Hydrodynamics of Gas-Liquid-Solid Fluidized and Semi-Fluidized Beds

Hara Mohan Jena

Department of Chemical Engineering
National Institute of Technology
Rourkela – 769008, India

PhD
Thesis

Hydrodynamics of Gas-Liquid-Solid Fluidized and Semi-Fluidized Beds

Hara Mohan Jena

NIT
Rourkela
2009

Hydrodynamics of Gas-Liquid-Solid Fluidized and Semi-Fluidized Beds

Thesis submitted to the
National Institute of Technology, Rourkela
for award of the degree

of

Doctor of Philosophy

By

Hara Mohan Jena

DEPARTMENT OF CHEMICAL ENGINEERING
NATIONAL INSTITUTE OF TECHNOLOGY, ROURKELA
ORISSA -769 008, INDIA

September 2009

Dedicated to

Lord Jagannath, Baladeva and Subhadra

DEPARTMENT OF CHEMICAL ENGINEERING
NATIONAL INSTITUTE OF TECHNOLOGY,
ROURKELA -769 008, INDIA

CERTIFICATE

This is to certify that the thesis entitled **Hydrodynamics of Gas-Liquid-Solid Fluidized and Semi-Fluidized Beds,** submitted by **Hara Mohan Jena** to National Institute of Technology, Rourkela is a record of bonafide research work under our supervision and is worthy of consideration for the award of the degree of Doctor of Philosophy of the Institute. The candidate has fulfilled all prescribed requirements and the thesis, which is based on candidate's own work, has not been submitted elsewhere for a degree or diploma.

Sd-

Co-supervisor
Prof. B. C. Meikap
Department of Chemical Engineering
Indianl Institute of Technology
Kharagpur - 721302
INDIA

Sd-

Supervisor
Prof. G. K. Roy
Department of Chemical Engineering
National Institute of Technology
Rourkela - 769008
INDIA

Acknowledgement

I would like to express my deep and sincere gratitude to my Supervisors Prof. G. K. Roy and Prof. B. C. Meikap for their valuable guidance, inspiration, constant encouragement and heartfelt good wishes. Their genuine interest in the research topic, free accessibility for discussion sessions, thoughtful and timely suggestions has been the key source of inspiration for this work. I feel indebted to both my supervisors for giving abundant freedom to me for pursuing new ideas. It was overall a great experience of working with both of them.

I record my sincere thanks and gratitude to Prof. S. K. Srarangi, Director, N.I.T., Rourkela for his cordial advice and suggestions on CFD modeling, and continued encouragement throughout this work.

I take this opportunity to express my deep sense of gratitude to the members of my Doctoral Scrutiny Committee Prof. S. K. Agarawal (HOD), Prof. K. C. Biswal, Prof. (Mrs.) A. Sahoo of Chemical Engineering Department and Prof. D. P. Tripathy of Mining Engineering Department for thoughtful advice during discussion sessions. I am also thankful to my teachers Prof. P. Rath and Prof. R. K. Singh for constant encouragement and good wishes throughout the current work. I record my sincere gratitude to Prof. G. R. Satpathy of Biotechnology and Medical Engineering Department for his constructive suggestions and continued pestering for early submission of the thesis.

I am very thankful to Prof. S. S. Mahapatra of Mechanical Engineering for his help in data analysis and thoughtful suggestions, Dr. Anil Kishan for his sessions in CFD modeling and Prof. S. Paria of Chemical Engineering Department for timely suggestions. I thank Mr. M. Madhan, Asst. Librarian for his help in getting literature needed for the work.

My special thanks to our students B.K.Sahoo, Kapil Rakh, Debasish Mohapatra and Amit Kumar for their help in performing various experiments and modeling work. I express my special thanks to my friends P. Kanungo, G. C. Sahoo for their readiness to help for anything and everything for the current work. I remain ever grateful to our technical staffs Mr. Rajendra Tirkey, Mr. S. Mohanty and Mr. Biswanath for their assistance in experimental work.

I owe a lot to my wife Dr. Puspanjali Rout for her night-long runs to the lab with me assisting in performing experiments over the time and taking care of proof-reading part of the thesis at the end. My daughter Monalisa deserves a special mention for her patient cooperation without which it would have been greatly difficult to finish the thesis in time. The thesis would remain incomplete without mentioning the contributions of my siblings and parents for making me what I am today.

(Hara Mohan Jena)

Preface

Two-phase and three-phase fluidized beds have been applied successfully to many industrial processes such as in the H-oil process for hydrogenation and hydro-desulfurization of residual oil, the H-coal process for coal liquefaction, Fischer-Tropsch process, and the bio-oxidation process for wastewater treatment. A semi-fluidized bed has the advantages of both the packed and the fluidized beds as it can partly over come the disadvantages of a fluidized bed, namely back-mixing of solids, attrition of particles and erosion of surfaces, and those of a packed bed, such as non-uniformity in bed temperatures, segregation of solids and channeling. Semi-fluidized beds have been applied successfully to many industrial processes (physical, chemical and biochemical) such as in the filtration, adsorption, catalytic reactions, heavy metal removal and recovery, coal pyrolysis, bio-oxidation, ethanol fermentation, granule tablet manufacturing etc.

During the last four decades, considerable research efforts have been made to understand the hydrodynamic aspects of three-phase fluidization. Over the years newer applications of fluidized bed systems are being explored which necessitate deeper understanding of the two and the three phase fluidization and the semi-fluidization systems. The problems related to the effect of distributor, irregular and regular shape particles, liquid viscosity and surface tension, scaling up, particle size and density, which affect the hydrodynamics, and its structure still create practical dilemma. Even though a large number of experimental investigations have been directed towards the quantification of various hydrodynamic parameters of gas-liquid-solid fluidized beds, the complicated phenomena have not yet been fully understood. Critical appraisal of the status of research on the hydrodynamics of fluidized bed reactors shows that majority of the cases reported the hydrodynamics of three phase fluidization with spherical and non-spherical isotropic particles. However, exhaustive studies on the hydrodynamics of irregular shape particles, hollow cylindrical particles possessing higher surface to volume ratio and wide range of operating variables in a single system have not been carried out so far. Of late, computational fluid dynamics (CFD) has been promoted as a useful tool for better understanding of the multiphase reactors for precise design and scale up. The report on the computational models for the hydrodynamic characteristics of a three-phase (gas-liquid-solid) fluidized bed is limited. Thus, there exist many grey areas requiring further extensive fundamental studies for the three-phase fluidized bed systems.

.As far as the semi-fluidized bed is concerned; the earlier studies are limited to liquid-solid or gas-solid systems and to a narrow range of operating variables. Information relating to the gas-liquid-solid semi-fluidization is meagre although the technique has excellent potential to be used in chemical reactors for catalytic as well as non-catalytic ones, biochemical process and wastewater treatment.

Therefore, in this work an attempt has been made to investigate a few more aspects on the hydrodynamics of both the regular and the irregular particles within a co-current upflowing gas-liquid-solid fluidized bed to gain a better understanding of the bed behaviour for potential industrial applications. The objective of the CFD analysis in this study is to investigate numerically the hydrodynamic behaviour of a three-phase gas-liquid-solid fluidized bed.

The hydrodynamic study of a liquid-solid semi-fluidized bed and a cocurrent gas-liquid-solid semi-fluidized bed with liquid as the continuous phase has been taken up to have a better understanding of the bed behaviour with respect to a large number of operating variables. The outcome of the investigations may be useful in the design a semi-fluidized bed reactor recommended for fast exothermic reactions with better performance.

Thus the present investigation relating to the gas-liquid-solid fluidized and the semi-fluidized beds and the outcomes thereof are a step forward towards a better understanding of an otherwise complex but useful fluid-solid contacting technique of immense industrial importance. The contents of the thesis are a new interpretation of established facts based on exhaustive study and critical analysis of a few published work of others.

Contents

List of Figures

List of Tables

List of Symbols

A_c	cross sectional area of the fluidized bed column, m^2
Ar	Archimedes number ($[d_p^3 \rho_l(\rho_s - \rho_l)g]/ \mu_L^2$), -
b_i	coefficient in factorial design analysis
C_D	drag coefficient, -
C_μ, σ_k, σ_ε,	coefficient in turbulent parameters
$C_{1\varepsilon}$, $C_{2\varepsilon}$, $C_{3\varepsilon}$	coefficient in turbulent parameters
d_b	bubble diameter, m
D_c	diameter of the column, m
d_e	equivalent diameter of solid particle, m
D_e	effective diameter of the channel, m
d_p	average particle diameter, m
d_{pi}	particle diameter, m
d_r	particle diameter to column diameter ratio (= d_p/D_c), -
Eo	Eötvös number (= $\Delta\rho g D_c^2/ \sigma_L$), -
e_{ss}	coefficient of restitution for particle collisions, -
$\boldsymbol{F}_D$	drag force, N
$F_{D,gL}$	gas-liquid inter phase drag force, N
$F_{D,gs}$	gas-solid inter phase drag force, N
$\boldsymbol{F}_{D,Ls}$	liquid–solid inter phase drag force, N
$\boldsymbol{F}_i$	inter phase force, N
$\boldsymbol{F}_L$	lift force, N
$\boldsymbol{F}_{VM}$	force of virtual mass, N
Fr_g	gas Froude number (= $U_g^2/(g D_c)$), -
Fr_L	liquid Froude number (= $U_L^2/(g D_c)$), -
g	acceleration due to the gravity, ms^{-2}
$g_{0,ss}$	radial distribution function
$G_{k,L}$	production of turbulent kinetic energy, J
H, H_e or H_f	height of expanded fluidized bed, m
H_c	height of the column, -
H_L	height of the liquid in the column after the escape of gas, m
H_{Pa}	height of the top packed bed, m
H_r	bed aspect ratio (= H_s/D_c), -
H_s	initial static bed height, m
H_t	height of the top restraint, m
ΔH	differential height, m
$\boldsymbol{I}$	identity matrix

k	ratio of the volume fraction of the wake region to that of the bubble region, -
k	turbulent kinetic energy, J
K_{gs}	inter-phase exchange coefficient between the gas and the solid phases, kg s^{-1}
K_{Lg}	inter-phase exchange coefficient between the liquid and the gas phases, kg s^{-1}
K_{Ls}	inter-phase exchange coefficient between liquid and solid phases, kg s^{-1}
$k_{\Theta s}$	diffusion coefficient
M_b	buoyant mass of the solid in the bed, kg
Mo	Morton number (=g $\mu_L^4/(\rho_L \sigma_L^3)$), -
M_s	mass of the solid in the bed, kg
N	total number of treatments in factorial design analysis
n	Richardson-Zaki index
p	pressure, Pa
p_s	solids pressure, Pa
$\frac{\Delta P}{\Delta H}$	pressure gradient in the bed, Pa m^{-1}
$\frac{\Delta P_d}{\Delta H}$	dynamic pressure gradient in the bed, Pa m^{-1}
$\frac{\Delta P_f}{\Delta H}$	frictional pressure gradient in the bed, Pa m^{-1}
Δp^{Ls}	pressure drop in liquid-solid fluidized bed, Pa
Δp^{gLs}	pressure drop in gas-liquid-solid fluidized bed, Pa
ΔP_f	pressure drop across the fluidized section in semi-fluidized bed, Pa
ΔP_{osf}	pressure drop at onset of semi-fluidization
ΔP_{pa}	pressure drop across the packed section of the semi-fluidized bed, Pa
ΔP_r	pressure drop across the top restraint, Pa
ΔP_{sf}	pressure drop across the semi-fluidized bed, Pa
R	bed expansion ratio (H_e/H_s) or (H/H_s) in fluidized bed, (H_{sf}/H_s), or (H_t/H_s) in semi-fluidized bed, -
Re_b	bubble Reynolds number, -
Re_c	liquid Reynolds number based on column diameter (= $\rho_L D_c U_L/\mu_L$), -
Re_L	liquid particle Reynolds number (= $\rho_L d_p U_L/\mu_L$), -
Re_g	modified gas Reynolds number (= $\rho_L d_p U_g/\mu_L$), -
Re_{msf}	Reynolds number at maximum semi-fluidization
Re_p	particle Reynolds number, -
Re_t	Reynolds number at terminal condition
S_p	surface area of particle, m^2
$\boldsymbol{u}_{dr}$	drift velocity, m s^{-1}
U_g	superficial gas velocity, m s^{-1}
$\boldsymbol{u}_{jL}$	relative velocity, m s^{-1}

U_L	superficial liquid velocity, m s^{-1}
$\boldsymbol{U}_L$	phase-weighted velocity, m s^{-1}
U_{Losf}	onset liquid velocity of semi-fluidization or minimum liquid semi-fluidization velocity, m/s
U_{Lmsf}	maximum liquid semi-fluidization velocity, m/s
U_{Lmf}	minimum liquid fluidization velocity, m/s
U_{mf}	minimum fluidization velocity, m/s
U_{msf}	maximum semi-fluidization velocity, m/s
U_{osf}	onset velocity of semi-fluidization or minimum semi-fluidization velocity, m/s
U_s	semi-fluidization velocity, m/s
U_t	particle terminal velocity, m/s
V_p	volume of particle, m^3
We	Weber number (= $\rho_L D_c U_L^2 / \sigma_L$), -
x	ratio of solid holdup in wake region to that in the liquid-solid fluidized bed region, -
x_i	mass fraction, -
Y or Y_i	response in factorial design analysis

Greek Symbols

α_i	level of the variable in factorial design analysis
β_d	ratio of densities (= ρ_p/ρ_L), -
$\Delta\beta_d$	ratio of buoyancy to liquid density (=$(\rho_L- \rho_g)/\rho_L$), -
$\Delta\rho$	buoyancy term (=$\rho_L- \rho_g$), kg m^{-3}
ε or ε_f	porosity of fluidized bed, -
ε	turbulent dissipation rate, m^2 s^{-3}
ε_g	gas holdup in fluidized bed, -
$\varepsilon_{g,p}$	gas holdup in packed bed, -
$\varepsilon_{g,sf}$	gas holdup in semi-fluidized bed, -
ε_L	liquid holdup in fluidized bed, -
$\varepsilon_{L,p}$	liquid holdup in packed bed, -
ε_{pa}	porosity of packed section, -
ε_s	solid holdup in fluidized bed, -
$\varepsilon_{,s}$	voidage of initial static bed, -
$(\varepsilon_s)_{osf}$	solid holdup in fluidized bed at onset of semi-fluidization, -
$\varepsilon_{s,p}$	solid holdup in packed bed, -
γ_{Θ_s}	collision dissipation energy, J
λ_g, λ_L, λ_s	bulk viscosity of gas, liquid and solid phase, Pa s
μ_L	liquid viscosity, Pa s

μ_t	turbulent viscosity, Pa s
μ_w	viscosity of water, Pa s
Φ_s, φ_s	sphericity of solid particle, -
ρ_f	density of fluid, kg m^{-3}
ρ_g	density of gas, kg m^{-3}
ρ_L	density of liquid, kg m^{-3}
ρ_p or ρ_s	density of solid particle, kg m^{-3}
σ_L	surface tension of liquid. kg m^{-2}
$\boldsymbol{\tau}$	stress tensor, Pa
τ_g	bubble relaxation time, s
$\boldsymbol{\tau}''_L$	Reynolds stress tensor for liquid phase, Pa
$\tau_{t,L}$	characteristic time of the energetic turbulent eddies, s
θ_g	gas holdup in packed bed based on gas and liquid phases, -
θ_L	liquid holdup in packed bed based on gas and liquid phases, -
Θ_s	granular temperature, K

Subscripts

g	gas phase
L	liquid phase
s	solid phase
,s	static bed

Superscripts

Ls	liquid-solid system
gLs	gas-liquid-solid system
T	transpose

Abbreviations

AARE	average absolute relative error
CFD	computational fluid dynamics
cal.	calculated
exp.	experimental
GI	galvanized iron
FB	fluidized bed
PVC	polyvinyl chloride
SFB	semi-fluidized bed

Abstract

Fluidized and semi-fluidized bed systems are efficient gas-liquid-solid contacting techniques and have tremendous potential for industrial use. In spite of a lot of research activities carried out for the understanding of fluidization technology in the past few decades, several aspects relating to the effect of distributor, irregular and regular shape particles as bed material, liquid viscosity and surface tension, scaling up of a developed system for industrial application are not fully investigated. In the present investigation, a fluidized bed and a semi-fluidized bed have been developed, designed and fabricated to characterize the hydrodynamic properties. Results on spherical particles indicate that the bed pressure drop decreases with gas velocity and increases with initial static bed height, the liquid minimum fluidization velocity decreases with gas velocity and liquid viscosity but increases with particle size. Under optimum operating conditions, a maximum gas holdup value of 28.2 % has been found by Genetic algorithm. A similar influence of different operating variables has been observed in case of hollow cylindrical particles as observed with the spherical ones. In case of *irregular particles the most significant observation* is that the liquid minimum fluidization velocity increases with particle density and expanded bed height decreases with particle density. An attempt has been made for *computational fluid dynamic simulation of hydrodynamic characteristics of a three-phase fluidized bed*. The dynamic characteristics of gas–liquid–solid flows obtained from the computational fluid dynamic simulation have been validated with the experimental results and a good agreement has been observed. In is concluded that the Eulerian-Eulerian granular multiphase flow approach is capable of predicting the overall performance of gas–liquid–solid fluidized bed. Hydrodynamic characteristics of *regular particles in a semi-fluidized bed* indicate that the minimum semi-fluidization velocity increases with particle size and bed expansion ratio, but decreases with liquid viscosity. It has also been observed that the top packed bed height increases with increase in the values of the liquid and the gas velocity, liquid viscosity, but decreases with particle size, initial static bed height and expansion ratio. Empirical and semi-empirical equations have been developed and the predicted values have been found to agree well with the experimental results. It is interesting to note that for certain cases, gas holdup has been found to be 40 % higher in case of the semi-fluidized bed than that in the fluidized bed under identical operating conditions. Empirical model has been proposed for the prediction of gas holdup. The effect of various operating parameters for *irregular particles in a semi-fluidized bed has been investigated. In view of difference observed in*

the dependency of hydrodynamic parameters on operating variables, separate correlations for the regular and the irregular particles have been developed for the prediction of the values of minimum and maximum semi-fluidization velocity and the height of the top packed bed. Prediction of pressure drop using the model equation with the initial static bed voidage has resulted in large deviation from the experimental values. In case of pressure drop calculated from the measured packed bed voidage gives a good agreement in case of the liquid-solid semi-fluidized bed. In the light of important results obtained scale-up and design of semi-fluidized bed system for industrial use has been proposed and the future scope of the work has been identified.

Keywords: Fluidization, three-phase fluidized bed, packed bed, fluidized bed, semi-fluidized bed, regular shape particles, irregular shape particle, hydrodynamics, pressure drop, minimum fluidization velocity, bed expansion, porosity, gas holdup, minimum and maximum semi-fluidization velocity, height of the top packed bed, viscosity effect, computational fluid dynamics, Eulerian-Eulerian granular multiphase flow.

Chapter 1

Introduction and Literature Survey

Chapter – 1

Introduction and Literature Survey

Fluidization is an operation by which fine solids are transformed into a fluid-like state through contact with gas or liquid or by both gas and liquid. It is a fluid-solid contacting technique, which has found extensive industrial applications over the last six decades. This method of contacting has a number of unusual characteristics, and fluidization engineering is concerned with its efforts to take advantage of this behaviour and put it to various industrial uses.

1.1. Types of fluidization and its applications

Fluidization can be broadly of two types, viz. aggregative or bubbling and particulate fluidization. Particulate fluidization is mostly encountered in a liquid-solid system and in gas-liquid-solid system with liquid as the continuous phase, while aggregative fluidization is a characteristic of the gas-solid type or gas-liquid-solid system with gas as the continuous phase. In the case of liquid-solid contact, the action in the bed is strongly influenced by the particle size. The efficiency of aggregative fluidization depends upon the uniformity of fluidization, which is a result of good gas-solid contact. However, aggregative fluidization has certain in inherent drawbacks like bubbling, channelling and slugging, which results in a poor gas-solid contact thereby affecting the quality of fluidization.

1.1.1. Advantages and disadvantages of fluidized beds

There are several advantages of fluidized beds relative to fixed bed processes (Shah, 1979; Beaton et al., 1986; Fan, 1989; Le Page et al., 1992) such as; ability to maintain a uniform temperature, significantly lower pressure drops which reduce pumping costs, catalysts may be withdrawn, reactivated, and added to fluidized beds continuously without affecting the hydrodynamic performance of the reactor (this also allows the catalyst activity to be controlled), bed plugging and channelling are minimized due to the movement of the solids, lower investments for the same feed and product specifications, new improved catalysts can replace older catalysts with minimal effort, high macromixing, yielding large axial dispersion of phases, high reactant conversions for reaction kinetics favouring completely mixed flow patterns, low intraparticle diffusion resistance, gas-liquid and liquid-solid mass transfer resistance.

There are, however, also some disadvantages to fluidized beds such as; catalyst attrition due to particle motion, entrainment and carryover of particles, relatively larger reactor size compared to for fixed beds due to bed expansion, catalyst-fluid contact per unit volume is reduced due to bed expansion, not suitable for reaction kinetics favouring plug flow pattern, low controllability over product selectivity for complex reactions and loss of driving force due to back mixing of particles in case of transfer operations.

Due to the above mentioned advantages of the fluidized bed, it has extensive industrial applications as compared to fixed beds, and has become a versatile fluid-solid contacting device in chemical, biochemical and metallurgical industries. Extensive use of fluidization began in the petroleum industry with the development of fluid bed catalytic cracking. Presently, fluidization technique has found extensive applications in various fields like: In Physical operations such as: Coating of metal with plastic, Drying of solids, Transportation, Heating, Adsorption, etc. In Chemical operations viz. Coal gasification, Synthesis reactions, Combustion and incineration, Carbonization and gasification, Roasting of sulphide ores, Reduction of iron oxide, Biochemical reactors, etc.

1.2. History of development of fluidized bed technology

Winkler is credited with describing the first fluidized bed in 1921 and industrial fluidized bed application began with a large-scale Winkler gasifier in 1926 (Kunii and Levenspiel, 1991). This was the first application of coarse-powder fluidization. Table 1.1 lists the development chronology of fluidization science and technology since the first use of the fluidized bed. Fluidized bed catalytic cracking of crude oil to gasoline (FCC) was commercialized in 1942, and is still the major application of fine-powder fluidization. Several catalytic applications such as acrylonitrile synthesis, phthalic anhydride and Fischer-Tropsch synthesis of liquid fuels from coal-based gas extended the range following the FCC.

In the 1970's, Lurgi commercialized the circulating fluidized bed (CFB) for coarse powders, which operates above the terminal velocity of all the bed particles. The bed inventory in a CFB is continually entrained out of the vessel, recovered and re-circulated. Polyethylene began to be produced in a fluidized bed, and the technology is now widely used in industry.

The 1980's saw commercialization of circulating fluidized bed combustion and production of polypropylene in fluidized beds. New areas of application were production

of semiconductors and ceramic materials by chemical vapour deposition in fluidized bed and the use of liquid fluidized beds for biological applications.

Table 1.1: Development chronology of fluidized bed technology

Year	Development of technique / application
1920's	Winkler Gasifier-Coarse Powder Fluidization Coal Liquefaction (Bergius-Pier Process)
1940's	Fluid Catalytic Cracking (FCC)-Fine Powder Fluidization Phthalic Anhydride Ore Roasting Drying
1950's	Fluid Hydroforming Fischer-Tropsch Synthesis Acrylonitrile Spouted Bed Technique
1960's	Three – Phase Biochemical Processes Bubbling Bed Combustors Semi-Fluidized Bed Technique
1970's	Circulating Fluidized Beds (CFB's Lurgi & Battelle) FCC Risers High Density Polyethylene
1980's	Polypropylene CFB Combustors Semiconductors By Chemical Vapour Deposition. Fluidization Technique for Geldart's Group C Powders Immobilization Of Enzymes/Mammalian Cell Fermentation Waste Incineration.
1990's	Desulfurization / Denitration Using Powder-Particle Fluidized Bed Petroleum Coke Combustion
2000's	Industrial Combustion Biomass And Sludge Catalytic Propane Dehydrogenation Partial Oxidation of Butane Maleic Anhydride Dry Coal Beneficiation

1.3. Three-phase fluidization

Gas-liquid-solid fluidization also known as three-phase fluidization is a subject of fundamental research since the last four decades due to its industrial importance. Since then considerable progress has been made with respect to an understanding of the phenomenon of gas-liquid-solid fluidization. The successful design and operation of a gas-liquid-solid fluidized bed system depends on the ability to accurately predict the fundamental properties of the system.

Gas-liquid-solid fluidization is defined as an operation in which a bed of solid particles is suspended in gas and liquid media due to the net drag force of the gas and/or liquid flowing opposite to the net gravitational force (or buoyancy force) on the particles. Such an operation generates considerable, intimate contact among the gas, liquid and the solid in the system and provides substantial advantages for application in physical, chemical or biochemical processing involving gas, liquid and solid phases. The state of the gas-

liquid-solid fluidization is strongly dependent on the geometry of the bed, methods of gas-liquid injection, and the presence of a retaining grid or internals. This is exemplified by the development and the operation of a tapered fluidized bed, spouted bed, semi-fluidized bed and draft tube spouted bed.

1.3.1 Modes of three-phase fluidization

Within the field of three-phase systems there are several configurations and contacting modes. Three-phase fluidization requires three distinct phases. Fluidized beds are further classified by the direction of flow: co-current up-flow, co-current down-flow, counter-current, and liquid batch with gas up-flow. The present work is limited to co-current up-flow of the gas and liquid, the most widely used type of three-phase flow (Muroyama and Fan, 1985; Wild and Poncin, 1996). When designing three-phase fluidized beds for industrial application, the kinetics, heat transfer, and mass transfer must al1 be considered? For a typical catalytic reaction, there are eight key steps to be considered (Smith, 1981) for scale-up and design of a fluidized bed reactor which are as follows:

- Gas-liquid interface mass transfer
- Liquid-solid interface mass transfer
- Interna1 diffusion to the catalyst surface
- Adsorption of reactants at the catalyst surface
- Reaction on the catalyst surface
- Desorption of adsorbed products
- Transport of products from catalyst interior sites to outer surface**,**
- Transport of product from catalyst surface to bulk fluid.

Depending on the system, any of these can be the rate-limiting step. To completely understand the behaviour of a fluidized bed, each of these aspects must be studied. The first of these steps is commonly the rate-controlling one, and it is clear that it depends strongly on the bed hydrodynamics. It is therefore very essential to study the bed hydrodynamics, specifically the phase hold-ups, bed expansion, pressure drop and the minimum fluidization velocity.

For a given reactor volume and fluid flow rates, a cloud of small, spherical, slow-moving bubbles will have a greater opportunity to allow mass transfer than a few large, quick-moving slugs. A better understanding of the hydrodynamics would also be helpful in understanding the axial and the lateral dispersions factors which are also important in the functioning of multiphase reactors.

Traditional engineering research has focused on "big" breakthroughs resulting in new processes or dramatic improvements of existing technologies. Without any doubts, this is a worthwhile goal; however, recent efforts have been directed more towards fundamental understanding and small but steady improvements to maximize process efficiency. The work in the present thesis is an attempt in this direction. By proposing and validating a method of simulating industrial processes, some fundamental engineering information have been obtained through exhaustive experimental investigations to help gain a better understanding of the process being simulated.

1.3.2. Flow regimes

Identification of flow regimes in fluidized bed is important for its stable operation in a particular set of operating variables. Fan (1989) identified three flow regimes in which three-phase fluidized beds can operate: bubbling, slugging, and transport. Within the bubbling regime, there are two sub-categories: the dispersed bubble and the coalesced bubble regimes. The separation between regimes is often qualitative and not well defined. Zhang (1996) and Zhang et al. (1997) identified seven distinct flow regimes for gas-liquid-solid co-current fluidized beds and identified a number of quantitative methods for determining the transitions as under:

- Dispersed bubble flow: Usually corresponds to high liquid velocities and low gas velocities. Results in small bubbles of relatively uniform size. Little bubble coalescence despite high bubble frequency.
- Discrete bubble flow: Usually occurs at low liquid and gas velocities. It is similar to the previous regime with respect to small bubble size and uniform size. However, the bubble frequency is lower.
- Coalesced bubble flow: Usually found at low liquid velocities and intermediate gas velocities. The bubbles are larger and show a much wider size distribution due to increased bubble coalescence.
- Slug flow: Not often seen in industrial applications, this regime is characterized by large bullet shaped bubbles with a diameter approaching that of the column and lengths that exceed the column diameter. Some smaller bubbles are also observed, especially in the wakes of the slugs.
- Churn flow: Churn flow is similar to the previous regime, but much more chaotic and frothy. As gas flow is increased, an increase in downward liquid flow near the wall is usually observed. Note that while Darton (1985) also identified a Churn-turbulence regime, he defined it as the transition between

bubbling and slug flow. However his definition, based upon two-phase fluidized systems, should probably be classified as a coalescing bubble regime.

- Bridging flow: A transitional regime between the churn flow and the annular flow where liquid and solids effectively form 'bridges" across the reactor which is continuously broken and re-formed.
- Annular flow: At extremely high gas velocities, a continuous gas phase appears in the core of the column.

A schematic representation of these flow regimes reprinted from Zhang (1996) is shown in Figure 1.1. Under Fan's (Fan, 1989), previous classification of regimes, Zhang's dispersed bubble flow, discrete bubble flow and coalesced bubble flow can be grouped under the heading "bubbling regime", while churn flow, bridging flow, and annular flow al1 be classified as belonging to the transport regime.

The bubble sizes and shapes in the bubbling, slugging, and transport regimes differ considerably from one another. As mentioned above, slug flow has bullet shaped bubbles with a cross-sectional dimension almost equal to the reactor column. In the transport regime, bubbles are practically non-existent since the gas forms a continuous phase as it conveys liquid droplets and solid particles through the fluidized bed. In the bubbling regime, under dispersed bubble flow, the bubbles tend to be spherical, small and relatively uniform in size. For coalesced flow, however, the bubbles tend to be larger, with a wider size distribution. Spherical-cap or spheroidal bubbles are also commonly found, and these can have significant wakes that also affect the reactor performance (Matsuura and Fan, 1984). Wakes are responsible often for increased particle mixing and is the reason for some beds to contract initially when the gas flow is increased (Epstein and Nicks, 1976).

Another important aspect of the flow regimes is the particle action. In a transport system, many particles are entrained and removed from the system; hence particles need to be replenished continuously. In a bubbling bed, entrainment of particles is much less significant, although some caution must still be taken to prevent emptying of the column over time.

Although most classifications of the fluidization regime are related to liquid and gas superficial velocities, it is important also to consider particle size, shape, and density (Muroyarna and Fan, 1985).

1.3.3. Applications of three-phase fluidized bed

Numerous applications of gas-liquid-solid fluidization system exist which vary from bench scale to commercial scale and include all the basic modes of operation. In most of the applications, the individual phases can be reactant, product, catalyst, or inert (L'Homme, 1979; Shah, 1979; Ramachandran and Chaudhari, 1983). Three-phase cocurrent gas-liquid-solid fluidized beds have been used in a wide range of applications including hydro-treating and conversion of heavy petroleum and synthetic crude, coal liquefaction, methanol production, sand filter cleaning, electrolytic timing, conversion of glucose to ethanol, aerobic waste water treatment, and various other hydrogenation and oxidation reactions (Fan, 1989; Wild and Poncin, 1996).

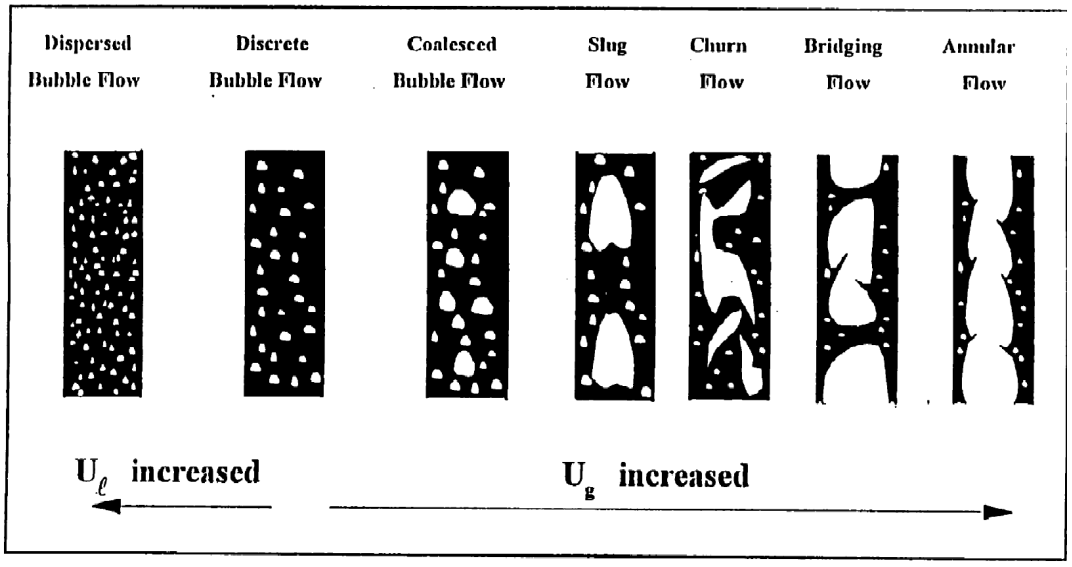

Fig. 1.1. Flow regimes in gas-liquid-solid co-current fluidized bed

The direct liquefaction of coal (Bergius-Pier process) in mini commercial scale first started in Germany in 1927 with a capacity of 2500 barrels per day (bbl/day) (Fan, 1989). The first large scale production (4.2 million tonnes per annum) of aviation gasoline in Germany was achieved during World War II (Donath, 1963). Gas-liquid-solid reactors for catalytic production of organic chemicals or polyolefins are in use since 1950s. Major reaction applications in commercial production included hydrogenation of glucose to sorbitol, benzene to cyclohexane, benzoic acid to cyclohexanecarbocylic acid, butynediol to butenediol, adiponitrile to hexamethylene diamine, esters to fatty alcohols, 3,5 nitrotoluene to 3,5 toluene diamine and aluminium and ethylene to Ziegler alcohol (ALFOL process), and ethylene polymerization (Solvey process using Ziegler-Natta catalyst) (Fan, 1989).

The three-phase fluidized bed (Mode E-I-a-1) was first used commercially in 1968 for hydrotreating petroleum residues (H-oil process) (Fan, 1989). Plants of capacity higher than 60,000 bbl/day are in use now. The direct coal liquefaction processes such as Exxon Donor Solvent (EDS) Process, Solvent Refined Coal (SRC) process, and H-coal process. Plants of capacities 250 ton/day for EDS and SRC process (Mode E-I-a-2) and 500 ton/day for H-coal process (Mode E-I-a-1) were started in 1973 (Fan, 1989). The first large scale three-phase fluidized bed reactor (Mode E-I-a-2) (10,000 litre fermentor for ethanol production) came to be in use in early 1980's (Samejima et al., 1984).

Critical literature survey reveals that, beyond the above large scale applications, there are numerous examples of application of three-phase fluidized bed systems demonstrated at relative small scales. Few such applications relatively in smaller scale of cocurrent gas-liquid-solid fluidized beds (liquid as continuous phase) have been given in Table 1.2. These applications are classified as: (a) physical, (b) chemical (petrochemical or electrochemical) and (c) biochemical.

Table 1.2: Relatively smaller scale applications of gas-liquid-solid fluidized beds

Applications	Process type	References
Physical processes		
Sand filter cleaning	Physical	Brownell (1951)
Crystallization	Physical	Thompson (1955)
Air flotation	Physical	Fuerstenau (1980), Foot et al. (1986)
Chemical processs		
Calcium bisulfite production	chemical	Volpicelli and Massimilla (1970)
Hydrogenation of heptane	chemical	Ermakova et al. (1973) cited in Fan (1989)
Coal gasification	chemical	Cover et al. (1973); Kohl et al. (1978)
Electrodes	chemical	Oloman and Watkinson (1975) Kusakabe et al. (1981)
Methanol production	chemical	Sherwin and Frank (1976)
Hydrogenation of 1-heptene	chemical	Gartsman et al. (1977)
Methanation	chemical	Blum and Toman (1977)
Coal liquefaction (H-Coal or ebullated bed reactor)	chemical	Li and Liu (1981)
Oxydesulfurization of coal	chemical	Joshi et al. (1981)
Production of zinc hydrosulfite	chemical	Sastri et al. (1983)
Coal liquefaction (Exxon Donor Solvent Reactor)	chemical	Tarmy et al. (1984)
Hydrotreating and conversion of heavy petroleum and synthetic crude (H-oil, LC-Fining or ebullated bed reactor)	chemical	Johnson et al. (1985) Beaton et al. (1986)
High pressure three-phase fluidization with heat transfer	chemical	Luo et al. (1997)
Dry impregnation of coarse alumina porous particles by a metallic salt	chemical	Barthe et al. (2009)
Pyrolysis of sewage sludge in fluidized bed to produce bio-oil	chemical	Fonts et al. (2009)
H_2 rich product gas by steam gasification of biomass with in situ CO_2 absorption	chemical	Koppatz et al. (2009)
Biochemical processes		
Treatment of Lactose wastewater	biochemical	Scott and Hancher (1976)

Treatment of phenol wastewater	biochemical	Holladay et al. (1978), Sokol and Halfani (1999)
Treatment of thiocyanate and coal hydrocarbonization wastewater	biochemical	Lee et al. (1979)
Treatment of slaughter house wastewater	biochemical	Qian (1980)
Treatment of municipal sewage wastewater	biochemical	Shen and Wang (1980)
Treatment of isobutanol or acetic acid wastewater	biochemical	Chatib et al. (1981); Grasmick et al. (1981)
Treatment of glucose-BOD wastewater	biochemical	Takase et al. (1983)
Conversion of sucrose to glucose by plant cells D. carota	biochemical	Prenosil and Pedersen (1983)
Treatment of gasification wastewater	biochemical	Donaldson et al. (1984)
Ethanol production by yeast cells		Samejima et al. (1984)
Treatment of synthetic milk wastewater sewage	biochemical	Forster et al. (1986)
Treatment of s-triazine wastewater	biochemical	Hogrefe et al. (1986)
Bioprocessing of coal for liquefaction and removal of sulphur, nitrogen and trace metals	biochemical	Wilson et al. (1986) cited in Fan (1989)
Simultaneous selective flocculation and microbial desulfurization of high sulphur coal	biochemical	Fan and Attia (1988)
Production of acetic acid using immobilized *Acetobacter aceti*	biochemical	Sun and Furusaki (1990)
Culture of *Solanum aviculare*	biochemical	Anata et al (1995)
As biofilm reactor	biochemical	Beyenal and Tanyolac (1998)
Cultivation of plant cells and tissues	biochemical	Sajc et al. (2000)
Biodegradation phenol using psychotropic Pseudomonas putida	biochemical	Hirata et al. (2000a), Gonzalez et al. (2001), Onysko et al. (2002)
Denitrification of nitrate-nitrogen wastewater	biochemical	Jianping et al. (2003)
Treatment of refinery wastewater	biochemical	Sokol (2003), Xianling et al. (2005)
Microbial removal of ionic mercury	biochemical	Deckwer et al. (2004)
Degrdation of atrazine in biofilm activated coerbon fluidized bed reactor	biochemical	Herzberg et al. (2005)
Aerobic digestion of starch wastewater	biochemical	Rajasimman and Karthikeyan (2007)
Biodesulfurization of refractory organic sulfur compounds	biochemical	Soleimani et al. (2007)
Monoaromatics removal from polluted water	biochemical	Farhadian et al. (2008)
Iron oxidation by acidophilic bacteria	biochemical	Nurmi et al. (2009)
Oxidation of limonene to perillic acid	biochemical	Mirata et al. (2009)
Biohydrogen production using sewage sludge	biochemical	Lin et al. (2009)

1.3.3.1. Waste water treatment

Wastewater discharged in various process industries needs proper treatment to meet the stringent environmental regulations. Biological treatment of waste water is attractive due to its potential to almost total degradation of the pollutants while producing innocuous end products. There are various types of bioreactors used in the treatment of waste water. The immobilization cell bioreactors like CSTR, packed bed, fluidized bed, air lift type, etc are better than the conventional type free-culture bio-reactors due to the potential advantages like continuous reactor operation at any desired liquid throughput without risk of cell washout, protection of cells from toxic substrates, higher growth rate resulting in high concentration of cells in the reactor, easy cell-treated water separation, enhanced gas-liquid mass transfer rate, plug flow operation by maintaining the immobilized cells as a stationary phase (Jena et al., 2005). The fluidized bed bioreactors

are superior in performance due to immobilization of cells on solid particles reducing the time of treatment, volume of reactor is extremely small, lack of clogging of bio-mass and removal of pollutant like phenol even at lower concentrations (Jena et al., 2005). The superior performance of a FBB stems from the higher biomass concentration (up to 30-40 kg/m^3) and very high specific surface area per bioreactor volume (800-1200 m^2/m^3) (Jena et al., 2005).

Numerous research on various types of waste water treatment using gas-liquid-solid fluidized bed bioreactor have been reported in literature (Schügerl, 1997; Choi et al., 1999; Nicolella et al., 2000; Xianling et al., 2005; Horn et al., 2008; Potumarthi et al., 2008; Wang et al., 2009). The wastewater from process industries or municipal sources after primary sedimentation is treated in a fluidized bed bioreactor. The water treated in the fluidized bed bioreactor contains mainly suspended particles, oils and greases, complex organic compounds etc. and thus possesses a viscosity higher than the ordinary water. Literature survey indicates that very limited work has been reported on the effect of viscosity on the hydrodynamics of a gas-liquid-solid fluidized bed. It is therefore very essential to use the simulated value of the possible liquid viscosity in a waste water plant on hydrodynamic characteristics of fluidized bed reactor for better scale-up, design and understanding the mechanism of hydrodynamic behaviour.

1.4. Scaling: The journey from laboratory unit to industrial application

There have been extensive studies into many aspects of three-phase fluidization and some excellent reviews are available since 1980 (Epstein, 1981; Wild et al., 1984; Darton, 1985; Muroyama and Fan, 1985; Fan, 1989; Wild and Poncin, 1996; Kim and Kang, 1997; Yang and Fan, 2007). However, three phase systems are complex and there remain many unanswered questions (Tarmy and Coulaloglou, 1992; Barkat and Diboun, 1995; Safoniuk, 1999).

Although there have already been extensive investigations on the hydrodynamics of three-phase fluidized beds, a major problem that continues to limit their industrial application involves the difficulties in scaling-up the results from small laboratory units to larger industrially significant units. It is common for results found with small-scale test units to be unachievable when the unit size is increased. This problem is due in part to the materials used in the bulk of the previous work: air, water and spherical glass beads, while industrial applications mostly involve non-spherical particles at high temperatures and pressures. These temperatures and pressures result in fluid properties

considerably different from that of air and water at normal laboratory conditions (Tarmy et al., 1984; Jiang et al., 1992; Luo et al., 1997).

This problem is not unique to three-phase systems and has also plagued two-phase fluidization. The first major documented case of a severe scale-up problem was in a Fischer-Tropsch synthesis plant in Brownsville, Texas in the early 1950s (Squires et al., 1985). The conversion achieved in the industrial unit was only about 50% of that achieved in the laboratory reactors. Such a large reduction in conversion would cripple most of the processes. Therefore scale-up consideration must be taken into account in the design of such reactors.

To design a three-phase fluidized bed chemical reactor many different aspects must be predicted and quantified. Most often, to achieve desired reactor goals, fundamental knowledge like the effect of various operating parameters on the hydrodynamics may be required. For the given fluid and solids properties, the operating gas and liquid superficial velocities must then be set and the reactor size determined based upon the expected bed expansion and hold-ups.

There are essentially three ways of addressing the above item: laboratory studies, pilot-plant studies, and mock-up studies (Euzen et al., 1993). In a laboratory study, the fluidized bed hydrodynamics, or any other aspect of the process (mass transfer for example), may be studied for different fluids and solids under idealized conditions. This is definitely the least expensive method and can generate significant amount of data within relatively a short time frame. In a pilot-plant study, the work is focused more closely on the expected operating conditions of the full-scale reactor. This may necessitate operating the unit for extended periods of time and varying process parameters such as operating conditions and feed impurities. Even at this level of process-directed research, not al1 scale-up issues are addressed adequately (Euzen et al., 1993). In mock-up studies, experiments are conducted in a unit that is typically about 1/10 the linear size of the expected final design. This is a very expensive process and can delay the final reactor design by several years (Euzen et al., 1993) because of the time it takes to commission and run such a unit. Often the implementation of a process can go through al1 three methods since scale-up problems, as discussed above, have led to caution within the industry.

1.5. Some definitions of fluidization phenomena

Some of the common terminology used to describe the fluidization phenomenon is defined in Table 1.3.

Table 1.3: Definitions of some three-phase fluidization phenomena

Term	Symbol	Significance
Bed Pressure drop	ΔP	Measures the drag in combination with the buoyancy and phase holdups
Minimum fluidization velocity	U_{mf}	The minimum superficial velocity at which the bed becomes fluidized. For the operating conditions in this work, the particles are fluidized primarily by the liquid.
Bed expansion ratio	β_{er}	Measures the extent of fluidization of the bed, $\beta_{er} = \frac{H_e}{H_s}$
Gas holdup	ε_g	Measures the fractional volume occupied by the gas, $\varepsilon_g = \frac{\text{volume of gas}}{\text{total bed volume}}$
Liquid holdup	ε_L	Measures the fractional volume occupied by the liquid, $\varepsilon_L = \frac{\text{volume of liquid}}{\text{total bed volume}}$
Solids holdup	ε_s	Measures the fractional volume occupied by the solids, $\varepsilon_s = \frac{\text{volume of solid}}{\text{total bed volume}}$ and $\varepsilon_g + \varepsilon_L + \varepsilon_s = 1$
Porosity	ε	Measures the volume occupied by both the liquid and the gas, $\varepsilon = \varepsilon_g + \varepsilon_L = 1 - \varepsilon_s$
Bubble rise velocity	U_b	The actual velocity of a bubble as it rises through the bed. Note that $\varepsilon_g \approx U_g/U_b$

1.6. Critical appraisal for hydrodynamic predictions

Review of literature on hydrodynamics in g-l-s fluidization reveals that a significant amount work has been carried out and the detailed research investigations based on experiments conducted in small-scale columns is listed in Table 1.4. This table also contains brief information on the techniques and models used and the systems studied.

Table 1.4: Hydrodynamic studies on gas-liquid-solid fluidization

Researcher	Type of system (Gas/liquid/solids), technique and approach used	Parameter studied
Ermakova et al. (1970)	Air/water and glycerine solution/glass bead, visual observation	Minimum fluidization velocity, pressure drop and gas holdup
Dakshinamurty et al. (1971, 1972)	Air/water/glass beads, iron shot, sand or Rockwool shot; air/kerosene/glass beads, iron shot or Rockwool shot; Air/water/glass beads and lead shot; nitrogen/elecboIyte/glass beads and RockwooI shot	Bed voidage
Bhatia and Epstein (1974)	Generalized wake model.	Bed voidage, gas holdup
Darton and Harrison (1975)	Air/water/sand particle, Wake model.	Bed voidage, gas and liquid holdup
Begovich and Watson (1978)	Air/water/various beads Electrical conductivity measurement	Minimum fluidization velocity, gas holdup, bed voidage
Soung (1978)	Nitrogen/heptane/cylindrical extrudates	Bed expansion

El-temtamy and Epstein (1979)	Air/water/glass beads and lead shot, Wake model	Bed contraction and expansion
Kato et al. (1981)	Air/water or aqueous solutions of CMC/glass beads	Liquid holdup
Kelkar et al. (1983)	Air/water-alcohol solutions/glass beads Surfactants added	Gas holdup
Chern et al. (1984)	Air/water/glass spheres and PVC cylinders	Gas holdup, pressure drop
Fan et al. (1985)	Air/water/binary mixtures of activated carbon, nylon, glass and alumina beads	Minimum fluidization velocity, bed expansion, gas holudup, mixing and segregation
Costa et al. (1986)	air, He, CO_2, CH4/Water and aqueous solutions of CMC/ glass, aluminum and benzoic acid covered with a paint film	Bed voidage
Fan et al. (1986)	Air/water/ glass and nylon beads, alumina particles, Visual observation of flow regime.	Pressure fluctuation measurement, flow regime transition
Jean and Fan (1987)	Air/water/glass, alumina or lead spherical or near-spherical particles, Force balance model	Particle terminal velocity, gas holdup
Saberian-Broudjenni et al. (1987)	N2, He, CO_2/water, cyclohexane, gas oil, kerosene, C_2Cl_4/ glass and alumina beads, alumina extrudates	Minimum fluidization, bed porosity, gas slip velocity, gas and liquid holdups
Fan et al. (1987)	Air/water-alcohol solutions/glass beads, surfactants added	Gas holdup, bubble size, solid holdup
Zheng et al. (1988)	Air/water/glass beads, Pressure fluctuation signals measurement using semi-conductor pressure transducers	Flow regimes, gas holdup
Tang and Fan (1989)	Air/water/polystyrene, nylon, acrylic and acetate particles, electrical resistive probe, development of mechanistic model for axial solid holdup	Axial distribution of holdup of gas, liquid and solid phases, bubble size distribution
Nikov et al. (1990)	Air/mineral oils, kerosene/glass beads, bubble wake model	Bed voidage, gas and liquid holdups
Han et al. (1990)	Air/water, aqueous solutions of glycerol/ glass beads	Bed voidage, gas and liquid holdups
Nacef et al. (1992)	Nitrogen/water-alcohol solution/glass and polypropylene beads	Minimum fluidization velocity, phase holdups, slip velocity
Kim et al. (1992)	Air/water-CMC, Triton X-100, ethanol solution /glass beads, tracer and conductivity probe	Phase holdup and axial dispersion coefficient
Chen et al. (1994)	Air/sodium iodide solution/glass and acetate beads, particle imaging velocimetry and lesser sheeting technique	Macroscopic flow structure, flow visualisation.
Liang et al. (1995)	Air/water/glass beads Electrical conductivity probe	Pressure gradient, axial phase holdup, solid particle circulation
Yu and Rittmann (1997)	Air/water/clean glass beads and biofilm coated particles, Wake model for phase holdup	Bed expansion, gas, liquid and solid holdup
Safoniuk et al. (1999)	Air/aqueous magnesium sulphate solution/ cylindrical aluminium particles, Scaling using Buckingham Pi theorem.	Bed expansion, gas holudup
Sokol and Halfani (1999)	Air/water/biomass laden low density particles	Minimum fluidization air velocity, gas holudup
Larachi et al. (2000)	Database containing diversified information related to over 540 measurements used, Artificial neural network model	Minimum fluidization velocity
Lee et al. (2001a)	Air/water/ glass beads, polymer beads Fluid maldistribution effect	Bed voidage, gas, liquid and holdups
Larachi et al. (2001)	Macroscopic hydrodynamic revisited using artificial neural networks & dimensional analysis and *hybrid k-x* generalized bubble wake model	bed porosity, liquid and gas holdups
Miura et al. (2001)	Air/ water and solutions of glycerol, CMC solution/glass beads	gas holdup, bed voidage
Zhang et al. (2002)	Air/water/glass bead and hydrophilic biurea and hydrophobic ADC particles	Terminal settling velocity, axial distribution of solid

		holdup.
Safoniuk et al. (2002)	Air/water-aqueous solutions of glycerol/glass beads, dual conductivity probe	Gas holdup
Wang et al. (2003)	Air/water/glass beads Fibre optic probe	Gas holdup, bubble size distribution, bubble rise velocity
Vinod et al. (2004)	Air/water /plastic beads Phase isolation	Gas holdup
Knesebeck and Guardani (2004a, b)	Air/water /porous alumina particles, Wake model	Particle concentration profile, particle velocity
Wen et al.(2005)	Air/water /TiO_2 nanoparticles, laser Doppler anemometer (LDA) and conductivity probes used to measure local hydrodynamics	Axial liquid velocity, gas holdup
Dargar and Macchi (2006)	Air/aqueous solutions of surface active agents/glass beads; Dynamic pressure drop	Gas, liquid and solid holdups
Cao et al. (2007)	Air/water-CMC solution /glass beads and styrene blend spheres, double-sensor micro-electric conductivity probe	Gas, liquid and solid holdups
Jena et al. (2008b)	Air/water /glass beads, phase isolation method	Pressure drop, minimum fluidization velocity bed expansion, gas holdup
Zhou et al. (2009)	Air/water /glass beads and activated carbon, Force balance model	Minimum fluidization velocity, pressure drop
Ramesh et al. (2009)	Nitrogen/electrolyte solution/glass beads Bed pressure drop measurement	Pressure drop, bed porosity, gas and liquid holdup

1.6.1. Status on influence of variables on hydrodynamic characteristics

A qualitative summary concerning operating variables and their effect on the hydrodynamics is shown in Table 1.5. The findings from the experiments of some of the previous work have been discussed briefly in the subsequent subsections. Although bubble rise velocity, U_b, is not included in the table, the consensus is that it is directly related to the bubble diameter, d_b (Kim et al., 1977; Clift et al., 1978; Matsuura and Fan, 1984; Fan, 1989), and, therefore, the qualitative influence of the variables on it is the same as for d_b.

Table 1.5: Summary of qualitative influence of operating variables

	ε_g	β_{er}	ε	d_b	Remarks/cited research
$\uparrow U_g$	↑	↑	↑	↑	As gas flow increases, bubble diameter tends to increase due to greater opportunity to coalesce. ε_g, increases despite this due to the greater gas flow (Wild and Poncin, 1996; Saberian-Broudjenni et al., 1987).
$\uparrow U_L$	↓ slight	↑	↑	Slight ↓	As liquid flow increases, bubbles have less time to coalesce as they pass through the system. Therefore d_b, is reduced. The influence on ε_g, is less well understood. The correlations in Table 1.6 predict both decreases and increases under similar circumstances. But most likely ε_g slightly decreases with increase in U_L.
$\uparrow \rho_p$	Not clear	↓	↓	Not clear	Intuitively one expects little influence of particle density. However as ρ_p, increases, the bed expansion must decrease for given operating conditions as the gravitational forces on a particle increase. Since the bed is more tightly packed, coalescence increases, bubble size increases slightly and ε_g decreases. Wild and Poncin (1996) predict decreases, as do some correlations (Costa et al., 1986), while others (Bloxom et al., 1975; Jean and Fan, 1986) predict increases.

$\uparrow\rho_L$	↓	↑	↑	↓	A decrease in gas hold-up, together with increased bed expansion with increasing liquid density, was reported by several groups (e.g. Bloxom et al., 1975; Wild and Poncin, 1996). It should be noted that Kato et al. (1985) predict an increase in ε_g, with increasing ρ_L.
$\uparrow\rho_g$	-	-	-	-	Saberian-Broudjenni et al. (1987) showed little or no effect of ρ_g. However, several people have indicated significant effects of pressure (Tarmy et al., 1984; Jiang et al., 1992).
$\uparrow\sigma$	↓	-	-	↑	The results show that as the surface tension is lowered with surfactants, measured gas holdups increase as the bubbles become smaller and more rigid, thereby lowering the bubble rise velocity and the tendency to coalesce. As σ increases, the bubbles become larger and hence ε_g decrease. (Kelkar et al., 1983; Fan et al., 1987; Gorowara and Fan, 1990)
$\uparrow\mu_L$	Not clear	↑	↑	Not clear	As liquid viscosity increases, the bed expansion increases due to increased drag. The maximum stable bubble size also increases. This may result in larger bubbles rising faster, and hence lower ε_g (Kim et al., 1977; Han et al., 1990; Bloxom et al., 1975). Higher liquid viscosity exerts higher drag on the gas bubble. A higher drag results in lower bubble rise velocity and hence higher holdup (Fan et al., 1987; Song et al., 1989; Safoniuk et al., 2002)
$\uparrow d_p$	↑	↓	↓	↓	Kim et al. (1975), Dargar and Macchi (2006) and Jena et al. (2008a, 2009b) have reported higher gas holdup and small bubble size for higher size particle due to better bubble disintegration behaviour of the particles, where as Fan et al. (1987) and Kim et al. (1987) have reported a small decrease in gas hold-up with increasing particle size.
Φ_s	No effect	-	-	-	Sinha et al. (1986)
$\uparrow D_c$	↓	-	-	-	Should have no effect for proper scale-up provided that Dc >> d_p and d_b. However, some researchers (e.g. Begovich and Watson, 1978; Hu et al., 1986) have found that the gas hold-up decreases with increasing column diameter.

Although the liquid viscosity in a typical industrial hydrocarbon unit can differ by an order of magnitude from that of water, there has been little work on the effect of viscosity. A few researchers have observed that an increase in viscosity, results in lower gas hold-ups while a few others have reported an increase in gas holdup with liquid viscosity. In contrast, Begovich and Watson (1978) have mentioned that the gas holdup was unaffected by liquid viscosity.

In the present work an attempt has been assumed that no significant local gradients in physical properties exist and that the bulk values are representative of the entire liquid. The values of liquid viscosity varied in the present work ranges from ones.

The successful design and operation of a gas-liquid-solid fluidized bed system depends on the ability to accurately predict the fundamental characteristics of the system, viz. the hydrodynamics, the mixing of individual phases, and the heat and mass transfer characteristics. Among the hydrodynamic characteristics, the most important ones are the minimum liquid fluidization velocity, the bed expansion and the gas holdup. Knowledge of the bed expansion helps in sizing the system and gas holdup helps in improving

performance of the system. Some of the more widely known correlations for gas hold-up and bed porosity relating to bed expansion, together with the authors who presented the work along with the systems studied, are listed in Table 1.6. Accurate prediction of minimum liquid fluidization condition is essential to the successful operation of gas-liquid-solid fluidized beds, especially when particle or liquid properties are involved. Table 1.7 summarizes the previous research on the minimum liquid fluidization velocity in gas-liquid-solid systems.

Table 1.6: Available correlations for gas holdup and bed porosity in gas-liquid-solid fluidized beds

Researcher	Correlations	System (Gas/liquid/solids) or approach
Dakshinamurty et al. (1971)	$\varepsilon = 2.12(U_L/U_t)^{0.41}(\mu_L U_g/\sigma)^{0.08}\ for\ \mathrm{Re}_t < 500$	Air-water/glass beads, iron shot, sand or Rockwool shot; air/kerosene/glass beads, iron shot or Rockwool shot
Dakshinamurty et al. (1972)	$\varepsilon = 2.65(U_L/U_t)^{0.6}(\mu_L U_g/\sigma)^{0.08}\ for\ \mathrm{Re}_t > 500$	Air/water/glass beads and lead shot; nitrogen/ electrolyte/glass beads and Rockwool shot
Bhatia and Epstein (1974)	$\varepsilon = \left[\frac{U_L - U_g k(1-x)}{U_t(1-\varepsilon_g - k\varepsilon_g)}\right]^{1/n}[1-\varepsilon_g(1+k-k\varepsilon_g)]+\varepsilon_g(1+k-k\varepsilon_g)$ $k = \left(0.61+\frac{0.037}{\varepsilon_g+0.013}\right)\varepsilon^3$	Generalized wake model
Darton and Harrison (1975)	$\varepsilon = \left[\frac{U_L - U_g k}{U_t(1-\varepsilon_g - k\varepsilon_g)}\right]^{1/n}[1-\varepsilon_g(1+k)]+\varepsilon_g(1+k)$ $k = 1.4\left(\frac{U_L}{U_g}\right)^{0.33} - 1$	Air/water/sand particles Wake model
Begovich and Watson (1978)	$\varepsilon_g = 0.048\,U_g^{0.720}\,d_p^{0.168}\,D_c^{-0.125}$ $\varepsilon = 1-\varepsilon_s = 0.371\,U_L^{0.271}\,U_g^{0.041}\,(\rho_s-\rho_L)^{-0.316}\,d_p^{-0.268}$ $\mu_L^{0.055}\,D_c^{-0.033}$ (best for ε reported by Han et al., 1990 and Wild and Poncin, 1996)	Air/water/various beads, data from Bhatia and Epstein, 1974; Kim et al., 1975
Catros et al. (1985)	$\varepsilon_g = 0.066\left(\frac{U_L}{U_L+U_g}\right)^{-0.424}\ for\ \frac{U_L}{U_L+U_g} > 0.08$	Air/water /glass beads
Lee and de Lasa (1987)	$\varepsilon = 1-0.631\exp(-0.418U_L - 0.004U_g)$ $\varepsilon_L = 0.006U_L^{0.246}U_g^{-0.059}$	Air/water /glass beads
Fan et al. (1987)	$\varepsilon_g = 1.837Fr_{g,dh}^{0.315}Fr_{L,dh}^{-0.098}Mo^{0.02}C^{0.145}(1+34.09\frac{d_p}{d_h})^{-0.346}$ where C is the term for the number of carbon atoms in the alcohol molecule	Air/water-alcohol solutions/glass beads surfactants added
Saberian-Broudjenni et al. (1987)	$\varepsilon = (14\phi_s)^{-1/3}\left(\frac{U_L}{U_{Lmf}^{LS}}\right)^{0.27}\left[1+0.070\left(\frac{\rho_L U_g d_p}{\mu_L}\right)^{0.34}\right]$ $\varepsilon_g = \varepsilon\frac{U_g - U_{gL}}{U_g+U_L};\ \varepsilon_L = \varepsilon\frac{U_{gL}+U_L}{U_g+U_L};\ U_{gL} = 0.017(\rho_L U_g^2)^{0.45}$	N_2, He, CO_2/water, cyclohexane, gas oil, kerosene, C_2Cl_4/ glass and alumina beads, alumina extrudates

Song et al. (1989)	$\varepsilon = 0.371\ U_L^{0.271}\ U_g^{0.041}\ (\rho_s - \rho_L)^{-0.316}\ d_p^{-0.268}\ \mu_L^{0.055}\ D_c^{-0.033}\ \phi_s^{-0.424}$ for coalesced bubble regime: $\varepsilon_g = 0.342 Fr_g^{0.0373}\ \mathrm{Re}_L^{-0.192}$ for dispersed bubble regime: $\varepsilon_g = 0.280 Fr_g^{0.126}\ \mathrm{Re}_L^{-0.0873}$ for surfactant system: $\varepsilon = 7.62 U_L^{0.204} U_g^{0.130} (\rho_s - \rho_L)^{-0.250} (d_e \phi)^{-0.175} \mu_L^{0.060}$ for dispersed large bubble regime: $\varepsilon_g = 1.81 Fr_g^{0.222}\ \mathrm{Re}_L^{-0.432}\ Mo^{0.020}$ for transition regime: $\varepsilon_g = 0.654 Fr_g^{0.385}\ \mathrm{Re}_L^{0.051}\ Mo^{0.020}$ for dispersed small bubble regime: $\varepsilon_g = 2.61 Fr_g^{0.210}\ \mathrm{Re}_L^{-0.372}\ Mo^{0.020}$	Air/ aqueous t-pentanol solution /cylindrical particles Air/ water /cylindrical particles
Gorowara and Fan (1990)	Low foaming solutions similar to water: $\varepsilon_g = 0.132 Fr_g^{0.2855}\ \mathrm{Re}_L^{-0.0892}$ Medium foaming: $\varepsilon_g = 0.132 Fr_g^{0.3117}\ \mathrm{Re}_L^{0.1166}$ Middle and high gas holdup regions: $\varepsilon_g = 0.8140 Fr_g^{0.3987}\ \mathrm{Re}_L^{-0.0977}$	Air/water-alcohol solutions/glass beads surfactants added
Han et al. (1990)	For initial expansion: $\varepsilon = (U_L / U_t)^{1/n} (1 + 0.123 Fr_g^{0.347} We_m^{0.037}$ For initial contraction: $\varepsilon = \left(\frac{U_L}{U_t}\right)^{1/n} \left[0.359 Fr_g^{0.552} We_m^{0.124} + \exp\left\{ -\left(\frac{U_L}{U_t}\right)^{0.305} Fr_g^{0.5} \right\} \right]$ $\varepsilon_L = (U_L / U_t)^{1/n} (1 - 0.374 Fr_g^{0.176} We_m^{-0.173}$	Air/water or solutions of glycerol/ glass beads combined with over 5000 points from the literature cited by Wild and Poncin (1996) as the best for ε_L and ε
Chen et al. (1995)	Homogeneous bubble flow regime: $\varepsilon_g = 12.0 Ar^{-0.23} Bo^{0.81} Fr_g^{0.51} (\frac{U_L}{U_g})^{-0.19} (1 - \varepsilon_s)^{1.47} (1 + 0.91x)^{1.59}$ Transition regime: $\varepsilon_g = 19.2 Ar^{-0.35} Bo^{0.74} Fr_g^{0.24} (\frac{U_L}{U_g})^{-0.13} (1 - \varepsilon_s)^{1.80} (1 + 0.58x)^{1.60}$ Turbulent bubble flow regime: $\varepsilon_g = 22.9 Ar^{-0.37} Bo^{0.69} Fr_g^{0.14} (\frac{U_L}{U_g})^{-0.11} (1 - \varepsilon_s)^{1.87} (1 + 0.36x)^{1.63}$	Air/water /glass beads
Buffière et al. (1998)	$\varepsilon_g = (8.66 \pm 0.05) d_p^{0.168} U_g^{0.69}$	CO_2/acidic water/Biolite and Pozzolana
Ramesh and Murugesan (2002)	$\varepsilon_g = 0.17 Fr_g^{0.33}\ \mathrm{Re}_L^{-0.065}\ Ar_L^{0.125}\ Mo^{0.05}$ *for* $\mathrm{Re}_L < 100$ $\varepsilon_g = 0.11 Fr_g^{0.35}\ \mathrm{Re}_L^{0.2}\ Ar_L^{0.11}\ Mo^{0.075}$ *for* $\mathrm{Re}_L > 100$	Air/water or solutions of glycerol/ glass beads, raschig rings
Vinod et al. (2004)	$\varepsilon_g = 0.4008 Fr_g^{0.38547}\ \mathrm{Re}_L^{-0.6712}$	Air/water /plastic beads
Ruiz et al. (2004)	$\varepsilon = 3.93 \mu_L^{0.055} U_L^{0.271} U_g^{0.041} (\rho_s - \rho_L)^{-0.316} d_p^{-0.268} D_c^{-0.033} \phi_s^{0.378}$	Air, N_2/water, diesel, jet fuel/cylindrical catalysts
Bakopoulos (2006)	$\varepsilon_g = 0.23 U_g^{0.3} (g \nu_g)^{-0.1}$	CO, CO_2, N_2, H_2/ methanol/ $Cu/ZnO/Al_2O_3$ catalyst
Nacef et al. (2007)	$\varepsilon = \varepsilon_g + \varepsilon_L;\ \varepsilon_g = \varepsilon \frac{U_g - U_{gL}}{U_g + U_L};\quad \varepsilon_L = \varepsilon \frac{U_{gL} + U_L}{U_g + U_L}$ $U_{gL} = 0.2 \mu_L^{0.1} Fr_g^{0.438}$	Nitrogen/water-aqueous solutions of alcohol /glass beads, polypropylene cylinders

Son et al. (2007)	$\varepsilon_g = 0.15 U_L^{-0.047} U_g^{0.303} \varepsilon_s^{-0.05}$	Air/synthetic waste water/polymeric anionic resins
Jena et al. (2008a)	$\varepsilon_g = 5.53 Fr_g^{0.4135} \mathrm{Re}_L^{-0.1808} H_r^{0.0597} d_r^{0.0873}$	Air/water /glass beads

Table 1.7: Summary of correlations on minimum fluidization velocity

Authors	Correlations	Gas/liquid/solids or approach
Ermakova et al. (1970)	$\frac{U_{Lmf}}{U_{Lmf}^{LS}} = 1 - \varepsilon_g 0.5 U_g^{0.075}$	Air/water and glycerine solution/glass bead
Begovich and Watson (1978)	$\frac{U_{Lmf}}{U_{Lmf}^{LS}} = 1 - U_g^{0.436} \mu_L^{0.227} d_p^{0.598} (\rho_s - \rho_L)^{-0.305}$ $\mathrm{Re}_{Lmf} = 5.121 \times 10^{-3} Ar^{0.662} Fr_g^{-0.118}$	Air/water/glass, alumina, aliminosilicate, plexiglass beads
Fortin (1984)	$U_{Lmf} = 0.427 U_g^{-0.198} d_p^{1.539} (\rho_s - \rho_L)^{0.775}$	Nitrogen/cyclohexane/alumina beads and cylinders
Costa et al. (1986)	$U_{Lmf} = 6.969 \times 10^{-4} U_g^{-0.328} (\phi d_p)^{1.086} (\rho_s - \rho_L)^{0.865}$ $D_c^{0.042} \mu_L^{-0.355}$	air, He, CO_2, CH_4/Water & CMC solutions/ various beds
Song et al. (1989)	$\frac{U_{Lmf}}{U_{Lmf}^{LS}} = 1 - 376 U_g^{0.327} (\rho_s - \rho_L)^{-0.423} \mu_L^{0.227} d_p^{0.213}$	Air/ aqueous t-pentanol solution /cylindrical particles
Nacef et al. (1991)	$\frac{U_{Lmf}}{U_{Lmf}^{LS}} = \exp(-13.8 Fr_g^{0.35} (\rho_s - \rho_L)^{-0.38})$	N_2/water-alcohol solution/glass and polypropylene beads
Zhang et al. (1995)	$\mathrm{Re}_{Lmf} = -42.86(1 - \varepsilon_{Lmf})\phi_s^{-1} + [1837 (1 - \varepsilon_{Lmf})^2 \phi_s^{-2}$ $+ 0.5715 \phi_s \varepsilon_{Lmf}^3 (1 - \varepsilon_{gmf})^3 Ar]^{0.5}$ where $\varepsilon_{gmf} = 0.16 / \varepsilon_{mf} [U_g / (U_g + U_L)]$	Air/water/glass and plastic beads
Zhang et al. (1998)	$\mathrm{Re}_{Lmf} = \sqrt{33.7^2 + 0.0406 Ar (1 - \varepsilon_{gmf})} - 33.7$ $\varepsilon_{gmf} = 0.16 / \varepsilon_{mf} [U_g / (U_g + U_{Lmf})$	Air/water/glass beads and steel shots
Larachi et al. (2000)	neural network $U_{Lmf} = f(U_g; U_L; \phi; d_p; \rho_s - \rho_L; \sigma_L; d_p / D_c$	Wide range of literature data
Lee et al. (2001b)	$\mathrm{Re}_{Lmf} = \sqrt{\left(51.4 \frac{(1 - \varepsilon_{mf})}{\phi_s}\right)^{2^2} + 0.0571 \phi_s \varepsilon_{mf}^3 Ar (1 - \varepsilon_{gmf})^3}$ $- 51.4 \frac{(1 - \varepsilon_{mf})}{\phi_s}$; $\varepsilon_{gmf} = 0.16 / \varepsilon_{mf} [U_g / (U_g + U_{Lmf})$	Literature data. Comparison of different liquid-buoyed-gas perturbed liquid models (LB-GPLM) and mixture-buoyed-gas perturbed liquid models (MB-GPLM)
Ramesh and Murugesan (2002)	$\mathrm{Re}_{Lmf} = 0.6[1 + Fr_g]^{-1.85} Ar^{0.30} Mo^{-0.09} \phi_s^{0.04}$	Air/water or solutions of glycerol/ glass beads, raschig rings
Ruiz et al. (2004)	$\frac{U_{Lmf}}{U_{Lmf}^{LS}} = (1 - 0.5 U_g^{0.075} - \varepsilon_{mf} \beta_{gmf}) \phi_s^{-0.93}$ where $\beta_{gmf} = 0.16 / \varepsilon_{mf} [U_g / (U_g + U_L)]$	Air, N_2/water, diesel, jet fuel /cylindrical catalysts of nickel and molybdenum oxide on porous alumina support

1.7. Recent research on three-phase fluidised bed reactors

1.7. 1. Flow structure quantification

The quantification of flow structure in three-phase fluidised beds mainly focuses on local and globally averaged phase hold-ups and phase velocity for different operating conditions and parameters. In literature, Rigby et al. (1970), Muroyama and Fan (1985),

Lee and de Lasa (1987), Yu and Kim (1988) investigated bubble phase holdup and velocity in three-phase fluidised beds for various operating conditions using experimental techniques like electroresistivity probe and optical fibre probe. Larachi et al. (1996), Kiared et al. (1999) investigated the solid phase hydrodynamics in three-phase fluidised bed using radio active particle tracking. Recently Warsito and Fan (2001, 2003) quantified the solid and gas holdups in three-phase fluidised bed using the electron capacitance tomography (ECT).

1.7.2. Flow regime identification

Muroyama and Fan (1985) developed the flow regime diagram for air–water–particle fluidised bed for a range of gas and liquid superficial velocities. Chen et al. (1995) investigated the identification of flow regimes by using pressure fluctuation measurements. Briens and Ellis (2005) used spectral analysis of the pressure fluctuation for identifying the flow regime transition from dispersed to coalesced bubbling flow regime based on various data mining methods like fractal and chaos analysis, discrete wake decomposition method etc. Fraguío et al. (2006) used solid phase tracer experiments for flow regime identification in three-phase fluidized beds.

1.7.3. Advanced modelling approaches

Even though a large number of experimental studies have been directed towards the quantification of flow structure and flow regime identification for different process parameters and physical properties, the complex hydrodynamics of these reactors are not well understood due to complicated phenomena such as particle–particle, liquid–particle and particle–bubble interactions. For this reason, computational fluid dynamics (CFD) has been promoted as a useful tool for understanding multiphase reactors (Dudukovic et al., 1999) for precise design and scale up. As regards to mathematical modeling, CFD simulations give very detailed information about the local values of pressure, components of mean velocity, viscous and turbulent stresses, turbulent kinetic energy, viscous and turbulent energy dissipation rates, etc. Such information can be useful in the understanding of the transport phenomena in the complex geometry like fixed beds. Basically two approaches are used namely, the Euler–Euler formulation based on the interpenetrating multi-fluid model, and the Euler–Lagrangian approach based on solving the Newton's equation of motion for the dispersed phase.

Recently, several CFD models based on Eulerian multi-fluid approach have been developed for gas–liquid flows (Cheung et al., 2007; Kulkarni et al., 2007) and liquid–solid flows (Roy and Dudukovic, 2001; Panneerselvam et al.,2007) and gas–solid flows

(Jiradilok et al., 2007). Some of the authors (Matonis et al., 2002; Feng et al., 2005; Schallenberg et al., 2005) have extended these models to three-phase flow systems. Comprehensive list of literature on modeling of these reactors are tabulated in Table 1.8. Most of these CFD studies are based on steady state, 2-D axisymmetric, Eulerian multi-fluid approach. But in general, three phase flows in fluidised bed reactors are intrinsically unsteady and are composed of several flow processes occurring at different time and length scales. The unsteady fluid dynamics often govern the mixing and transport processes and is inter-related in a complex way with the design and the operating parameters like reactor and sparger configuration, gas flow rate and solid loading.

Table 1.8: Summary of investigations on CFD modeling of three-phase reactors

Researcher	Multiphase approach	Models used	Parameters studied
Bahary et al. (1994)	Multi fluid Eulerian approach for three-phase fluidized bed	Gas phase was treated as a particulate phase having 4mm diameter and a kinetic theory granular flow model applied for solid phase. They have simulated both symmetric and axis-symmetric mode.	Verified the different flow regimes in the fluidized bed and compared the time averaged axial solid velocity with experimental data
Grevskott et al. (1996)	Two fluid Eulerian–Eulerian model for three-phase bubble column	The liquid phase along with the particles is considered pseudo homogeneous by modifying the viscosity and density. They included the bubble size distribution based on the bubble induced turbulent length scale and the local turbulent kinetic energy level.	Studied the variation of bubble size distribution, liquid circulation and solid movement
Mitra-Majumdar et al. (1997)	2-D axis-symmetric, multi-fluid Eulerian approach for three-phase bubble column	Used modified drag correlation between the liquid and the gas phase to account for the effect of solid particles and between the solid of gas bubbles. A k-ε turbulence model was used for the turbulence and considered the effect of bubbles on liquid phase turbulence	Examined axial variation of gas holdup and solid hold up profiles for various range of liquid and gas superficial velocities and solid circulation velocity
Jianping and Shonglin (1998)	2-D, Eulerian–Eulerian method for three-phase bubble column	Pseudo-two-phase fluid dynamic model. k_{sus}-ε_{sus}– k_b-ε_b turbulence model used for turbulence	Validated local axial liquid velocity and local gas holdup with experimental data
Li et al. (1999)	2-D, Eulerian–Lagrangian model for three-phase fluidization	The Eulerian fluid dynamic (CFD) method, the dispersed particle method (DPM) and the volume-of-fluid (VOF) method are used to account for the flow of liquid, solid, and gas phases, respectively. A continuum surface force (CSF) model, a surface tension force model and Newton's third law are applied to account for the interphase couplings of gas–liquid, particle–bubble and particle–liquid interactions, respectively. A close distance interaction (CDI) model is included in the particle–particle collision analysis, which considers the liquid interstitial effects between colliding particles	Investigated single bubble rising velocity in a liquid–solid fluidized bed and the bubble wake structure and bubble rise velocity in liquid and liquid–solid medium are simulated

Padial et al. (2000)	3-D, multi-fluid Eulerian approach for three-phase draft- tube bubble column	The drag force between solid particles and gas bubbles was modeled in the same way as that of drag force between liquid and gas bubbles	Simulated gas volume fraction and liquid circulation in draft tube bubble column
Matonis et al. (2002)	3-D, multi-fluid Eulerian approach for slurry bubble column	Kinetic theory granular flow (KTGF) model for describing the particulate phase and a k-ε based turbulence model for liquid phase turbulence	Studied the time averaged solid velocity and volume fraction profiles, normal and shear Reynolds stress and comparison with experimental data
Chen and Fan (2004)	2-D, Eulerian–Lagrangian model for three-phase Fluidization	Level-set method for interface tracking and Sub-Grid Scale (SGS) stress model are used for bubble-induced turbulence.	Studied the bubble rise velocity, bubble shapes and their fluctuations, and bubble formation. Discussed the effect of particle concentration on these phenomena.
Feng et al.(2005)	3-D, multi-fluid Eulerian approach for three-phase bubble column	The liquid phase along with the solid phase considered as a pseudo homogeneous phase in view of the ultrafine nanoparticles. The interface force model of drag, lift and virtual mass and k-ε model for turbulence are included	Compared the local time averaged liquid velocity and gas holdup profiles along the radial position
Schallenbe-rg etal. (2005)	3-D, multi-fluid Eulerian approach for three-phase bubble column	Gas–liquid drag coefficient based on single bubble rise, which is modified for the effect of solid phase. Extended k-ε turbulence model to account for bubble-induced turbulence. The interphase momentum between two dispersed phases is included.	Validated local gas and solid holdups as well as liquid velocity with experimental data
Zhang and Ahmadi (2005)	2-D, Eulerian – Lagrangian model for three-phase slurry reactor	The interactions between bubble–liquid and particle–liquid are included. The drag, lift, buoyancy, and virtual mass forces are also included. Particle–particle and bubble–bubble interactions are accounted for by the hard sphere model approach. Bubble coalescence is also included in the model	Studied transient characteristics of gas, liquid, and particle phase flows in terms of flow structure and instantaneous velocity. The effect of bubble size on variation of flow patterns is also studied
Cao et al. (2009)	2-D, Eulerian–Eulerian–Lagrangian (E/E/L) model for gas-liquid-solid circulating fluidized bed	E/E/L model combined with Two Fluid Model (TFM) and Distinct Element Method (DEM). Based on generalized gas–liquid two fluids k-ε model, the modified gas–liquid TFM is established.	Studied the local liquid velocity and radial distribution of local phase hold-ups
Panneersel-vam et al. (2009)	3D, Eulerian multi fluid approach for gas-liquid-solid fluidized bed	Kinetic theory granular flow (KTGF) model for describing the particulate phase and a k-ε based turbulence model for liquid phase turbulence. The interphase momentum between two dispersed phases is included. Various energy flows are also computed.	Radial distribution of axial and radial solid velocities, axial and radial solid turbulent velocities, shear stress, axial bubble velocity, axial liquid velocity and averaged gas holdup
O'Rourke et al. (2009)	3D, Eulerian finite difference approach for gas-liquid-solid fluidized bed	The mathematical model using multiphase particle-in-cell (MP-PIC) method is used for calculating particle dynamics (collisional exchange) in the computational-particle fluid dynamics (CPFD).	Mass averaged velocity of solid and liquid and particle velocity fluctuation, collision time, liquid droplet distribution

1.8. Semi-fluidization

Semi-fluidization is a type of fluid-solid contacting technique which has been reported in the sixties only. Like the packed and the fluidized bed techniques, this is also a two-phase or three-phase phenomenon. A semi-fluidized bed is a compromise between the packed and the fluidized bed conditions and can be achieved in a conventional fluidizer by incorporating certain modifications in the column construction.

A semi-fluidized bed can be viewed as the combination of a batch fluidized bed at the bottom and a fixed bed at the top within a single vessel. Such a bed can be formed by providing sufficient space for the free expansion of a fluidized bed and then arresting the escape of particles by means of a top restraint. The degree of semi-fluidization occurring in the bed can range from minimum semi-fluidization (the first particle of the expanded fluidized bed just touches the top restraint of the semi-fluidizer) to maximum semi-fluidization (when all the solid particles of the bed are attached to the top restraint) by varying the fluid velocity or by altering the position of the upper constraining plate. A semi-fluidized bed has the advantages of both the packed and the fluidized beds.

As described in section 1.1.1, the fluidized bed technique has specific advantages over the packed bed like; uniform contact of the fluid with all the particle surfaces, prevents segregation of solids because of the turbulence, minimizes the temperature variation i.e., local hot spots are avoided, and has a lesser pressure drop than the fixed bed. The fluidized bed also suffers from certain inherent defects like; loss of driving potential for transfer processes within the bed because of the intense back-mixing, attrition and elutriation of solid particles which necessitate costly dust recovery system, non-availability of necessary free space above the bed, and erosion of the containing vessel.

As a result, a wholesome substitution of a fixed bed method by a fluidized one can not been recommended for a smooth and efficient process application in many cases. To overcome some such problems of the fluidized bed, a semi-fluidized bed can be used. By choosing suitable parameters like restraint position, fluid velocity etc., it is possible to have both the packed and fluidization conditions in the same set-up. Further semi-fluidization offers greater flexibility of operation and eliminates partially the disadvantages of fluidized beds, namely back-mixing of solids, attrition of particles and erosion of surfaces, and those of packed beds, such as non-uniform bed temperatures, segregation of solids and channelling.

Since semi-fluidized beds comprise the features of both the packed and the fluidized beds these may be employed to serve as a unique combination of back-mix and tubular-

flow reactors in series, whose relative lengths can be varied simply by adjusting the overall concentration of solids, to yield the most optimum driving potentials for momentum, heat and mass transfer without disturbing the other operating variables. Semi-fluidization technique has immense applications in various fields of Chemical Engineering processes and a few of them have been listed in table 1.9. As the semi-fluidized bed behaviour is not elaborately studied till date, the application is found to be limited.

Table 1.9: Applications of semi-fluidized beds

Applications	Process type	References
Physical processes		
Filtration of fine particles from liquid or gases	physical	Wen and Fan (1979)
Adsorption of trace organics	physical	Mathews and Fan (1983)
Filtration of fines-hydrocarbon suspensions	physical	Dehkissia et al. (2008)
Chemical processes		
Extraction	chemical	Weiss and Swinton (1958)
Reduction of iron ore	chemical	Agaletskii and Ruban (1959)
Mass transfer	chemical	Fan et al. (1959, 1960)
Continuous coking	chemical	Shcherbakov et el. (1963)
Ion exchange	chemical	Hwang and Lu (1995)
Removal of lead and nickel ions using strong cation exchange resin	chemical	Kim et al. (1998)
Boiler furnace	chemical	Is'emin et al. (1995, 2001)
Removal of Cyanide and Copper Ions	chemical	Kim et al. (1999, 2001)
Removal of Cyanide complexes of Cu, Cd, Zn	chemical	Kim et al. (2002)
Mercury sorption by activated carbon	chemical	Ho et al. (2002)
Mercury emission control from combustion flue gas	chemical	Ho et al. (2005)
Separation of phenoxyacetic acids	chemical	Kim et al. (2006)
Pyrolysis of coal particles	chemical	Liu et al. (2008)
Biochemical processes		
Phenol biodegradation	biochemical	Fan (1983)
Extractive fermentation of ethanol	biochemical	Dias (1991)
Structured granule tablets formation	biochemical	Roshchin (1992)
Pediatric medicinal preparation containing an extract of the milk-white iris (*IRIS LACTEA*)	biochemical	Minina et al. (2008)

The present study aims at understanding the hydrodynamic behaviour of liquid-solid and co-current gas-liquid-solid semi-fluidization with liquid as the continuous phase which are extensively used for operations like; ion exchange operations, separation of hazardous materials from waste water and recently as bioreactor for anaerobic and aerobic applications.

1.8.1. Semi-fluidized bed bioreactor a novel system for waste water treatment

Fluidized bed bio-reactors had been successfully applied in the treatment of several kinds of wastewater such as ammonia-nitrogen containing wastewater, photographic processing wastewater, phenolic waste water, coke oven wastewater, and other domestic and industrial wastes (Meikap and Roy, 1995; Onysko et al. 2002; Vinod and Reddy, 2003; Sokol and Korpal, 2004; Jena et al., 2005). These reactors have also been

successfully used for the reductive biotransformation of mercuric ions to elemental mercury present in the effluents from industrial amalgam process, combustors and power stations (Deckwer et al., 2004).

A fluidized bed bioreactor (FBB) is capable of achieving treatment in low retention time because of the high biomass concentration. FBB offers distinct mechanical advantages, which allow small and high surface area media to be used for biomass growth (Sokol, 2003). A practical problem, which occurs in the operation of an FBB, is the excessive growth of biomass on support media. This can lead to the channeling of bioparticles in fluidized beds since biomass loading can increase to such extent that the bioparticles begin to be carried over from a bioreactor. The problem of over expansion of fluidized bed due to biomass growth has generally been solved by the removal of heavily biomass-laden particles from bioreactor, followed by the addition of biomass-free particles. However this solution complicates operation of a bioreactor and introduces the need for additional equipment external to the bioreactor, such as a vibrating screen or an incinerator (Sokol and Halfani, 1999; Sokol and Korpal, 2004).

The nutrients for microbial growth are transported first from bulk phase to the surface of the biofilm, and then transported to the inner regions of the biofilm via diffusion. The limiting mass transport rate controls the performance of the biofilm reactor (Beyenal and Tanyolac, 1998; Sokol, 2001). The external resistance can be neglected in the case of a high fluidization flow rate (Beyenal and Tanyolac, 1998). In a three-phase fluidized bed bioreactor it is found that the reaction rate follows first order kinetics with respect to oxygen and zero-order one with respect to phenol (Hirata et al., 2000a). For chemical and bio-chemical processes, where mass transfer is the rate-limiting step, it is important to know the gas hold-up as this is related directly to mass transfer (Hirata et al., 2000b; Vinod et al., 2004). The gas hold up at high pressures is always larger than that at low pressures, regardless of the liquid velocity and particle size in three-phase fluidization (Luo et al. 1997).

In a semi-fluidized bed higher velocity of fluid is possible which will lessen the external mass transfer resistance. As a top packed bed is formed in such a bioreactor, the reactor pressure drop is high that means it is operated under high-pressure condition. Hence the gas hold-up in the fluidizing section of the column will be more thus enhancing the mass transfer rate. If the semi fluidized bed can be used as a bioreactor, it will overcome the disadvantages of fluidized bed, namely back mixing, attrition and erosion of immobilized solids, reduction of concentration of culture by elutriation, instability due to fluctuation

in flow rate of waste water, particles agglomeration and also overcomes the drawbacks of packed bed such as particle segregation, non-uniformity in temperature and channeling. As the top restraining plate is adjustable slugging by bacterial growth can be prevented. Improved mass transfer in semi-fluidized bed at the cost of higher pressure drop is compensated by lower operation cost through efficient use of oxygen. The top packed bed portion complements to the fluidized bed portion by acting as a polishing section, so that the level of contaminants is low compared to fluidized bed bioreactor (Jena et al., 2005).

Viewing these advantages of the semi-fluidized bed system as an aerobic bioreactor, it is necessary to understand the hydrodynamic behaviour of the system for better design and operation of the system.

1.9. Hydrodynamic studies on semi-fluidization

Literature survey reveals that studies relating to the hydrodynamics of semi-fluidization are limited and not much detail is available in the literature for liquid-solid and gas-liquid-solid semi-fluidized bed reactor. The studies related to hydrodynamics are normally subdivided into following categories:

- Prediction of the values of minimum and the maximum semi-fluidization velocity.
- Prediction of the top packed bed formation.
- Total pressure drop in a semi-fluidized bed.
- Gas holdup in a gas-liquid-solid semi-fluidized bed.
- Miscellaneous hydrodynamic studies.

A few of the information on hydrodynamics studies available in the literature based on experiments are listed in Table 1.10. This table also contains brief information on the systems studied.

The successful design and operation of a gas-liquid-solid fluidized bed system depends on the accurate prediction of the fundamental characteristics of the system, viz. the hydrodynamics. Among the hydrodynamic characteristics, the most important ones are the minimum and maximum semi-fluidization velocity between which the semi-fluidized bed exists, the height of the top packed bed, semi-fluidized bed pressure drop and the gas holdup. Some of the more widely known correlations and models for the prediction of minimum and the maximum semi-fluidization velocity, the height of packed bed and pressure drop in liquid-solid semi-fluidized bed are listed in Table 1.11. The available

information on hydrodynamics of co-current gas-liquid-solid semi-fluidization is meagre and has been discussed in the following section 1.9.1.

Table 1.10: Hydrodynamic studies on two and three phase semi-fluidization

Researcher	System (Gas/liquid/solids) , technique and approach	Parameter studied
Fan and Wen (1961)	Water/ glass bead	Minimum and maximum semi-fluidization velocities, pressure drop, packed bed height
Kurian and Raja Rao (1970)	Water/ glass bead, polystyrene, silica sand, crushed raschig rings	Minimum and maximum semi-fluidization velocities, pressure drop
Roy and Sarma (1972)	Water/various spherical and non-spherical particles	Minimum semi-fluidization velocity
Roy and Sarma (1973)	Water/various spherical and non-spherical particles	Packed bed height
Roy and Sarma (1974)	Water/various non-spherical particles	Maximum semi-fluidization velocity
Roy and Sharat Chandra (1976)	Water/binary mixtures of dolomite, barite, chromite iron ore	Minimum and maximum semi-fluidization velocity
Roy and Sarma (1978)	Water/various spherical and non-spherical particles	Pressure drop
Singh et al. (1980)	Water/magnetite, chalcopyrite, magnesite, limestone, graphite, electrode-carbon	Packed bed height
Chern et al. (1983)	Air/water/polyethylene, polypropylene beads Countercurrent flow of gas and liquid with liquid as the continuous phase Mathematical model	Onset velocity of semi-fluidization, pressure drop, gas and liquid holdup, height of packed section.
Chern et al. (1984)	Air/water/glass beads, PVC cylinders Mathematical model	Onset velocity of semi-fluidization, pressure drop, gas holdup, height of top packed bed.
Beaver and Fan (1984)	Air/water/five different solid particles	Packed bed height, solid holdup
Mydlarz (1987)	Water/agalit	Packed bed height
Ho et al. (1987)	Air/-/glass bead, sand coal, polyethylene	Minimum semi-fluidization velocity, pressure drop, top packed bed formation
Murthy et al. (1990)	Water/ glass bead, crushed calcite particles Electrolytic tracer technique.	Residence time distribution
Hwang and Chiou (1990)	Air/water/glass beads, PVC cylinders Electrolytic tracer technique	Axial dispersion of liquid, packed bed height
Singh et al. (2005)	Air/water/ irregular shape solid particles	Bed pressure drop

Table 1.11: Summary of correlations and models on minimum and maximum semi-fluidization velocity, the top packed bed height and the bed pressure drop

Authors	Correlations /models	Liquid/solids
Minimum semi-fluidization velocity		
Kurian and Raja Rao (1970)	$\frac{U_{osf}-U_{mf}}{U_t-U_{mf}}=0.61\left(\frac{R}{R-1}\right)^{-1.2}$	Water/ glass bead, polystyrene, silica sand, crushed raschig rings
Roy and Sarma (1972)	$\frac{U_{osf}}{U_{mf}}=1.625\left(\frac{D_c}{d_p}\right)^{0.266}\left(\frac{\rho_s}{\rho_f}\right)^{-0.228}(R)^{0.585}$ (for non-spherical particles) $\frac{U_{osf}}{U_{mf}}=1.875\left(\frac{D_c}{d_p}\right)^{0.266}\left(\frac{\rho_s}{\rho_f}\right)^{-0.228}(R)^{0.585}$ (for spherical particles)	Water/various spherical and non-spherical particles

Roy and Sharat Chandra (1976)	$\frac{U_{osf}}{U_{msf}} = 0.473\left(\frac{D_c}{d_p}\right)^{-0.20}\left(\frac{\rho_s}{\rho_f}\right)^{0.17}(R)^{0.38}$	Water/binary mixtures of dolomite, barite, chromite iron ore
Maximum semi-fluidization velocity		
Poddar and Dutta (1969)	$18\,\mathrm{Re}_{msf} + 2.7\,\mathrm{Re}_{msf}^{1.687} = Ga$	Water/spherical and non-spherical particles
Roy and Sarma (1974)	$\frac{U_{msf}}{U_{mf}} = 5.71\left(\frac{D_c}{d_p}\right)^{0.42}\left(\frac{\rho_s}{\rho_f}\right)^{0.67}$	Water/various non-spherical particles
Roy (1975)	$U_{msf} = 1.85\times10^{4} d_p^{0.65}(\rho_s - \rho_f)^{0.55}\rho_f^{-0.45}\mu_f^{-0.1}$	Water/various spherical and non-spherical particles
Height of the top packed bed		
Kurian and Raja Rao (1970)	$\frac{U_s - U_{mf}}{U_t - U_{mf}} = 0.61\left(\frac{H_{sf} - H_{pa}}{H_{sf} - H_s}\right)^{-1.2}$	Water/ glass bead, polystyrene, silica sand, crushed raschig rings
Roy and Sarma (1973)	$\frac{H_{pa}}{H_s} = 1.09\left(\frac{U_{sf}}{U_{msf}}\right)^{1.51}\left(\frac{D_c}{d_p}\right)^{0.23}\left(\frac{\rho_s}{\rho_f}\right)^{0.17}\left(\frac{H_s}{D_c}\right)^{-0.15}(R)^{-0.86}$ (for non-spherical particles) $\frac{H_{pa}}{H_s} = 2.21\left(\frac{U_{sf}}{U_{msf}}\right)^{2.08}\left(\frac{D_c}{d_p}\right)^{0.23}\left(\frac{\rho_s}{\rho_f}\right)^{0.17}\left(\frac{H_s}{D_c}\right)^{-0.15}(R)^{-0.88}$ (for spherical particles)	water/various spherical and non-spherical particles
Singh et al. (1980)	$\frac{H_{sf} - H_s}{H_{sf} - H_{pa}} = 0.974 + 0.324\ln\left(\frac{U_s - U_{mf}}{U_t - U_{mf}}\right)$	Water/magnetite, chalcopyrite, magnesite, limestone, graphite, electrode-carbon
Mydlarz (1987)	$\frac{U_s - U_{mf}}{U_t - U_{mf}} = \left(\frac{H_{sf} - H_{pa}}{H_{sf} - H_s}\right)^{-3.15}$ (for $1.0 < (H_{sf}-H_{pa})/(H_{sf}-H_s) < 1.3$)	Water/agalit
Semi-fluidized bed pressure drop		
Fan and Wen (1961)	$\Delta P_{sf} = \left[H_f - \frac{(1-\varepsilon_{pa})(H_f - H_{sf})}{(\varepsilon - \varepsilon_{pa})}\right](1-\varepsilon)(\rho_s - \rho_L)$	Water/ glass bead
Kurian and Raja Rao (1970)	$+\left[150\frac{(1-\varepsilon_{pa})^2}{(\varepsilon_{pa})^3}\frac{\mu_l U_l}{(\varphi_s d_p)^2} + 1.75\frac{1-\varepsilon_{pa}}{(\varepsilon_{pa})^3}\frac{\rho_L U_L^2}{\varphi_s d_p}\right] \times\frac{(1-\varepsilon)(H_f - H_{sf})}{(\varepsilon - \varepsilon_{pa})}$	Water/ glass bead, polystyrene, silica sand, crushed raschig rings
Roy and Sarma (1978)	$\frac{\Delta P_{sf}}{\Delta P_{osf}} = 19.5\left(\frac{D_c}{d_p}\right)^{-0.17}\left(\frac{\rho_s}{\rho_f}\right)^{0.48}\left(\frac{H_{Pa}}{Hs}\right)^{0.89}(R)^{0.28}$	Water/various spherical and non-spherical particles

1.9.1. Existing information on co-current gas-liquid-solid semi-fluidization

As discussed earlier the hydrodynamic study on gas-liquid-solid fluidization is rare. Chern et al. (1984) have studied the hydrodynamic behaviour of a co-current gas-liquid-solid fluidization with liquid as the continuous phase. They have conducted separate investigation on a packed bed and a fluidized bed under gas-liquid flow conditions similar to that for the semi-fluidized bed. They have, however not performed the true experiment in a semi-fluidized bed. Separate model equations have been proposed by them for describing the packed bed behaviour and the fluidized behaviour. They have

combined the model equations of the packed bed and the fluidized bed to predict the behaviour of a semi-fluidized bed. The model equations have been found to describe satisfactorily the hydrodynamic behaviour of a semi-fluidized bed and found to agree well with results obtained from their experiment. Singh et al. (2005) have developed an empirical equation for the pressure drop but no fundamental aspect has been studied by them.

The hydrodynamic parameters studied by Chern et al. (1984) includes; pressure drop, gas holdup, onset liquid velocity of semi-fluidization or the minimum liquid semi-fluidization velocity and height of the top packed bed. The effects of variables studied are gas velocity, liquid velocity, particle size, shape and density. The minimum liquid semi-fluidization velocity (U_{Losf}) is defined as the liquid velocity at which a particle of the bed touches the upper retaining grid at a fixed value of gas velocity. The transition from fluidization to semi-fluidization is evident from a sharp increase of the pressure drop in the bed. U_{Losf} can also be predicted from the extrapolation of the bed expansion relationship for the fluidized bed. Semi-fluidization would occur when bed expands to such an extent that the holdup of solid in the fluidized bed (ε_s) equals the solid holdup at the onset of semi-fluidization ($(\varepsilon_s)_{osf}$) which is defined as;

$$(\varepsilon_s)_{osf} = \frac{M_s}{\rho_s A_c H_{sf}} \tag{1.1}$$

According to Chern et al. (1984), (ε_s=1-ε) in the fluidized bed can be calculated from the generalized k-x wake model of El-Temtamy and Epstein (1978). For particles of size more than 1 mm, the particles would not be held in the wake region. Thus x can be set as zero (El-Temtamy and Epstein, 1978). With x = 0, the wake model is given by;

$$\varepsilon = \varepsilon_g + \varepsilon_L = \left[\frac{U_L - U_g k}{U_t(1-\varepsilon_g - k\varepsilon_g)}\right]^{1/n}\left[1-\varepsilon_g(1+k)\right]+\varepsilon_g(1+k) \tag{1.2}$$

In the above equation, U_t is the extrapolated superficial liquid velocity in the liquid-solid fluidized bed as the bed voidage approaches to unity or the particle terminal velocity, k is the ratio of the wake region to that of the bubble region and n is the Richardson-Zaki index. Chern et al. (1984) empirically expressed k as;

$$k = 0.398 U_L^{0.246} U_g^{-0.646} \tag{1.3}$$

From the material balance Chern et al. (1984) developed a model for the height of the packed bed section in a semi-fluidized bed expressed as;

$$H_{pa} = \frac{M_s/(\rho_s A_c) - H_{sf}\varepsilon_s}{\varepsilon_{s,p} - \varepsilon_s} \tag{1.4}$$

In using the above equation for calculation of height of the top packed bed, the solids holdup in the fluidized section has been approximated by the solids holdup in the fully fluidized bed as obtained from Eq. (1.2).

For the prediction of pressure drop in the semi-fluidized bed (ΔP_{sf}), Chern et al. (1984) have proposed the following model (Eq. (1.5)), which is the combination of fluidized bed pressure drop (ΔP_f) and the packed bed pressure drop (ΔP_{pa}).

$$\Delta P_{sf} = \Delta P_f + \Delta P_{pa} \tag{1.5}$$

$$\Delta P_f = (\rho_g \varepsilon_g + \rho_L \varepsilon_L + \rho_s \varepsilon_s) Hg \tag{1.6}$$

$$\varepsilon_s = 1 - \varepsilon = \frac{M_s}{\rho_s A_c H} \tag{1.7}$$

$$\varepsilon_g + \varepsilon_L + \varepsilon_s = 1 \tag{1.8}$$

$$\Delta P_{pa} = \theta_L \Delta P_f^{Ls} + (\theta_L \rho_L + \theta_g \rho_g) H_{pa} g \tag{1.9}$$

$$\theta_L = \frac{\varepsilon_{L,p}}{1 - \varepsilon_{s,p}} \tag{1.10}$$

$$\theta_g = \frac{\varepsilon_{g,p}}{1 - \varepsilon_{s,p}} \tag{1.11}$$

$$\theta_L + \theta_g = 1 \tag{1.12}$$

ΔP_f^{Ls} is the frictional pressure drop between the liquid and the solid and can be expressed by Fanning's equation as;

$$\Delta P_f^{Ls} = 4f\left(\frac{1}{D_e}\right)\left[\frac{1}{2}\rho_L\left(\frac{U_L}{\varepsilon_{L,p}}\right)^2\right] H_{pa} \tag{1.13}$$

where, f is the modified friction factor and D_e is the effective diameter of the channel for liquid flow. D_e has been expressed by;

$$D_e = \frac{2(1-\varepsilon_{s,p})}{\varepsilon_{s,p}}\left[1 - \sqrt{\theta_g}\right]\phi_s d_p \tag{1.14}$$

where, ϕ_s is the sphericity of the particle and d_p is the equivalent particle diameter.

The modified friction factor (f) relates to the liquid Reynolds number and has been empirically correlated by Chern et al. (1984) as;

$$f = 0.1075 + 6.359\,\mathrm{Re}^{-0.368} \tag{1.15}$$

Here, the liquid Reynolds number is defined as;

$$\mathrm{Re} = \frac{D_e \rho_L U_L}{\mu_L \varepsilon_{L,p}} \tag{1.16}$$

The gas holdup (θ_g) in the packed bed based on gas and liquid phases, has been correlated with liquid and gas velocity as given by;

$$\theta_g = 0.0296 U_L^{-0.35} U_g^{0.977} \tag{1.17}$$

For the prediction of average gas holdup in the semi-fluidized bed the following model has been proposed by Chern et al. (1984).

$$\varepsilon_{g,sf} = \left(\frac{H_{pa}}{H_{sf}}\right)\varepsilon_{g,p} + \left(1 - \frac{H_{pa}}{H_{sf}}\right)\varepsilon_g \tag{1.18}$$

The gas holdup in the packed bed $\varepsilon_{g,p}$ can be calculated from Eq. (1.17). For the gas holdup calculation in the fluidized section in the dispersed bubble flow regime, Chern et al. (1984) have used the following equations in combination.

$$\frac{U_g}{\varepsilon_g} = \frac{U_g}{1-\varepsilon_s} + \frac{U_L}{1-\varepsilon_s} + U_o \tag{1.19}$$

U_o the velocity due to buoyancy is given by;

$$U_o = 10.16 + 14.88\sqrt{\frac{U_g}{1-\varepsilon_s}} \tag{1.20}$$

1.10. Scope and objective of the present investigation

Critical appraisal of the status of research on the hydrodynamics of fluidized bed reactors shows that majority of the cases reported the hydrodynamics of three phase fluidization with spherical and non-spherical isotropic particles. However, exhaustive studies on the hydrodynamics of irregular shape particles, hollow cylindrical particles possessing higher surface to volume ratio and wide range of operating variables in single system have not been carried out so far. Therefore, in this work an attempt has been made to investigate the hydrodynamics of both regular and irregular particles within a co-current upflowing gas-liquid-solid fluidized bed. The major motive is to gain a better understanding of the bed behaviour for miscellaneous industrial applications varying from the production of synthetic crude oil from bitumen to aerobic bioreactor and to explore an approach for using a small-scale cold-flow experimental unit to predict the behaviour under industrial conditions. For a given reactor volume and fluid flow rates, a cloud of small, spherical, slow-moving bubbles will have a greater opportunity to allow mass transfer than a few large, quick-moving slugs. A better understanding of the hydrodynamics would also be helpful in understanding the axial and the lateral dispersion, factors which are also important in multiphase reactors.

Further in the present work a novel approach to prevent scale-up surprises and to make experimental results from a small laboratory unit more pertinent to industrially relevant reactors has been used. In particular, the approach focuses on ensuring effective scaling of bed hydrodynamics. Since bed hydrodynamics control the degree of fluids-solid contact, a good understanding of the hydrodynamics is essential to eliminate significant scale-up defects. Safoniuk et al. (1999) were the first to use, dimensional similitude and the Buckingham Pi Theorem to form a set of parameters for achieving dynamic similarity. This approach is especially important for systems which are mass-transfer controlled and hence controlled by the bed hydrodynamics. In this work the dimensional analysis using Buckingham Pi Theorem has also been used to derive dimensionless groups to explain the gas holdup and other hydrodynamic parameters.

The gas holdup characteristic depends upon the bubble size and its dispersion in the bed. Thus the generation of fine gas bubbles is important which is possible by the suitable design of an air sparger (Thorat et al., 1998). Although the use of various types of sparger is seen in literature, but little attention has been made for the precise design of an air sparger which can avoid high pressure drop in the distributor section. In the present study an antenna type air sparger has been used which is quite efficient in producing fine

air bubbles with less pressure drop in the distributor section. Such a type of air sparger has been recommended by Meikap et al. (2002).

The complex hydrodynamics of three-phase reactors are not well understood due to the complicated phenomena such as particle–particle, liquid–particle and particle–bubble interactions. For this reason, computational fluid dynamics (CFD) has been promoted as a useful tool for understanding multiphase reactors for precise design and scale up. The report on the computational models for the hydrodynamic characteristics of three-phase (gas-liquid-solid) fluidized bed is scarce. Very little information is available in literature which is focused on the effect of the number of variables on the liquid minimum fluidization velocity, bed expansion behaviour and phase holdups. The objective of this study is to investigate numerically the hydrodynamic behaviour of a three-phase gas-liquid solid fluidized bed. The hydrodynamic behaviour studied numerically is mainly the bed pressure drop, minimum fluidization velocity, bed expansion or bed voidage and phase holdups.

Literature survey reveals that the hydrodynamic studies relating to of both liquid-solid and gas-liquid-solid semi-fluidized bed are limited. As far as the two-phase liquid-solid semi-fluidization is concerned, although a good number of research articles are available but the study is limited to a narrow range of operating variables. The particle sizes studied are either too small (< 1 mm) or large (> 4 mm). Mostly in the hydrodynamic studies irregular particles have been used and the use of spherical particle is scanty. Effect of liquid viscosity on hydrodynamics has not yet been studied.

In case of the gas-liquid-solid fluidization, Chern et al. (1984) reported the hydrodynamic parameters like pressure drop, minimum semi-fluidization velocity, height of packed section and fluidized section, and gas holdup based on separate experiments in fluidized and packed beds. It is also clear from the literature survey that, there is no work on semi-fluidized bed with liquid as the continuous phase and using irregular shape particles. The study of gas-liquid-solid semi-fluidization with the variation in the liquid viscosity and density and the solid density have not been studied (Chern, 1984). Effect of the position of the top grid and initial static bed height on various hydrodynamic parameters has also not been investigated by previous investigators. Therefore, the hydrodynamic study of a liquid-solid semi-fluidized bed and a cocurrent gas-liquid-solid semi-fluidized bed with liquid as the continuous phase has been taken up to have a better understanding of the bed behaviour with variation in a large number of operating variables.

The experimental system used in the present study ultimately aims at the performance characteristic study both as fluidized and semi-fluidized beds aerobic and anaerobic bioreactors. To design a semi-fluidized bed reactor a better understanding of the hydrodynamics of the liquid-solid and gas-liquid-solid semi-fluidization is essential.

1.11. The plan of investigation

Fluidized bed and semi-fluidized bed systems are the useful equipment for efficient gas-liquid-solid contacting process and can be used in chemical reactors, both for catalytic and non-catalytic ones, biochemical processes and wastewater treatment. During the last three decades, considerable research efforts have been put into understand the hydrodynamic aspects of fluidization as well as micro scale structure, identification and characterization of various regimes, gas-solids mixing, etc. Over the years newer applications of fluidized bed systems are being explored necessitating deeper understanding of the two and the three phase fluidization systems. The problems related to the effect of distributor, irregular and regular shape particles, liquid viscosity and surface tension, scaling up, particle sizes and their density, which affect the hydrodynamics, and its detailed structure still create practical dilemma. Thus, there exists many thrust areas requiring further detailed fundamental studies in the fluidized as well as the semi-fluidized bed reactor. In view of reported literature on advantages of fluidized and semi-fluidized bed reactor with regular and irregular shape particles, the major objective of the present work is as follows:

(1) Design and fabricate a fluidized and a semi fluidized bed system with an air sparger and distributor arrangement which ensures less pressure drop and uniform distribution of a large number of small gas bubbles.
(2) Hydrodynamics of the three phase fluidized bed reactor using regular shape spherical and hollow cylindrical particle systems.
(3) Hydrodynamics of the fluidized bed reactor with irregular shape particles.
(4) Theoretical analysis and CFD simulation of a fluidized bed reactor for prediction of its characteristics.
(5) Hydrodynamic characteristics like minimum and the maximum semi-fluidization velocities, the top packed bed height, the pressure drop across the semi-fluidized bed and the gas holdup of semi-fluidized bed reactor with spherical particles.
(6) Hydrodynamic characteristics of the semi-fluidized bed with non-spherical and irregular shape particles.

Chapter 2

Experimental Set-up and Techniques

Chapter – 2

Experimental Set-up and Techniques

2.1. Introduction

A three-phase (gas-liquid-solid) fluidized bed is designed and fabricated to study the hydrodynamic characteristics (like: pressure drop, minimum fluidization velocity, bed expansion and phase holdup) of regular and irregular shape particle systems using water and dilute solution of water-glycerol as liquid phase and air as the gas phase. The same setup with suitable modification has also been used for the hydrodynamic study of a three-phase semi-fluidized bed with identical particle systems and fluid phases as used in case of fluidization.

2.2. Experimental setup

The fluidized bed assembly consists of three sections, viz., the test section, the gas-liquid distributor section, and the gas-liquid disengagement section. Fig. 2.1 shows the schematic representation of the experimental setup used in the three-phase fluidization study. Fig. 2.2 gives the photographic representation of the experimental setup. The test section is the main component of the fluidized bed where fluidization takes place. It is a vertical cylindrical Plexiglas column of 0.1 m internal diameter and 1.88 m height consisting three pieces of persepex columns assembled by flange and nut bolt arrangement with rubber gasket in-between. This has been done for the purpose of varying the height of the fluidizer for different hydrodynamic studies.

During the experiment there is a chance for the generation of fines which may be entrained from the bed. To prevent particle entrainment a 16-mesh screen has been attached to the top of the column for the fluidization study. For semi-fluidization study the above 16-mesh screen has been used as a movable grid to retain the particle for the formation of a packed bed beneath it. The top grid is shown in Fig 2.3(a). The gas-liquid distributor is located at the bottom of the test section and is designed in such a manner that uniformly distributed liquid and gas mixture enters the test section. The distributor section made of Perspex is fructo-conical of 0.31 m in height, and has a divergence angle of 4.5^0. The liquid inlet of 0.0254 m in internal diameter is located centrally at the lower cross-sectional end. The higher cross-sectional end is fitted to the test section, with a perforated distributor plate made of G.I. sheet of 0.001 m thick, 0.12 m diameter having

open area equal to 20 % of the column cross-sectional area with either a 16 mesh (BSS) stainless steel screen or a plastic net in between.

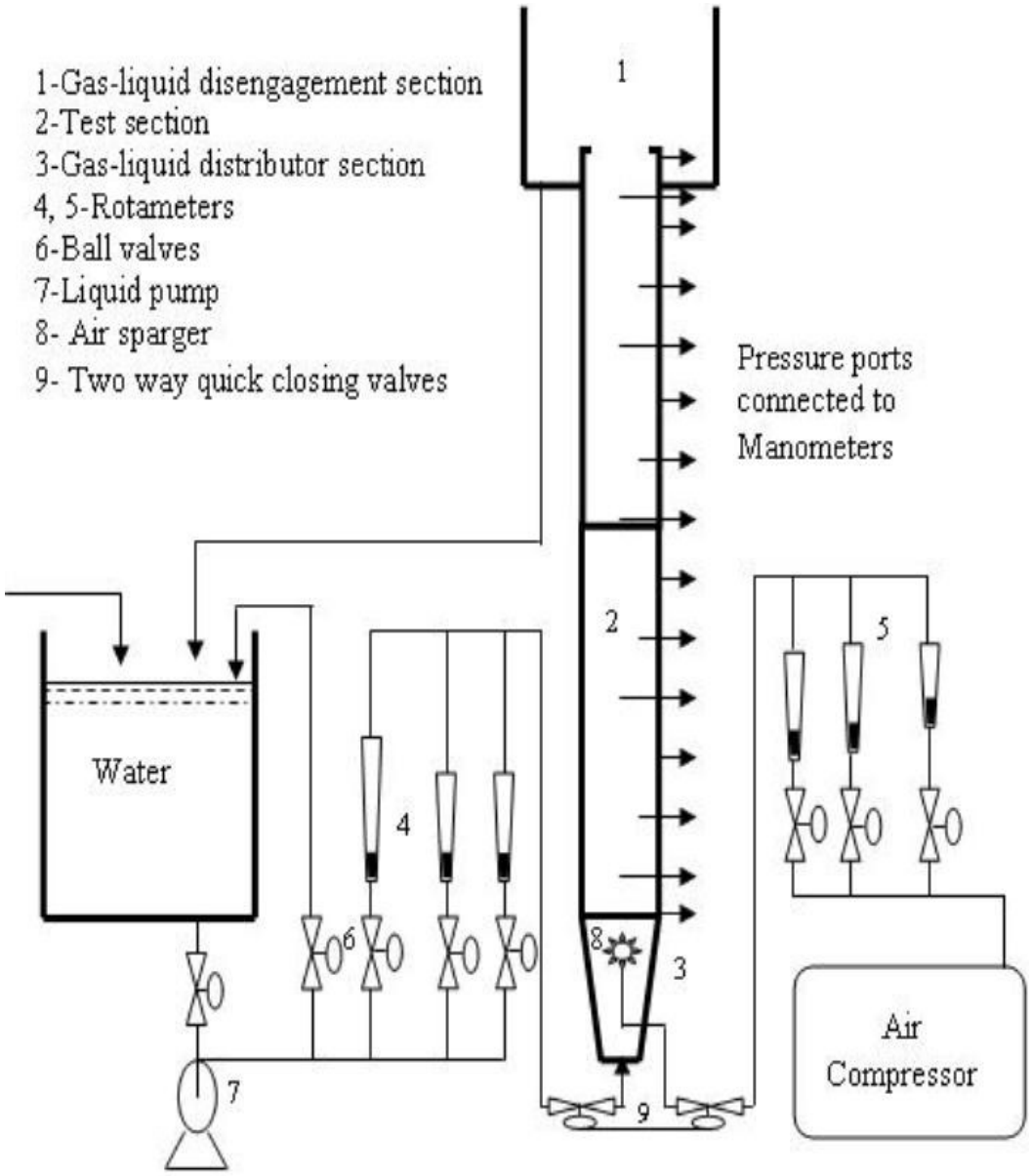

Fig. 2.1. Schematic representation of the experimental setup.

The distributor plate has 288 openings of 0.002 m, 0.0025 m and 0.003 m in triangular pitch arranged in 10 concentric circles of about 0.005 m radial gap. The size of the holes has been increased from the inner to the outer circle. This has been done with a view to have less pressure drop at the distributor plate and a uniform flow of the gas-liquid mixture into the test section. By convention the flow rate is higher at the centre than towards the wall thus driving the gas bubbles in the central zone to a greater extent causing there a higher holdup of gas. To avoid this unequal distribution at the entrance of

the test section, the distributor plate has been designed so that relatively uniform flow can be achieved throughout the cross-section. Figs. 2.3(b) through 2.3(d) represent the photographic view of the gas-liquid distributor section and the distributor plate. An antenna-type air sparger (Fig. 2.3(e)) of 0.09 m diameter with 50 number of 0.001 m holes has been fixed below the distributor plate with a few layers of plastic and glass beads in between for the generation of fine bubbles uniformly distributed along the column cross-section of the fluidizer. The antenna type air sparger has been previously used by Meikap et al. (2000). They have mentioned the generation of well distributed fine bubbles with much less pressure drop values by this design compared to the conventional air distributor.

Fig. 2.2. Photographic view of the experimental set-up.

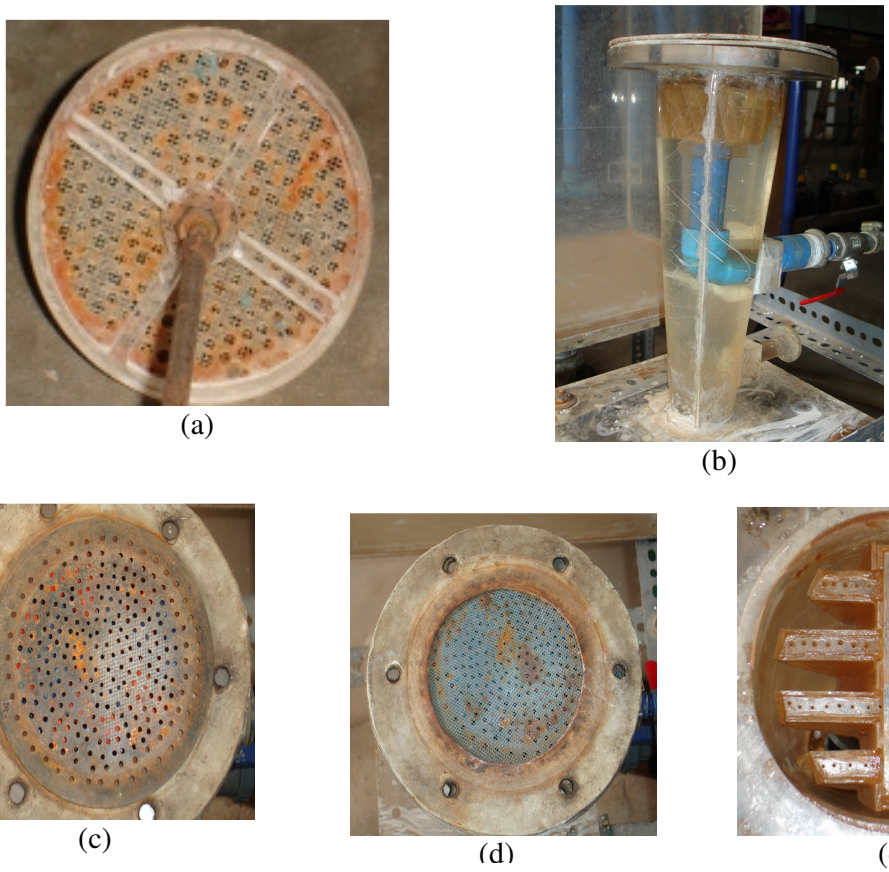

Fig. 2.3. Photographic view of: (a) the top grid or restraint, (b) the gas-liquid distributor, (c) distributor plate, (d) surmounted plastic net, (e) air sparger.

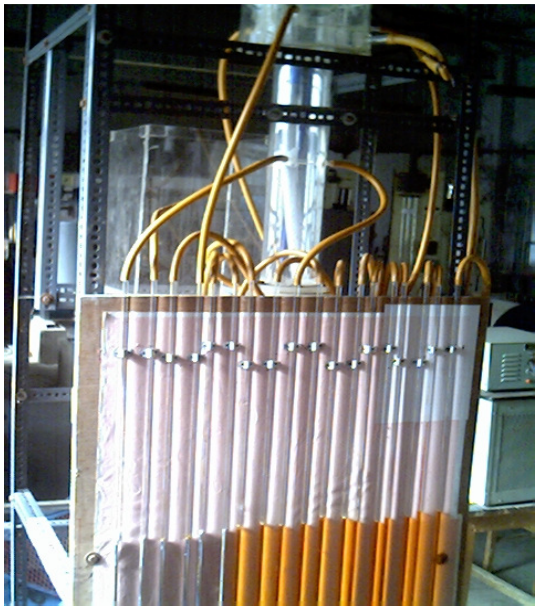

Fig. 2.4. Manometers connected with the set-up.

Use of various other types of distributor is seen in literature viz. a packed bed of solids of size 2 to 6 mm (Saberian-Broudjenni et al., 1987; Song et al., 1989; Zhou et al., 2009), distributor containing single nozzle (Ramesh and Murugesan, 2002) and multiple nozzles (Lee and Lasa, 1987; Liang et al., 1995), vertical pipes evenly spaced across a grid containing fine holes (Lee et al., 2001c; Cao et al., 2007), a ring containing large number of holes (Safoniuk et al., 2002). The packed type distributor although generates uniform mixture of gas and liquid which enters the test section of the three-phase system, results in large pressure drop in comparison to distributor containing different types of air sparger. The pressure drop through the distributor used by Saberian-Broudjenni et al. (1987), Song et al. (1989) and Zhou et al. (2009) has been calculated and is found to be 2.62, 6.6 and 2.98 times higher respectively than the pressure drop for the present distributor for a superficial air velocity of 0.084926 m/s.

The bubbles generated by single and multiple nozzle air sparger are comparatively large in size. The ring type air sparger results in unequal distribution of the gas in the liquid which enters the test section. As the gas-liquid mixture moves up in the column a vigorous contact with the solid phase results in uniform distribution of gas across the cross-section in the three-phase system. Safoniuk et al. (2002) have reported a uniform gas distribution (equal radial gas holdup) at a height of nearly 55 cm in the test section, below which the local gas holdup is unequal across the cross-section.

In the present study, it has been observed visually that the distributor arrangement used allows a uniform flow of gas and liquid to the text section containing fine gas bubbles. In the gas-liquid distributor section, the gas and the liquid streams are merged and passed through the perforated grid. The mixing section and the grid ensured that the gas and the liquid are well mixed and evenly distributed into the bed.

The gas-liquid disengagement section at the top of the fluidizer is a cylindrical section of 0.26 m internal diameter and 0.34 m height, assembled to the test section with 0.08 m of the test section inside it, which allows gas to escape and liquid to be circulated through the outlet of 0.0254 m internal diameter at the bottom of this section.

For the measurement of pressure drop in the bed, the pressure ports have been provided and fitted to the manometers filled with carbon tetrachloride and mercury as the manometric fluids for the accurate measurement of pressure at different ranges. Fig. 2.4 shows the photographic view of the manometers connected to the column. Pressure ports are available at seven different levels of equal spacing including one at bottom and one at the top of the test section. In one of the three Perspex columns pressure ports have been made at an interval of 0.1m. This has been done to measure the pressure drops at a

particular section at three different radial positions, viz., at the wall, at the centre of the column and at one-fourth of the diameter of the column from the wall. With this arrangement, the wall effect, expanded bed height, distribution of particle concentration and the gas holdup can be studied clearly. The inner end of the pressure ports have been covered by means of 16 wire mesh SS sieve to prevent solids entering into the pressure tubing connected to the manometer.

Table 2.1: Equipment characteristics and operating conditions

SET-UP	
Test section (Cylindrical Plexiglas column)	
Diameter, m	0.1
Height, m	1.88
Gas-liquid distributor section (fructo-conical)	
Height, m	0.31
Diameter of the ends, m	0.0508, 0.1
Tapered angle	4.5^0
Gas-liquid disengagement section (Cylindrical)	
Diameter, m	0.26
Height, m	0.34
Air sparger (antenna type)	
Orifice size, m	0.001 (50 nos.)
Distributor plate (GI)	
Diameter, m; thickness, m	0.12; 0.001
(holes in 10 concentric circles extend to 0.001m from centre)	
Gap between circumference of holes, m	0.005
0.002 m holes (40 nos)	centre:1, circle-1 (c-1): 6, c-2: 12, c-3: 21
0.0025 m holes (142 nos)	c-4: 22, c-5: 28, c-6: 34, c-7: 39, c-8: 19
0.003 m holes (106 nos)	c-8: 19, c-9: 40, c-10: 47
Liquid reservoirs	
Reservoir-1: dimension, m; capacity, lit.	0.42 x 0.32 x 0.70; 94
Reservoir-2: dimension, m; capacity, lit.	ID = height = 1; 1000
OPERATING RANGE OF GAS AND LIQUID VELOCITY	
Gas-liquid-solid fluidization of regular particles	
Superficial liquid velocity (U_L), m/s	0.004246 to 0.1486
Superficial gas velocity (U_g) , m/s	0.0 to 0.1274
Gas-liquid-solid fluidization of irregular particles	
Superficial liquid velocity (U_L), m/s	0.004246 to 0.1486
Superficial gas velocity (U_g) , m/s	0.0 to 0.1274
Gas-liquid-solid semi-fluidization of regular particles	
Superficial liquid velocity (U_L), m/s	0.004246 to 0.3057
Superficial gas velocity (U_g) , m/s	0.0 to 0.1274
Gas-liquid-solid semi-fluidization of irregular particles	
Superficial liquid velocity (U_L), m/s	0.004246 to 0.3057
Superficial gas velocity (U_g) , m/s	0.0 to 0.1274

In actual practice, oil free compressed air from a centrifugal compressor (3 phase, 1 Hp, 1440 rpm) with a receiver and an air accumulator / constant pressure tank used to supply

the air at nearly constant pressure gradient as fluidizing gas. The purpose of air accumulator is to dampen any pressure fluctuation. A silica gel tower was used to absorb moisture and oil carried out by the compressed air. The air was injected into the column through the air sparger at a desired flow rate using calibrated rotameter. Water or aqueous solution of glycerol was pumped to the fluidizer at a desired flow rate using water rotameter. Two centrifugal pumps of different capacity (pump-1: Texmo, single phase, 1 HP, 2900 rpm, discharge capacity of 150 lpm; pump-2: CRI, single phase, 0.5 HP, 2880 rpm, discharge capacity of 120 lpm) were used to deliver water to the fluidizer. Three calibrated rotameters with different ranges each for water as well as for air were used for the accurate record of the flow rates. Water rotameters used were of the range 0 to 20 lpm, 5 to 100 lpm and 20 to 200 lpm. Air rotameters were of the range 0 to 10 lpm, 0 to 50 lpm and 10 to 100 lpm.

2.3. Measurement of properties of the solids and the fluids

2.3.1. Flow rate measurement of glycerol solutions

The flow rate of glycerol solutions were measured using calibrated water rotameters. Due to difference in density of water and glycerol solutions, the observed flow rate of glycerol solutions were corrected by using the following formula as given by Nakra and Chaudhury (1985).

$$Q_w = K\sqrt{(\rho_f - \rho_w)/\rho_w} \tag{2.1}$$

$$Q_{sol} = K\sqrt{(\rho_f - \rho_{sol})/\rho_{sol}} \tag{2.2}$$

Where, Q_w and Q_{sol} represent the volumetric flow rate of water and glycerol solution in lpm respectively, K, constant for the rotameter, ρ_f, ρ_w and ρ_{sol} represent the density of the float of the rotameter, density of water and density of the glycerol solution respectively.

2.3.2. Particle size

The diameter of various regular (spherical) and irregular shape particles has been determined by sieve analysis using British standard sieves (BSS). The particle size determined by sieve analysis is the average of the size or opening of two consecutive screens. The diameters used are the mass mean particle diameter for spherical and irregular particles obtained from sieve analysis. The solids used in fluidized beds are never identical in size and usually follow a size distribution. An average particle diameter, d_p used is the Sauter mean diameter and is given by.

$$d_p = \frac{1}{\sum(x_i / d_{pi})} \tag{2.3}$$

The diameter of hollow cylindrical raschig rings is the equivalent volume diameter, which is the diameter of a sphere whose volume is the same as that of the solid volume of actual particle. The equivalent volume diameter of the hollow cylindrical particle has been calculated by using the following formula,

$$\frac{\pi}{6} d_p^3 = \frac{\pi((OD)^2 - (ID)^2)L}{4} \tag{2.4}$$

Where, *OD*, *ID* and *L* represent the outer diameter, inner diameter and length of the hollow cylindrical particle respectively and have been determined with a slide calipers. The average diameter of 10 individual particles randomly selected has been used as the particle size.

2.3.3. Particle density

The density of the different kind of fluidized particles has been measured using the water displacement method in which the packing voidage was obtained by displaced water volume when the particles were placed into a graduated cylinder filled with water.

2.3.4. Sphericity

The shape of an individual particle is expressed in terms of the sphericity, which is independent of particle size. The sphericity, ϕ_s, of a solid particle is the ratio of the surface area of a sphere, whose volume is equal to that of the particle, divided by the actual surface area of the particle. For a non-spherical particle, the sphericity is defined as:

$$\phi_s = \frac{6V_p}{d_p S_p} \tag{2.5}$$

For a spherical particle of diameter, d_p, $\phi_s = 1.0$. For non-spherical particle, the sphericity has been determined using air permeability apparatus. Permeability of air through a bed of solid particles is defined by volume rate of flow per unit cross section per unit pressure gradient and is expressed by

$$permeabilty = \frac{volumetric\ flow\ rate\ of\ air \times length\ of\ the\ bed}{crossctional\ area \times pressure\ drop} \tag{2.6}$$

The surface to volume ratio of particle (S_p/V_p) is calculated as;

$$\frac{S_p}{V_p} = 14\sqrt{\frac{(porosity\ of\ bed)^3}{permeability \times viscosity\ of\ air \times (1 - porosity\ of\ bed)^2}} \tag{2.7}$$

Where, $porosity = \dfrac{packed\ bed\ volume - (mass\ of\ particles / density\ of\ particle)}{packed\ bed\ volume}$ (2.8)

2.3.5. Liquid phase density

The liquid phase density of water and aqueous solutions of glycerol has been measured using standard 25 ml specific gravity bottle. The aqueous solutions of glycerol of different mass % have been prepared by adding required volumes of pure glycerol (99.5% glycerol of MERCK) to a definite quantity of water from the mass volume relationship using the formula.

$$V_{sol} = V_w + V_G \tag{2.9}$$

$$\%\ by\ mass\ of\ glycerol\ in\ solution = \frac{V_G \rho_G}{V_G \rho_G + V_w \rho_w} \tag{2.10}$$

Where, V_{sol}, V_w and V_G represents the required volumes of solution, water and glycerol respectively and ρ_w and ρ_G are the densities of water and glycerol respectively.

2.3.6. Viscosity of liquid

Viscosity of the liquids used in the experiment has been determined by using standard Ostwald (U-tube) viscometer (Paul's size B, BS-188). To attain the desired temperature of measurement (30^0C), the viscometer was kept in a water bath. The standard procedure for determination of viscosity as recommended for Ostwald viscometer has been followed.

2.3.7. Surface tension of liquid

Surface tension of water and aqueous solutions of glycerol has been determined by Wilhelmy plate method using a surface tensiometer Data Physics, Germany (DCAT 11EC). DCAT 11 is equipped with a high-tech weighing system, efficient microelectronics and MS Windows based software which gives the value of surface tension of the sample with the temperature measurement. For the check of calibration at the beginning surface tension of distilled water is measured and compared with standard value. If the value does not agree, then Platinum plate is cleaned very carefully with acetone. Normally the platinum plate used for measurement has been cleaned and burned for each reading. 30 ml of the sample solution has been taken in the jacketed sample vessel. A temperature of (30 ± 0.1^0C) was maintained by circulating thermostatic water by a circulator through a jacked vessel containing the solution.

2.4. Experimental procedure

The three-phase solid, liquid and gas are glass beads, tap water (and aqueous solution of glycerol in some cases) and oil free compressed air, respectively. Tap water is treated water used for drinking and sanitation and is fairly pure for industrial operation. The tap water used in the present study had no suspended solids and the dissolved solid content was also quite

low. The scope of the experiment is presented in Table 2.2. The air-water flow was co-current and upwards. Accurately weighed amount of material was fed into the column and adjusted for a specified initial static bed height. Water was pumped to the fluidizer at a desired flow rate using water rotameter. The air was then introduced into the column through the air sparger at a desired flow rate using air rotameter. Three calibrated rotameters with different ranges each for water as well as for air have been used for the accurately record of the flow rates.

All experiments have been started with the column completely filled with water and glass beads and the initial level of manometer adjusted to have zero level. For liquid-solid experiment the liquid flow rate was gradually increased. Approximately five minutes were allowed to make sure that the steady state was reached. Then the readings of the manometers and the expanded heights of the bed were noted. For gas-liquid-solid experiment, with a little flow of liquid close to zero, the air was slowly introduced and gradually increased to the desired flow rate after which the liquid flow rate was increased and the readings were noted down, as mentioned above. From the total pressure drop in the bed, the gas holdup was determined. The procedure was repeated for different values of initial static bed height, particle size and gas velocity.

Table 2.2: Scope of the present investigation

A. Properties of gas, liquid and solid phase

Gas phase	**Density (kg/m^3)**	**Viscosity (Pa.s)**	**Surface tension (kg/m^2)**
Air at 30^{0}C	1.166	1.794x10^{-5}	-
Liquid phase at 30^{0}C			
Water	995.7	0.000798	0.0712
6% glycerol solution	1009.7	0.000984	0.0706
12% glycerol solution	1024.0	0.001082	0.0701
18% glycerol solution	1039.0	0.001268	0.0696
24% glycerol solution	1054.0	0.001567	0.0691
30% glycerol solution	1068.6	0.001852	0.0685

Solid phase	**Particle Size (d_p), mm**	**Particle density (ρ_p), kg/m^3**	**Solid phase**	**d_p, mm**	**ρ_p kg/m^3**
Glass beads	1.55	2470	Raschig		
	2.18	2216, 2470	rings	6.864	1670
	2.58	2253, 2470	Coal	4.05	1492
	3.07	2253, 2470	Dolomite	1.55, 2.18, 3.07, 4.05	2652
	4.05	2470	Laterite	4.05	3313
	6.29	2470	Iron ore	4.05	3994

B. Experimental conditions

Operating variables	**Range**
Superficial gas velocity:	$0.0 < U_g < 0.1274$ m/s
Superficial liquid velocity (for fluidization study):	$0.0 < U_L < 0.1486$ m/s
Superficial liquid velocity (for semi-fluidization study):	$0.0 < U_L < 0.3057$ m/s
Bed Parameters	
Initial static bed height in cm:	17.1, 17.7, 21.3, 21.6, 25.6, 26.7, 29.6, 30.1, and 36.7
Bed expansion ratio (R)	2.0, 2.5, 3.0, and 3.5

Chapter 3

Hydrodynamics of Regular Particles in Fluidized Bed

Chapter-3

Hydrodynamics of Regular Particles in Fluidized Bed

3A. *Hydrodynamics of spherical particles*

3A.1. Introduction

Three-phase fluidized beds have been applied successfully to many industrial processes such as in the H-oil process for hydrogenation and hydro-desulfurization of residual oil, the H-coal process for coal liquefaction, Fischer-Tropsch process, and the bio-oxidation process for wastewater treatment. Three-phase fluidized beds are also often used in physical operations (Muroyama and Fan, 1985). Among the various modes of operation of gas-liquid-solid fluidized beds, the most striking one is the co-current three-phase fluidization with liquid as the continuous phase (Epstein, 1981; Muroyama and Fan, 1985). The co-current gas-liquid-solid fluidization is defined as an operation in which a bed of solid particles is suspended in upward flowing gas and/or liquid media due to the net gravitational force (i.e. gravitational force – buoyancy force) on the particles. Such an operation generates considerable intimate contact among the gas, liquid and solid particles in the system and provides substantial advantages for applications in physical, chemical or biochemical processing involving gas, liquid and solid phases (Dhanuka and Stepanek, 1978).

The successful design and operation of a gas-liquid-solid fluidized bed system depends on the ability to accurately predict the fundamental characteristics of the system, viz. the hydrodynamics, the mixing of individual phases, and the heat and mass transfer characteristics (Begovich and Watson, 1978; Lin and Tzu, 2003). The hydrodynamic properties such as the bed pressure drop, minimum fluidization velocity, bed porosity (or bed expansion), phase holdups, bubble properties etc. have to be studied in order to provide the basic information required for the design of such fluidized bed systems (Jena et al., 2008a). A comprehensive literature survey of the hydrodynamics of gas-liquid-solid fluidized bed has been discussed in chapter-1.

The gas holdup characteristic depends upon the bubble size and its dispersion in the bed. Thus the generation of fine gas bubbles is important which is possible by the suitable design of an air sparger (Thorat et al., 1998). Although the use of various types of sparger is seen in literature, but little attention has been made for the precise design of an air sparger which can avoid high pressure drop in the distributor section. In the present study an antenna type air sparger has been used which is quite efficient in producing fine air bubbles with less pressure drop in the distributor section. Such a type of air sparger

has been recommended by Meikap et al. (2002). In the present investigation, a gas-liquid-solid three phase fluidized bed reactor has been designed, fabricated and hydrodynamic characteristics have been investigated using regular shape spherical and hollow cylindrical particles.

Before using the reactor for specific purpose, the hydrodynamics of the fluidized bed reactor must be studied in detail so as to maximize the efficiency of the system. In the present chapter, an attempt has therefore been made to acquire precise knowledge of the hydrodynamic characteristics of fluidized bed reactor for three phase flow. Experiments have been conducted to study the hydrodynamic behavior viz. the pressure drop, minimum liquid fluidization velocity, bed expansion (bed voidage) and phase hold up of a co-current gas-liquid-solid three-phase fluidized bed with a wide range of operating variables. This has been done to develop a good understanding of the hydrodynamic behaviour in gas-liquid-solid fluidization in low to moderately high Reynolds number range.

3A.2. Experimental set-up and techniques

The same experimental setup as presented in Fig. 2.1 and discussed in chapter-2 has been used in present case. The scope of the experiment has been presented in Table 3.1. In actual practice, accurately weighed amount of bed material was fed into the column and adjusted for a specified initial static bed height (reproducible) by repeated fluidizing and defluidizing the bed with water. Liquid was pumped to the fluidizer at a desired flow rate using calibrated rotameter. The air was then introduced into the column through the air sparger at a desired flow rate. Approximately five minutes was allowed to make sure that the steady state has been reached. The readings for pressure drop and the expanded heights of the bed were then noted. All experiments have been conducted at temperature of $(30\pm5)^0$C. The procedure was repeated for different liquids, particles of different sizes and varying initial static bed heights. For a change of $\pm5^0$C in temperature, the viscosity of water varies up to ±11.53%, which can cause a variation of ±1.54% in minimum fluidization velocity (calculated from equation of Wen and Yu (1966)) for 4.05 mm glass beads (GB) and a variation of ±4.16% in the pressure drop for 2.18 mm GB of a bed height 17.7 cm at water velocity of 0.03397 m/s (calculated from Ergun's equation).

3A.3. Pressure drop and minimum fluidization velocity

3A.3.1. Pressure drop

The pressure drop through the bed is strongly related to the individual phase holdups in the bed. In the fluidized bed with no or low solid entrainment, the solid holdup is given by;

$$\varepsilon_s = 1-\varepsilon = \frac{M_s}{\rho_s A_c H_e} \tag{3.1}$$

The relation between individual phase holdups is expressed as;

$$\varepsilon_g + \varepsilon_L + \varepsilon_s = 1 \tag{3.2}$$

Table 3.1: Scope of the experiment

A. Experimental conditions			
Operating variables	**Range**		
Superficial gas velocity	0.0< U_g < 0.1274 m/s		
Superficial liquid velocity	0.004246< U_L < 0.1486 m/s		
Initial static bed height	17.1, 17.7, 21.3, 25.6, 26.7, 30.1, and 36.7 cm		
B. Properties of gas, liquid and solid phase			
Gas phase	**Density (kg/m^3)**	**Viscosity (Pa.s)**	**Surface tension (kg/m^2)**
Air at 30^{0}C	1.166	1.794x10^{-5}	-
Liquid phase at 30^{0}C			
Water	995.7	0.000798	0.0712
6% glycerol solution	1009.7	0.000984	0.0706
12% glycerol solution	1024.0	0.001082	0.0701
18% glycerol solution	1039.0	0.001268	0.0696
24% glycerol solution	1054.0	0.001567	0.0691
30% glycerol solution	1068.6	0.001852	0.0685
Solid phase	**Particle Size, mm**	**Particle density (kg/m^3)**	
Glass beads	1.55	2470	
	2.18	2216, 2470	
	2.58	2253, 2470	
	3.07	2253, 2470	
	4.05	2470	
	6.29	2470	

At quasi steady state condition, the total bed pressure gradient (Fan, 1989) neglecting the frictional drag on the column wall and the acceleration terms for the gas and liquid flows is given by;

$$\frac{\Delta P}{\Delta H} = g(\rho_g \varepsilon_g + \rho_L \varepsilon_L + \rho_s \varepsilon_s) \tag{3.3}$$

For liquid continuous phase the dynamic pressure gradient for the liquid is defined as the total pressure gradient corrected for the hydrostatic head of the liquid.

$$\frac{\Delta P_d}{\Delta H} = g(\rho_g \varepsilon_g + \rho_L \varepsilon_L + \rho_s \varepsilon_s) - \rho_L g = \varepsilon_s(\rho_s - \rho_L)g - \varepsilon_g(\rho_L - \rho_g)g \tag{3.4}$$

The frictional pressure gradient is defined as the total pressure gradient is corrected for the hydrostatic head of the gas-liquid two phase mixture (Epstein, 1981) and is given by;

$$\frac{\Delta P_f}{\Delta H} = \frac{\Delta P}{\Delta H} - \rho_f g; \ \ where\ \rho_f = \frac{\varepsilon_g \rho_g + \varepsilon_L \rho_L}{\varepsilon_g + \varepsilon_L} = \frac{\varepsilon_g \rho_g + \varepsilon_L \rho_L}{1 - \varepsilon_s} \tag{3.5}$$

Combining Eqs. (3.2), (3.3), and (3.5) the frictional pressure gradient becomes;

$$\frac{\Delta P_f}{\Delta H} = \varepsilon_s(\rho_s - \rho_f)g = (1-\varepsilon)(\rho_s - \rho_f)g \tag{3.6}$$

This equation shows that the frictional pressure gradient balances the effective weight of solid particles in the two-phase medium. In the absence of gas, Eqs. (3.4) and (3.6) reduces to the characteristics equation for the liquid-solid system.

$$\frac{\Delta P_d}{\Delta H} = \frac{\Delta P_f}{\Delta H} = (1-\varepsilon_L)(\rho_s - \rho_L)g \tag{3.7}$$

In the present study, pressure drop in the fluidized bed has been measured by using manometers filled with carbon tetrachloride as manometric fluid connected to pressure tappings in the column as described in chapter-2. All experiments have been started with the column completely filled with water and glass beads up to a desired height with the initial level of manometer adjusted to have zero. For liquid-solid experiment the liquid flow rate was gradually increased. For gas-liquid-solid experiment with little flow of liquid close to zero, the air was slowly introduced and gradually increased to the desired flow rate after which the liquid flow rate was increased and the readings were noted down.

Figs. 3.1 and 3.2 show the variation of pressure drop with superficial liquid velocity in gas-liquid-solid system for different static bed heights and particle sizes. An increase in bed pressure drop has been observed with increased initial static bed height as seen in Fig. 3.1. It is obvious that higher static bed height (higher bed mass) requires a higher amount of drag to make the bed fluidize, thus a higher value of pressure drop as observed. Fig. 3.3 shows the effect superficial liquid velocity at different constant superficial gas velocities on pressure drop. It is interesting to note that with increase in gas velocity the bed pressure drop decreases, this may be due to the increased gas holdup in the bed.

In Figs. 3.1, 3.2 and 3.3 the pressure drop after incipient of fluidization has been assumed to be constant. But in actual case the pressure drop slightly increases as the liquid holdup is likely to increase with the increase in liquid velocity at a constant gas velocity. The experimental pressure drop in two phase fluidization has been found to be very close to that can be obtained from basic force balance as shown in Fig 3.4, indicating there by the absence of wall effect in the present case. The dotted line in the figure shows the effective bed weight (i.e. buoyant weight) per unit area.

Fig. 3.4 shows the variation of bed pressure drops in the fluidization regime (i.e. at higher fluid flow rates than at minimum fluidization) with superficial liquid velocity at constant values of gas velocity. The little increase in bed pressure drop with liquid velocity may be due to increased liquid holdup in the system. The pressure drop obtained

from manometer reading for a three phase system does not represent the true frictional drag on the solid particles which holds the particles in suspended conditions as the hydrostatic pressure in the column changes due to gas holdup. On the other hand the pressure drop measurement is used to calculate the phase holdup in the bed.

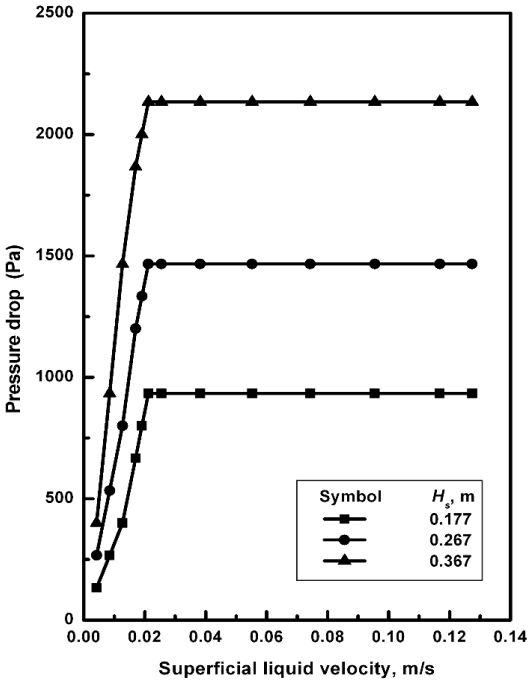

Fig. 3.1. Variation of bed pressure drop with liquid velocity for different initial static bed heights at [U_g = 0.02123 m/s, d_p = 2.18mm].

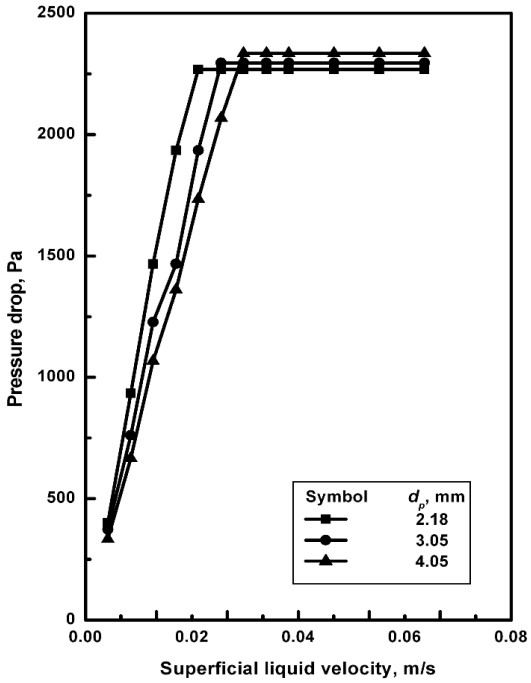

Fig. 3.2. Variation of bed pressure drop with liquid velocity for different particle sizes at [U_g = 0.02123 m/s, H_s = 0.367 m]

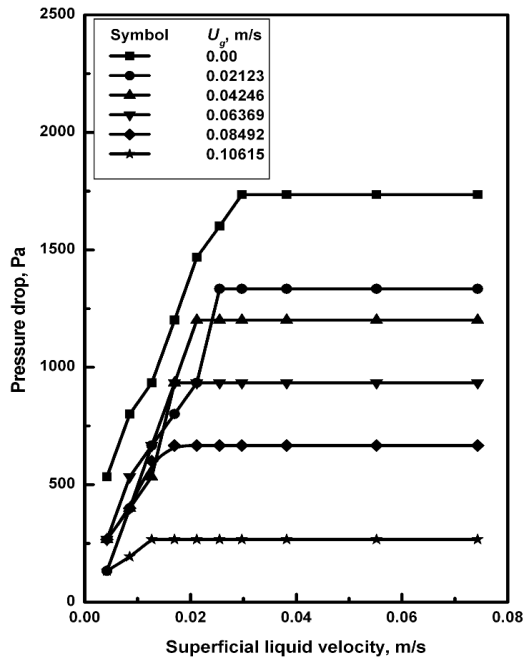

Fig. 3.3. Variation of bed pressure drop with liquid velocity for different values of gas velocity at [H_s = 0.267 m, d_p = 3.07 mm]

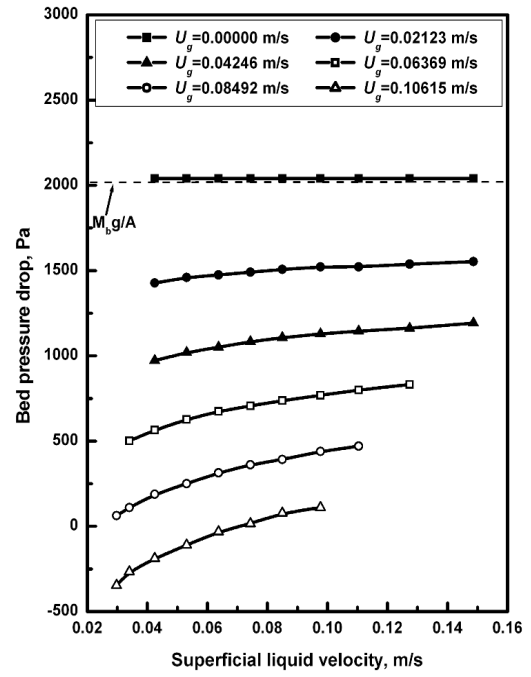

Fig. 3.4. Variation of bed pressure drop with liquid velocity for different values of gas velocity at [H_s = 0.256 m, d_p 3.07 mm]

3A.3.2. Minimum fluidization velocity

In case of gas-liquid-solid fluidization with liquid as the continuous phase, the minimum fluidization velocity is called as the minimum liquid fluidization velocity (U_{Lmf}). U_{Lmf} is the superficial liquid velocity at which the bed becomes fluidized for a given superficial gas velocity (Briens et al., 1997a). The minimum liquid flow rate required to achieve fluidization is determined from the bed pressure drop vs. superficial liquid velocity plot at a constant gas velocity. The point of intersection of the line of different slope is taken as U_{Lmf} (Begovich and Watson, 1978). Visual observation determines U_{Lmf} as either the velocity at which the bed first begins to expand or as the velocity at which any particle within the bed continuously shifts position with neighboring particles (Briens et al., 1997b).

U_{Lmf} in this study has been obtained from the plot of pressure drop and superficial liquid velocity (like Figs.3.1 and 3.2). In case of environmental applications of liquid-solid fluidized bed as anaerobic bioreactor and gas-liquid-solid fluidized bed as aerobic bioreactor for waste water treatment, a higher bed inventory is preferred as it increases the removal efficiency of the operation. Biological treatment is a slow process and needs long residence time for the wastewater in the bed. Thus in this particular application, the design and operation of the fluidized bed should ensure a good quality of fluidization as well as sufficiently large residence time for the liquid. Sufficient contact time between micro-organisms and the pollutants is achieved in the system and maximum solid surface is available to the liquid. This emphasizes the study of the effect of bed mass on liquid-solid and gas-liquid-solid fluidization characteristics (Delebarre et al., 2004). From Fig. 3.1 it is observed that there is no effect of initial static bed height on U_{Lmf} and a typical value of 0.0212 m/s was observed for all the cases, which is in agreement with findings of Begovich and Watson (1978). However, Delebarre et al. (2004) have reported the reverse phenomena of variation of minimum fluidization velocity with the initial static bed height. Since fluidization of a bed is achieved when the upward inertial and drag forces exerted on the particles by the fluids equal the buoyant weight of the bed, an effect of initial static bed height on the minimum fluidization velocity would only be expected if end effects were present in the bed (Jena et al., 2008b).

From Fig. 3.2, it is observed that U_{Lmf} increases with increase in particle size. Fig. 3.3 shows the effect of superficial gas velocity on U_{Lmf}. The figure indicates that U_{Lmf} decreases with the increase in gas velocity. Fig. 3.5 shows the variation of U_{Lmf} with superficial gas velocity for different particle sizes. It can be seen from the figure that the U_{Lmf} decrease with an increase in gas velocity, which indicates bubble supported fluidization. The rate of decrease in velocity is large at lower gas velocity but the rate

decreases as gas velocity increases. However at higher gas velocity, the minimum liquid fluidization velocity becomes almost constant. The same trend has been reported by Briens et al. (1997a). In addition, a similar trend has also been observed for all particle sizes, which agrees well to the findings of Song et al. (1989). It is also observed that initially with introduction of gas, the decrease in U_{Lmf} is large, but with increase in the gas velocity the decrease is relatively small. U_{Lmf} for liquid-solid fluidization is within 5% deviated from the values predicted by the correlation of Wen and Yu (1966) (marked as short horizontal line in Fig. 3.5). The qualitative nature of the variation in U_{Lmf} with the operating variables observed in the present study also agrees with the findings of Lee et al. (2001c).

The experimental data for minimum liquid fluidization velocity has been correlated by non-linear regression analysis and the following equations (Eqs. (3.8) and (3.9) have been developed which can be used for the prediction of U_{Lmf} for similar systems. The non-linear regression equation developed is based on least square estimation using Gauss-Newton method.

$$U_{Lmf} = 0.0065 U_g^{-0.268} d_p^{0.551} \mu_L^{-0.434} (\rho_s - \rho_L)^{0.066} \tag{3.8}$$

(with coefficient of determination (R-square) = 0.993)

$$\frac{U_{Lmf}}{U_{Lmf}^{Ls}} = 0.465 U_g^{-0.268} d_p^{-0.08} \mu_L^{-0.216} (\rho_s - \rho_L)^{-0.218} \tag{3.9}$$

(with coefficient of determination (R-square) = 0.982)

The values of the experimental minimum liquid fluidization velocity have been compared with those calculated from Eqs. (3.8) and (3.9) and from a few available correlations in literature in Fig. 3.6. Using Eq. (3.9) prior knowledge of U_{Lmf} in liquid-solid system is required. The predicted values of U_{Lmf} from Eqs. (3.8) and (3.9) agree with experimental data with an Average Absolute Relative Error (AARE) of 1.31 % and 1.62 % respectively. The equations of Begovich and Watson (1978) and of Nacef (1991) predict higher values of U_{Lmf} except for a few cases. The values of U_{Lmf} predicted from the neural network model of Larachi et al. (2000) distributed equally both in lower and upper side of the diagonal in Fig. 3.6 with a relatively larger deviation than the other correlations. This may be due to fact that the model has been developed from a wide range of literature data with wide rage of operating variables and liquid-particle system, which might not be able for accurate prediction of U_{Lmf} for some specific conditions. But most of the predicted values from all correlations have been found to agree within 20 % with the experimental values. The values of U_{Lmf} predicted from the liquid-buoyed-gas perturbed liquid model (LB-GPLM) suggested by Lee et al. (2001b) agrees with the experimental values with an AARE of 16.2 %.

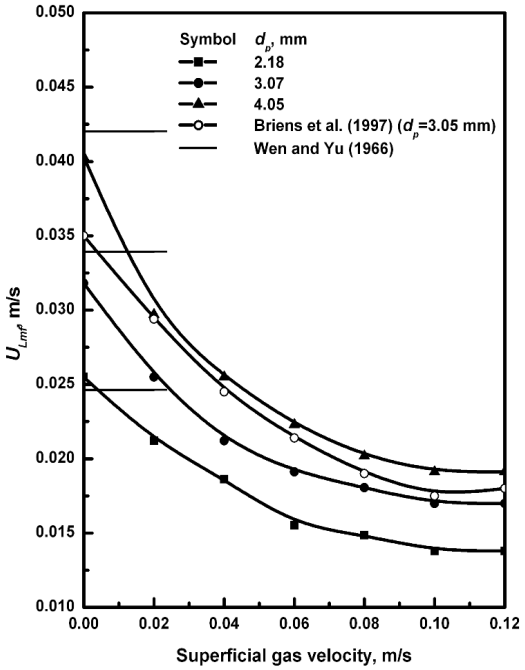

Fig. 3.5. Variation of minimum liquid fluidization velocity with gas velocity for different particle sizes.

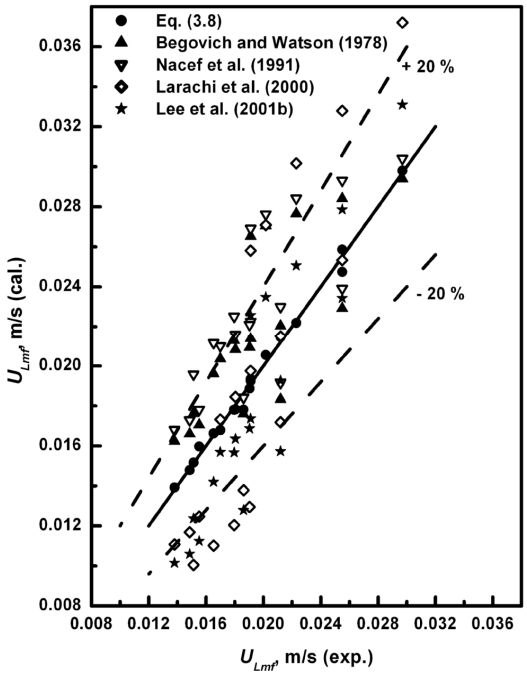

Fig. 3.6. Comparison of minimum liquid fluidization velocity.

3A.4. Bed expansion

The expanded bed height can be obtained either visually or from the measured pressure drop gradient (Kim et al., 1975, Dargar and Macchi, 2006). In determining the bed height, the axial static pressure profile of the entire height of the column is drawn (Kim et al., 1972, 1975). The bed height is taken as the point at which there is a sharp change in the slope of the pressure profile. Previous studies on the bed characteristics in three-phase fluidized bed include broader range of gas velocities, liquid surface tensions and viscosities. However the investigation on the effect of a larger number of variables on the bed voidage in a single experimental plan is scarce. In the present case, the effects of a wide range of operating variables on the bed expansion characteristics have been studied.

The expanded bed height in the present study has been measured by visual observation and the data have been compared as shown in Fig. 3.7 with the pressure drop profile along the length of the column measured by manometers. In Fig 3.7 the expanded bed height has been represented as bed expansion ratio (H/H_s). Fairly good agreement has been observed between two measurements. In visual observation a very dilute bed which appears at the top of the three-phase region has been neglected and the height of the relatively dense bed has been reported as expanded bed height. The bed expansion study as carried out by varying liquid velocity (at a constant gas velocity) and particle sizes

have been presented in terms of bed expansion ratio as shown in Figs. 3.8 and 3.9 respectively. It is seen from Fig. 3.8 that the bed expansion ratio increases with increase in both the liquid velocity and the gas velocity. Fig. 3.9 shows the decrease in bed expansion with particle size.

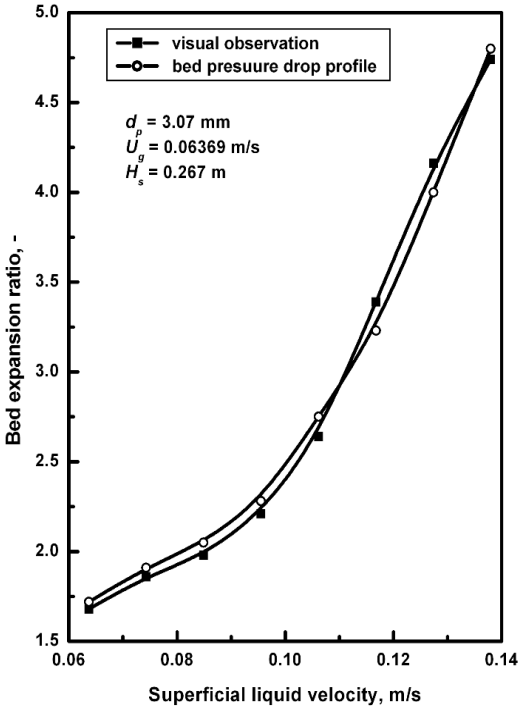

Fig. 3.7. Comparison of expanded bed height obtained from visual observation and pressure drop profile.

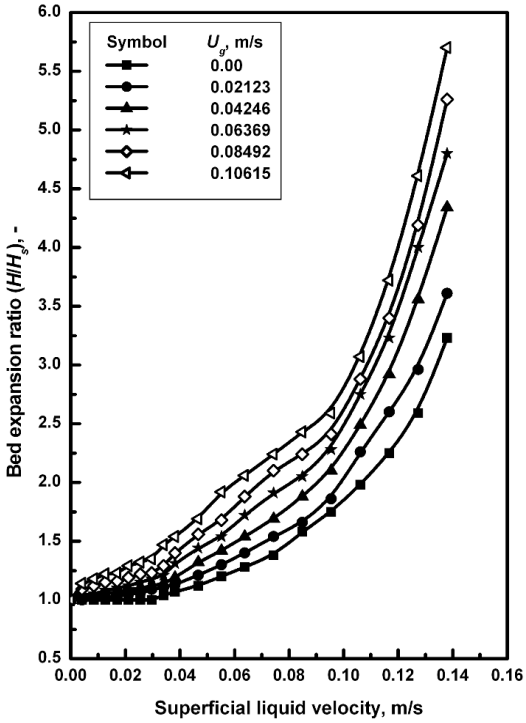

Fig. 3.8. Variation of bed expansion ratio with liquid velocity for different values of gas velocity at [H_s = 0.267 m, d_p = 3.07 mm].

3A.4.1. Development of correlation based on factorial design analysis

Factorial design analysis brings out the interaction effects of variables, which would not be found otherwise by conventional experimentation and to explicitly find out the effect of each of the variables quantitatively on the response. In this method the experiments have been repeated twice or thrice at two levels of each of the operating variables i.e. one at lower level (-1 level) and the other at higher level (+1 level).The scope of the factors considered for factorial experimentation have been presented in Table 3.2. The variables, which affect the bed expansion ratio in fluidization, are initial static bed height, particle size, liquid and gas velocities. Thus total numbers of experiments required at two levels for the four variables is 16. Each experiment has been repeated three times and the average of the values has been reported as the response value. A correlation based on the factorial design analysis (Davies, 1978) has been developed for the bed expansion ratio of the fluidized bed.

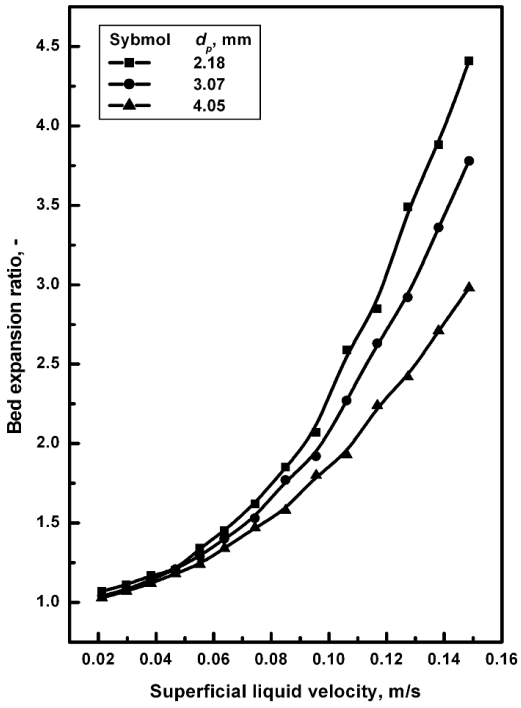

Fig. 3.9. Variation of bed expansion ratio with liquid velocity for different particle sizes at [H_s = 0.267 m, U_g = 0.02123 m/s].

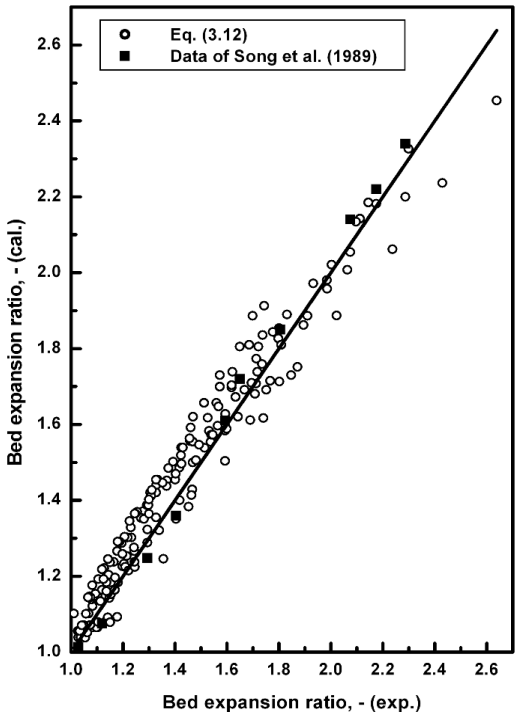

Fig. 3.10. Comparison of calculated and experimental values of bed expansion ratio.

The model equation for four factors is represented in the general form as;

$$Y = (b_0 + b_1A + b_2B + b_3C + ... + b_{12}AB + b_{13}AC + ... + b_{123}ABC + ... + b_{1234}ABCD) \qquad (3.10)$$

(i) Coefficients are calculated by the Yates standard technique (Davies, 1978) as;

$$b_i = \Sigma \frac{\alpha_i Y_i}{N} \qquad (3.11)$$

Where b_i is the coefficient, Y_i is the response, α_i is the level of the variable and N is the total number of treatments.

ii) Calculations of the level of variables

A: Level for static bed height= (Static bed height – 0.272)/0.095

B: Level for particle diameter = (Particle diameter - 0.003115)/0.000935

C: Level for gas velocity = (Gas velocity – 0.06)/0.04

D: Level for liquid velocity = (Liquid velocity – 0.03925)/0.02655

Table 3.2: Scope of the factors for bed expansion ratio (factorial design analysis)

Sl. No.	Actual variable	Factorial design symbol	Min. level (-1)	Max. level (+1)	Magnitude of variables
1	H_s, m	A	0.177	0.367	0.177,0.267,0.367
2	d_p, m	B	0.00218	0.00405	0.00218,0.00305,0.00405
3	U_g, m/s	C	0.02	0.10	0.02 - 0.10
4	U_L, m/s	D	0.0212	0.0743	0.0212 - 0.0743

The experimental data based on factorial design and the nature of the effects has been presented for bed expansion ratio in Table 3.3.

Table 3.3: The effects of parameters on bed expansion ratio as per factorial design analysis

Sl. No.	TC[$]	R (exp)	1	2	3	4	Effect (4)/8	Sum of squares $(4)^2/16$	PC[#]
1	1	1.07	2.11	4.19	9.06	24.04			
2	a	1.04	2.08	4.87	14.98	-0.86	-0.1075	0.000722	1.35
3	b	1.03	2.55	6.28	-0.02	-1.22	-0.1525	0.001454	2.72*
4	ab	1.05	2.32	8.70	-0.84	0.4	0.05	0.000156	0.29
5	c	1.30	3.19	-0.01	-0.26	3.1	0.3875	0.009385	17.57*
6	ac	1.25	3.09	-0.01	-0.96	-1.04	-0.13	0.001056	1.98
7	bc	1.14	4.78	0.10	0.14	-0.96	-0.12	0.0009	1.69
8	abc	1.18	3.92	-0.94	0.26	-0.1	-0.0125	9.77E-06	0.02
9	d	1.62	-0.03	-0.03	0.68	5.92	0.74	0.034225	64.08*
10	ad	1.57	0.02	-0.23	2.42	-0.82	-0.1025	0.000657	1.23
11	bd	1.47	-0.05	-0.10	0	-0.7	-0.0875	0.000479	0.90
12	abd	1.62	0.04	-0.86	-1.04	0.12	0.015	1.41E-05	0.03
13	cd	2.64	-0.05	0.05	-0.2	1.74	0.2175	0.002957	5.54*
14	acd	2.14	0.15	0.09	-0.76	-1.04	-0.13	0.001056	1.98
15	bcd	2.18	-0.5	0.20	0.04	-0.56	-0.07	0.000306	0.57
16	abcd	1.74	-0.44	0.06	-0.14	-0.18	-0.0225	3.16E-05	0.06
							Total sum of squares = 0.053408		

[$]Treatment combination, [#] Percentage contribution, * Significant variable

Note: The variables C and D are most significant. B is very close for significance. The interaction CD is significant. The interactions AC, BC, and ACD have been included in the Eq. (3.12) to improve accuracy even though these are not significant.

The following model equation (correlation) has been obtained, from statistical design of experiment analysis.

$$Y = (1.5025 - 0.07625B + 0.19375C - 0.065AC - 0.06BC + 0.37D + 0.10875CD - 0.0675ACD) \quad (3.12)$$

The value of a coefficient indicates the magnitude of that effect of the variable. The sign of the coefficient gives the direction of the effect of the variable i.e. positive coefficient indicates an increasing in the value of the response with increase in the value of the variable while a negative coefficient indicates that the response decreases with increase in the value of the variable. The calculated values of the bed expansion ratio from Eq. (3.12) have been compared with the experimental ones taken at conditions other than those used for development of the correlation and have been found to agree with a standard deviation of 4.62 % and an error of ± 10 %. The comparison of the data for the bed expansion ratio has been presented in the Fig. 3.10. Fairly good agreement has been observed between the experimental and the predicted values from the correlation of Song et al. (1989) for air-water system.

3A.5. Phase Holdup

The gas holdup is one of the most important characteristics for analyzing the performance of a three-phase fluidized bed. For chemical processes, where mass transfer is the rate-limiting step, it is important to be able to estimate the gas holdup since this relates directly to the rate of mass transfer (Fan et al., 1987; Schweitzer et al., 2001; Safoniuk et al., 2002). Eqs. (3.1) through (3.3) have typically been used to determine the holdup of each phase in a three phase fluidized bed. Bed height in Eqs. (3.1) and (3.3) is obtained either visually or from the measured pressure drop gradient (Kim et al., 1972; Bhatia and Epstein, 1974; Muroyama and Fan, 1985; Dargar and Macchi, 2006). A more direct method of measuring gas holdup is to simply isolate a representative portion of the test section by simultaneously shutting two quick closing valves and measuring the fraction of the isolated volume occupied by the gas (Meikap et al., 2002; Epstein, 1981). Other most promising methods of measuring the local phase holdup are electrical impedance (resistance) measurement (Razzak et al., 2007, 2009a) and electro conductivity methods (Bhatia and Epstein, 1974; Dhanuka and Stepneck, 1978; Warsito and Fan, 2001, 2003), γ - ray transmission measurements (Ostergaard, 1977; Lee and Al-Dabbagh, 1978), using fiber optic probe (Lee and de Lasa, 1987; Lee et al., 1990; Thompson and Worden, 1997; Wang et al., 2003; Razzak et al., 2009b).

In the present study the solid holdup has been measured using Eq. (3.1) and the experimentally observed expanded bed height. For gas holdup measurement, the methods used are (i) the phase isolation method, and (ii) the bed pressure drop measurement. There is a marginal difference between the two measurements techniques. The variables used in both the methods are also to some extent different as discussed in the corresponding sections.

3A.5.1. Phase holdup measurement by phase isolation method

In the phase isolation method the quick closing valves in the water and air lines were closed simultaneously. At first free board experiment with wide variation of gas and liquid flows were conducted to calculate the two phase fractional gas hold up using Eq. (3.13).

$$\varepsilon_g = \left(\frac{H_c - H_L}{H_c} \right) \tag{3.13}$$

Similarly the gas holdup was calculated for the fluidization experiment with particles. The gas holdup in the three-phase region has been calculated by subtracting the gas

holdup in the two-phase region above the three-phase zone. The region above the expanded bed is the two-phase region. The ranges of the variables studied are: (a) liquid velocity (0.004246 to 0.07436 m/s), (b) gas velocity (0.02123 to 0.10615 m/s), (c) static bed heights (0.177, 0.267 and 0.367 m) and particle sizes (2.18, 3.07 and 4.05 mm).

Fig. 3.11 shows the variation of fractional gas holdup with superficial liquid velocity at different values of fixed superficial gas velocity. It is seen from the figure that with increasing liquid velocity, the gas holdup decreases. However the variation of fractional gas holdup with liquid velocity is very small. It has been reported by Safoniuk et al. (2002) that the fractional gas holdup is practically unaffected by the liquid velocity except at very high liquid superficial velocities. According to Breins et al. (1997a) the gas holdup decreases with liquid velocity but at higher liquid velocity range it remains almost constant. Begovich and Watson (1978), Dhanuka and Stepanek (1978), Lee and de Lasa (1987) have reported a slight decrease in gas holdup with liquid velocity over a large range of the later. At higher liquid velocity, large number of fine bubbles are produced as the flow regime is completely distributed or dispersed, for which the gas holdup should be more. But the decrease in gas holdup with liquid velocity may possibly be due to the fact that at higher liquid velocity the bubbles are fast driven by the liquid. The residence time of the bubbles decreases with the increase in liquid velocity and hence the gas holdup is likely to decrease.

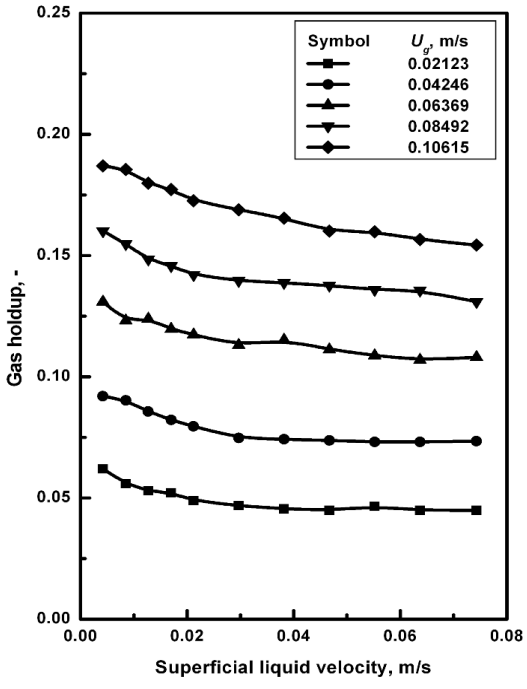

Fig. 3.11. Variation of gas holdup with liquid velocity for different values of gas velocity at [H_s = 0.177 m, d_p 2.18 mm].

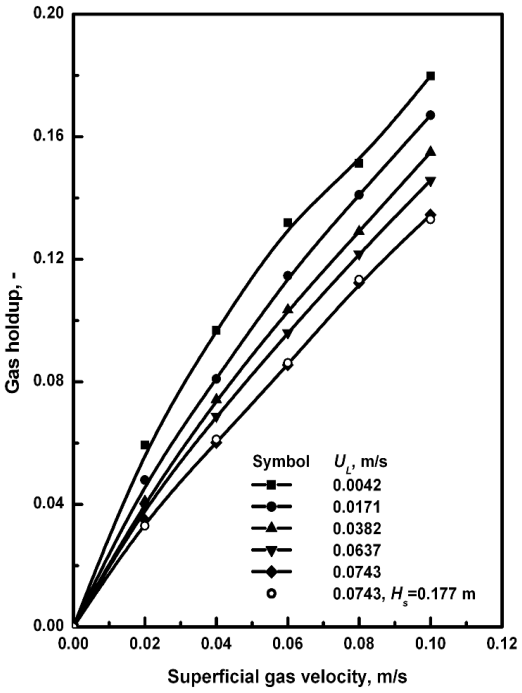

Fig. 3.12. Variation of gas holdup with gas velocity for different values of liquid velocity at [H_s = 0.367 m, d_p = 2.18 m].

Fig. 3.12 represents the variation of fractional gas holdup with superficial gas velocity, at constant liquid velocities. As seen from the figure, the fractional gas holdup increases monotonically with the gas velocity having little higher value of the slope at low gas velocities. This corroborates the findings of Begovich and Watson (1978), Dhanuka and Stepanek (1978), Lee and de Lasa (1987), Briens et al. (1997a), Safoniuk et al. (2002), and Dargar and Macchi (2006). In the lower range of gas velocity, an increase in gas velocity results in the formation of a larger number of gas bubbles without appreciable increase in the bubble diameter. Therefore an increasing fractional gas holdup is observed. As gas velocity increases, the bubble size grows due to bubble coalescence, and consecutively there is a small decrease in the gas holdup. As the experiment has been conducted for the gas velocity range pertaining to the distributed bubble regime, the decrease in slope is not significant which is observed for the transformation from the distributed bubble to the slug flow regime.

In Fig. 3.13 a peculiar behaviour of the variation of fractional gas holdup with superficial liquid velocity is seen for different particle sizes. The gas holdup decreases with liquid velocity. But the variation of gas holdup is different for different particle sizes. This can be divided into two ranges of liquid velocities for each particle size. In the low liquid velocity range, higher the particle size lower is the fractional gas holdup. But in the higher velocity range, the value of gas holdup increases with particle size. Actually the plot presents the gas holdup for both the fixed and the fluidized bed regimes. The gas holdup is low in the fixed bed regime for higher size particle. It is a well known fact that smaller the bubble size i.e. in the distributed bubble flow regime the gas holdup is more. This phenomenon can explain the lower gas holdup for higher size particle in the low liquid velocity range. Higher the particle size higher is the liquid minimum fluidization velocity. In the fixed bed of higher size particles, the interstitial void is large thus higher size of bubbles may be possible which produce a low value of observed gas holdup. But in the higher liquid velocity range i.e. in fluidization regime due to interaction with higher mass of particles, the bubble size may be less for particles of higher sizes due to frequent bubble breakage. Kim et al. (1975) have reported the existence of critical particle size of 2.5 mm in diameter for glass beads of same density for the air-water system, which separates the “bubble coalescing regime” from the “bubble disintegrating regime”. Fan et al. (1987) have shown opposite behaviour for 1, 3, 4 and 6 mm glass beads in aqueous solution of 0.5 wt% of t-pentanol. With increase in particle size, reduced gas holdup has been reported by them.

The effect of static bed height on gas holdup has been found to be negligible, and has not been presented here.

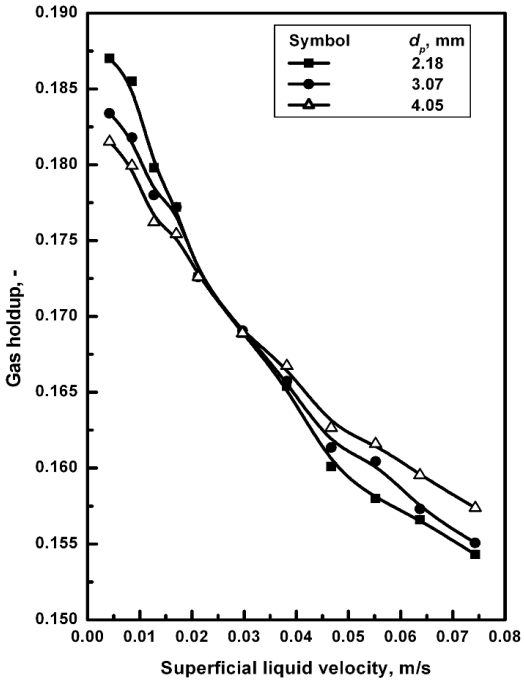

Fig. 3.13. Variation of gas holdup with liquid velocity for different particle sizes at [H_s = 0.367 m, U_g = 0. 10615 m/s].

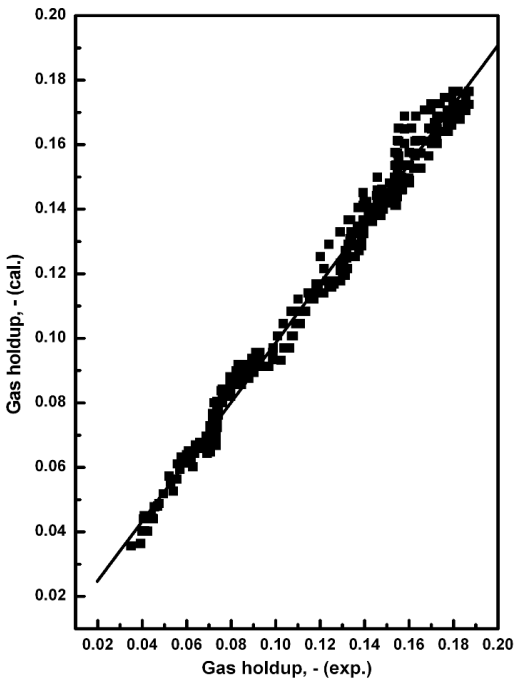

Fig. 3.14. Comparison of experimental values of gas holdup with those calculated from factorial design equation (Eq. (3.14)).

3A.5.1.1. Development of correlation for gas holdup from factorial design analysis

Model equation based on factorial design analysis (Davies, 1978) as discussed in section 3A.4.1 has been used to develop a correlation for the gas holdup. The variables which affect the gas holdup in fluidization are static bed height, particle size, liquid and gas velocity, sparger orifice diameter, density of gas, liquid and solid, viscosity of gas and liquid, surface tension of liquid and the gravitational constant. In the present investigation only four important parameters viz. static bed height, particle size, liquid velocity and gas velocity have been varied.

The scope of the factors considered for factorial experimentation has been presented in Table 3.4. The same procedure as discussed in section 3.3.1 has resulted in the following correlation.

$$Y = 0.104729 + 0.052555C - 0.01564D - 0.00429BC) \qquad (3.14)$$

The calculated values of gas holdup from Eq. (3.14) have been compared with experimental ones in Fig. 3.14 and have been found to agree within a standard deviation of ± 10 %. Fig. 3.15 shows the comparison of experimental values of gas hold up with the calculated ones from the correlations developed by Hughmark (1967), Hitika et al.

(1974 and 1980), Kato et al. (1985), Saberian-Broudjenni et al. (1987) and Nikov et al. (1990). A very close agreement between the gas hold values obtained from the present experiment and predicted from literature correlations has been obtained as is evident from Fig. 3.15.

Table 3.4: Scope of the factors for gas and liquid holdup

Sl. No.	Actual variable	Factorial design symbol	Min. level (-1)	Max. level (+1)	Magnitude of variables
1	H_s, m	A	0.177	0.367	0.177,0.267,0.367
2	d_p, m	B	0.00218	0.00405	0.00218,0.00305,0.00405
3	U_g, m/s	C	0.02	0.10	0.02,0.04,0.06,0.08,0.10
4	U_L, m/s	D	0.0042	0.0743	0.0042,0.0085,0.0127,0.0170, 0.0212,0.0297,0.0382,0.0467, 0.0552,0.0637,0.0743

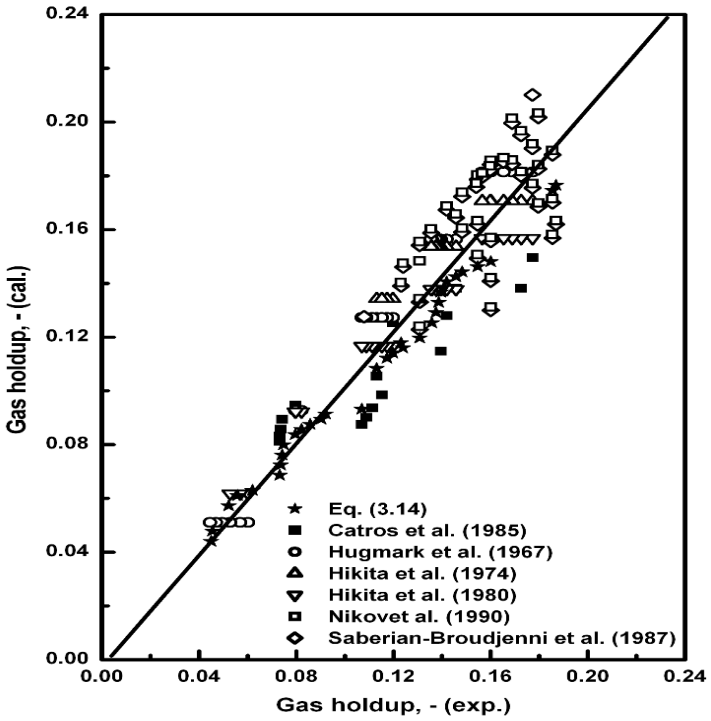

Fig. 3.15. Comparison of experimental values of gas holdup with those calculated from correlations reported values in the literature.

Fig. (3.16) and (3.17) present the variation of liquid holdup with superficial liquid velocity at various constant gas velocities and with gas velocity at different values of constant liquid velocity respectively. It has been observed that with the increase in liquid velocity the liquid holdup increases sharply and with increase in gas velocity at constant liquid velocity the liquid holdup decreases. The effect of liquid velocity and particle size on liquid holdup is shown in Fig. (3.18). It is seen that with increase in particle size the

liquid holdup decreases. The observed trends are in agreement with reported values (Dhanuka and Stepank, 1978).

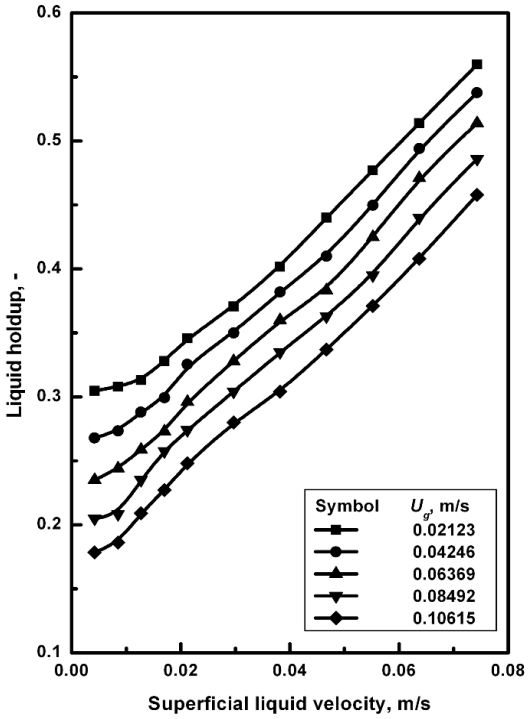

Fig. 3.16. Effect of liquid velocity on liquid holdup for different values of gas velocity at [H_s = 0.267, d_p = 2.18 mm].

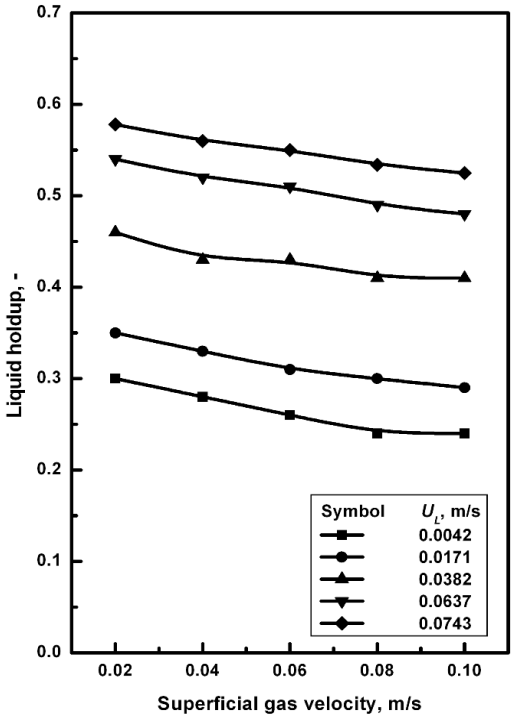

Fig. 3.17. Effect of gas velocity on liquid holdup for different values of liquid velocity at [H_s = 0.367 m, d_p = 2.18 mm].

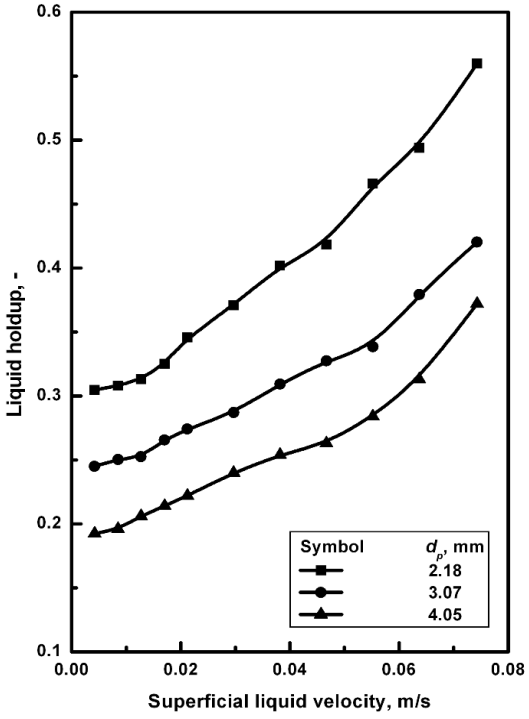

Fig. 3.18. Effect of liquid velocity on liquid holdup for different particle sizes at [U_g = 0.02123 m/s, H_s = 0.267 m].

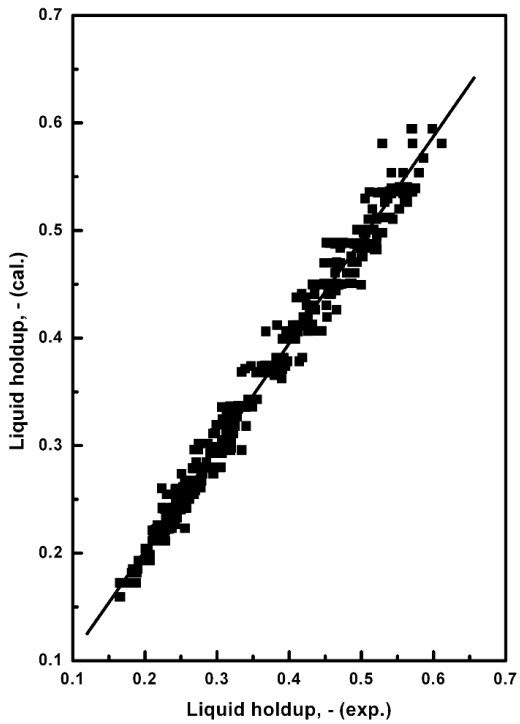

Fig. 3.19. Comparison of experimental values of liquid holdup with those calculated from factorial design equation (Eq. (3.15)).

For the prediction of liquid holdup a model equation based on factorial design analysis (Davies, 1978) has been developed. The scope of the factors considered for factorial experimentation is same as for the gas holdup and has been presented in Table 3.4. Identical variables affect the liquid holdup as well as the gas hold-up.

The following equation has been obtained,

$$Y = 0.370493 - 0.03472B + 0.156263D - 0.02654BCD) \quad (3.15)$$

The calculated values of liquid holdup from Eq. (3.15) have been compared with the experimental ones in Fig. 3.19 and have been found to agree within a standard deviation of ±10 %. The comparison of experimental values of liquid holdup with the values calculated from different correlations available in literature has been presented in Fig. 3.20. A fairly good agreement between the experimental values and those predicted from literature correlations has been observed.

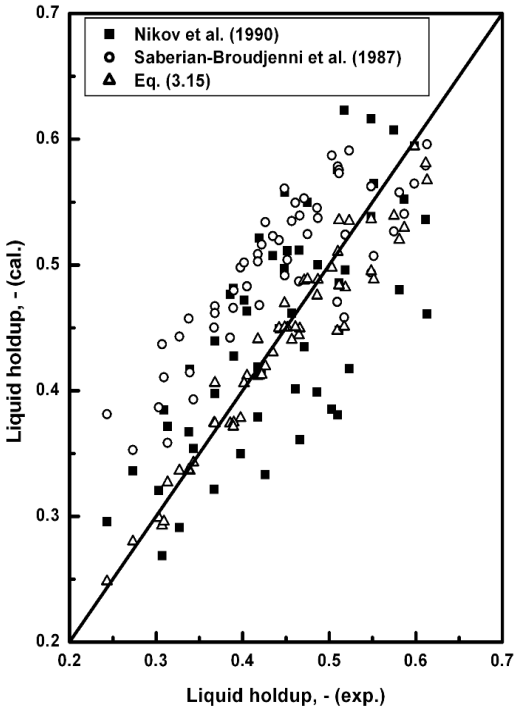

Fig. 3.20. Comparison of experimental values of liquid holdup with those calculated from Nikov et al. (1990) and Saberian et al. (1987).

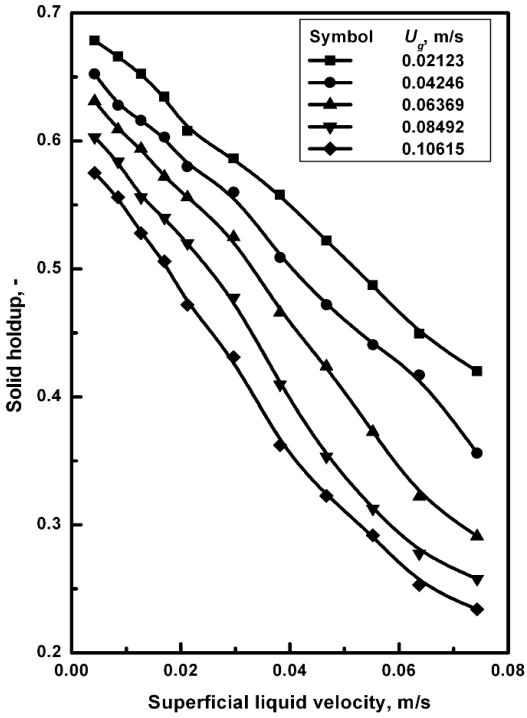

Fig. 3.21. Effect of liquid velocity on solid holdup for different values of gas velocity at [H_s = 0.177 m, d_p = 2.18 mm].

Figs.3.21 and 3.22 present the variation of solid holdup with liquid velocity at various values of fixed gas velocity and with gas velocity at different fixed values of liquid velocity respectively. It is seen that with increase in liquid and gas velocity the solid holdup decreases. As it was previously observed, the expanded bed height increases with increase in both liquid and gas velocities, thus with increased expanded bed height the particles concentration decreases so also the solid holdup. The effect of liquid velocity

and particle size on solid holdup is shown in Fig. 3.23. It is seen that solid holdup increases with increase in particle size. With increase in particle size the expanded bed height decreases, thus particle concentration remains high for particles of higher size under the same liquid and gas velocities and so also the solid holdup.

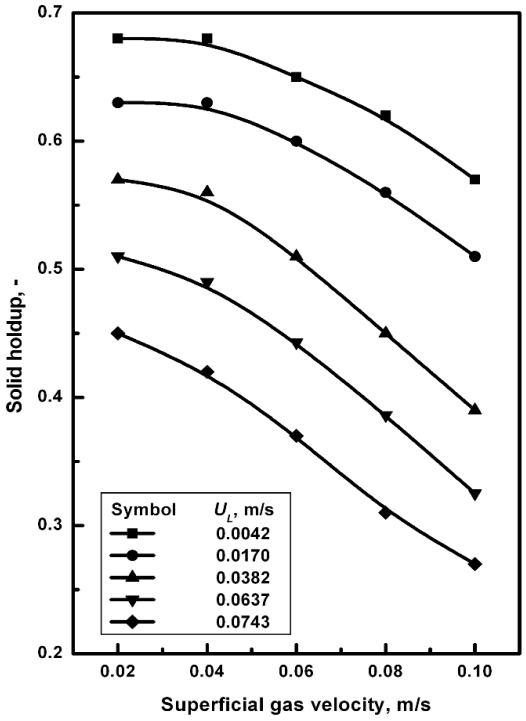

Fig. 3.22. Effect of gas velocity on solid holdup for different values of liquid velocity at [H_s = 0.367 m, d_p = 2.18 mm].

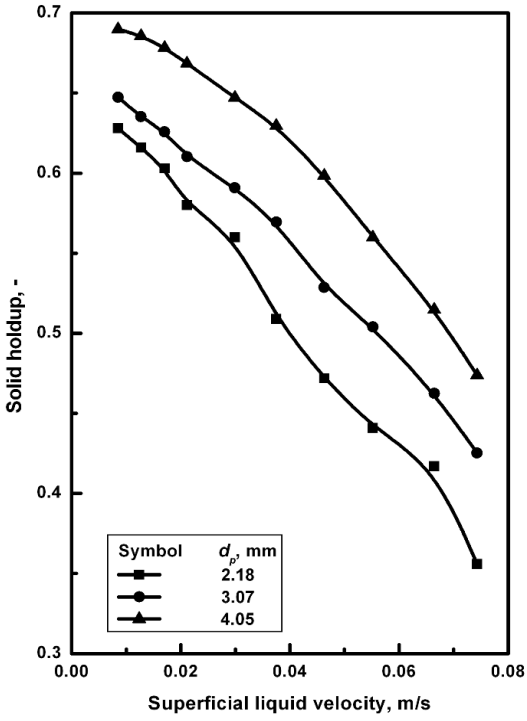

Fig. 3.23. Effect of liquid velocity on solid holdup for different particle sizes at [U_g = 0.04246 m/s, H_s = 0.367 m].

3A.5.2. Gas holdup determination from bed pressure drop measurement

An attempt has been made to measure the gas hold-up from pressure drop measurement for comparison. The variation of bed pressure drops in the fluidization regime (i.e. at higher fluid flow rates than at minimum fluidization) with superficial liquid velocity at constant values of gas velocity has been shown in Fig.3.4. The dotted line in the figure shows the effective bed weight per unit area. The experimental pressure drop in the fluidization regime for liquid-solid system agrees well with that of the calculated buoyant weight per unit area. For gas-liquid-solid system the observed bed pressure drop recorded in manometer is found to be less than that for liquid-solid bed. With higher values of gas flow rate, the observed bed pressure drop decreases further. This is due to the increased gas holdup in the bed which decreases the hydrostatic pressure. For superficial gas velocity of 0.10615 m s^{-1}, negative bed pressure drop has been measured by the manometer. The equivalent liquid column of the difference in bed pressure drop

of the liquid-solid and gas-liquid-solid bed has been considered to be the region of the column filled with gas. The gas holdup has been calculated using the following equation.

$$\varepsilon_g = \frac{(\Delta p^{Ls} - \Delta p^{gLs})/(\rho_L g)}{H_e} \tag{3.16}$$

In Eq. (3.16) H_e is the expanded fluidized bed height. The measured bed pressure drop ΔP reported has been taken to be the pressure drop between the same two tappings. This has been done in order to avoid the interference of the gas holdup of the bubble column region on the top of the gas-liquid-solid bed. The range of variables studied in this study includes all presented in Table 3.1 except the static bed heights of 0.177, 0.267, and 0.367 m. In this method a broader range of gas and liquid velocities have been studied which was not possible in the phase isolation method in this study. In addition, the effect of liquid viscosity and surface tension on gas holdup has also been included in this work, since the use of high viscous and low surface tension liquids, enhanced the gas hold up (Safoniuk et al., 2002).

3A.5.2.1. Dimensional analysis

An industrial three-phase fluidized bed can be simulated and scaled up perfectly from a laboratory small-scale cold flow model by developing an extensive set of dimensionless groups from dimensional analysis of transport equations. The scaling is proper if the dimensionless groups are perfectly respected. Both geometric and dynamic similarity should be considered for understanding and developing correlations which can provide predictions which are valid for industrial units. In doing so the first step is to identify all the variables that are expected to have a significant effect on the gas holdup dynamics. Then an appropriate set of dimensionless groups can be developed by applying Buckingham Pi theorem.

Previous studies on three-phase fluidized beds by Fan et al. (1987), Safoniuk et al (1999), and Jena et al. (2008a) have identified ten variables (U_L, U_g, μ_L, σ_L, ρ_L, $\Delta\rho g$, ρ_p, d_p, H_s, D_c) which are expected to influence the gas holdup significantly. The gas density has been incorporated in the buoyancy ($\Delta\rho g$). Using these ten significant variables which involve three fundamental dimensions (mass, length and time), seven independent dimensionless groups can be formed according to Buckingham Pi theorem. Keeping in mind the advantage of using groups that are relevant to multiphase flow, two sets of seven independent dimensionless groups has been developed by rearrangement as;

Set-1: $\mathrm{Re}_c = \frac{\rho_L D_c U_L}{\mu_L}$, $Fr_g = \frac{U_g^2}{gD_c}$, $We = \frac{\rho_L D_c U_L^2}{\sigma_L}$, $\Delta\beta_d = \frac{(\rho_L - \rho_g)}{\rho_L}$, $\beta_d = \frac{\rho_p}{\rho_L}$, $d_r = \frac{d_p}{D_c}$, and $H_r = \frac{H_s}{D_c}$

Set-2: $Mo = \frac{g\mu_L^4}{\rho_L \sigma_L^3}$, $Eo = \frac{\Delta\rho g D_c^2}{\sigma_L}$, $Fr_L = \frac{U_L^2}{gD_c}$, $Fr_g = \frac{U_g^2}{gD_c}$, $\beta_d = \frac{\rho_p}{\rho_L}$, $d_r = \frac{d_p}{D_c}$, and $H_r = \frac{H_s}{D_c}$

The combinations Weber number (*We*), Reynolds number (Re), and Froude number (*Fr*) or Morton number (*Mo*) and Eötvös number (*Eo*) are used to characterize the multiphase flow of bubbles or drops moving in a surrounding fluid. Morton number (*Mo*) is the combination of Weber number (*We*), Reynolds number (Re), and Froude number (*Fr*). In the present work it has also been found that the second set gave a better value of coefficient of determination (R-square) of 0.972 in comparison to the first set which resulted in a R-square value of 0.947 in developing the model equation from traditional regression analysis. Therefore in the present study an attempt has been made to use the second set for analysis of the gas holdup dynamics. The experimental results have been presented graphically using the dimensionless groups and in some cases as dimensional variable.

Fig. 3.24 shows the variation of fractional gas holdup with liquid Froude number at different values of fixed gas Froude number. It is seen from the figure that with increasing liquid Froude number, the gas holdup decreases. However the variation of fractional gas holdup with liquid Froude number is small. At higher liquid Froude number large number of fine bubbles are possible as the flow regime is completely distributed or dispersed, for which the gas holdup should be more. But the decrease in gas holdup with liquid Froude number may possibly be due to the fact that at higher liquid Froude number the bubbles are fast driven by the liquid. The residence time of the bubbles decreases with the liquid Froude number and hence the gas holdup is likely to decrease.

Fig. 3.25 represents the variation of fractional gas holdup with gas Froude number, at constant liquid Froude numbers. As seen from the figure, the fractional gas holdup increases monotonically with the gas Froude number having higher value of the slope at low gas Froude numbers. In the lower range of gas Froude number, an increase in gas Froude number results in the formation of a larger number of gas bubbles without

appreciable increase in the bubble diameter. Therefore an increasing fractional gas holdup is observed. As gas velocity increases, the bubble size grows due to bubble coalescence, and relatively the slope of gas holdup line decreases. The decrease in slope may be due to the transformation of flow from the bubble to the slug flow regime.

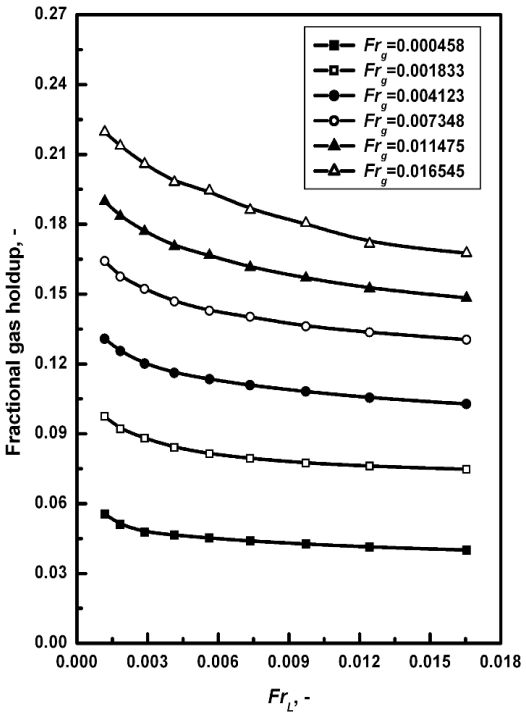

Fig. 3.24. Variation of gas holdup with liquid Froude number for different gas Froude numbers at [H_s/D_c = 2.56, d_p/D_c = 0.0307, ρ_P/ρ_L = 2.263, Mo = 1.1078x10^{-11} and Eo = 1370.66].

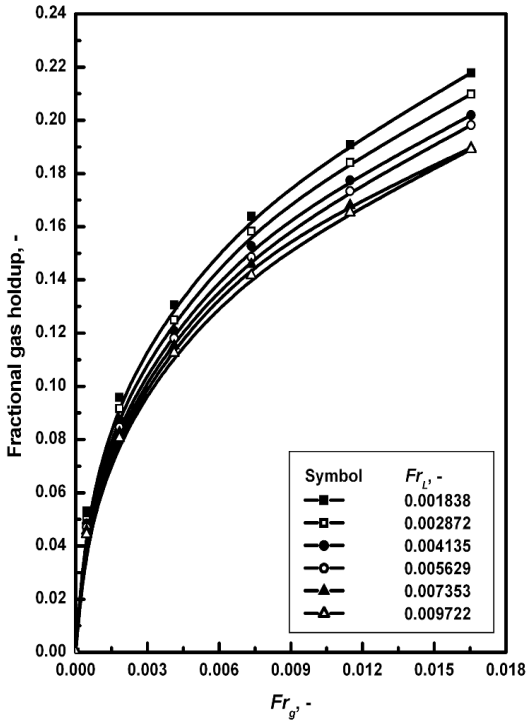

Fig. 3.25. Variation of gas holdup with gas Froude number for different liquid Froude numbers at [H_s/D_c = 2.56, d_p/D_c = 0.0405, ρ_P/ρ_L = 2.270, Mo = 1.1078x10^{-11} and Eo = 1370.66].

In Fig. 3.26 the variation of fractional gas holdup with liquid Froude number has been represented for different ratios of particle size to column diameter keeping all other variables constant. As the density of particles of different sizes is different, there is a variation in the ratio of the density of the particle to the density of the liquid as mentioned on the figure. The gas holdup decreases with liquid velocity like the above finding (Fig. 3.24). But the measured gas holdup is found to increase with particle size. A significant variation of the fractional gas holdup is seen between the particle sizes of 2.18mm to 4.05mm, but the variation magnitude is less for particles smaller than 2.18 mm and larger than 4.05mm. Similar results have been obtained in the phase isolation method as shown in Fig. 3.13. This may be due to the same phenomena as discussed for Fig. 3.13. The difference in gas holdup for particles of different sizes is more in the higher liquid Froude number. This may be due to the better fluid particle interaction and higher mass of particles adds up to its bubble breaking behaviour in such a situation, thus

resulting in large number of small size bubbles which is in agreement with Dargar and Macchi (2006)in air-water system.

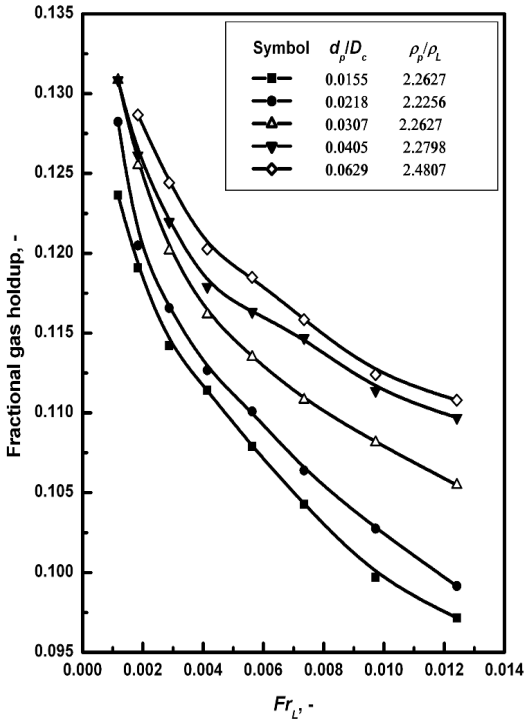

Fig. 3.26. Variation of gas holdup with liquid Froude number for different d_p/D_c at [H_s/D_c = 2.56, Fr_g = 0.004123, Mo = 1.1078x10^{-11} and Eo = 1370.66].

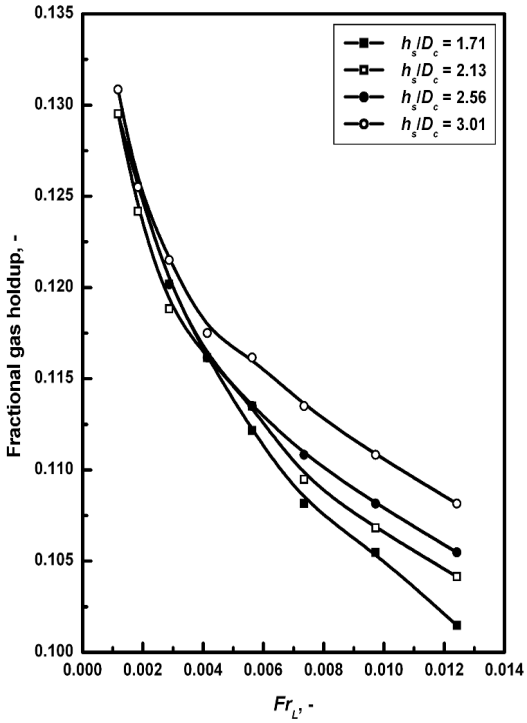

Fig. 3.27. Variation of gas holdup with liquid Froude number for different H_s/D_c at [d_p/D_c = 0.0307, ρ_P/ρ_L = 2.263, Fr_g = 0.004135, Mo = 1.1078x10^{-11} and Eo = 1370.66].

The variation of fractional gas holdup with liquid Froude number for different ratios of the initial static bed height to the column diameter (H_s/D_c) at constant values of other variables is shown in Fig. 3.27. It is clear from the figure that at low liquid Froude number range the gas holdup is almost same for different values of H_s/D_c. But at high liquid Froude number range, i.e. at higher bed voidage, there is a little increase in the gas holdup with H_s/D_c. This may possibly be due to the gas-liquid-solid interaction for a longer time in the bed for higher initial static bed height or H_s/D_c. Study on the effect of bed inventory on gas holdup is not seen in the literature.

Fig. 3.28 represents the variation of fractional gas holdup with gas Froude number for different liquid solutions, at constant values of liquid Froude number, d_p/D_c, H_s/D_c. Similar trend of gas holdup with the variation of gas Froude number has been observed in this case as was observed in case of water (Fig. 3.25). As represented in Fig. 3.28, due to variation of the liquid density, viscosity and surface tension with aqueous solutions of glycerol, there is a change in Morton number (Mo) and Eötvös number (Eo) and ρ_p/ρ_L. With increase in both Morton number (Mo) and Eötvös number (Eo), the gas holdup has

been found to increase. Similar results have been obtained by other investigators like Fan et al. (1987), Song et al. (1989), Safoniuk et al. (1999, 2002). The enhancement of gas hold up with the use of high viscous and low surface tension liquids is due to the following reasons. Higher liquid viscosity exerts higher drag on the gas bubble; the same is done by lower surface tension of liquid due to formation of surface tension gradient on the bubble surface. A higher drag results in lower bubble rise velocity and hence higher holdup. Lower surface tension of liquids also makes the generation and existence of fine bubbles possible thus by possessing higher residence time in the system increases the gas holdup.

Fig. 3.29 shows the effect of liquid to gas velocity ratio on the fractional gas holdup. It is seen from the figure that the fractional gas holdup versus the velocity ratio plot shows two distinct regimes. With the decrease in velocity ratio, there is a small increase in the fractional gas holdup in the beginning but below a certain value of velocity ratio the holdup fraction starts increasing at a faster rate. Hence it can be concluded that there is an optimum velocity ratio below which it is advantageous to operate the three-phase fluidized bed system. The separation of the higher and lower gas holdup regime at the optimum velocity ratio has been represented as a dotted line in Fig.3.29.

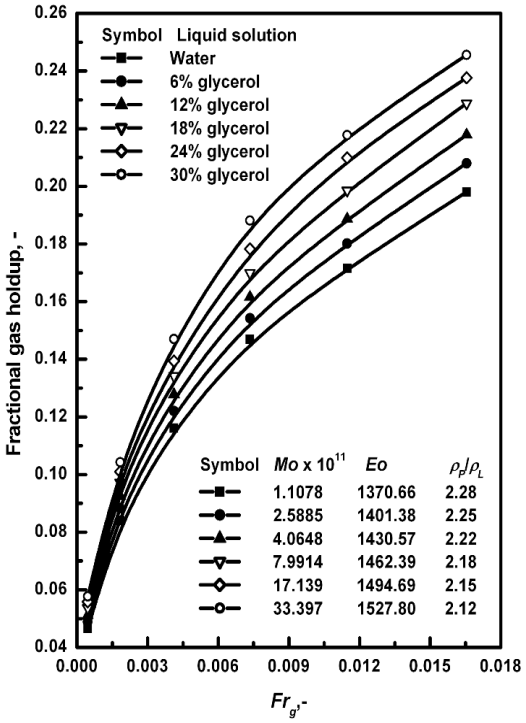

Fig. 3.28. Variation of gas holdup with gas Froude number for different liquids at [H_s/D_c = 2.56, d_p/D_c = 0.0405, Fr_L = 0.004135].

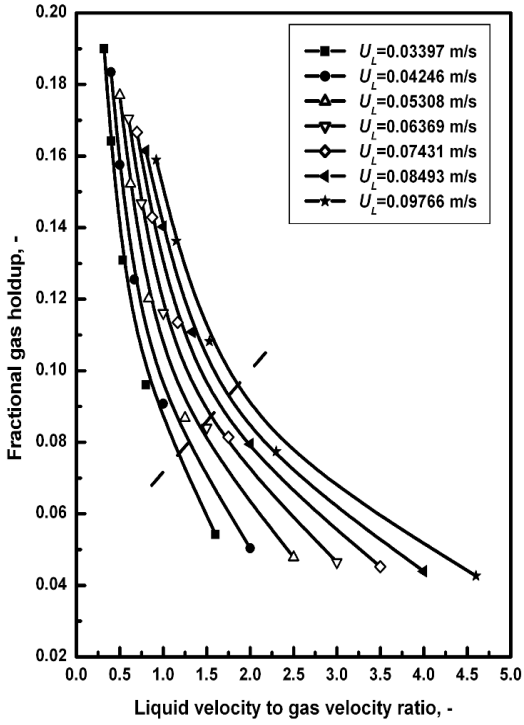

Fig. 3.29. Variation of gas holdup with liquid to gas velocity ratio for different values of liquid velocity at [H_s = 0.256 m, d_p = 3.07 mm].

Fig. 3.30 shows the variation of the fractional gas holdup obtained from the experiment and those predicted from the correlations proposed by various researchers with gas velocities at a constant liquid velocity. The experimental data is almost the same as predicted by the correlation of Begovich and Watson (1978). There is also a very close agreement between the experimental and the predicted gas hold up from the correlation of Yu and Rittman (1997) at low gas velocity, but as the gas velocity increases the gas velocity deviates negatively from the experimental. Correlation of Safoniuk et al. (2002) for all the ranges predict high values for the gas hold up, where as correlations of Catros et al. (1985) and Song et al. (1989) predict the gas holdup values around the experimental ones, which is differs with the variation in gas velocity. For gas velocities less than 0.04 m/s and 0.06 m/s correlations of Catros et al. (1985) and Song et al. (1989) respectively, predict gas holdup more than the experimental, where as for the higher gas velocity than these, the predicted gas holdup is less than the experimental ones for liquid velocity of 0.07431 m/s.

3A.5.2.2. Development of model equation by regression analysis

Empirical model equations have been developed to express the gas holdup behaviour from the experimental data by traditional regression analysis and least square estimation using Gauss-Newton method with the aid of SYSTAT R7 software. In this method , first the dependency of the response on each individual group has been expressed as the power law relationship keeping all other groups constant as, ε_g = A1 $(Mo)^{a1}$, with Eo, Fr_L… etc constant, ε_g = A2 $(Eo)^{a2}$, with, Mo, Fr_L… etc constant. Then the response ε_g expressed as ε_g = C$((Mo)^{a1}(Eo)^{a2}(Fr_L)^{a3}\ldots)^{B}$, where A1, A2, …, C are the coefficients and a1, a2, …., B are the exponents. The following Eq. (3.17) has been obtained. In developing the model 36 numbers of data sets have been used. The R-square value of the developed equation is 0.972. The equation fits another 204 number of data sets with a standard deviation of 0.07.

$$\varepsilon_g = 8\times10^{-7}(Mo)^{0.051}(Eo)^{2.046}(Fr_L)^{-0.079}(Fr_g)^{0.360}(\beta_d d_r)^{0.063}(H_r)^{0.074} \qquad (3.17)$$

An attempt has been made to develop a more precise model taking large number of data sets with high R-square value and low standard deviation using non-linear regression method. Any regression analysis needs that data to be uncorrelated. Therefore, Pearson's correlation coefficient for all pairs of variables considered in this study has been calculated. The correlation analysis suggests that most of the input variables are not correlated to each other except for a few combinations like Mo and Eo, Mo and β_d and Eo and β_d due to involvement of a common parameter like liquid density in these

combinations. The correlation coefficients between the input variables and the output variable (gas holdup) are quite good and satisfy the statistical acceptable limit. Hence, the data can be reasonably assumed to be independent. Non-linear regression equation is developed based on least square estimation using Gauss-Newton method. The model so developed using software SYSTAT R7 is given as Eq. (3.18).

$$\varepsilon_g = (Mo)^{0.05}(Eo)^{0.157}(Fr_L)^{-0.093}(Fr_g)^{0.401}(\beta_d)^{-0.096}(d_r)^{0.081}(H_r)^{0.026} \qquad (3.18)$$

In order to validate the model, coefficient of determination (R^2) has been calculated and it is found to be 0.997. Further, residual analysis has been made to check the robustness of the model. It is found that the residual is normally distributed with mean 0.001 (almost zero) and standard deviation of 0.003 (very small).It is observed that there is small fluctuation of residuals between -0.009 to 0.007 about the zero value (Fig. 3.31). This confirms that the model can predict the values with sufficient accuracy. Upper and lower confidence interval of model parameters at 95% has been estimated and is found to be in the range of -0.005 to 0.404.

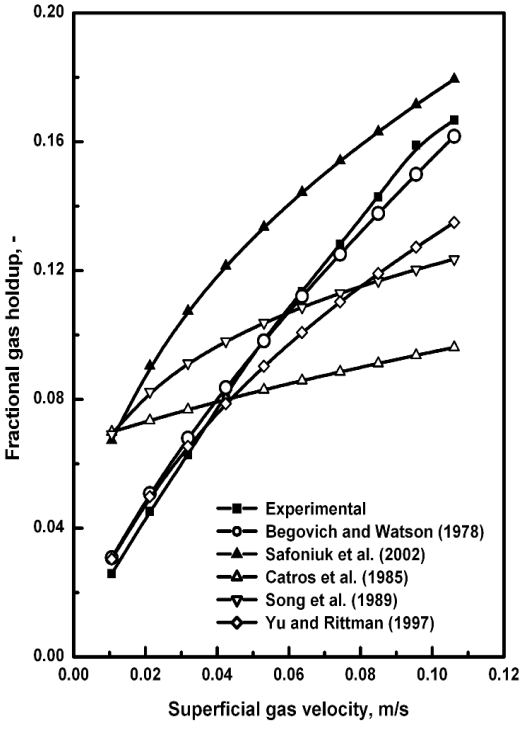

Fig. 3.30. Comparison of gas holdup from literature correlations with present investigation.

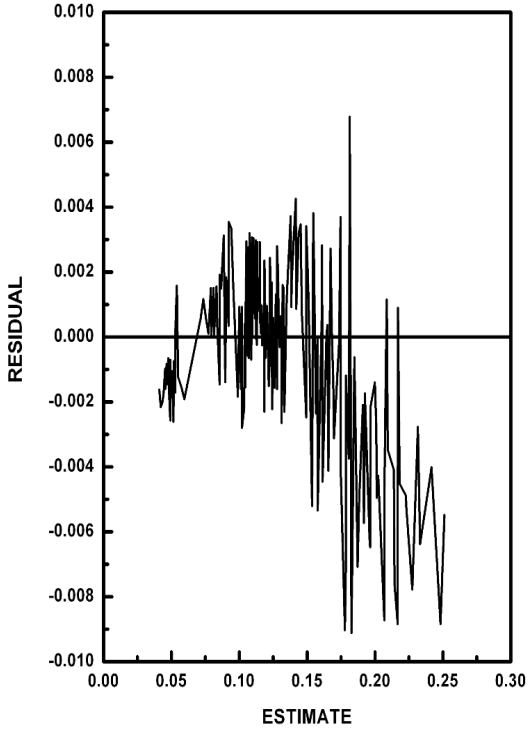

Fig. 3.31. Distribution of residuals.

The experimentally found gas holdup has been compared with the ones calculated from Eqs. (3.17) and (3.18) in Fig. 3.32. It is seen that the Eq. (3.18) is a better fit to the experimental gas holdup. Thus the empirical model (Eq. (3.18)) is precise enough for the

prediction of gas holdup and has been used to optimize the operating conditions for finding the highest possible gas holdup in the experimental domain.

To check the validity of the proposed Eq. (3.18), experiments have been conducted at another concentration of glycerol (44% by mass) as appeared in literature (Safoniuk et al., 2002). The experimental result has been compared with the predicted values from Eq. (3.18) and the correlation available in literature (Fan et al., 1987; Gorowara and Fan, (1990); Ramesh and Murugesan (2002); Safoniuk et al. (2002)) and presented in Fig. 3.33. It is seen from Fig. 3.33 that there is a close agreement between the experimental values and those predicted from Eq. (3.18). The correlation of Safoniuk et al. (2002) predict higher values of gas holdup at lower gas velocities (lower Fr_g) and lower values of gas holdup at higher gas velocities, but the agreement is within 25% with the present experimental values. This difference may be due to the non-existence of all other parameters except the modified gas Reynolds number in correlation of Safoniuk et al. (2002).

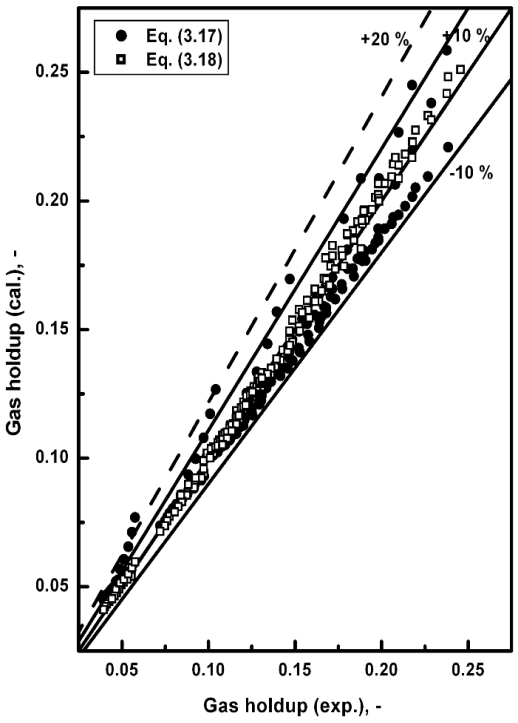

Fig. 3.32. Comparison of the experimental values of gas holdup with the calculated ones.

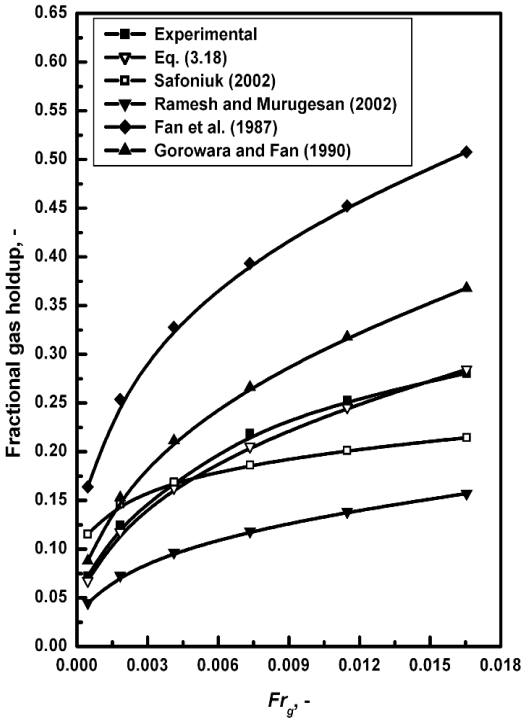

Fig. 3.33. Comparison of the gas holdup (experimental) with those calculated from the literature correlations.

The predicted values of gas holdup from the correlation of Ramesh and Murugesan (2002) although shows the same trend in the variation of gas holdup with Fr_g, but the predicted values are lower than the experimental ones. The cause may be the air sparger

used by them is a single nozzle type which might be producing large size bubbles moving centrally in the column without proper distribution. Surfactant has not been a consideration in the present study but as the glycerol possesses low surface tension, using glycerol the surface tension of the solution has altered and its effect on the gas holdup has been expressed in form of *Mo* and *Eo* in the proposed correlation. From Fig. 3.33 it is observed that under similar flow conditions, the gas holdup predicted from the correlations (Fan et al., 1987; Gorowara and Fan, 1990) developed using surfactants predict higher values of gas holdup. On the whole the trend in the variation of gas holdup for the present study agrees well with the predicted values from the correlations proposed by other investigators.

3A.5.3. Optimization of operating conditions

Hydrodynamic behaviour of a three-phase fluidized bed is quite complex and the empirical equations used to explain the system behavior is highly nonlinear; thus making the analysis difficult. Any attempt to optimize process parameters for maximum gas hold up, becomes still cumbersome. As many interacting variables operate in non-linear fashion, it is difficult to obtain global solution using traditional optimization tools. Hence, parametric optimization has been done using genetic algorithm, a popular evolutionary technique, with the aim to obtain global best values with reasonable computational time and less mathematical rigor.

The optimization problem for maximization gas holdup can be defined as follows:

Maximize ε_g (3.19)

Subjected to constraints (operating limits of each dimensionless group in the experimental domain):

$1.1078\text{x}10^{-11} \leq Mo \leq 3.3397\text{x}10^{-10}$ (3.20)

$1370.663 \leq Eo \leq 1527.798$ (3.21)

$4.59\text{x}10^{-4} \leq Fr_L \leq 2.52\text{x}10^{-2}$ (3.22)

$4.58\text{x}10^{-4} \leq Fr_g \leq 2.52\text{x}10^{-2}$ (3.23)

$2.124 \leq \beta_d \leq 2.481$ (3.24)

$0.0155 \leq d_r \leq 0.0629$ (3.25)

$1.71 \leq H_r \leq 3.01$

(3.26)

Genetic algorithms (GAs) are mathematical optimization techniques that simulate a natural evolution process. They are based on the Darwinian Theory, in which the fittest species survives and propagates while the less successful tends to disappear. The concept of genetic algorithm is based on the evolution process and was introduced by Holland

(1975). Genetic algorithm mainly depends on the following types of operators: reproduction, crossover, and mutation. Reproduction is accomplished by copying the best individuals from one generation to the next, in what is often called an elistic strategy. The best solution is monotonically improving from one generation to the next. The selected parents are submitted to the crossover operator to produce one or two children. The crossover is carried out with an assigned probability, which is generally rather high. If a number randomly sampled is inferior to the probability, the crossover is performed. The genetic mutation introduces diversity in the population by an occasional random replacement of the individuals. The mutation is performed based on an assigned probability. A random number is used to determine if a new individual will be produced to substitute the one generated by crossover. The mutation procedure consists of replacing one of the decision variable values of an individual, while keeping the remaining variables unchanged. The replaced variable is randomly chosen, and its new value is calculated by randomly sampling within its specific range. The pseudo-code for standard genetic algorithm is presented below. Where S_a is initial population.

The standard genetic algorithm
{
Generate initial population, S_a
Evaluate population, S_a
While stopping criteria not satisfied repeat
{
Select elements from S_a to put into S_{a+1}
Crossover elements of S_a and put into S_{a+1}
Mutate elements of S_a and put into S_{a+1}
Evaluate new population S_{a+1}
$S_a = S_{a+1}$
}
}

The computational algorithm was implemented in C^{++} code. In this work, roulette wheel selection, single point crossover, and standard bit-wise mutation have been adopted. In genetic optimization, population size, probability of crossover and mutation are set at 20, 25%, and 5% respectively. Number of generation is varied till the output is converged. The flow chart of the method is depicted in Fig. 3.34.

The optimum conditions of the group variables with the optimum performance output i.e. the maximum gas holdup are given by;

$[Mo, Eo, Fr_L, Fr_g, \beta_d, d_r, H_r, \varepsilon_g]$

$= [3.21\text{x}10^{-10}, 1487.57, 1.10\text{x}10^{-3}, 1.55\text{x}10^{-2}, 2.2797, 0.0588, 2.747, 0.282].$ (3.27)

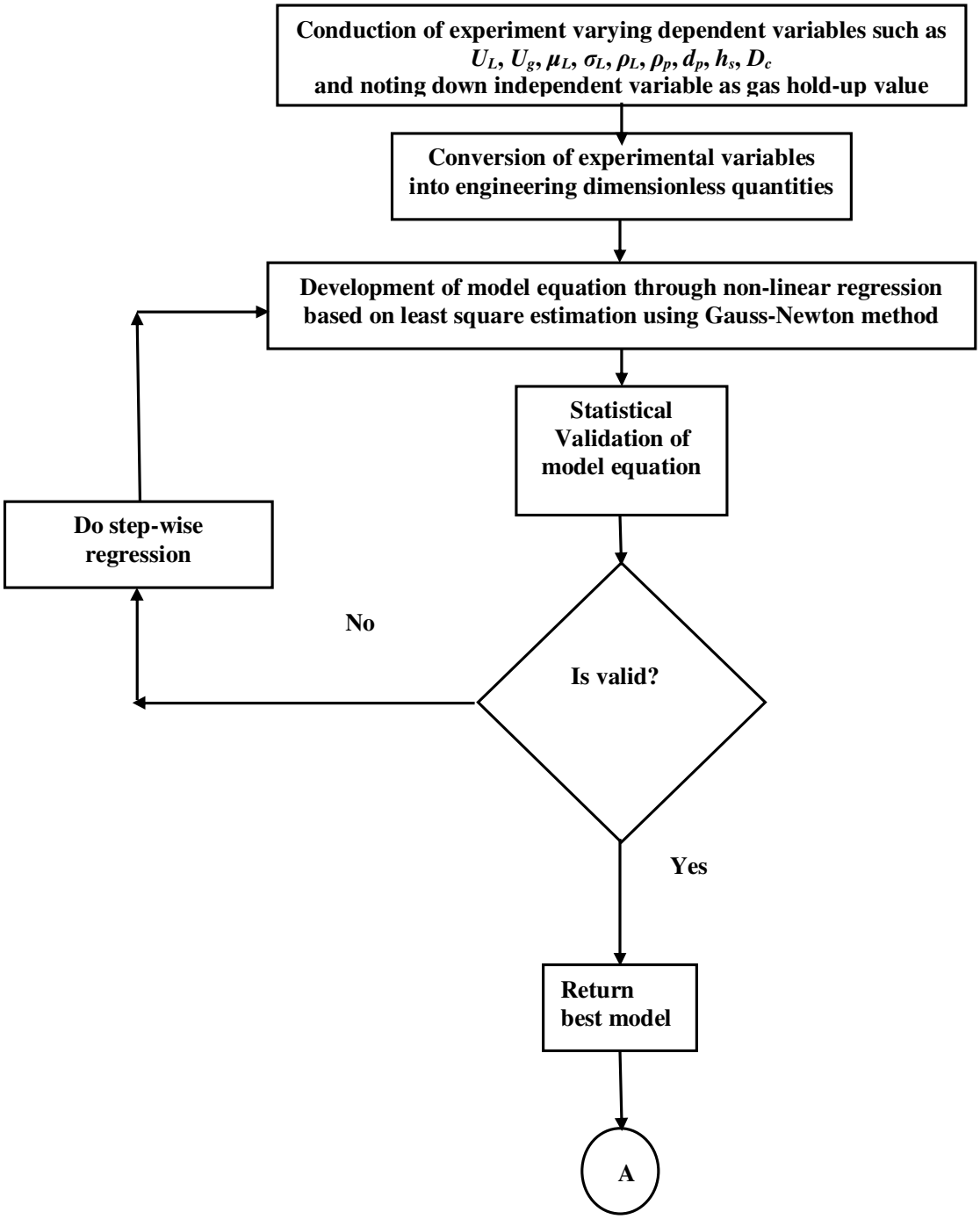

Fig. 3.34. Flow chart of the method.

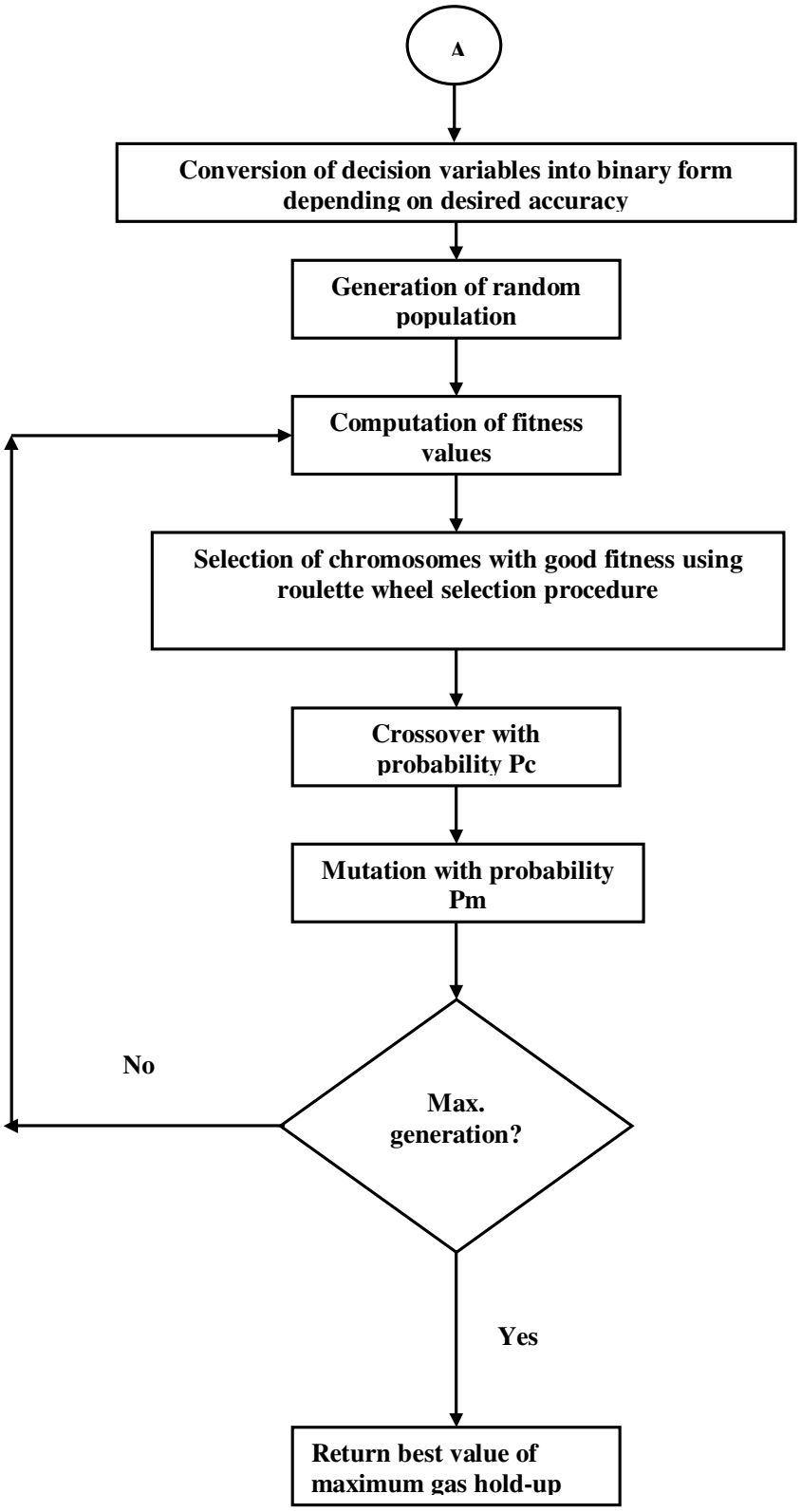

Fig. 3.34. Flow chart of the method (continued).

The convergence curve is shown in Fig. 3.35. The optimum gas holdup in the experimental domain is found to be 0.282. As discussed in the preceding gas holdup dynamics section 3.4.2.1, the gas holdup increases with Mo, Eo, Fr_g, d_r and H_r but decreases with Fr_L and β_d. Thus a higher gas holdup is expected at higher values of Mo, Eo, Fr_g, d_r and H_r and lower value of Fr_L and β_d. The determined maximum gas holdup in the experimental domain is not at the extreme values of these variables because of the presence of interaction among the variables. The trade-off among them yields an optimum combination of the engineering groups with a maximum possible gas holdup value.

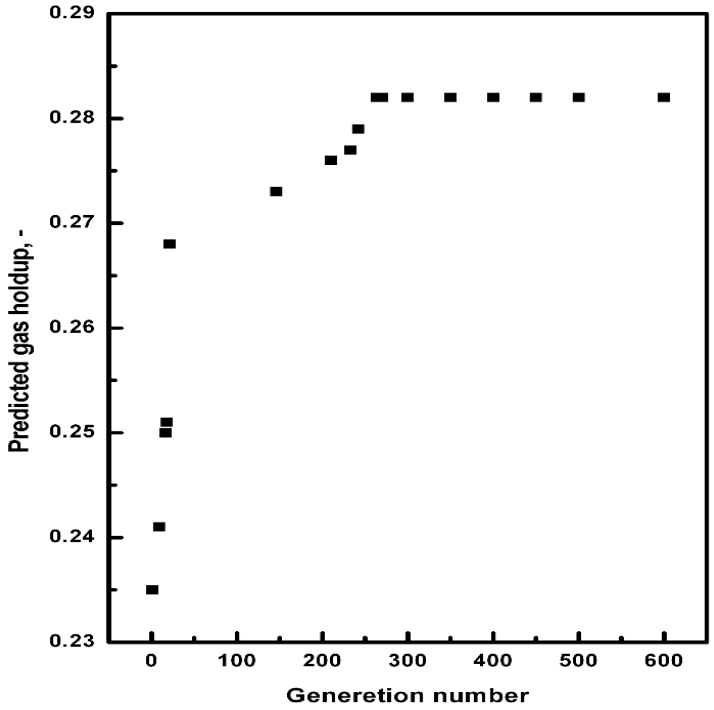

Fig. 3.35. Convergence curve.

3B. *Hydrodynamic study of hollow cylindrical particles*

3B.1. Introduction

The critical review of the literature as discussed in chapter-1, reveals that the solid phase used in the hydrodynamic study is either (a) spherical particles: like glass beads, steel balls, plastic beads and other spherical catalyst particles, (b) cylindrical particles: like aluminum cylinders and pvc cylinders, other cylindrical catalyst particles and (c) irregular particles like: sand, irregular gravel, quartz particles etc. having sphericity ranging from 0.68–1.0 approximately. Three-phase fluidized beds have been applied successfully in the bio-oxidation process for wastewater treatment in which various low-to-moderate density solid particles of different shape and size are used as cell support. In such reactors high surface area of the particle is desirable, which can be used as solid support for microorganisms, thus resulting in higher mass transfer rate. This can be achieved by the use of hollow cylindrical particles as, these possess very high surface to volume ratio i.e. of low sphericity.

3B.2. Experimental

The present study has been conducted to examine the hydrodynamic behavior viz. the pressure drop, minimum liquid fluidization velocity, bed expansion and phase hold up of a co-current gas-liquid-solid three-phase fluidized bed (as shown in Fig. 2.1) with an antenna air sparger using liquid as the continuous phase and gas as the discontinuous phase. Ceramic raschig rings having sphericity of 0.58 have been used as the solid phase as it is of moderate density and high surface to volume ratio due to its hollow cylindrical structure. The other phases, liquid and gas are tap water and the oil free compressed air respectively. Experiments have been conducted at a temperature of 25^0 C. The same experimental procedure has been adopted as discussed for the spherical particles. The scope of the experiment is presented in Table 3.5.

Table 3.5: Scope of the experiment

A. Properties of bed materials				
Materials	**L = OD, m**	**ID, m**	**Spherical volume-equivalent diameter, m**	**ρ_p (kg/m^3)**
Ceramic raschig ring	0.0066	0.0033	0.006864	1670
Initial static bed height (m)	0.154	0.214	0.264	0.314
B. Properties of fluidizing medium			**ρ (kg/m^3)**	**μ (Pa.s)**
Air at 25^0C			1.187	0.0000181
Water at 25^0C			997.15	0.000891
C. Properties of manometric fluid			**ρ (kg/m^3)**	**μ (Pa.s)**
Mercury			13,574	0.001526
Carbon tetra-chloride (CCl_4)			1,600	0.000942

The phase isolation method has been used to measure the gas holdup in the low-moderate fluid flow rates. Experiments have been conducted with the gas and liquid flow rates which varied from 0 - 0.1274 m/s and from 0 – 0.1486 m/s respectively.

3B.3. Pressure drop and minimum fluidization velocity

Fig. 3.36 shows the variation of pressure drop with superficial liquid velocity in gas-liquid-solid system for different initial static bed heights. Experimental pressure drop values are close to those obtained from basic force balance in two phase fluidization, indicating no wall effect to fluidization in this case. As the ratio of column diameter to the equivalent diameter of the cylindrical particle is 14.5 wall effect is not expected, since wall effect is prominent when the ratio is less than 8. It has been observed that bed mass (or initial static bed height) has no effect on minimum fluidization velocity. At all the bed heights the minimum liquid fluidization velocity has been found to be 0.02654 m/s. The pressure drop profile with variation of superficial liquid velocity for gas-liquid-solid system at different constant superficial gas velocities is shown in Fig. 3.37. It can be seen from this figure that the minimum liquid fluidization velocity decreases with the gas velocity. The decrease in minimum liquid fluidization velocity may be due the contribution of the gas to the total drag on the particles by the gas-liquid up ward flow. The relative velocity may promote fluidization at a lower liquid fluidization velocity.

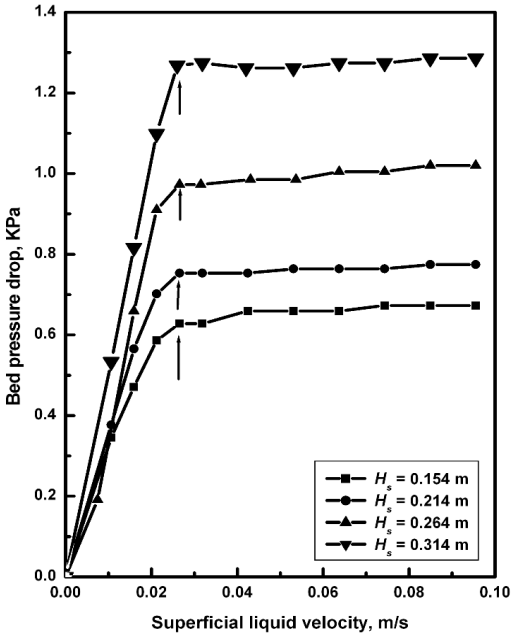

Fig. 3.36. Variation of bed pressure drop with liquid velocity for different static bed heights at U_g = 0.06369 m/s.

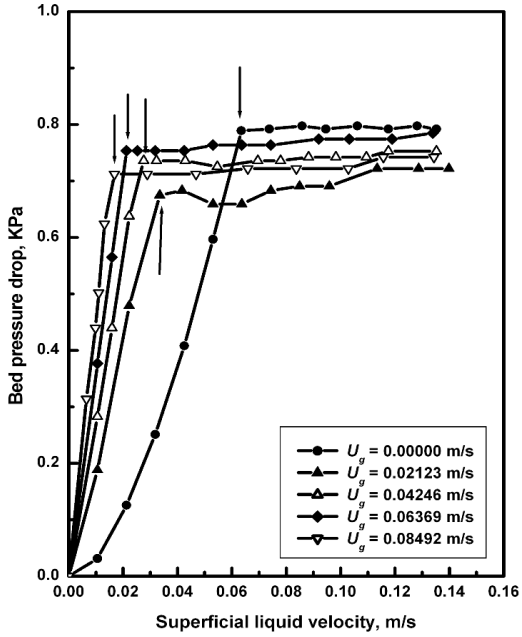

Fig. 3.37. Variation of bed pressure drop with liquid velocity for different values of gas velocity at H_s = 0.214 m.

Fig. 3.38 shows the variation of minimum liquid fluidization velocity (U_{Lmf}) with superficial gas velocity. It can be seen from the figure that the rate of decrease in minimum liquid fluidization velocity is large at lower gas velocity but the rate decreases as gas velocity increases. The sharp decrease in minimum liquid fluidization velocity with introduction of the gas indicates the bubble supported fluidization in presence of gas, but with increase in the gas velocity the contribution of the gas to fluidization decreases. In the present study continuous decrease in U_{Lmf} has been observed with gas velocity whatever small the change may be. This corroborates the previous finding with spherical particles. The minimum liquid fluidization velocity for liquid-solid fluidization is within 5% that predicted from the correlation of Wen and Yu (1966) marked as short horizontal line in Fig. 3.38. Song et al. (1989) have experimentally predicted the minimum liquid fluidization velocity by pressure gradient method for cylindrical hydrotreating catalysts in a three-phase fluidized bed. They have proposed the following correlation (Eq. (3.28)) for the prediction of U_{Lmf} in a three-phase fluidized bed with cylindrical particles.

$$\frac{U_{Lmf}}{U_{Llmf}^{Ls}} = 1 - 376 U_g^{0.327} \mu_L^{0.227} d_e^{0.213} (\rho_s - \rho_L)^{-0.423} \tag{3.28}$$

Eq. (3.28) has been used to calculate the U_{Lmf} for the present case of hollow cylindrical particles. The calculated values using the equivalent diameter have been compared in Fig. 3.38. Very close agreement is seen between the calculated and the experimental values. In some cases both the values have been found to be almost the same. In the present case only gas velocity and initial static bed height have been varied keeping all other parameters constant. From Fig. 3.36, it is observed that bed mass (initial static bed height) has no effect on minimum liquid fluidization velocity. Thus superficial gas velocity being the only variable, a correlation in the dimensional form has been developed for U_{Lmf} as under;

$$U_{Lmf} = 0.0049 U_g^{-0.518} \tag{3.29}$$

(with a correlation factor of 0.9564 and standard deviation of 0.0698).

By using the above correlation values of U_{Lmf} have been calculated for different gas velocities and have been compared with their respective experimental values. The values calculated from correlation have been found to agree well with the experimental ones with standard and mean deviation of 0.06975 and 0.06014 respectively. Thus, the correlation given by Eq. (3.29) can be used for such systems to predict U_{Lmf} at all values of gas velocity except the zero gas velocity.

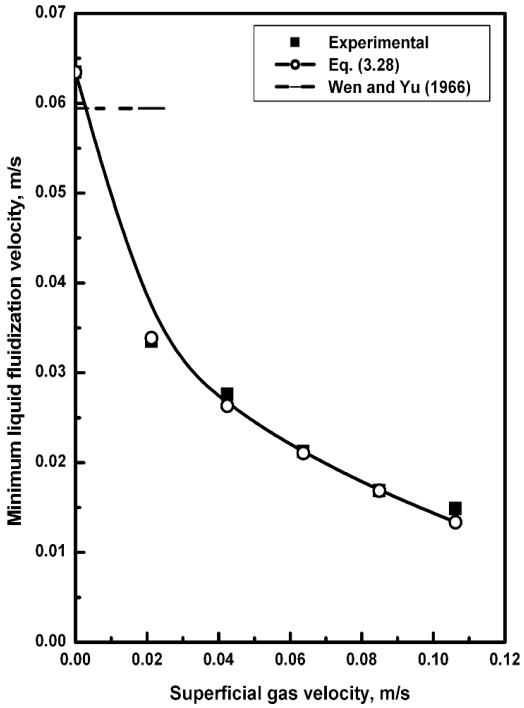

Fig. 3.38. Variation of minimum liquid fluidization velocity with gas velocity.

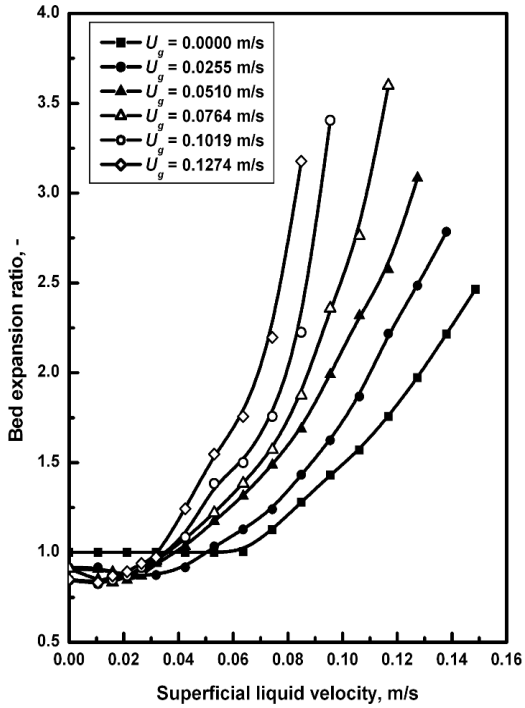

Fig. 3.39. Variation of bed expansion ratio with liquid velocity for different values of gas velocity at H_s = 0.214 m.

3B.4. Bed voidage

The same method as used for the spherical particles has been used for the measurement of expanded bed height. The bed expansion study carried out by varying liquid velocity (at a constant gas velocity) has been presented in terms of bed expansion ratio in Fig. 3.39. It is seen from the figure that the bed expansion ratio increases with increase in both the liquid and the gas velocities. The bed voidage or bed porosity is defined as the fraction of the bed volume occupied by both liquid and gas phases and as such directly proportional to the expanded bed height. As in the present study hollow cylindrical particles have been used as the solid phase, the bed expansion simply does not relate to the bed voidage unless the volume of the hollow section is taken into account. The bed voidage has been calculated by considering the hollow volume and has been represented graphically in Fig. 3.40 for the conditions above the minimum fluidization. Song et al. (1989) have modified the original Begovich and Watson (1978) correlation by introducing shape factor term for calculation of bed voidage of cylindrical particles in three-phase fluidized bed with air and water as the gas and the liquid phases respectively, which is given as:

$$\varepsilon = 3.93\phi_s^{-0.424} U_L^{0.271} U_g^{0.041} \mu_L^{0.055} d_e^{-0.268} D_c^{-0.033} (\rho_s - \rho_L)^{-0.316} \qquad (3.30)$$

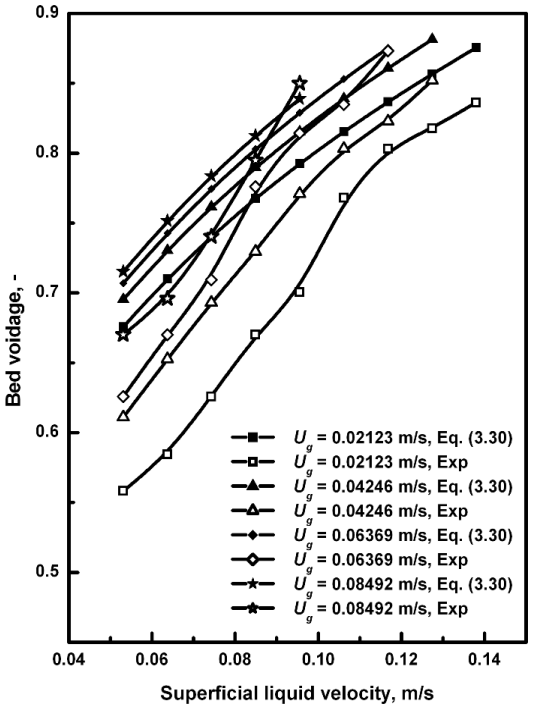

Fig. 3.40. Variation of bed voidage with liquid velocity for different values of gas velocity at H_s = 0.214 m.

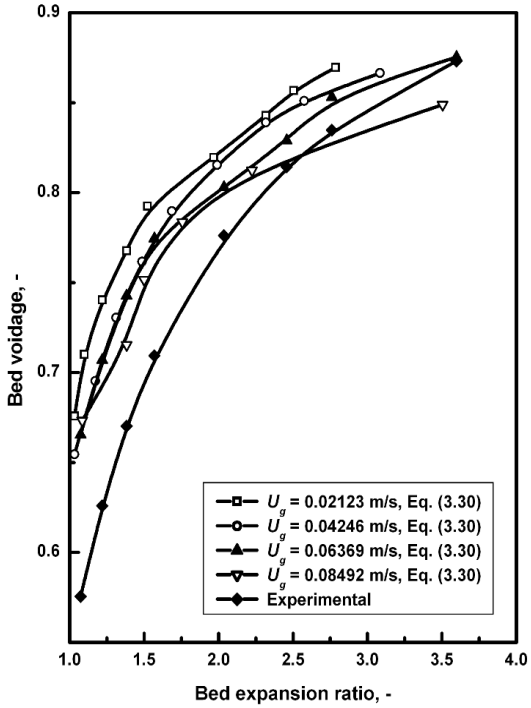

Fig. 3.41. Variation of bed voidage with bed expansion ratio for different values of gas velocity at H_s = 0.214 m.

The values of bed voidage both experimental and calculated from Eq. (3.30) have been plotted against superficial liquid velocity at different constant gas velocities in Fig 3.40. It is clear from the plot that the bed voidage increases with increase in both the liquid and the gas velocities. The bed voidage is a strong function of liquid velocity, but is a weak function of gas velocity. In most of the cases the values of the experimental bed voidage have been found to be less than those calculated from Eq. (3.30), the deviation being relatively higher at lower liquid velocities and near close agreement for the higher ones. This may be due to the fact that the correlation developed by song et al. (1989) might have based on their experimental bed voidage obtained at higher gas and liquid velocities than the present study. Thus it can be emphasized that Eq. (3.30) can be used for calculating the bed voidage at higher gas and liquid velocities where the bed expansion ratio is nearly greater than 2.5. In Fig. 3.41 the plot of bed voidage (experimental and calculated from Eq. (3.30)) vs. bed expansion ratio shows the same trend. A singe line for experimental bed voidage is seen in the figure for all gas velocities as the former has been calculated from the experimental bed expansion ratio. Fig. 3.42 shows the variation of bed voidage with the ratio of superficial liquid to gas velocity. It is clear from the plot that for higher gas velocities (liquid to gas velocity ratio < 2.0), there exists very close agreement between the experimental bed voidage and that calculated from Eq. (3.30).

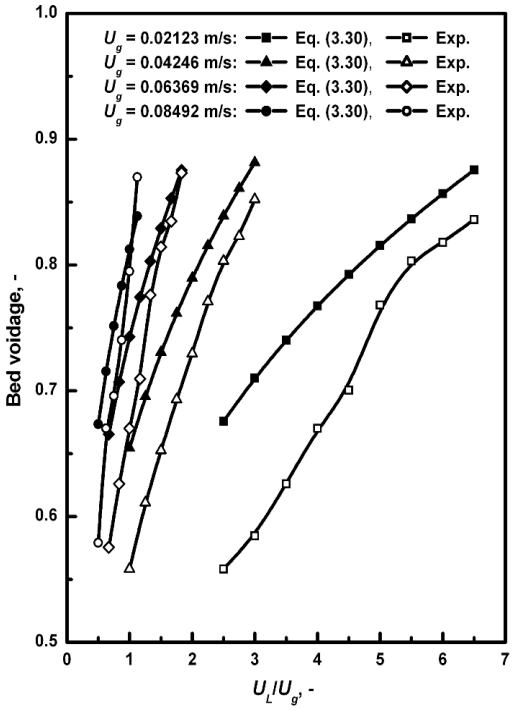

Fig. 3.42. Variation of bed voidage with ratio of liquid to gas velocity for different values of gas velocity at H_s = 0.214 m.

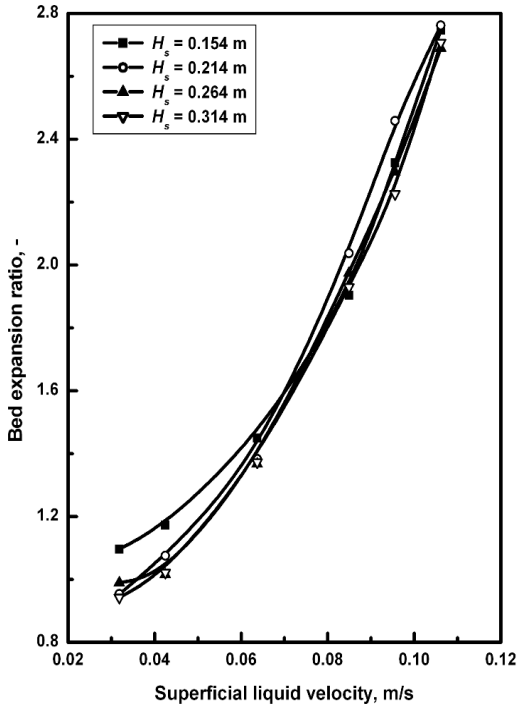

Fig. 3.43. Variation of bed expansion ratio with liquid velocity for different initial static bed heights at gas velocity of 0.06369 m/s.

A simple correlation has been developed from the experimental data of bed voidage above the minimum fluidization condition up to a bed expansion ratio of about 3.5 times that of the initial static bed height. In this experiment the particle size, sphericity and density of the solid, viscosity and density of liquid, and column diameter are constant. Thus the bed expansion (or bed voidage) determined here is a simple function of gas and liquid velocities and initial static bed height. Fig. 3.43 is the plot of the variation of bed expansion ratio with superficial liquid velocity at a constant gas velocity for different initial static bed heights. It is clear from the plot that the bed voidage is not a function of the initial static bed height as the bed expansion ratio is more or less same for all the cases. Thus the bed voidage for the present case is a function of the gas and the liquid velocities only and for the range of 0.04246 m/s $\leq U_L \leq$ 0.1486 m/s and 0.02123 m/s $\leq U_g \leq$ 0.1247 m/s, can be presented as:

$$\varepsilon = 3.29 U_L^{0.422} U_g^{0.147} \tag{3.31}$$

(with a standard deviation of 0.02483, mean deviation of 0.01910 and a correlation coefficient of 0.9701)

The bed voidage values calculated from Eqs. (3.30) and (3.31) have been compared with the experimental ones in Fig. 3.44. Fairly good agreement is seen between the experimental values and with those calculated by both the equations for air-water system.

More than 65% of the data of Song et al. (1989) and all values from present correlation are within 10%, where as all the values from Eq. (3.30) is within 20% but with almost positive deviation from experimental ones.

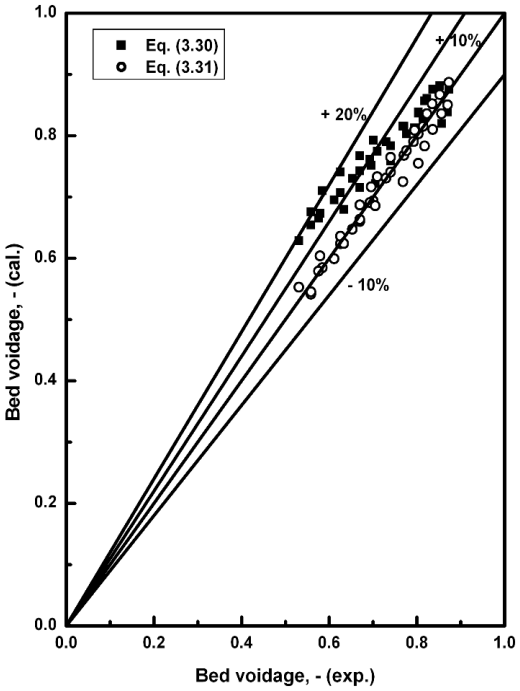

Fig. 3.44. Comparison of calculated values of bed voidage from Eqs. (3.30) and (3.31) with the experimental values.

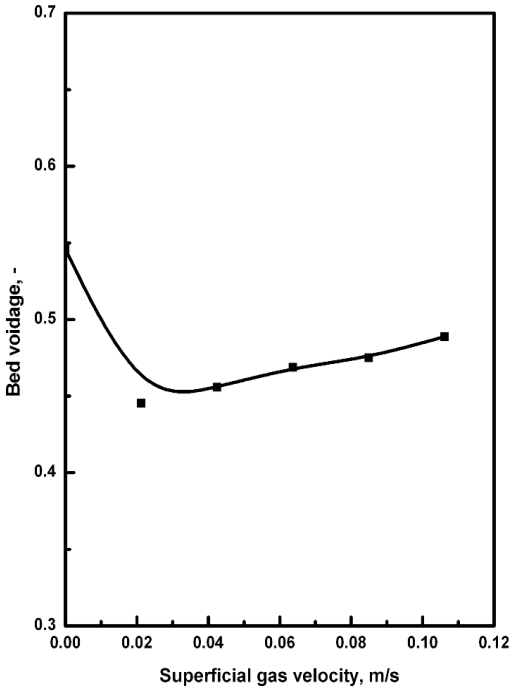

Fig. 3.45. Variation of bed voidage with gas velocity at minimum fluidization at H_s = 0.214 m.

Fig. 3.45 shows the variation of bed voidage with superficial gas velocity at minimum fluidization. The minimum fluidization condition has been determined from pressure drop profile and the bed height by visual observation. Then the bed voidage has been calculated from bed height at minimum fluidization. It is clear from the plot that bed voidage of three-phase bed is less than that of the liquid-solid bed for all gas velocities. At the introduction of the gas the bed voidage is first reduced and then with increase of the gas velocity it increases. Kim et al. (1975) have shown a continuous increase in bed voidage for 6 mm glass beads and 2.6 mm irregular gravels, but decrease in bed voidage for 1mm glass beads for air-water system. It is indicated from the figure that in the presence of gas phase a more compact bed is possible than in two-phase liquid solid system. The injection of small amount of gas causes the bed to collapse, but with increase in gas velocity the bed voidage again increased. The increasing trend is same as of Kim et al. (1975) for large particles as with increase of gas velocity the bubble size increases.

3B.5. Gas holdup

Fig. 3.46 shows the variation of fractional gas holdup with superficial liquid velocity at different values of fixed superficial gas velocity. It is seen from the figure that with increasing liquid velocity, the gas holdup decreases. However the variation of fractional gas holdup with liquid velocity is very small. Several workers have reported that the fractional gas holdup is practically unaffected by liquid velocity except at very high liquid superficial velocities (Safoniuk et al., 2002). According to Dhanuka and Stepanek (1978) and Song et al. (1989) there is a slight decrease in gas holdup with liquid velocity. This may possibly be due to the lower residence time of the gas bubbles in the bed at higher liquid velocities.

Fig. 3.47 represents the variation of fractional gas holdup with superficial gas velocity, at constant liquid velocities. As seen from the figure, the fractional gas holdup increases monotonically with the gas velocity with relatively higher values of the slope at low gas velocities. This corroborates the findings of Dhanuka and Stepanek (1978) and Safoniuk et al. (2002). In lower range of gas velocity, an increase in gas velocity results in the formation of a larger number of gas bubbles without appreciable increase in the bubble diameter. Therefore an increasing fractional gas holdup is observed. As gas velocity increases the bubble size grows due to bubble coalescence, with relative decrease in gas holdup. As the experiment has been conducted for the gas velocity range pertaining to the distributed bubble regime, the decrease in slope is not significant which is observed for the transformation to the slug flow regime.

In air-water systems, both coalesced bubbling and dispersed bubbling regime are observed and the gas holdup behaviour strongly depends upon the flow regime. In the present experimental range of gas liquid velocities mainly dispersed bubbling regime is observed. For dispersed bubbling regime, the gas holdup in three-phase fluidized beds containing cylindrical catalysts, correlation in terms of gas particle Froude number (Fr_g) and the liquid particle Reynolds number (Re_L) has been proposed by Song et al. (1989), which is as under,

$$\varepsilon_g = 0.28 Fr_g^{0.126} \, \mathrm{Re}_L^{-0.087} \tag{3.32}$$

This correlation predicts much lower values of gas holdup than the experimental ones as shown in Figs. 3.48 and 3.49. At low gas velocity the gas holdup calculated from Eq. (3.32) is close to experimental value, but as the gas velocity increases the deviation becomes more and more. The latest correlation for predicting gas holdup available in

literature for cylindrical solid particles is by Safoniuk et al. (2002). They have proposed the correlation for gas holdup in terms of modified gas Reynolds number (Re_g), which is given by Eq. (3.33).

$$\varepsilon_g = 0.014\,\mathrm{Re}_g^{\,0.426} \tag{3.33}$$

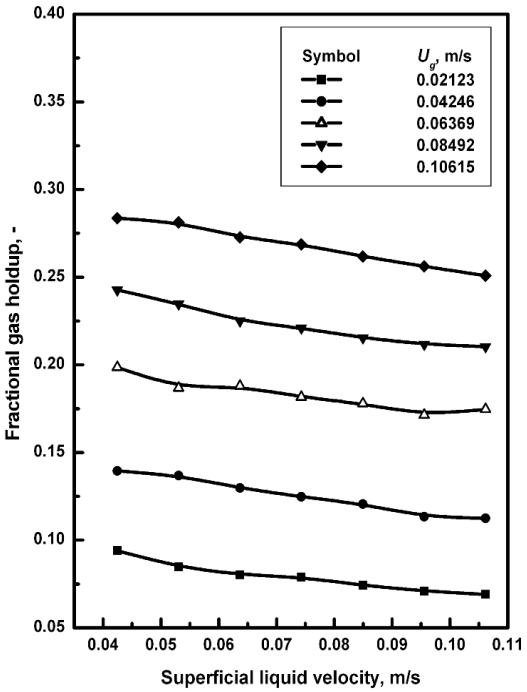

Fig. 3.46. Variation of gas holdup with liquid velocity for different values of gas velocity at H_s = 0.214 m.

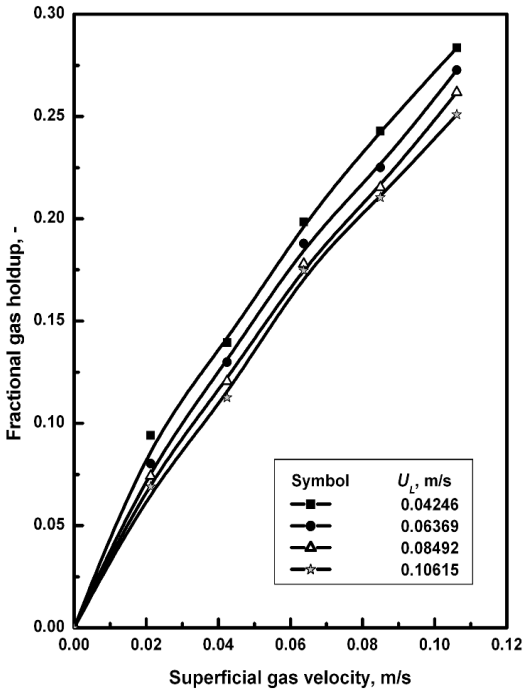

Fig. 3.47. Variation of gas holdup with gas velocity for different values of liquid velocity at H_s = 0.214 m.

Gas holdup predicted from Eq. (3.33) has been compared with that obtained from the present experiment in Figs. 3.48 and 3.49. It is seen from Fig. 3.48 that Eq. (3.33) predicts the gas holdup higher than the experimental ones at lower gas velocities, but close agreement is there at higher gas velocities. As both the correlations are not accurately predicting the gas holdup for hollow cylindrical particles for the present range of experiments, a correlation in the form of Eq. (3.32) has been proposed here to predict the gas holdup. For this the results have been fitted to a power-law equation passing through origin (zero gas holdup at zero gas flow). For the range of $362.275 \le \mathrm{Re}_L \le 905.772$ and $0.0067 \le Fr_g \le 0.1674$, this leads to:

$$\varepsilon_g = 1.357\,Fr_g^{0.384}\,\mathrm{Re}_L^{-0.147} \tag{3.34}$$

(with a standard deviation of 0.039 and a correlation coefficient of 0.994).

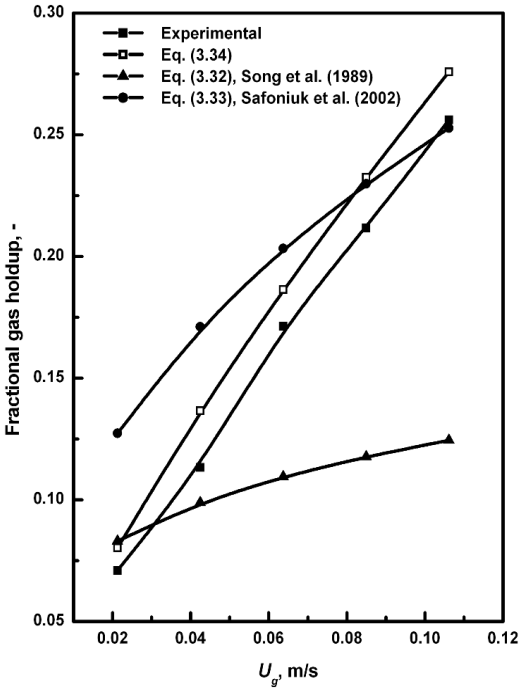

Fig. 3.48. Variation of experimental and calculated values (from correlations) of gas holdup with gas velocity at H_s = 0.214 m.

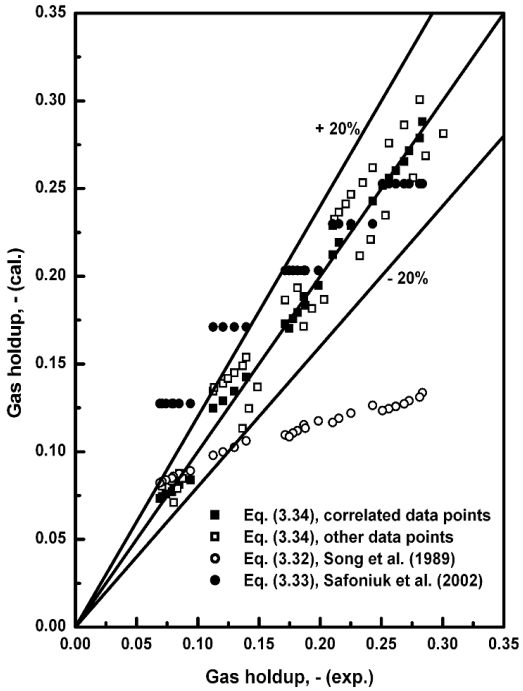

Fig. 3.49. Comparison of experimental values of gas hold-up with those calculated from Eqs. (3.32), (3.33) and (3.34).

Close agreement between the values of gas holdup predicted from Eq. (3.34) and the experimental ones is seen from Figs. 3.48 and 3.49. From the experimental data some have been taken for the development of correlation as Eq. (3.34). Rest of the experimental data along with those used for developing the correlation has been compared with those of the calculated values of gas holdup from Eq. (3.34). More than 95% are within 10%, where as all are within 20%. This shows a very good agreement and the significance of the developed correlation. Except at lower values of gas velocity i.e. at lower gas hold up range for all other cases the predicted gas holdup from Eq. (3.33) of Safoniuk et al. (2002) is within 20% deviation from the developed correlation. The reverse trend is shown by Eq. (3.32) of Song et al. (1989) i.e. the predicted gas holdup except for the lower range have a negative deviation of more than 20% and the deviation increases at higher values of gas holdup.

3.6. Conclusions

In this chapter a systematic step by step detailed investigation has been carried out to study the effect of initial static bed height, particle size, liquid velocity and viscosity and gas velocity on different hydrodynamic parameters in a gas-liquid-solid system for two varieties of particles viz. spherical and hollow cylindrical particles. The outcome of the findings has been presented in two section of this chapter the first sections deals with the regular shape particles and the later is for hollow cylindrical particles. An antenna type air sparger has been used in the gas-liquid distributor section, for uniform mixing of the fluids with the gas moving as fine bubbles to the fluidizing section. This arrangement also reduces the pressure drop encountered through a conventional distributor used for the purpose. To overcome the non-uniformity of flow through the column (i.e. the central region), a distributor plate with 20% open area has been fabricated with concentric circular punched holes of increased diameter from centre to the wall.

The results and discussion relating to minimum liquid fluidization velocity, bed expansion and phase holdup provide an insight to the dynamics of co-current gas-liquid-solid three phase fluidized systems, which is a prerequisite to be considered for its potential application. The values of expanded bed height measured from both the visual observation and the pressure profile have been found to agree well. Thus any of the method can suitably be used for the measurement of expanded bed height for particles of size more than 1mm.

Gas holdups were measured under various operating conditions dynamically similar to some industrial reactor. Nearly the same value of gas holdup under similar conditions has been obtained from both the pressure drop measurement and the phase isolation method. Results indicate that the gas holdup increased monotonically with increasing gas velocity. At a fixed gas velocity, gas holdup decreases with increase in liquid velocity. In general, gas holdup increase is meagre with increase in particle size. The overall gas holdup has been a strong function of Eötvös number and gas Froude number. The gas hold-up is a strong function of gas to liquid velocity ratio which drastically reduces up to the velocity ratio of 1.5. Measurement of gas holdup has further confirmed the fact that the structure of the bed is different for the small and the large size particles, with a transition taking place at particle size of 2.58 mm.

Liquid holdup increases steadily with increase in liquid velocity and decreased with increase in gas velocity. Liquid holdup also decreases with increase in particle size. Solid holdup decreases with increase in liquid and gas velocity and increases with increase in

particle size. Experimental study based on factorial design has been made to obtain the phase holdup of a three-phase fluidized bed. The experimental values thus obtained have been compared with those predicted by the correlations and have been found to agree well.

By matching the geometric and dynamic similitude, an industrial reactor can be scaled up with high gas holdup. Thus dimensional analysis has been carried out by applying Buckingham Pi theorem to develop dimensionless groups which can be used to scale up such a system. Using the dimensionless groups an empirical model (Eq. (3.18)) has been proposed for the prediction of gas holdup. The equation has been found to be satisfactory with high value of coefficient of determination (0.997). The residual analysis shows the robustness of the model.

Using Eq. (3.18) the operating conditions have been optimized for the highest gas holdup in the experimental domain. As the empirical model represents the gas holdup dynamics to be highly nonlinear, the parametric optimization has been done using genetic algorithm. The optimum operating conditions in terms of various dimensionless groups have been found to be [Mo, Eo, Fr_L, Fr_g, β_d, d_r, H_r] = [$3.21\text{x}10^{-10}$, 1487.57, $1.10\text{x}10^{-3}$, $1.55\text{x}10^{-2}$, 2.2797, 0.0588, 2.747] with a maximum gas holdup value of 0.282 for the present case.

In case of hollow cylindrical particles the bed pressure drop measurement, a standard technique gives the minimum liquid fluidization velocity in the range of 0.06344 to 0.01485 m/s**,** which continuously decreases with superficial gas velocity over range of the experimental conditions. The bed voidage has been found to increase with both gas and liquid velocities in the fluidization regime. The bed voidage at minimum fluidization has been found to be 0.55 for liquid-solid fluidization, which suddenly decrease with the introduction of the gas. Later with increase in gas velocity the bed voidage increase but for all the cases the bed voidage at minimum fluidization in the three-phase system has been found to be less than that of the liquid-solid bed. The gas holdup increase with gas velocity and decrease with liquid velocity but is a weak function of the latter. The experimental data and the developed correlations may be useful for better understanding of the behaviour and design of a gas-liquid-solid fluidized bed system using hollow cylindrical particles as the solid phase.

Chapter 4

Hydrodynamics of Irregular Particles in Fluidized Bed

Chapter-4

Hydrodynamics of Irregular Particles in Fluidized Bed

4.1. Introduction

In chapter-1, it has been discussed that fluidized bed reactor has gained importance for various types of chemical engineering applications. Before using the reactor for specific purpose, the hydrodynamics of the fluidized bed reactor must be studied in detail so as to maximize the efficiency of the system. Particle shape affects the hydrodynamic characteristics. It is obviously expected that the hydrodynamic characteristics of irregular particles is different from the regular ones. The effect of particle shape on hydrodynamics of gas-liquid-solid fluidized bed have been studied by many investigators viz.: Soung et al. (1978), Fortin (1984), Song et al. (1989), Nacef (1991), Safoniuk et al. (1999), Ramesh and Murugesan (2002), Nacef et al. (2007). Song et al. (1989) have studied the effect of particle shape on minimum fluidization velocity and bed voidage. They have used cylindrical particles and developed a generalized empirical correlation for minimum fluidization velocity using equivalent particle diameter and taking into account the avilable literature data on spherical particles. They have modified the equation of Begovich and Watson (1978) for the bed expansion characteristics by replacing particle diameter d_p by ($\Phi_s d_p$). Sinha et al. (1986) have mentioned that there is no effect of particle shape on gas holdup. Saberian-Broudjenni et al. (1987) have proposed a bed voidage equation for non-spherical particles based on their investigations carried out for various cylindrical aluminum catalyst particles.

Since the initial static bed voidage and particle shape is likely to affect the bed pressure drop, minimum fluidization and expanded bed voidage due to the variation in the tortousity of the bed and the surface area of contact with the fluid, the study of bed hydrodynamics using irregular particles is of specific importance. While the work in literature on non-spherical particles are mainly with the use of cylindrical extrude, the use of irregular particles like coal and dolomite particles of size 1 to 5 mm has been limited. In the present study, the irregular particles used are coal, dolomite, laterite and iron ore and the study has been separated from hydrodynamics of regular shape particles. A bed with a sieved size of a material is likely to contain particles of varied shapes although the experimentally found sphericity of the aggregate has been used to represent the particle shape. The bed expansion behaviour of such irregular particles is different from that of the regular ones and higher expanded bed height is expected due to less

sphericity and variation in shape of the particles. For a particular sieved fraction, the particle concentration seems to vary in the bed containing particles of higher sphericity and size at the bottom and of lower sphericty and size in form of a dilute bed observed at the top.

In the present investigation, the gas-liquid-solid three phase fluidized bed used for the hydrodynamic study of regular particles (chapter-3) has been also used to study the hydrodynamic characteristics of irregular particles. In the present chapter, an attempt has therefore been made to acquire precise knowledge of the hydrodynamic characteristics of fluidized bed reactor for three phase flow using irregular particles and by broadly varying a large number of operating variables like liquid velocity, viscosity, surface tension, gas velocity, particle size, shape and density. The hydrodynamic properties such as the bed pressure drop, minimum fluidization velocity, bed porosity (or bed expansion), phase holdups have been studied and discussed in this chapter.

4.2. Experimental set-up and techniques

The experimental setup as shown in Fig. 2.1 and discussed in Chpter-2 has been used in the present investigation. The scope of the experiment is presented in Table 4.1. Accurately weighed amount of material was fed into the column and adjusted for a specified initial static bed height (reproducible) by repeated fluidizing and de-fluidizing the bed with water. Liquid was pumped to the fluidized bed at a desired flow rate using calibrated rotameters. Air was then injected into the column through the air sparger at a desired flow rate. After a lapse of about five minutes to allow for the steady state to be reached, the readings for pressure drop and the expanded bed heights were noted. All experiments have been conducted at temperature of $(30\pm5)^0$C. The procedure was repeated by varying liquids, particle size and density and initial static bed height. The measured bed pressure drop has been used for the determination of gas holdup in the bed, by following the procedure outlined in chapter-3 section 3.6.

4.3. Pressure drop

The method of measurement of pressure drop is same as that given in chapter-3. In case of each of the experimental run the column was completely filled with water and a particular type and size of the irregular particles, with the initial level of manometer adjusted to have zero drop value. For experiment with the liquid-solid system, liquid flow rate was gradually increased. In case of gas-liquid-solid experiment, with a very little flow of liquid close to zero, the air was slowly introduced and gradually increased

to a specified flow rate. Later the liquid flow rate was increased and the readings were noted down.

Table 4.1: Characteristics of gas-liquid-solid system used in the study

Gas-liquid-solid system	d_px10^3,m	ρ_s, kg/m^3	ε_s, -	φ_s, -	h_s, m	ρ_L, kg/m^3	μ_Lx10^3, Pa.s
Air-water-dolomite	3.07	2652	0.49	0.71	0.176	995.7	0.789
do	3.07	2652	0.49	0.71	0.216	995.7	0.789
do	3.07	2652	0.49	0.71	0.256	995.7	0.789
do	3.07	2652	0.49	0.71	0.296	995.7	0.789
do	1.55	2652	0.47	0.72	0.176	995.7	0.789
do	2.18	2652	0.48	0.715	0.176	995.7	0.789
do	4.05	2652	0.50	0.70	0.176	995.7	0.789
do	4.05	2652	0.50	0.70	0.176	995.7	0.789
do	4.05	2652	0.50	0.70	0.176	995.7	0.789
do	4.05	2652	0.50	0.70	0.176	995.7	0.789
Air-water-Coal	4.05	1492	0.52	0.63	0.176	995.7	0.789
Air-water -Laterite	4.05	3313	0.51	0.68	0.176	995.7	0.789
Air-water-Iron ore	4.05	3994	0.47	0.73	0.176	995.7	0.789
Air- aqueous solution of glycerol-dolomite (% by mass of glycerol)							
6.0	3.07	2652	0.49	0.71	0.216	1009.7	0.948
12.0	3.07	2652	0.49	0.71	0.216	1024.0	1.082
18.0	3.07	2652	0.49	0.71	0.216	1039.0	1.268
24.0	3.07	2652	0.49	0.71	0.216	1054.0	1.567
Operating range of superficial gas velocity:			0.0< U_g < 0.1274 m/s				
Operating range of superficial liquid velocity:			0.0< U_L < 0.1486 m/s				

The bed pressure drop has been found to increase with initial static bed as it was observed for regular particles. Fig. 4.1 shows the variation of pressure drop with superficial liquid velocity in air-water-dolomite system at different gas velocities for 4.05 mm particles at a static bed height of 0.176 m. From the figure it is observed that there is a sudden decrease in the measured bed pressure with the introduction of the gas and thereafter the pressure drop increases. The decrease in measured bed pressure may be due to a significant amount gas holdup in the system. The increase in pressure thereafter represents the drag of the fluid on the solid particles. With increase in gas velocity the measured bed pressure drop decreases indicating thereby the presence of higher gas holdup at higher gas velocity.

Fig. 4.2 shows the variation of pressure drop with superficial liquid velocity in air-water-dolomite system for different particle sizes at an initial static bed height of 0.176 m and gas velocity of 0.05096 m/s. The weighed bed mass for the same bed height being nearly the same (for different sizes of particles), almost an equal amount of pressure drop was observed. Fig. 4.3 presents the variation of bed pressure drop with liquid velocity for air-dolomite system with different liquid phase viscosity for 3.07 mm particles at static bed height of 0.216 m and gas velocity of 0.05096 m/s. For the variation in viscosity

aqueous solutions of glycerol of different concentration was used. A little decrease in the bed pressure drop has been observed with higher concentration of glycerol. This may be due to higher gas holdup in the system with higher liquid viscosity and surface tension as was observed for regular particles. Fig. 4.4 shows the variation of bed pressure drop with liquid velocity for air-water system at different solid phase density (different material) for 4.05 mm particles with initial static bed height of 0.176 m and gas velocity of 0.05096 m/s. With density, the bed mass being more for a constant static bed height, the bed pressure drop is found to be more with particles of higher density.

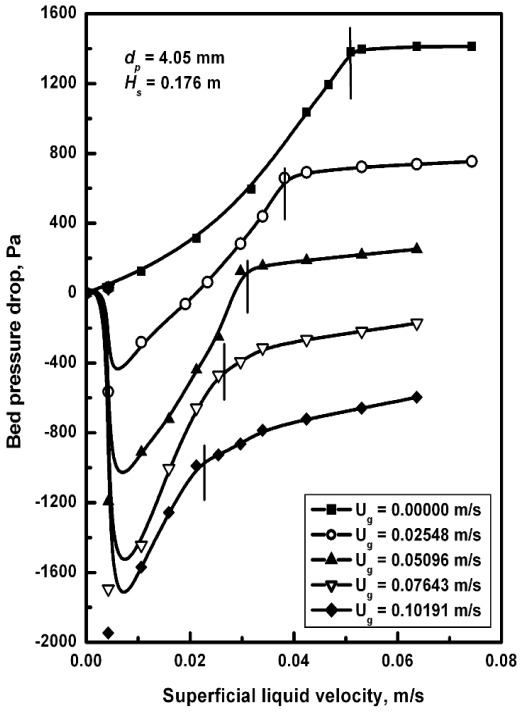

Fig. 4.1. Variation of bed pressure drop with liquid velocity for different values of gas velocity.

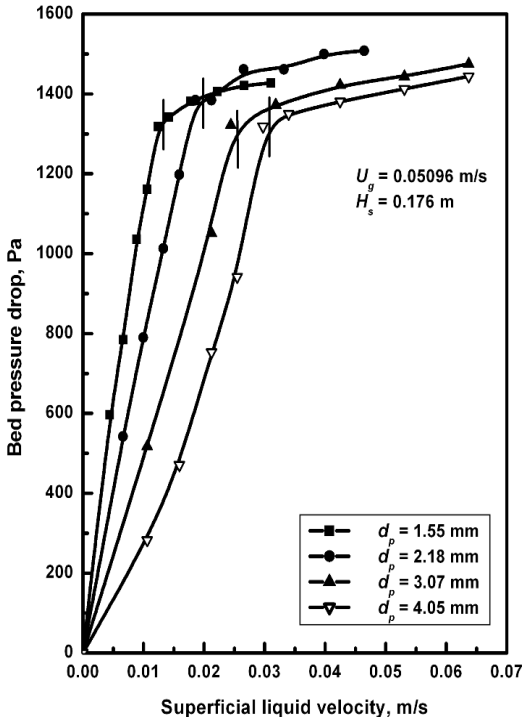

Fig. 4.2. Variation of bed pressure drop with liquid velocity for different particle sizes of dolomite.

4.4. Minimum fluidization velocity

The importance of the study of minimum fluidization velocity and its method of measurement has been discussed in chapter-1 and chapter-3. The minimum fluidization velocity in this study has been measured visually and also from the bed pressure drop measurement. In this work both the methods gives nearly the same values for minimum fluidization velociy. The values of minimum fluidization velocity obtained from bed pressure drop measurement have been reported here. The minimum fluidization velocity has been found to be independent of static bed height. In Fig. 4.1, it is seen that the minimum liquid fluidization velocity decreases with increase in gas velocity, thus indicating significant contribution of gas velocity to fluidization.

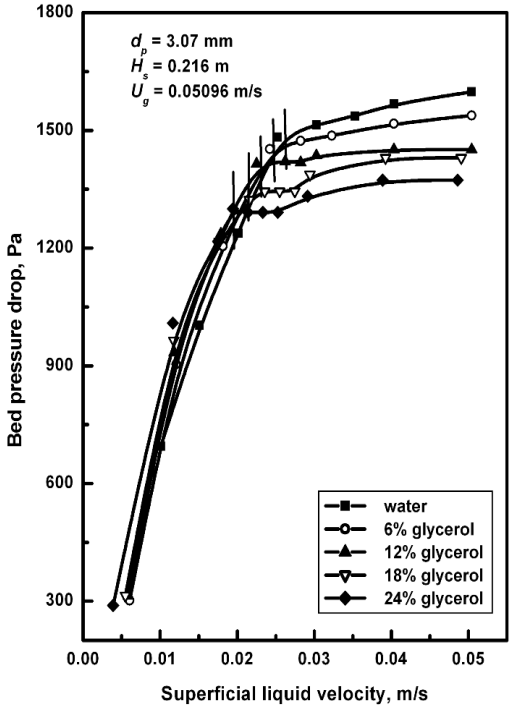

Fig. 4.3. Variation of bed pressure drop with liquid velocity for liquids of different viscosity.

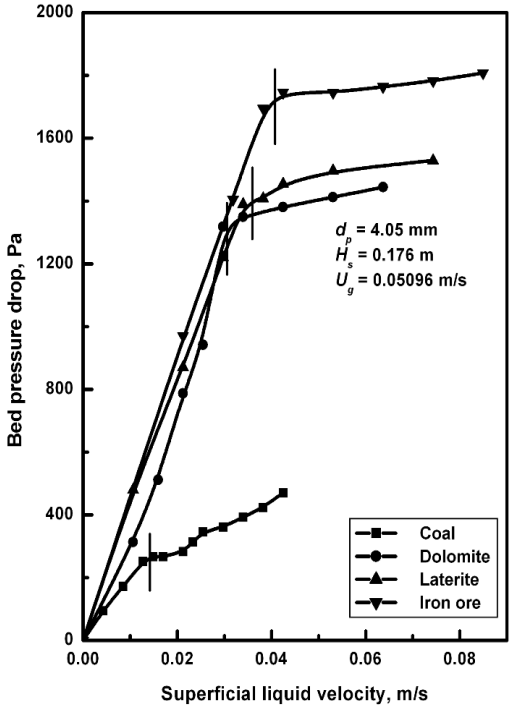

Fig. 4.4. Variation of bed pressure drop with liquid velocity for different kinds of solids.

Fig. 4.2 shows that the minimum liquid fluidization velocity (U_{lmf}) increases with particle size. With increase in liquid viscosity, U_{lmf} decreases (Fig 4.3). This indicates the contribution of the liquid viscosity to the drag offered by the liquid on the solid particles. Fig 4.4 indicates significant increase in U_{lmf} with solid phase density. The values of the minimum liquid fluidization velocity at various operating conditions for liquid-solid system and gas-liquid-solid systems are presented in Table 4.2.

With nonlinear regression analysis carried out over the experimentally observed values of minimum fluidization velocity for liquid-solid bed and the operating variables, the following correlation (Eq. (4.1) with a correlation coefficient of 0.99 has been obtained. The experimental values of minimum fluidization velocity for liquid-solid bed has been compared with those calculated from the balance of the drag force and the buoyant weight (Eq. 18, Chapter-3, Kunii and Levenspiel, 1991) and the equations proposed by Wen and Yu (1966), Babu et al. (1978) and Chitester et al. (1984) in Fig 4.5. A very close agreement between the experimental values and those predicted using the force balance equation and equation of Chitester et al. (1984) is observed in Fig. 4.5. The predicted values from equation of Wen and Yu (1966) agree within 15 %, whereas those predicted from equation of Babu et al. (1978) deviate at the rate more than 20%.

$$U_{Lmf}^{Ls} = 0.04\, d_p^{0.887} \mu_L^{-0.183} (\rho_s - \rho_L)^{0.560} \phi_s^{0.854} \qquad (4.1)$$

Table 4.2: Values of minimum liquid fluidization velocities (U_{Lmf}) in liquid-solid and gas-liquid-solid system

d_px10^3, m	ε_s, -	φ_s, -	ρ_p, kg/m^3	h_s, m	ρ_l, kg/m^3	μ_lx10^3, Pa.s	U_{Lmf}^{Ls}, m/s	U_g, m/s	U_{Lmf}, m/s
1.55	0.47	0.72	2652	0.176	995.7	0.789	0.02123	0.05096	0.01328
2.18	0.48	0.715	2652	0.176	995.7	0.789	0.03185	0.05096	0.01984
3.07	0.49	0.71	2652	0.176	995.7	0.789	0.04246	0.05096	0.02504
4.05	0.50	0.70	2652	0.176	995.7	0.789	0.05096	0.05096	0.03082
4.05	0.52	0.63	1492	0.176	995.7	0.789	0.02336	0.05096	0.01382
4.05	0.51	0.68	3313	0.176	995.7	0.789	0.06157	0.05096	0.03570
4.05	0.47	0.73	3994	0.176	995.7	0.789	0.07006	0.05096	0.04058
3.07	0.49	0.71	2652	0.216	1009.7	0.948	0.04034	0.05096	0.02345
3.07	0.49	0.71	2652	0.216	1024.0	1.082	0.03822	0.05096	0.02217
3.07	0.49	0.71	2652	0.216	1039.0	1.268	0.03609	0.05096	0.02094
3.07	0.49	0.71	2652	0.216	1054.0	1.567	0.03397	0.05096	0.01971
4.05	0.50	0.70	2652	0.176	995.7	0.789	0.05096	0.02548	0.03822
4.05	0.50	0.70	2652	0.176	995.7	0.789	0.05096	0.07643	0.02642
4.05	0.50	0.70	2652	0.176	995.7	0.789	0.05096	0.10191	0.02254

In literature the correlations proposed for the minimum liquid fluidization velocities are either in dimensional or in dimensionless form. Here the correlations in both dimensional and dimensionless form have been developed from the experimental data by carrying out nonlinear regression analysis. The following significant correlations with very high values of correlation coefficients as mentioned have been developed.

$$U_{Lmf} = 0.003 U_g^{-0.371} d_p^{0.814} \mu_L^{-0.269} (\rho_s - \rho_L)^{0.542} \phi_s^{0.928} \tag{4.2}$$

(correlation coefficient of 0.989)

$$\frac{U_{Lmf}}{U_{Lmf}^{Ls}} = 0.103 U_g^{-0.369} d_p^{-0.068} \mu_L^{-0.060} (\rho_s - \rho_L)^{-0.018} \phi_s^{0.088} \tag{4.3}$$

(correlation coefficient of 0.979)

$$\frac{U_{Lmf}}{U_{Lmf}^{Ls}} = 0.148\ Mo^{-0.025} Ar^{-0.022} Fr_g^{-0.185} \phi_s^{0.131} \tag{4.4}$$

(correlation coefficient of 0.979)

All the correlations predict nearly the same value of minimum liquid fluidization velocity. The values of the experimental minimum liquid fluidization velocity have been compared with those predicted from Eq. (4.3) and the ones predicted from a few correlations of literature as represented in Fig. 4.6.

It is seen from the comparison plot of the minimum liquid fluidization velocity that the values of U_{Lmf} predicted from the developed correlation (Eq. (4.3)) are in very close agreement with the experimental values with an AARE of 1.24 %. The values obtained from the correlations of Costa et al. (1986), Song et al. (1989) and Ruiz et al. (2004) are lower than the experimental ones. This may be due to the fact that in the above mentioned correlations the dependency of U_{Lmf} on gas velocity is more. But correlations

of Begovich and Watson (1978) and Nacef (1991) predict much higher values of U_{Lmf}. The liquid-buoyed-gas perturbed liquid model suggested by Lee et al. (2001b) agrees with the experimental values with an AARE of 31.8 %. All the correlations possess the same overall trend as with the present ones although their dependency on the operating variables differs a little.

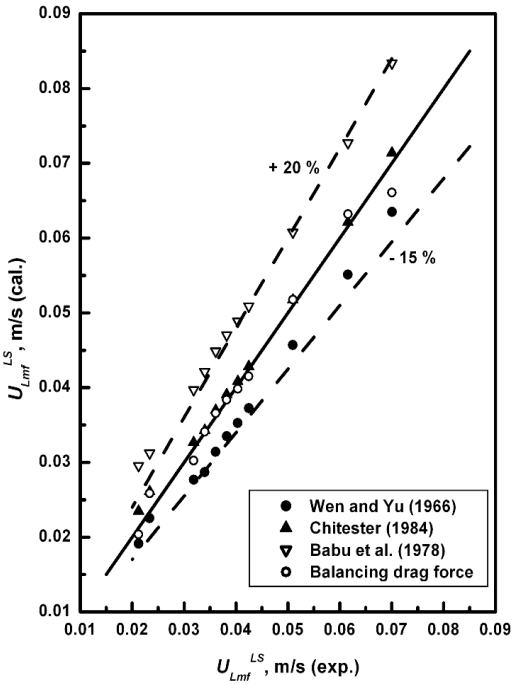

Fig. 4.5. Comparison of the values of minimum liquid fluidization velocity for liquid-solid system.

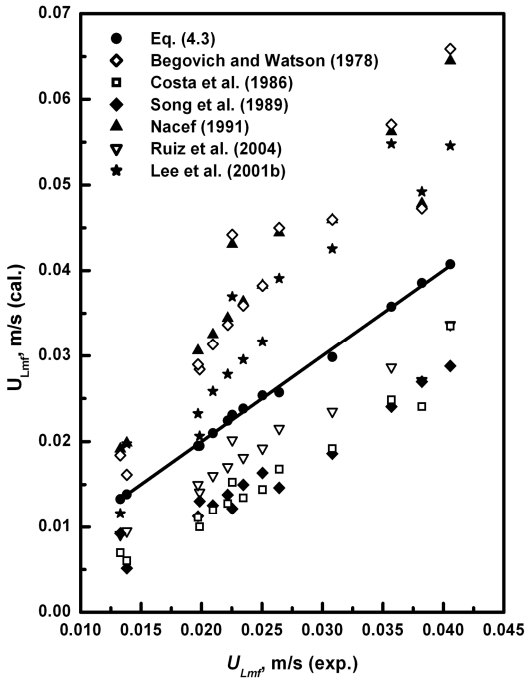

Fig. 4.6. Comparison of the values of minimum liquid fluidization velocity for gas-liquid-solid system.

4.5. Bed expansion

The expanded bed height in the present study has been measured by visual observation. In measuring the bed expansion, the agitated bed (where few particles are lifted by air bubbles below the condition of minimum fluidization) height and the portion very dilute in particles have been neglected. The bed expansion study carried out by varying liquid velocity (at a constant gas velocity) and particle size are presented in terms of bed expansion ratio in Figs. 4.7 and 4.8 respectively. It is seen from the plot of Fig. 4.7 that the bed expansion ratio increases with increase of both the liquid velocity and the gas velocity. It is further observed from the plot that with the introduction of the gas to the bed below the condition of minimum fluidization, the bed voidage decreases and compact bed is formed with reorientation of the particles. Even at minimum fluidization condition (as obtained from the pressure drop plot) the bed voidage (bed height) is lower than that of the liquid-solid bed. Above the minimum fluidization condition, the bed voidage is higher with increased values of gas velocity. Fig. 4.8 shows the decrease in

bed expansion with particle size. This may be due to the requirement of higher drag to lift the bigger size particles up to the same height, which is achieved at higher liquid velocities.

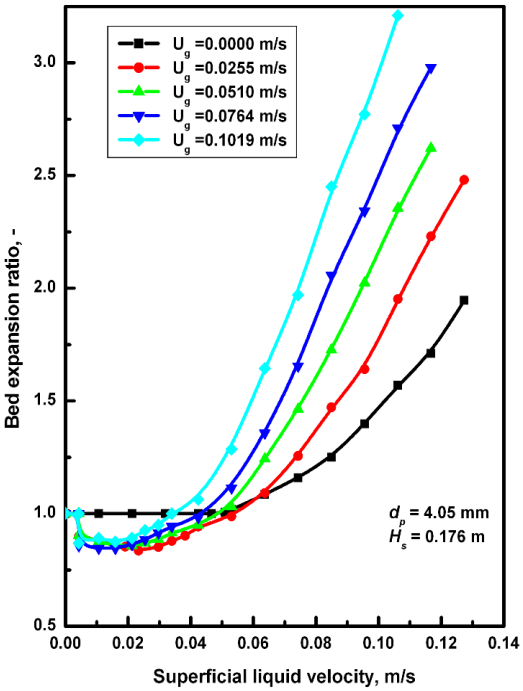

Fig. 4.7. Variation of bed expansion ratio with liquid velocity for different gas velocities for dolomite-water system.

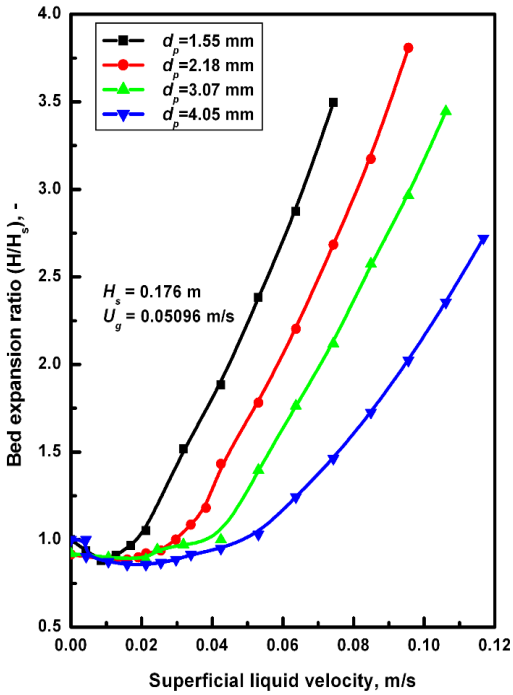

Fig. 4.8. Variation of bed expansion ratio with liquid velocity for particles of different size for dolomite-water system.

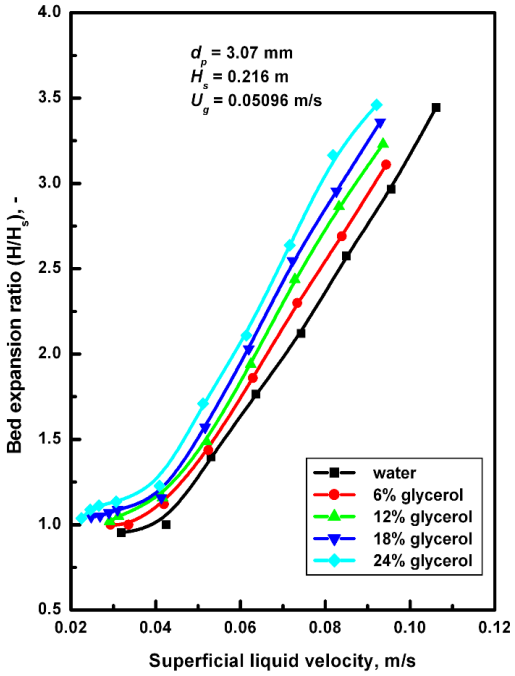

Fig. 4.9. Variation of bed expansion ratio with liquid velocity for liquids of different density and viscosity.

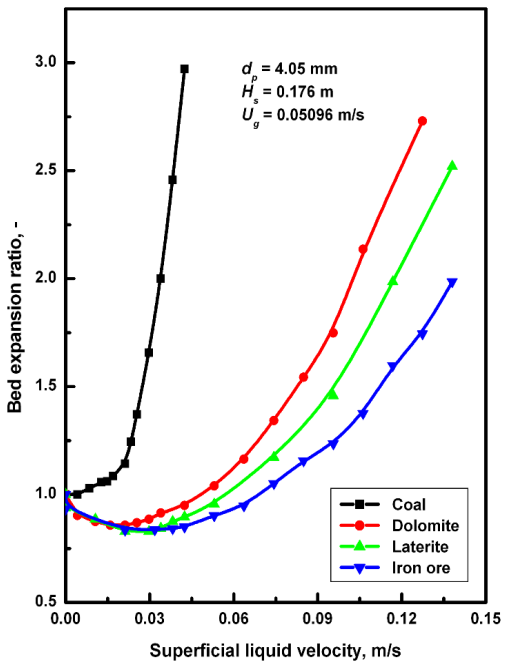

Fig. 4.10. Variation of bed expansion ratio with liquid velocity for particles of different density.

Fig. 4.9 represents the effect of liquid phase viscosity on the bed expansion. It is observed from the figure that for a constant liquid velocity, the bed expansion is more for liquid with higher viscosity, although the variation is small in the present experimental range of the liquid viscosity. The higher bed expansion may obviously be due to higher drag exerted by the high viscous liquid on the particles. The effect of particle density on the bed expansion has been represented in Fig. 4.10. The figure indicates a decrease in bed expansion value with increase in particle density. This behaviour may be due to the requirement of higher drag by the high density particle to get lifted to a particular position in the bed. A negligible effect of initial static bed height on bed expansion has been observed experimentally and therefore has not been presented here.

The experimental bed expansion data for liquid-solid system (in the absence of gas) have been correlated with the operating variables and the following equations in for bed expansion ratio and bed voidage have been developed.

$$\left(\frac{H}{H_s}\right)^{Ls} = 16.487 U_L^{0.811} d_p^{-0.418} \mu_L^{-0.041} (\rho_s - \rho_L)^{-0.444} \phi_s^{-0.700} \tag{4.5}$$

(with a correlation factor of 0.956)

$$\varepsilon^{Ls} = 2.426 U_L^{0.413} d_p^{-0.170} \mu_L^{0.003} (\rho_s - \rho_L)^{-0.212} \phi_s^{-0.807} \tag{4.6}$$

(with a correlation factor of 0.99)

The values of bed expansion ratio calculated from equation Eq. (4.5) have been compared with the corresponding ones obtained from experiment in Fig. 4.11. A good agreement of approximately 10 % between the values has been obtained, which indicates that Eq. (4.5) significantly describes bed expansion behaviour in a liquid-solid fluidized bed.

Fig. 4.12 presents a comparison of the values of bed voiadage in the liquid-solid bed obtained from experiment and those calculated from the developed correlation Eq. (4.6) and the equation of Richardson and Zaki (1954). In the equation of Richardson and Zaki (1954), the values of terminal velocity calculated from the prescribed equation of Geldart (1990) for non-spherical have been used. The close agreement between the experimental values and those predicted from Eq. (4.6) with AARE of 2.84 % indicates the robustness of the equation in predicting the bed voidage behaviour of the liquid-solid bed with irregular particles as used in the present case. The values calculated from the equation of Richardson and Zaki (1954) are within 10 % of the experimental ones, with a large

number of the calculated values being lower than the experimental ones. This indicates relatively higher bed voidage for non-spherical irregular particles.

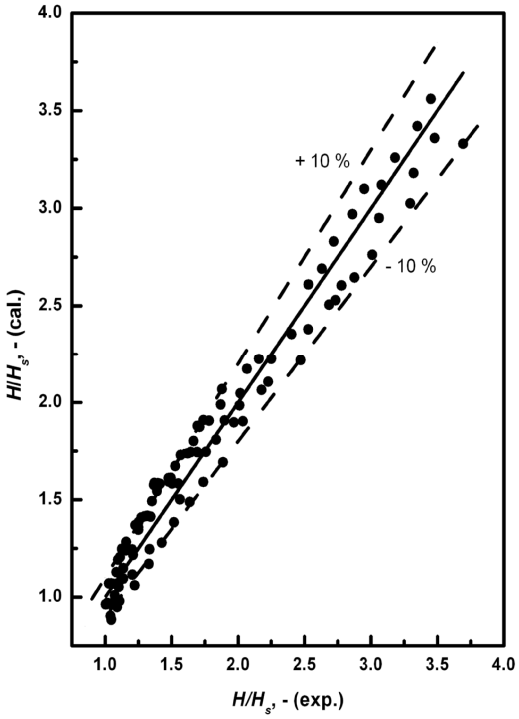

Fig. 4.11. Comparison of bed expansion ratio in liquid-solid fluidized bed.

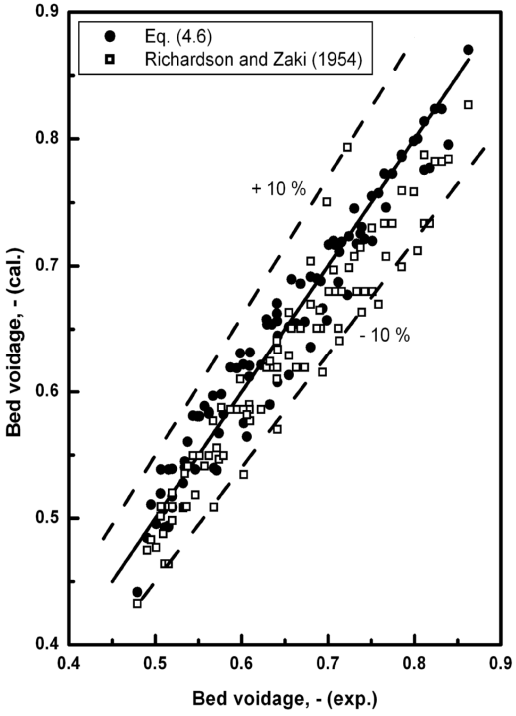

Fig. 4.12. Comparison of bed voidage in liquid-solid fluidized bed.

An empirical model equation for the bed expansion ratio (H/H_s) has been developed by carrying out nonlinear regression analysis over the experimental data of bed expansion ratio obtained at various operating conditions. The following model equation with a correlation coefficient of 0.956 has been obtained.

$$\frac{H}{H_s} = 7561.67 U_L^{1.020} U_g^{0.288} d_p^{-0.814} \mu_L^{0.481} (\rho_s - \rho_L)^{-0.819} \phi_s^{-0.227} \tag{4.7}$$

Comparison of the experimental values of bed expansion ratio has been made with those predicted from Eq. (4.7) as represented in Fig. 4.13. The predicted values have been found to agree with the experimental ones with an ARRE of 7.17 %.

In literature quite a good number of equations based on experimental findings and phenomenological models are available, which represent the bed expansion behaviour in terms of bed voidage. In the present work an attempt has been made to develop an empirical model equation for bed voidage from the experimental data and to compare the results with those predicted using a few correlations available in literature.

$$\varepsilon = 5.831 U_L^{0.387} U_g^{0.092} d_p^{-0.186} \mu_L^{0.201} (\rho_s - \rho_L)^{-0.141} \phi_s^{-1.661} \tag{4.8}$$

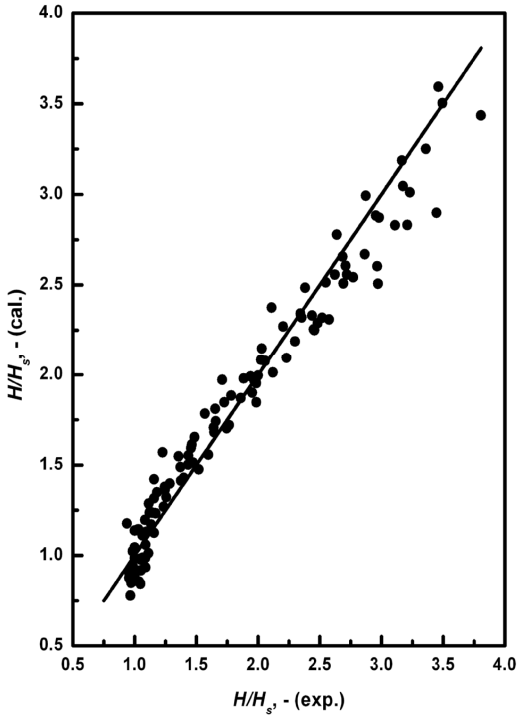

Fig. 4.13. Comparison of bed expansion ratio in gas-liquid-solid fluidized bed.

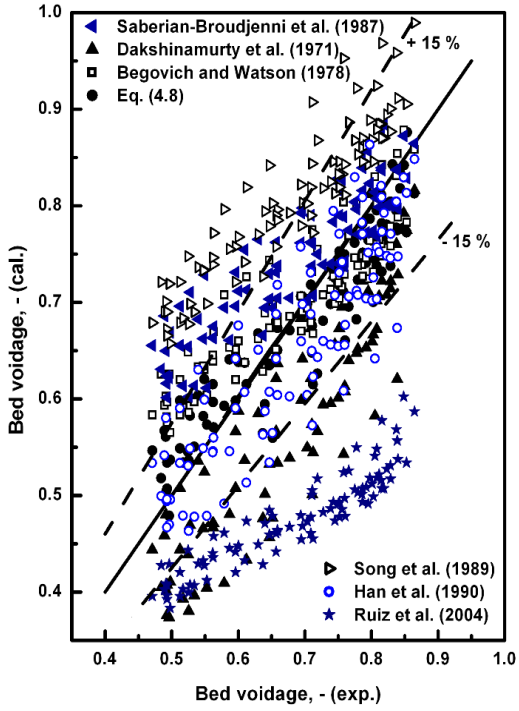

Fig. 4.14. Comparison of bed voidage in gas-liquid-solid fluidized bed.

Eq. (4.8) is the empirical model equation developed from nonlinear regression analysis of the experimental bed voidage data for gas-liquid-solid bed. The equation bears a correlation coefficient of 0.952 and the values predicted from it agrees with the experimental ones with an AARE of 7.2 %. A comparison of the bed voidage values calculated from the available correlations and the present model (Eq. (4.8) with the experimental ones has been presented in Fig. 4.14. Most of the values predicted by correlations of Begivich and Watson (1978) and Han et al. (1990) agree within 15 % with the experimental values. Except in the lower range of bed voidage the values calculated from the equation of Saberian-Broudjenni et al (1987) also agree within 15 %. The equation of Song et al. (1989) predicts higher values of bed voidage where only about 45 % of the values agree within 15 %. Except 20 % of the bed voidage values predicted by the correlation of Dakshinamurthy et al. (1971, 1972), remaining ones agree within 15 % with the experimental. But the deviation of the predicted values is almost negative w.r.t. the experimental. Hardly any value predicted by the equation of Ruiz et al. (2004) agrees within 15 % and the values predicted are much lower than the experimental ones.

To give a comparative picture of the bed expansion behaviour for gas-liquid-solid bed with that for a liquid-solid bed, the following empirical equations for bed expansion ratio and bed voidage have been developed from nonlinear regression analysis.

$$\left(\frac{H}{H_s}\right)\Bigg/\left(\frac{H}{H_s}\right)^{Ls} = 1030.71 U_L^{0.563} U_g^{0.196} d_p^{-0.574} \mu_L^{0.389} (\rho_s - \rho_L)^{-0.626} \phi_s^{1.133} \qquad (4.9)$$

(with a correlation coefficient of 0.942)

$$\frac{\varepsilon}{\varepsilon^{Ls}} = 2.973 U_L^{0.082} U_g^{0.121} d_p^{-0.113} \mu_L^{0.084} (\rho_s - \rho_L)^{-0.053} \phi_s^{-0.009} \qquad (4.10)$$

(with a correlation coefficient of 0.924)

To check the accuracy and validity of the developed correlations (Eqs. (4.9) and (4.10)), these have been used to predict the values of the ratio of bed expansion ratio and the bed voidage and compared with the experimental ones as shown in Figs. 4.15 and 4.16 respectively. The values predicted using Eqs. (4.9) and (4.10) are in agreement with the experimental values with an AARE of 6.16 % and 3.7 %. Figs 4.15 and 4.16 indicate that the maximum deviation in case of ratio of the bed expansion ratio in gas-liquid-solid bed to liquid-solid bed is nearly 10 %, where as the maximum deviation of ratio of bed voidage is well within 10%.

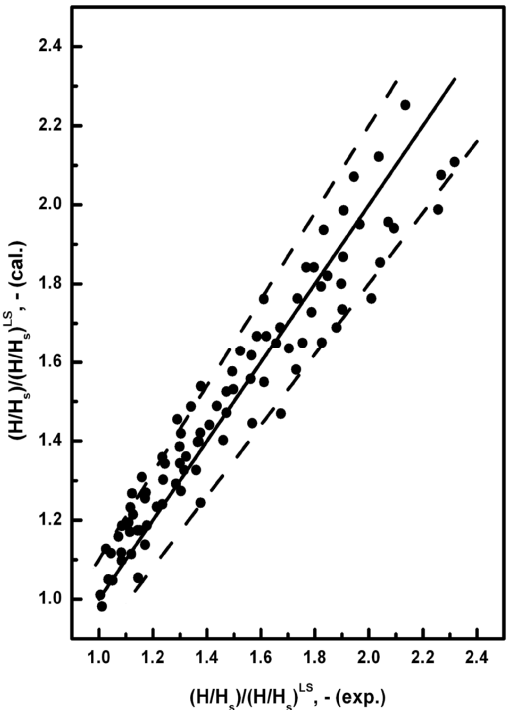

Fig. 4.15. Comparison of the ratio of bed expansion ratio in gas-liquid-solid fluidized bed to liquid-solid fluidized bed.

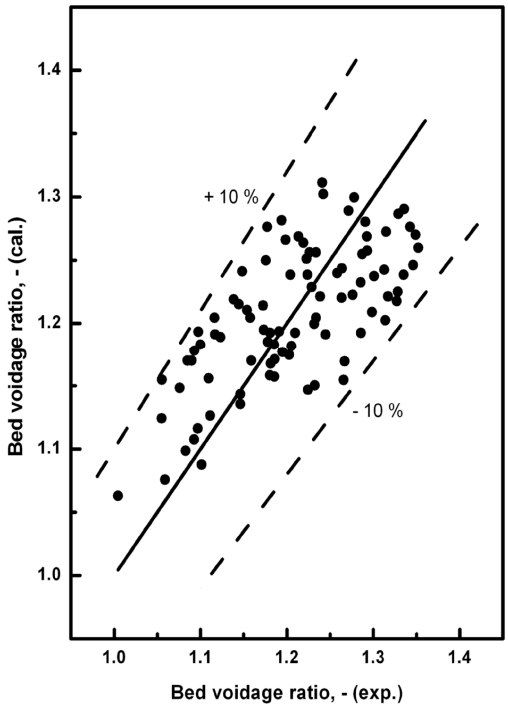

Fig. 4.16. Comparison of the ratio of bed voidage in gas-liquid-solid fluidized bed to liquid-solid fluidized bed.

4.6. Gas holdup

As discussed in chapter-3, the gas holdup is one of the most important characteristics of a three-phase fluidized bed specially the one dealing with chemical processes, where gas-liquid mass transfer is the rate-limiting step. Various possible methods of measurement of gas holdup in a gas-liquid-solid fluidized have been discussed in chapter-3. In the previous chapter, two different methods of measurement of gas hold i.e. the phase isolation and the pressure drop method have been used and a comparison of the values determined by both the methods has been presented. The comparison indicates a good agreement between the measured values by both the methods.

In the present hydrodynamic study of irregular particles, the gas holdup in the three-phase region of the bed have been determined from the bed pressure drop measurement using the same procedure as discussed in chapter-3. The ranges of the variables studied are: (a) liquid velocity (0.0 to 0.138 m/s), (b) gas velocity (0.02123 to 0.1019 m/s), (c) initial static bed heights (0.176, 0.216, 0.256, and 0.296 m), (d) particle size (1.55, 2.18, 3.07 and 4.05 mm) and (e) particle of different density (1492, 2652, 3313 and 3994 kg/m^3).

As it seen from Fig 4.1, the measured bed pressure drop in the bed is less at higher gas velocity. The lesser bed pressure drop in the bed is an indication of the higher holdup of the gas phase in the bed. Also a little increase in bed pressure drop with liquid velocity above the minimum fluidization condition is observed as indicated in the figure (Fig 4.1), which indicates a decrease in the gas holdup with increase in liquid velocity. As discussed in chapter-3 the gas holdup in the bed has been determined from difference in the measured bed pressure drop in the liquid-solid bed to the corresponding gas-liquid-solid bed. The detailed method has been discussed in the previous chapter.

In this chapter the values of gas holdup obtained experimentally have been represented graphically. Empirical equations have been developed from nonlinear regression analysis to represent the behaviour of gas holdup in the gas-liquid-solid bed at different operating conditions.

Fig. 4.17 represents the variation of gas holdup in the three-phase fluidized bed with superficial gas velocity at a fixed gas velocity for dolomite-water system. The plot of gas holdup vs. superficial liquid velocity also presents the values of gas holdup calculated from literature correlations. The gas holdup is found to decrease with an increase in liquid velocity, which agrees with the findings of Catros et al. (1985), Saberian-Broudjenni et al.(1987), Song et al. (1989), Son et al. (2007), Jena et al. (2008a). A

similar trend has also observed for regular particles as reported in chapter-3. An increase in gas holdup with the liquid velocity has been observed from the correlations of Gorowara and Fan (1990), Ramesh and Murugesan (2002) and Nacef et al. (2007). While the correlation of Begovich and Watson (1978) does not show any variation of gas holdup with the liquid velocity.

The variation of gas holdup with superficial gas velocity at a constant liquid velocity has been presented in Fig 4.18. The figure also represents the gas holdup values calculated from literature correlations at the same operating conditions. In Fig. 4.19, a comparison of the values of gas holdup calculated from literature correlations with those obtained from experiment have been presented.

In both Figs. 4.18 and 4.19, an increase in the values of gas holdup with the gas velocity has been observed for the experimental case as well as the calculated ones from available correlations. The dependency of gas holdup on gas velocity reported by various investigators is found to be different. In some cases very strong dependence has been reported but other reports shows a moderate dependence. Fig. 4.19 presents the gas holdup, both experimental and those calculated from available correlations for various combinations of gas and liquid velocities. In the figure the discontinuous group of points represents the gas holdup values for different liquid velocities at a constant gas velocity. Although an increase in gas holdup with gas velocity has been observed for all correlations but the quantitative increase is different. Some correlations which predict a higher gas holdup at lower gas velocity results a lower value of gas holdup at higher gas velocity than the experimental ones and from other correlations. This may be due to the difference in the air sparging device, distributor, size and density of particles and the gas-liquid system used.

The effect of particle density on the gas holdup has been presented in Fig. 4.20. A little increase in gas holdup with the particle density has been observed. This behaviour agrees with the findings of Bloxom et al. (1975) and Jean and Fan (1986). Wild and Poncin (1996), Costa et al. (1986), have shown a decrease in gas holdup with particle density. As per Wild and Poncin (1996) with increase in particle density ρ_p, the bed expansion decreases and the bed is more tightly packed. This may lead coalescence increased with slight increase in bubble size and decrease of gas holdup. This explanation may not be true. Rather the higher particle concentration in the bed will have stronger interactions between the gas and the solid phase with increased impact of higher density particles. This may lead to increased bubble disintegration and higher gas holdup. The gas holdup

is always more in the three-phase region than the two-phase gas-liquid region above the fluidized bed. Coalescence of bubble occurs in the two-phase region but not in the three-phase region.

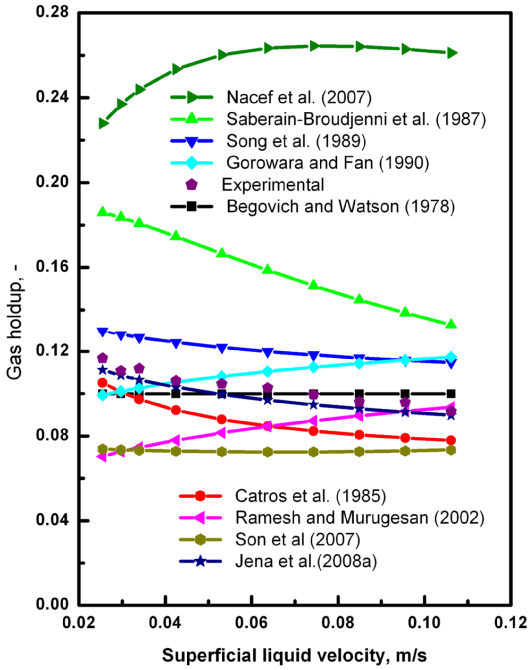

Fig. 4.17. Variation of gas holdup with liquid velocity for 4.05 mm particles of dolomite in water at [U_g=0.05096 m/s, H_s = 0.176 m].

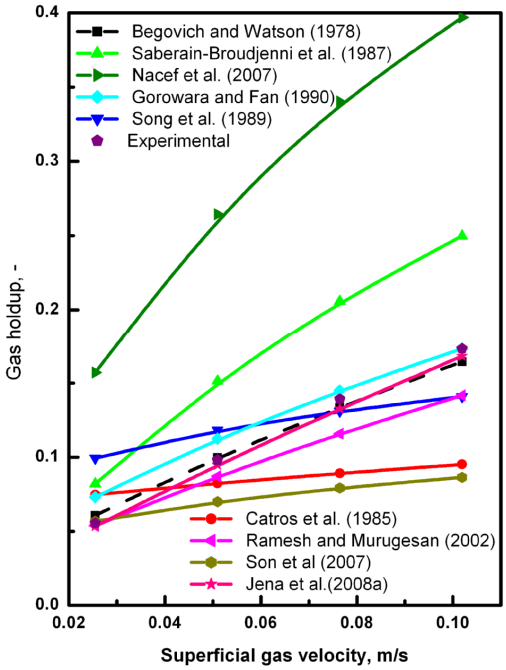

Fig. 4.18. Variation of gas holdup with gas velocity for 4.05 mm particles of dolomite in water at [U_L=0.07643 m/s, H_s = 0.176 m].

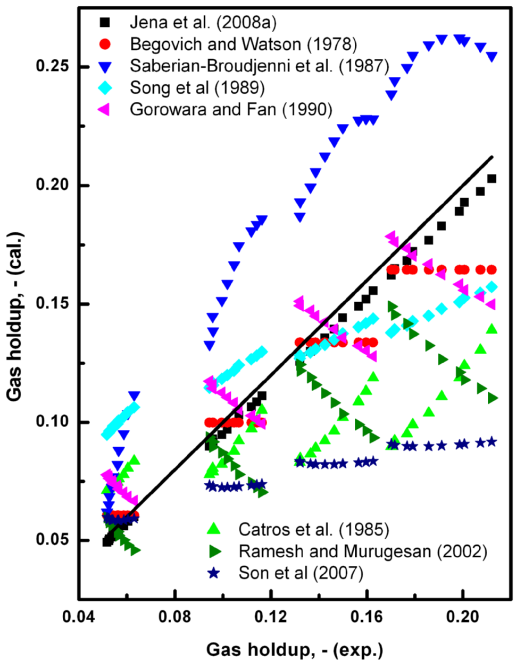

Fig. 4.19. Comparison of gas holdup values calculated from literature correlations with the experimental ones for 4.05 mm dolomite in water at different values of gas and liquid velocity.

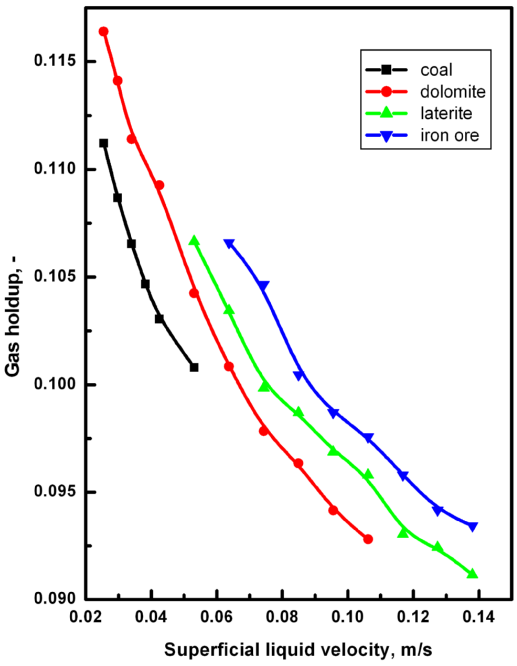

Fig. 4.20. Variation of gas holdup with liquid velocity for 4.05 mm particles of different materials in water at [U_g=0.05096 m/s, H_s = 0.176 m].

By non-linear regression analysis, the experimental data have used to develop the following empirical model equations for the prediction of gas holdup in a gas-liquid-solid fluidized bed system for such system with irregular particles both in dimensional form as well as dimensionless form. The following model equations both in dimensional form and dimensionless form have been obtained.

$$\varepsilon_g = 8.9\times10^{-9} U_L^{-0.147} U_g^{0.841} d_p^{0.123} H_s^{0.268} \mu_L^{0.044} (\rho_s - \rho_L)^{0.042} \times \sigma_L^{-7.379} \phi_s^{-0.025} \quad (4.11)$$

(with coefficient of determination of 0.99 and AARE of 1.46 %)

$$\varepsilon_g = 9.28\times10^{-8} Mo^{0.018} Eo^{2.304}\ Fr_L^{-0.076} \beta_d^{0.074} d_r^{0.128} H_r^{0.279} Fr_g^{0.420} \phi_s^{0.060} \quad (4.12)$$

(with coefficient of determination of 0.991 and AARE of 1.29 %)

Fig. 4.21 presents a comparison of the experimental gas holdup values with those calculated from Eq. (4.11) under the same flow conditions. A fairly good agreement has been observed between the values with an AARE of 1.46 %.

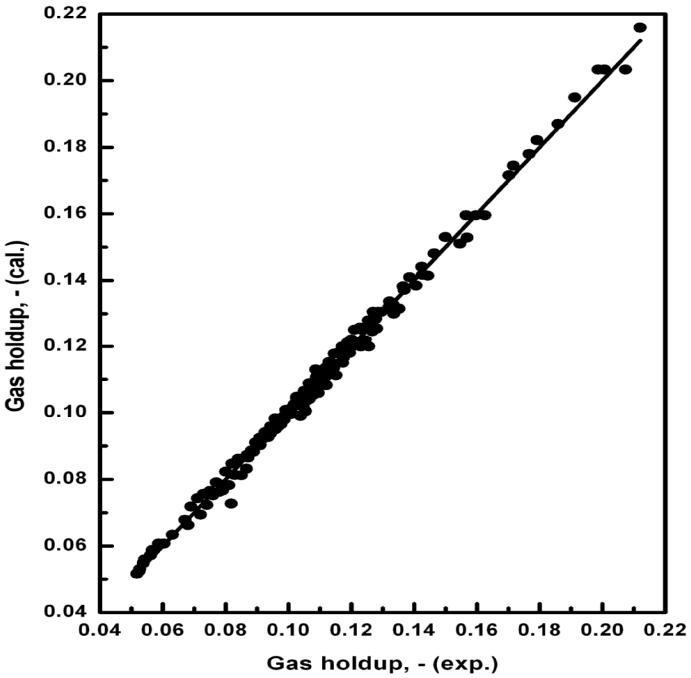

Fig. 4.21. Comparison of gas holdup values.

4.7. Conclusions

To develop a good understanding of the gas-liquid-solid fluidization phenomenon with irregular particles, a systematic and detailed investigation has been carried out to by varying different operating conditions widely. The effect of different variables studied in this chapter includes initial static bed height, particle size, particle density, liquid

velocity and viscosity and gas velocity. The hydrodynamic parameters studied are pressure drop, minimum fluidization velocity, bed expansion ratio and the gas holdup.

Similar behaviour of the hydrodynamic parameters with different quantitative dependence on the operating variables has been observed for irregular particles as it was observed for the regular ones in chapter-3.

Under similar flow conditions, the measured bed pressure drop in the fluidization regime has been found to be more for particles of higher density. The measured pressure drop does not represent the drag on the particles rather is a measure of the gas holdup in the gas-liquid-solid bed. The minimum fluidization velocity has been found to agree with a few literature data and deviate from some others within 20 %. Correlations have been developed for the prediction of minimum fluidization velocity in liquid-solid and gas-liquid-solid fluidized beds with the irregular particles, which reflects different quantitative influence of the variables when compared with the regular particles.

A little higher value of bed voidage has been obtained from the experiment than the literature data for liquid-solid system. A fairly good agreement has been observed between the experimental data and those predicted from a few correlations of literature for gas-liquid-solid system. Eqs. (4.5) and (4.6) have been developed for the calculation of bed expansion ratio and bed voidage respectively in liquid-solid system. For gas-liquid-solid fluidized beds the bed expansion ratio can be predicted from Eqs. (4.7) and (4.9) while Eqs. (4.8) and (4.10) can be used to predict bed voidage.

The experimental values of gas holdup agree well with those calculated from few literature correlations. The qualitative influence of particle density on gas holdup was not clear as the reports were contradicting. In the present investigation an increase in the value of gas holdup with increase in particle density has been observed. Almost similar qualitative influence of the other variables on the gas holdup as it was observed in case of regular particles (chapter-3), has also been observed with irregular particles. Empirical model equations in dimensional form (Eq. (4.11) and in dimensionless form (Eq. (4.12)) using dimensionless groups have been developed from experimental data for future prediction of gas holdup. Both the equations have been found to be significant with high value of coefficient of determination (0.99) and agree with the experimental values with a lower average absolute relative error.

Chapter 5

CFD Simulation of the Hydrodynamic Characteristics of Fluidized Bed

Chapter – 5

CFD Simulation of the Hydrodynamic Characteristics of Fluidized Bed

5.1. Introduction

CFD is a powerful tool for the prediction of the fluid dynamics in various types of systems, thus, enabling a proper design of such systems. It is a sophisticated way to analyze not only for fluid flow behaviour but also the processes of heat and mass transfer. The availability of affordable high performance computing hardware and the introduction of user-friendly interfaces have led to the development of CFD packages available both for commercial and research purposes. The various general-purpose CFD packages in use are PHONICS, CFX, FLUENT, FLOW3D and STAR-CD etc. Most of these packages are based on the finite volume method and are used to solve fluid flow and heat and mass transfer problems.

The Finite Volume Method (FVM) is one of the most versatile discrimination techniques used for solving the governing equations for fluid flow and heat and mass transfer problems. The most compelling features of the FVM are that the resulting solution satisfies the conservation of quantities such as mass, momentum, energy and species. This is exactly satisfied for any control volume as well as for the whole computation domain. Even a coarse grid solution exhibits exact integral balances. Apart from this, it can be applied to any type of grids (structured or unstructured, Cartesian or body fitted), and especially to complex geometries. In the finite volume method, the solution domain is subdivided into continuous cells or control volumes where the variable of interest is located at the centroid of the control volume forming a grid. The next step is to integrate the differential form of the governing equations over each control volume. Interpolation profiles are then assumed in order to describe the variation of the concerned variables between cell centroids. There are several schemes that can be used for discretization of governing equations e.g. central differencing, upwind differencing, power-law differencing and quadratic upwind differencing schemes. The resulting equation is called the discretized equation. In this manner the discretization equation expresses the conservation principle for the variable inside the control volume. These variables form a set of algebraic equations which are solved simultaneously using special algorithm.

Advances in physical models, numerical analysis and computational power enable simulation of the multi-phase flow characteristics in two and three dimensional

circumstances. Three-phase (gas-liquid-solid) fluidized bed is one of the most promising and widely used multi-phase system which finds applications in several industrial processes. The design of three-phase fluidized beds is usually done using correlations available for hydrodynamic characteristics (Matonis et al., 2002). Tarmy and Coulaloglu (1992) showed that there was no three-phase hydrodynamic model in the literature and that there was a need for such a model, as illustrated by the development of a three-phase hydrodynamic model at EXXON presented at the 1996 Computational Fluid Dynamics in Reaction Engineering Conference (Heard et al., 1996). The complex hydrodynamics of these reactors are not well understood due to complicated phenomena such as particle–particle, liquid–particle and particle–bubble interactions. For this reason, computational fluid dynamics (CFD) has been promoted as a useful tool for the understanding multiphase reactors (Dudukovic et al., 1999) for precise design and scale up. Today, computational fluid dynamics CFD has emerged as a new paradigm for modeling multiphase flow and fluidization, as seen from the literature review for three-phase reactors. The report on the computational models for the hydrodynamic characteristics of three-phase (gas-liquid-solid) fluidized bed is very limited. Hardly there is any literature which is focused on the effect of various variables on the liquid minimum fluidization velocity and the bed expansion behaviour. As described in the objective, the purpose of this study is to investigate numerically the hydrodynamic behaviour of a three-phase gas-liquid-solid fluidized bed. The hydrodynamic behaviour studied numerically is the bed pressure drop, minimum fluidization velocity, bed expansion or bed voidage and phase hold-ups.

In this work a two dimensional (2D) transient model is developed to simulate the local hydrodynamics of a gas–liquid–solid three- phase fluidized bed reactor using the CFD method. The 2D geometry is considered with the quadrilateral-meshing scheme. Simulation of hydrodynamics of three-phase fluidized bed based on Eulerian granular multiphase model is computationally intensive. Hence this model has been solved to simulate the flow behaviour using the commercial CFD package Fluent 6.2.16. The prime objective of this work is to capture the dynamic characteristics of the gas–liquid–solid flows using the above mentioned Eulerian model and then validate the same with the experimental results. The validation of the proposed CFD model is done with the experimental data for the solid phase, the liquid phase and for the gas phase hydrodynamics. The hydrodynamic parameters validated are bed pressure drop, bed expansion (bed voidage), and gas holdup. Computation of the solid mass balance and various energy flows in fluidized bed reactors are carried out.

5.2. Computational flow model

In the present work, an Eulerian granular multiphase model is adopted where gas, liquid and solid phases are all treated as continua (i.e. an Eulerian treatment is used for each phase), interpenetrating and interacting with each other everywhere in the computational domain. The pressure field is assumed to be shared by all the three phases, in proportion to their volume fraction.

5.2.1. Conservation equations

The motion of each phase is governed by respective mass and momentum conservation equations.

Continuity equation:

$$\frac{\partial}{\partial t}(\varepsilon_k \rho_k) + \nabla(\varepsilon_k \rho_k \boldsymbol{u}_k) = 0 \tag{5.1}$$

where ρ_k is the density, ε_k is the volume fraction and $\boldsymbol{u}_k$ is the velocity of phase $k = L, g, s$. The volume fraction of the three phases satisfy the following condition:

$$\varepsilon_L + \varepsilon_g + \varepsilon_s = 1 \tag{5.2}$$

Momentum equations:

For liquid phase:

$$\frac{\partial}{\partial t}(\rho_L \varepsilon_L \boldsymbol{u}_L) + \nabla.(\rho_L \varepsilon_L \boldsymbol{u}_L \boldsymbol{u}_L) = -\varepsilon_L \nabla p + \nabla.\boldsymbol{\tau}_L + \rho_L \varepsilon_L g + \boldsymbol{F}_{i,L} \tag{5.3}$$

For gas phase:

$$\frac{\partial}{\partial t}(\rho_g \varepsilon_g \boldsymbol{u}_g) + \nabla.(\rho_g \varepsilon_g \boldsymbol{u}_g \boldsymbol{u}_g) = -\varepsilon_g \nabla p + \nabla.\boldsymbol{\tau}_g + \rho_g \varepsilon_g g + \boldsymbol{F}_{i,g} \tag{5.4}$$

For solid phase:

$$\frac{\partial}{\partial t}(\rho_s \varepsilon_s \boldsymbol{u}_s) + \nabla.(\rho_s \varepsilon_s \boldsymbol{u}_s \boldsymbol{u}_s) = -\varepsilon_s \nabla p - \nabla p_s + \nabla.\boldsymbol{\tau}_s + \rho_s \varepsilon_s g + \boldsymbol{F}_{i,s} \tag{5.5}$$

where P is the pressure shared by all phases. The second term on the R.H.S of solid phase momentum Eq. (5.5) is the term that accounts for additional solid pressure due to solid collisions. The terms $\boldsymbol{F}_{i,L}$, $\boldsymbol{F}_{i,g}$, and $\boldsymbol{F}_{i,s}$ of the above momentum equations represent the inter-phase momentum exchange term for liquid, gas and solid phase, respectively.

The terms $\boldsymbol{\tau}_L$, $\boldsymbol{\tau}_g$ and $\boldsymbol{\tau}_s$ in Eqs. (5.3) – (5.5) are the stress-strain tensors of liquid, gas and solid phase, respectively and are defined as;

$$\boldsymbol{\tau}_L = \varepsilon_L \mu_L \left(\nabla \boldsymbol{u}_L + \nabla \boldsymbol{u}_L{}^T\right) + \varepsilon_L \left(\lambda_L - \frac{2}{3}\mu_L\right) \nabla.\boldsymbol{u}_L \boldsymbol{I} \tag{5.6}$$

$$\boldsymbol{\tau}_g = \varepsilon_g \mu_g \left(\nabla \boldsymbol{u}_g + \nabla \boldsymbol{u}_g{}^T \right) + \varepsilon_g \left(\lambda_g - \frac{2}{3} \mu_g \right) \nabla . \boldsymbol{u}_g \boldsymbol{I} \tag{5.7}$$

$$\boldsymbol{\tau}_s = \varepsilon_s \mu_s \left(\nabla \boldsymbol{u}_s + \nabla \boldsymbol{u}_s{}^T \right) + \varepsilon_s \left(\lambda_s - \frac{2}{3} \mu_s \right) \nabla . \boldsymbol{u}_s \boldsymbol{I} \tag{5.8}$$

where μ_L, μ_g and μ_s are the shear viscosity and λ_L, λ_g and λ_s are the bulk viscosity of liquid, gas and solid phase, respectively.

5.2.2. Interphase momentum exchange

The inter phase momentum exchange terms $\boldsymbol{F}_i$ are composed of a linear combination of different interaction forces between different phases such as the drag force, the lift force and the added mass force, etc., and is generally represented as

$$\boldsymbol{F}_i = \boldsymbol{F}_D + \boldsymbol{F}_L + \boldsymbol{F}_{VM} \tag{5.9}$$

In a recent review, the effect of various interfacial forces has been discussed by Rafique et al. (2004). They reported that the effect of added mass can be seen only when high frequency fluctuations of the slip velocity occur and they also observed that the added mass force are much smaller than the drag force in bubbly flow. By default, Fluent does not include the added or virtual mass force. In the previous studies, lift force has been applied to a few 2D simulations of gas–liquid flows. But, it has been often omitted in 3D simulation of bubble flows. The main reason for this is the lack of understanding about the complex mechanism of lift forces in gas–liquid flows (Bunner and Tryggvason, 1999). Also depending on the bubble size, a negative or positive lift coefficient is used in the literature in order to obtain good agreement between simulation and experiment. Recently Sokolichin et al. (2004) suggested that the lift force should be omitted as long as no clear experimental evidence of their direction and magnitude is available and neglecting the lift force can still lead to good comparison with experimental data as reported by Pan et al. (1999, 2000). The lift force is insignificant compared to the drag force. Hence, only the drag force is included for inter-phase momentum exchange in the present CFD simulation.

The inter-phase force depends on the friction, pressure, cohesion and other effects and is subject to the conditions that $\boldsymbol{F}_{D,jk} = -\boldsymbol{F}_{D,kj}$ and $\boldsymbol{F}_{D,jj} = 0$, where, subscripts j and k represent various phases. The inter-phase force term is defined as:

$$\boldsymbol{F}_{D,jk} = K_{jk} \left(\boldsymbol{u}_j - \boldsymbol{u}_k \right) \tag{5.10}$$

where K_{jk} (= K_{kj}) is the inter-phase momentum exchange coefficient

In the present work, the liquid phase is considered as a continuous phase and both the gas and the solid phases are treated as dispersed phases. The inter phase drag force between the phases is discussed below.

Liquid-solid interphase drag force

Liquid–solid inter phase drag force ($\boldsymbol{F}_{DLs}$) is given by

$$\boldsymbol{F}_{D,Ls} = K_{Ls}\left(\boldsymbol{u}_L - \boldsymbol{u}_s\right) \tag{5.11}$$

The inter-phase exchange coefficient between the liquid and the solid phases, K_{Ls} is obtained by Gidaspow drag model (1994) (it is combination of Wen and Yu model and the Ergun equation) as:

$$K_{Ls} = \frac{150\varepsilon_s^2\mu_L}{\varepsilon_L d_p^2} + \frac{1.75\varepsilon_s\rho_L\left|\boldsymbol{u}_L - \boldsymbol{u}_s\right|}{\varepsilon_L d_p}, \quad (\varepsilon_L \le 0.8) \tag{5.12}$$

$$K_{Ls} = \frac{3}{4}C_D\varepsilon_s\varepsilon_L\rho_L\frac{(\boldsymbol{u}_L - \boldsymbol{u}_s)}{d_p}f(\varepsilon_L), \quad (\varepsilon_L > 0.8) \tag{5.13}$$

where C_D is the drag coefficient proposed by Wen and Yu (1966) and is given as

$$C_D = \frac{24}{\varepsilon_L \operatorname{Re}_p}(1 + 0.15(\varepsilon_L \operatorname{Re}_p)^{0.687}), \quad \operatorname{Re}_p \le 1000 \tag{5.14}$$

$$C_D = 0.44, \quad \operatorname{Re}_p \ge 1000 \tag{5.15}$$

Here the particle Reynolds number is defined as

$$\operatorname{Re}_p = \frac{\rho_L d_p \left|\boldsymbol{u}_L - \boldsymbol{u}_s\right|}{\mu_L} \tag{5.16}$$

and

$$f(\varepsilon_L) = \varepsilon_L^{-2.65} \tag{5.17}$$

Gas-Liquid interphase drag force

Gas-Liquid inter phase drag force ($F_{D,gL}$) is given by

$$\boldsymbol{F}_{D,Lg} = K_{Lg}\left(\boldsymbol{u}_L - \boldsymbol{u}_g\right) \tag{5.18}$$

K_{Lg} is the exchange coefficient between the liquid and the gas phases. The secondary phase gas is assumed to form bubbles. The exchange coefficient for bubbly flow of gas-liquid mixtures is expressed in the general form:

$$K_{Lg} = \frac{\varepsilon_L\varepsilon_g\rho_g f}{\tau_g} \tag{5.19}$$

Where f, the drag function, is defined differently for different exchange-coefficient models and τ_g is the particulate (bubble) relaxation time, defined as;

$$\tau_g = \frac{\rho_g d_b^2}{18\mu_L} \tag{5.20}$$

where d_b is the diameter of the bubbles. The drag model of Schiller and Naumann (1935), acceptable for general use for all fluid-fluid pairs of phases and is given by

$$f = \frac{C_D \,\mathrm{Re}}{24} \tag{5.21}$$

where

$$C_D = \frac{24}{\mathrm{Re}_p}(1 + 0.15(\mathrm{Re}_b)^{0.687}), \quad \mathrm{Re}_b \le 1000 \tag{5.22}$$

$$C_D = 0.44, \quad \mathrm{Re}_b \ge 1000 \tag{5.23}$$

the bubble Reynolds number (Re_b) is defined as

$$\mathrm{Re}_b = \frac{\rho_L \,|\, \boldsymbol{u}_L - \boldsymbol{u}_g \,|\, d_b}{\mu_L} \tag{5.24}$$

Gas-solid interphase drag force

The momentum exchange between the two dispersed phases viz, gas and solid phases have to be taken into account for CFD simulation of three-phase flows, since the particles in the vicinity of bubbles tend to follow the bubbles (Mitra-Majumdar et al., 1997; Schallenberg et al., 2005). Even though the drag force between continuous phase and dispersed phase is discussed widely in literature, the interaction between dispersed bubbles and dispersed solids in liquid–solid–gas three-phase flows has not been modelled so far in the literature. Since the two dispersed phases are assumed to be continua in our simulation, it is reasonable to model the drag force between solid particles and bubbles in the same way as that between the continuous and the dispersed phase. Similar approach has also been used by Padial et al. (2000), Schallenberg et al. (2005), Wang et al. (2006). The equation used for drag force in the present simulation is the same as that of Wang et al. (2006). This interaction force is implemented as additional source term in the momentum equations of the gas and the solid phase through a user defined function in Fluent. Gas-solid inter phase drag force ($F_{D,gs}$) is given by

$$\boldsymbol{F}_{D,gs} = K_{gs}\left(\boldsymbol{u}_g - \boldsymbol{u}_s\right) \tag{5.25}$$

$$K_{gs} = \frac{150\varepsilon_s^2 \mu_g}{\varepsilon_g d_p^2} + \frac{1.75\varepsilon_s \rho_g \left|\boldsymbol{u}_g - \boldsymbol{u}_s\right|}{\varepsilon_g d_p}, \quad (\varepsilon_g \le 0.8) \tag{5.26}$$

$$K_{gs} = \frac{3}{4} C_D \varepsilon_s \varepsilon_g \rho_g \frac{(\boldsymbol{u}_g - \boldsymbol{u}_s)}{d_p}, \quad (\varepsilon_g > 0.8) \tag{5.27}$$

$$C_D = \frac{24}{\varepsilon_g \, \mathrm{Re}_p}(1 + 0.15(\varepsilon_g \, \mathrm{Re}_p)^{0.687}), \quad \mathrm{Re}_p \le 1000 \tag{5.28}$$

$$C_D = 0.44, \quad \mathrm{Re}_p \ge 1000 \tag{5.29}$$

Here the particle Reynolds number is defined as

$$\mathrm{Re}_p = \frac{\rho_g d_p |\boldsymbol{u}_g - \boldsymbol{u}_s|}{\mu_g} \tag{5.30}$$

5.2.3. Solids pressure

The solid phase pressure gradient results from normal stresses resulting from particle–particle interactions, which becomes very important when the solid phase fraction approaches the maximum packing. In literature, two closure models are used. The first model is constant viscosity model (CVM), where the solid phase pressure is defined only as a function of the local solid porosity using empirical correlations and the dynamic shear viscosity of the solid phase is assumed to be constant. Second model is based on the kinetic theory of granular flow (KTGF) which is based on the application of the kinetic theory of dense gases to particulate assemblies. This model gives more insight in terms of particle–particle interactions. Recently Patil et al. (2005) compared the performance of both the models for gas–solid fluidized beds and reported that both KTGF model and CVM give similar predictions in terms of bubble rise velocity and bubble size when compared to the experimental data. Zhang et al. (2008) using the KTGF model have simulated the solid volume fraction, solid axial velocity and pressure profiles and have found very reasonable agreement with the experimental data. As KTGF model is more computationally expensive, Panneerselvam et al. (2009) have used the CVM model in the simulation of a three-phase fluidized bed. In the present work the KTGF model has been used. In this model the Maxwellian velocity distribution is used for the particles, a granular temperature is introduced into the model, and appears in the expression for the solids pressure and viscosities. The solids pressure is composed of a kinetic term and a second term due to particle collisions:

$$p_s = \varepsilon_s \rho_s \Theta_s + 2\rho_s (1 + e_{ss}) \varepsilon_s^2 g_{0,ss} \Theta_s \tag{5.31}$$

where e_{ss} is the coefficient of restitution for particle collisions, the value used in this work is 0.9, which is the default value in Fluent. $g_{0,ss}$, the radial distribution function, is a correction factor that modifies the probability of collisions between grains when the solid granular phase becomes dense, given by;

$$g_0 = \left[1 - \left(\frac{\varepsilon_s}{\varepsilon_{s,\max}}\right)^{\frac{1}{3}}\right]^{-1} \tag{5.32}$$

and Θ_s is the granular temperature. The granular temperature Θ_s is proportional to the kinetic energy of the fluctuating particle motion. The transport equation used for the granular temperature calculation is given by;

$$\frac{3}{2}\left[\frac{\partial}{\partial t}(\rho_s \varepsilon_s \Theta_s) + \nabla.(\rho_s \varepsilon_s \boldsymbol{u}_s \Theta_s)\right] = (-p_s \boldsymbol{I} + \boldsymbol{\tau}_s) : \nabla \boldsymbol{u}_s + \nabla.(k_{\Theta_s} \nabla \Theta_s) - \gamma_{\Theta_s} + \phi_{ks} \tag{5.33}$$

where $(-p_s \boldsymbol{I} + \boldsymbol{\tau}_s) : \nabla \boldsymbol{u}_s =$ the generation of energy by the solid stress tensor.

$k_{\Theta_s} \nabla \Theta_s =$ the diffusion energy, k_{Θ_s} is the diffusion coefficient and is given by;

$$k_{\Theta_s} = \frac{15 d_s \rho_s \varepsilon_s \sqrt{\Theta_s \pi}}{4(41-\eta)}\left[1 + \frac{12}{5}\eta^2(4\eta - 3)\varepsilon_s g_{0,ss} + \frac{16}{5\pi}(41 - 33\eta)\eta \varepsilon_s g_{0,ss}\right] \tag{5.34}$$

where $\eta = \frac{1}{2}(1 + e_{ss})$

$\gamma_{\Theta_s} =$ the collision dissipation energy, represents the rate of energy dissipation within the solids phase due to collisions between particles. This term is represented by the expression derived by Lun et al. (1984) as;

$$\gamma_{\Theta_s} = \frac{12(1 - e_{ss}^2) g_{0,ss}}{d_s \sqrt{\pi}} \rho_s \varepsilon_s^2 \Theta_s^{3/2} \tag{5.35}$$

$\phi_{ks} =$ the energy exchange between the k^{th} fluid phase and the solid phase is represented by; $\phi_{ks} = -3 K_{ks} \Theta_s$.

The solids stress tensor contains shear and bulk viscosities arising from particle momentum exchange due to translation and collision. The solids shear viscosity contains collisional, kinetic and frictional components of viscosity as:

$$\mu_s = \mu_{s,\text{col}} + \mu_{s,\text{kin}} + \mu_{s,\text{fr}} \tag{5.36}$$

$$\mu_{s,\text{col}} = \frac{4}{5}\varepsilon_s \rho_s d_s g_{0,ss}(1 + e_{ss})\left(\frac{\Theta_s}{\pi}\right)^{1/2} \tag{5.37}$$

$$\mu_{s,\text{kin}} = \frac{\varepsilon_s \rho_s d_s \sqrt{\Theta_s \pi}}{6(3 - e_{ss})}\left[1 + \frac{2}{5}(1 + e_{ss})(3e_{ss} - 1)\varepsilon_s g_{0,ss}\right] \tag{5.38}$$

$$\mu_{s,\text{fr}} = \frac{p_s \sin\phi}{2\sqrt{I_{2D}}} \tag{5.39}$$

where, p_s is the solids pressure, ϕ is the angle of internal friction, and I_{2D} is the second invariant of the deviatoric stress tensor.

5.2.4. Closure laws for turbulence

To describe the effects of turbulent fluctuations of velocity and scalar quantities the simplest but complete model is the two-equation standard *k*-ε model. In comparison to single-phase flows, the number of terms to be modeled in the momentum equations in multiphase flows is large, and this makes the modeling of turbulence in multiphase simulations extremely complex. There are three methods for modeling turbulence in multiphase flows within the context of the *k*-ε model. Those are (a) mixture turbulence model, (b) dispersed turbulence model, and (c) turbulence model for each phase. In this work the *k*-ε dispersed turbulence model has been used for the turbulence modeling, as this model is applicable when there is clearly a primary continuous phase and the rest are dispersed secondary phases and seem to be the most probable model.

Using the *k*-ε dispersed turbulence model the turbulence in the continuous phase is calculated using the following equations. The eddy viscosity model is used to calculate averaged fluctuating quantities. The Reynolds stress tensor for continuous phase (liquid) takes the following form:

$$\boldsymbol{\tau}_L'' = -\frac{2}{3}\left(\rho_L k_L + \rho_L \mu_{t,L} \nabla . \boldsymbol{U}_L\right)\boldsymbol{I} + \rho_L \mu_{t,L}\left(\nabla \boldsymbol{U}_L + \nabla \boldsymbol{U}_L{}^T\right) \tag{5.40}$$

where $\boldsymbol{U}_L$ is the phase-weighted velocity.

The turbulent viscosity $\mu_{t,L}$ is written in terms of the turbulent kinetic energy as:

$$\mu_{t,L} = \rho_L C_\mu \frac{k_L^2}{\varepsilon_L} \tag{5.41}$$

and a characteristic time of the energetic turbulent eddies is defined as

$$\tau_{t,L} = \frac{3}{2} C_\mu \frac{k_L}{\varepsilon_L} \tag{5.42}$$

where ε_L is the dissipation rate and C_μ=0.09

The length scale of the turbulent eddies is

$$L_{t,L} = \frac{3}{2} C_\mu \frac{k_L^{3/2}}{\varepsilon_L} \tag{5.43}$$

The values of k_L and ε_L are directly obtained from the differential transport equations for the turbulence kinetic energy and turbulence dissipation rate represented as:

$$\begin{aligned} &\frac{\partial}{\partial t}\left(\rho_L \varepsilon_L k_L\right) + \nabla .\left(\rho_L \varepsilon_L \boldsymbol{U}_L k_L\right) \\ &= \nabla .\left(\varepsilon_L \frac{\mu_{t,L}}{\sigma_k} \nabla k_L\right) + \varepsilon_L G_{k,L} + \rho_l \varepsilon_L \varepsilon_L + \rho_L \varepsilon_L \Pi_{KL} \end{aligned} \tag{5.44}$$

and

$$\frac{\partial}{\partial t}(\rho_L \varepsilon_L \varepsilon_L) + \nabla.(\rho_L \varepsilon_L \boldsymbol{U}_L \varepsilon_L)$$
$$= \nabla.\left(\varepsilon_L \frac{\mu_{t,L}}{\sigma_\varepsilon} \nabla \varepsilon_L\right) + \varepsilon_L \frac{\varepsilon_L}{k_L}\left(C_{1\varepsilon} G_{k,L} - C_{2\varepsilon} \rho_l \varepsilon_L\right) + \rho_L \varepsilon_L \Pi_{\varepsilon_L} \tag{5.45}$$

Here Π_{k_L} and Π_{ε_L} represent the influence of the dispersed phases on the continuous liquid phase and $G_{k,L}$ is the production of turbulent kinetic energy. The term Π_{k_L} can be derived from the instantaneous equation of the continuous phase and takes the following form, where J represents the number of secondary phases:

$$\Pi_{k_L} = \sum_{j=1}^{J} \frac{K_{jL}}{\varepsilon_L \rho_L}\left(k_{jL} - 2k_L + \boldsymbol{u}_{jL}.\boldsymbol{u}_{dr}\right) \tag{5.46}$$

where k_{jL} is the covariance of the velocities of the continuous liquid phase and the dispersed phase *j* (calculated from Eq. below), $\boldsymbol{u}_{jL}$ is the relative velocity, and $\boldsymbol{u}_{dr}$ is the drift velocity (defined by Eq. below).

Π_{ε_L} is given by, $\Pi_{\varepsilon_L} = C_{3\varepsilon} \frac{\varepsilon_L}{k_L} \Pi_{k_L}$ (5.47)

where $C_{3\varepsilon} = 1.2$

In calculating the turbulence in the dispersed phase, the dispersion coefficients, correlation functions, and the turbulent kinetic energy of each phase are evaluated from time and length scales that characterize the motion. The characteristic particle relaxation time connected with inertial effects acting on a dispersed phase j is defined as

$$\tau_{F,jL} = \rho_L \varepsilon_L K_{jL}^{-1}\left(\frac{\rho_j}{\rho_L} + C_V\right) \tag{5.48}$$

The Lagrangian integral time scale calculated along particle trajectories, mainly affected by the crossing-trajectory effect is defined as

$$\tau_{t,jL} = \frac{\tau_{t,L}}{\sqrt{\left(1 + C_\beta \xi^2\right)}} \tag{5.49}$$

where $\xi = \frac{\left|\boldsymbol{u}_{jL}\right| \tau_{t,L}}{L_{t,L}}$ and $C_\beta = 1.8 - 1.35\cos^2\theta$ (5.50)

where θ is the angle between the mean particle velocity and the mean relative velocity. The ratio between these two characteristic times is written as

$$\eta_{jL} = \frac{\tau_{t,jL}}{\tau_{F,jL}} \tag{5.51}$$

The turbulence quantities for dispersed phase *j* are written as

$$k_j = k_L\left(\frac{b^2 + \eta_{jL}}{1+\eta_{jL}}\right) \tag{5.52}$$

$$k_{jL} = 2k_L\left(\frac{b + \eta_{jL}}{1+\eta_{jL}}\right) \tag{5.53}$$

$$D_{t,jL} = \frac{1}{3}k_{jL}\tau_{t,jL} \tag{5.54}$$

$$D_j = D_{t,jL} + \left(\frac{1}{3}k_j - b\frac{1}{3}k_{jL}\right)\tau_{F,jL} \tag{5.55}$$

$$b = (1 + C_V)\left(\frac{\rho_j}{\rho_L} + C_V\right) \tag{5.56}$$

And $C_V = 0.5$ is added mass coefficient.

The turbulent drag term for multiphase flow ($K_{jk}(\boldsymbol{u}_j - \boldsymbol{u}_k)$ is modelled for the dispersed phase and the continuous liquid phase as:

$$K_{jL}(\boldsymbol{u}_j - \boldsymbol{u}_L) = K_{jL}(\boldsymbol{U}_j - \boldsymbol{U}_L) - K_{jL}\boldsymbol{u}_{dr} \tag{5.57}$$

The drift velocity is defined as:

$$u_{dr} = \frac{D_j}{\sigma_{jL}\varepsilon_j}\nabla\varepsilon_j - \frac{D_L}{\sigma_{jL}\varepsilon_L}\nabla\varepsilon_L \tag{5.58}$$

Here D_j and D_L are diffusivities, and σ_{jL} is dispersion Prandtl number. The diffusivity values are assumed to be equal i.e. $D_j = D_L = D_{t,jL}$ and the value of σ_{jL} is 0.75.

5.3. Numerical methodology

The model equations described above are solved using the commercial CFD software package Fluent 6.2.16. The fluidized bed reactor considered for the present simulation study is a cylindrical Plexiglas column of diameter 0.1m and height 1.88m. Fig. 5.1 depicts the typical numerical mesh used for this simulation. The governing equations are discretized using element based finite volume method (Raw, 1994) and for spatial discretization of the governing equations, high-resolution discretization scheme is applied which accounts for accuracy and stability. For time discretization of the governing equations, a second order backward Euler scheme is used. The discretized equations are solved using the advanced algebraic multi-grid solver (AMG) technology

of Fluent 6.2.16. Fig. 5.2 shows the general procedure for the simulation using Fluent software.

Geometry and mesh

Two dimensional computational geometry of the fluidization column have been generated by using top-down technique (Face primitive - Rectangle) by using commercial software GAMBIT 2.2.30 as shown in Fig 5.1. After geometry creation, a uniform mesh has been generated with map structured Quadrilateral elements containing height to width ratio of 1. Totally 7520 cells with size of each cell 0.005m x 0.005m have been used for computation.

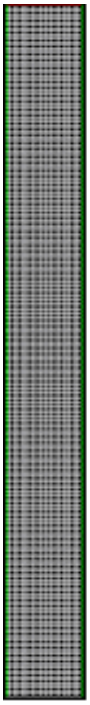

Fig. 5.1. 2D mesh

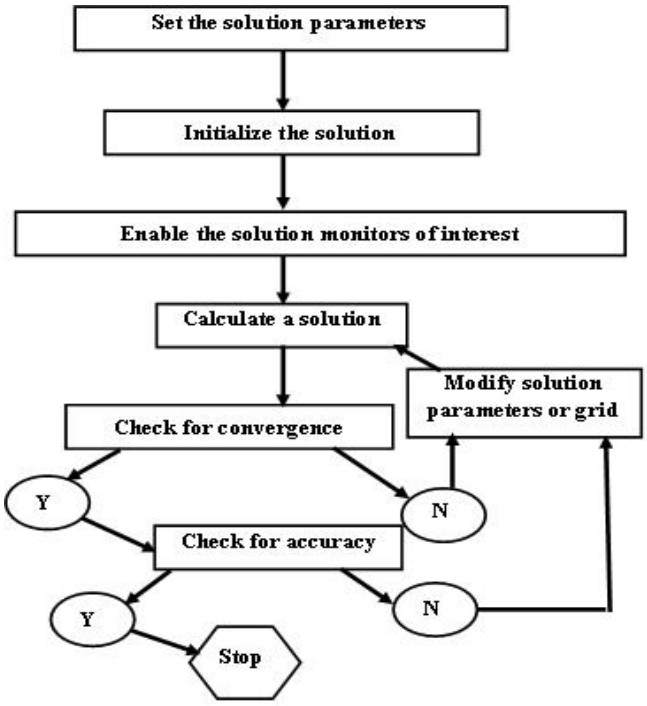

Fig. 5.2. Flowchart showing the general procedure for the simulation using Fluent.

Boundary and initial conditions

In order to obtain a well-posed system of equations, reasonable boundary conditions for the computational domain have to be implemented. Inlet boundary condition is a uniform liquid and gas velocity at the inlet, and outlet boundary condition is the pressure boundary condition, which is set as1.013×10^5 Pa. Wall boundary conditions are no-slip boundary conditions for the liquid phase and free slip boundary conditions for the solid phase and the gas phase. The higher viscous effect and higher velocity gradient near the wall have been dealt with the standard wall function method. At initial condition the solid volume fraction of 0.59 of the static bed height of column has been used and the

volume fraction of the gas at the inlet and in the free board region is based on the inventory. Table 5.1 shows the boundary and initial conditions.

Solution

The solution procedure involves the following steps: (i) generation of suitable grid system; (ii) conversion of governing equation into algebraic equations; (iii) selection of discretization schemes; (iv) formulation of the discretized equation at every grid location; (v) formulation of pressure equation; (vi) development of a suitable iteration scheme for obtaining a final solution.

Table 5.1: Description of system used in simulation

Diameter of column:	0.1 m	Liquid phase (water), 30^0C	
Height of column:	1.88 m	Viscosity, Pas:	7.98×10^{-4}
Solid phase (glass beads):		Density, Kg/m^3:	995.7
Particle size, mm:	2.18	Gas phase (air), 30^0C	
Particle density, Kg/m^3:	2470	Viscosity, Pas:	1.794×10^{-5}
Initial static bed height, m:	0.171, 0.213	Density, Kg/m^3:	1.166
Bed inventory, kg:	1.965, 2.450	Superficial liquid velocity:	0.004246 to 0.1746 m/s
Static bed voidage:	0.41	Superficial gas velocity:	0 to 0.1019 m/s

The Phase Coupled SIMPLE method (Patanker, 1980) has been chosen for pressure–velocity coupling. The second-order upwind scheme has been used for discretization of momentum, turbulence kinetic energy and turbulence dissipation rate and the first-order upwind scheme has been used for discretization of volume-fraction equations. The time step size of 0.001s has been used. The convergence criteria for all the numerical simulations are based on monitoring the mass flow residual and the value of $1.0e^{-04}$ was set as converged value. The residual plot of the progress of the simulation is shown in Fig.5.3.

The following under relaxation factors have been used for different flow quantities: pressure = 0.3, density = 1, body forces = 1, momentum = 0.2, volume fraction = 0.5, granular temperature = 0.2, turbulent kinetic energy = 0.8, turbulent dissipation rate = 0.8 and turbulent viscosity =1. The simulations have been carried out till the system reached the quasi-steady state i.e., the averaged flow variables are time independent; this can be achieved by monitoring the expanded bed height or phase volume fractions. Fig. 5.4 shows the variation in the bed profile with time. It can be observed from the figure that, the bed profile is almost the same between 18-30 s of simulation time. Simulations continued for 60 s and the averages over the last 20 s were used in the analysis. Once the fully developed quasi-steady state is reached, the averaged quantities in terms of time, axial and radial direction have been calculated.

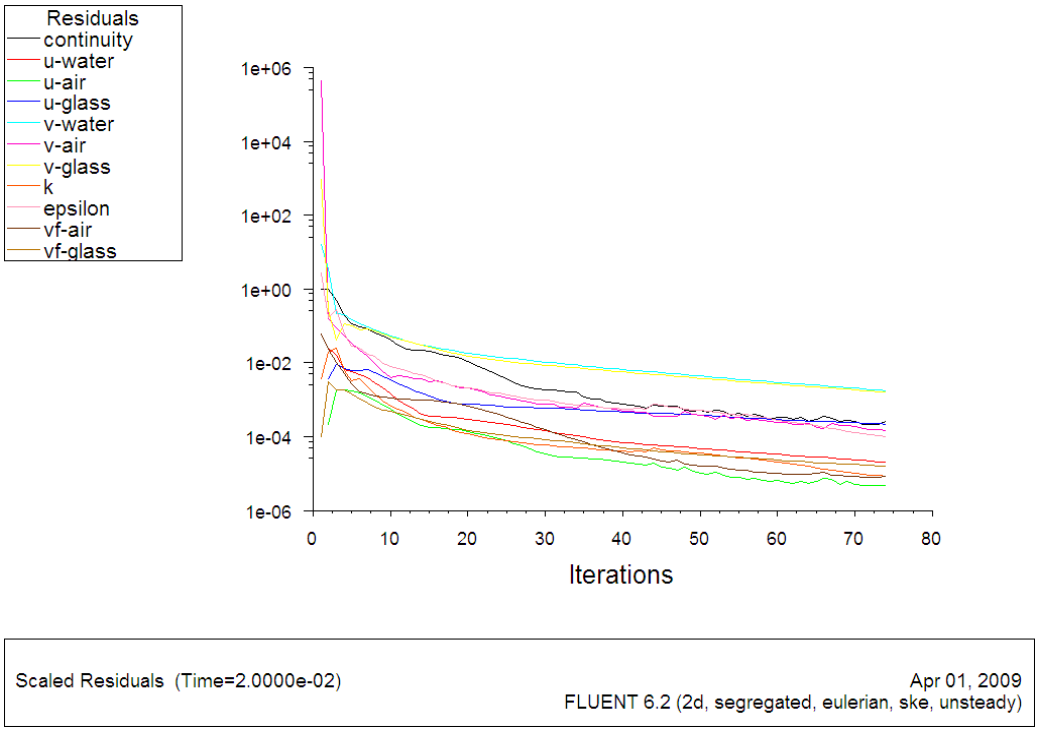

Fig. 5.3. Plot of residuals with the progress of simulation.

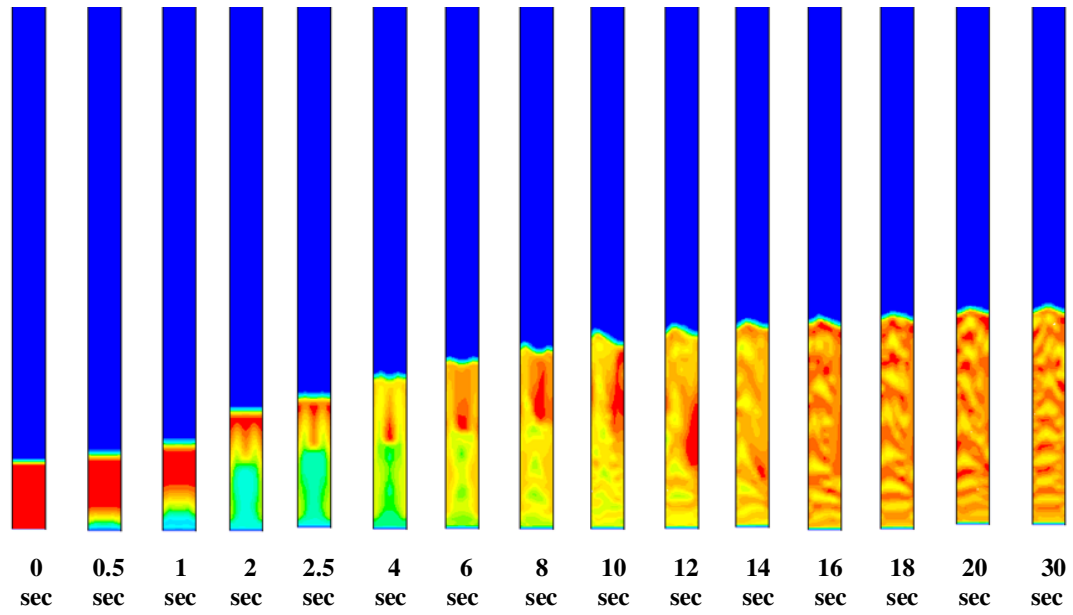

Fig. 5.4. Contours of volume fraction of 2.18 mm glass beads at water velocity of 0.12 m/s and air velocity of 0.0125 m/s with respect of time for initial bed height 0.213 m.

5.4. Results and discussion

Solid, liquid and gas phase dynamics have been represented in the form of contours, vectors and XY plots. Fig. 5.5 shows the contours of volume fractions of solid, liquid and gas in the column obtained at water velocity of 0.12 m/s and air velocity of 0.0125 m/s for initial static bed height 0.213 m and glass beads of diameter 2.18 mm after the

quasi steady state is achieved. The colour scale given to the left of each contours gives the value of volume fraction corresponding to the colour. The contours for glass beads illustrates that bed is in fluidized condition. The contour for water illustrates that volume fraction of the liquid is less in fluidized section than the two-phase region above it. The contour for air illustrates that gas holdup is significantly more in fluidized section of the bed compared to the two-phase region above.

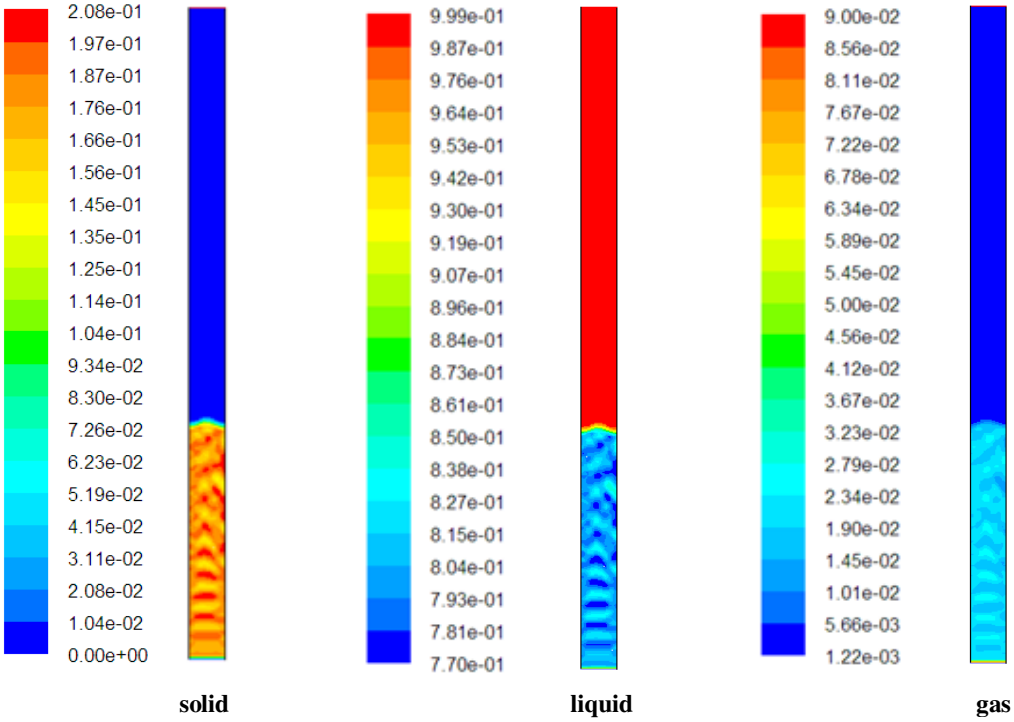

Fig. 5.5. Contours of volume fraction of solid, liquid and gas at water velocity of 0.12 m/s and air velocity of 0.0125 m/s for initial static bed height of 0.213 m.

Fig. 5.6 shows the velocity vectors of glass beads, water and air in the column obtained at inlet water velocity of 0.12 m/s and inlet air velocity of 0.0125 m/s for initial static bed height 0.213 m and glass beads of size 2.18 mm after the quasi steady state has been achieved. The velocity vectors are helpful in determining flow patterns in fluidized bed. From the vector of solids it can be seen that, there is a small length vigorous movement of the solid particles at the bottom part of the bed. In the upper part of the fluidizing section there is a circulatory motion of the particles with movement near the wall in the down ward direction while that in the central zone is upward.

The XY plot (Fig. 5.7) shows the radial distribution of the axial velocity of liquid phase obtained from the simulation at an inlet water velocity of 0.12 m/s and inlet air velocity of 0.0125 m/s. This indicates a fully developed flow in the bed. The plot gives a peak velocity of water of about 0.14 m/s.

Fig 5.8 is the XY plot for the magnitude of velocity of the gas phase (air). The plot also indicates a fully developed flow that the axial velocity along the centre line being maximum and that at the wall is less. The velocity of air bubbles is not zero like it was for the liquid phase (Fig. 5.7). This is due to no slip boundary condition for the liquid, and free slip boundary condition for gas. The peak value of air velocity is about 0.48m/s.

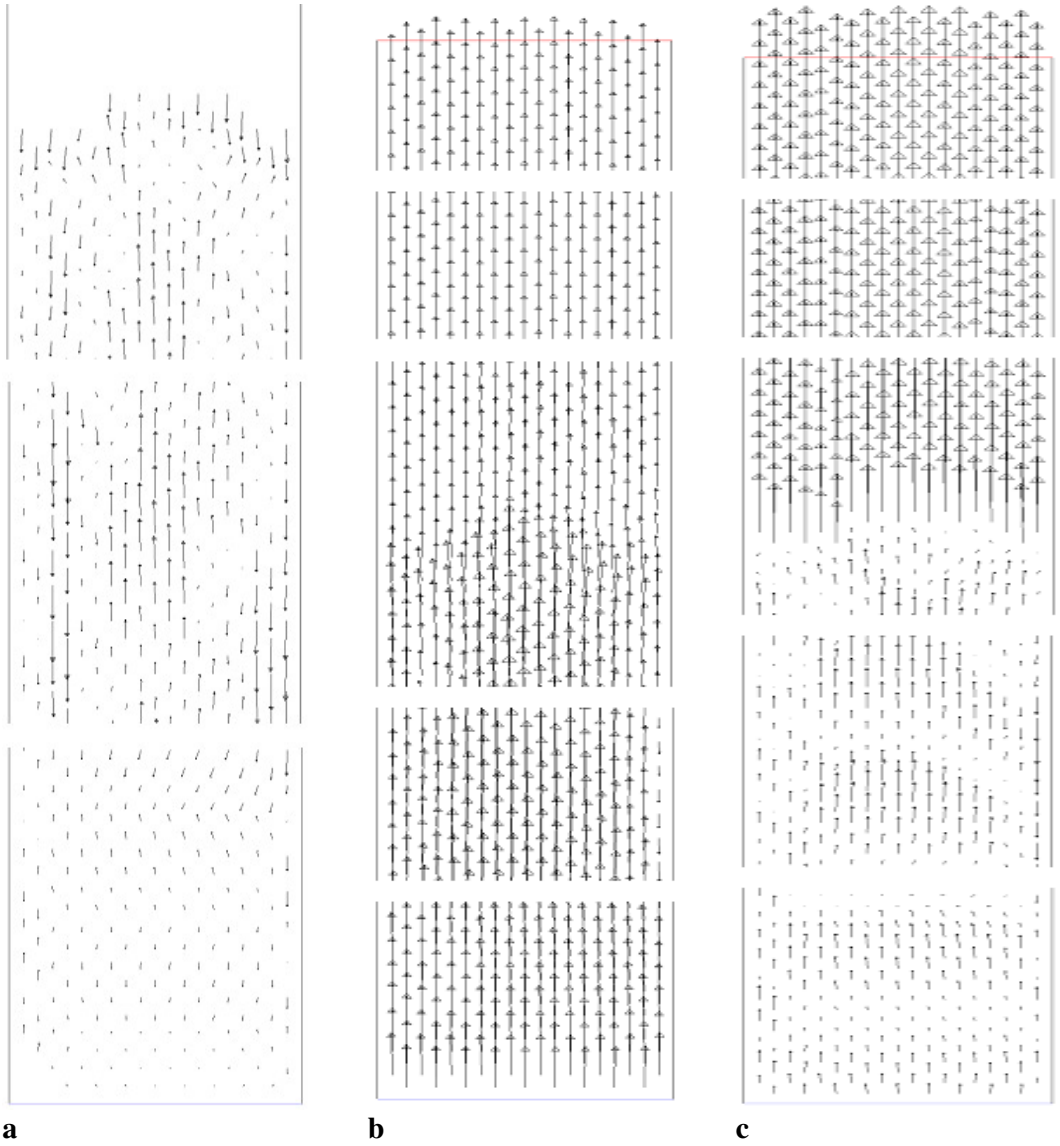

Fig 5.6. Velocity vector of the (a) solid phase, (b) liquid phase, (c) gas phase.

5.4.1. Bed expansion (Bed voidage)

In gas-liquid-solid system with increase in liquid velocity at a constant gas velocity, the expanded bed height increases and the voidage of the bed also increases. Experimentally this phenomenon has been observed for both regular and irregular particles in chapter-3 and chapter-4. CFD simulation result also shows an increase in bed expansion with

liquid velocity at a constant gas velocity. It can be seen from the contours of solid volume fraction (as shown in Fig. 5.9) that there is steady increase in bed height with liquid velocity above the minimum fluidization condition. The bed height can be determined from the XY plot of the solid volume fraction w.r.t. the axial distance from the base of the column (in 2D mesh it is noted as y-coordinate) as shown in Fig. 5.10. The point where the the solid fraction sharply decreases to zero value can be taken as the height of the bed.

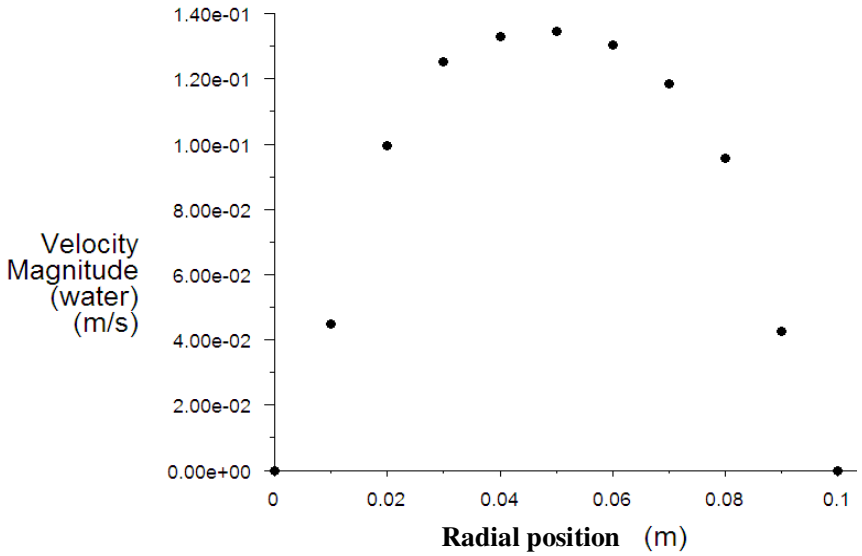

Fig.5.7. XY plot of velocity magnitude of liquid phase.

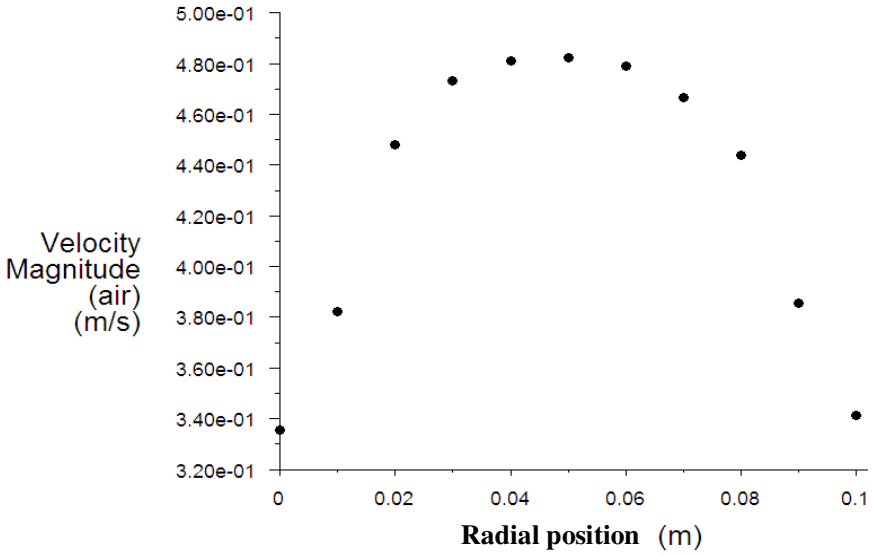

Fig. 5.8. XY plot of velocity magnitude of air.

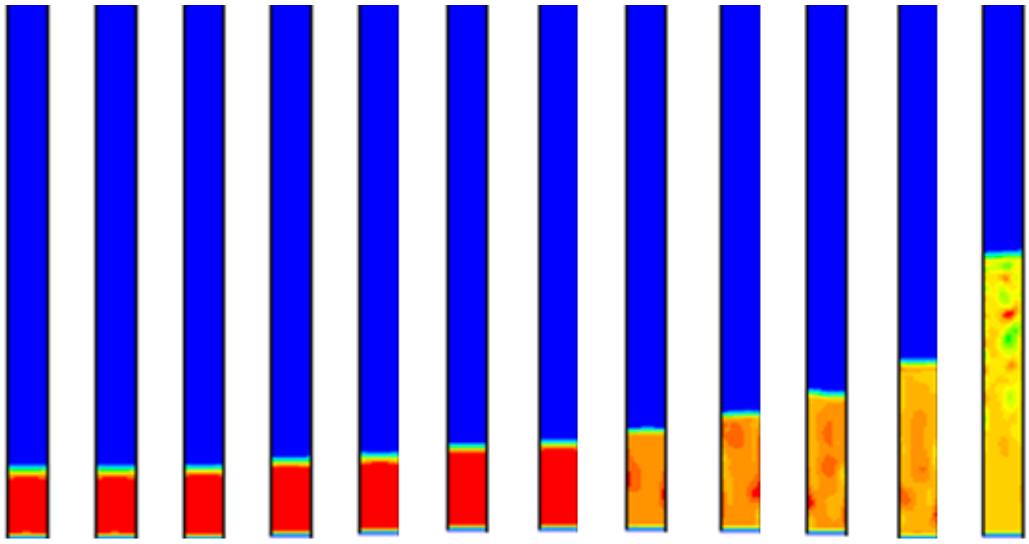

Fig. 5.9. Contour plot of solid volume fraction with variation in liquid velocity.

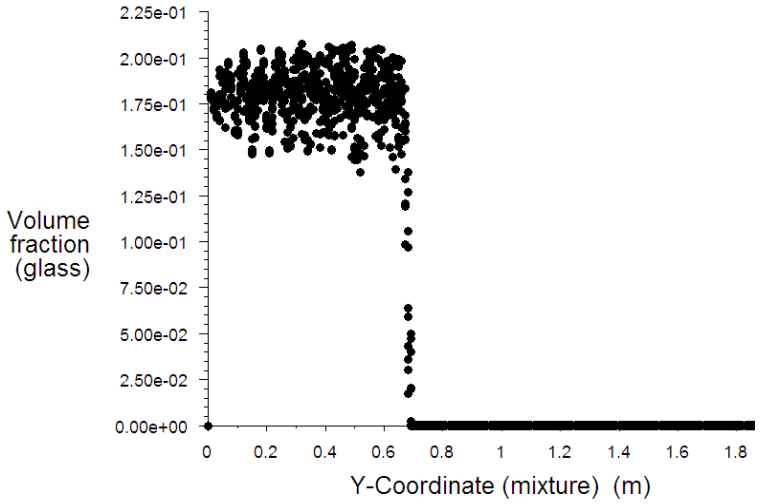

Fig. 5.10. XY plot of solid volume fraction.

Fig. 5.11 shows the plot of expanded bed height vs. liquid velocity obtained at different values of inlet gas velocity. It is indicated from figure that there is slight decrease in the expanded bed height with increase in the gas velocity. This may be due to the bed contraction with increase in gas velocity but in our experiment as discussed in chapter-3, an increase in bed expansion has been observed.

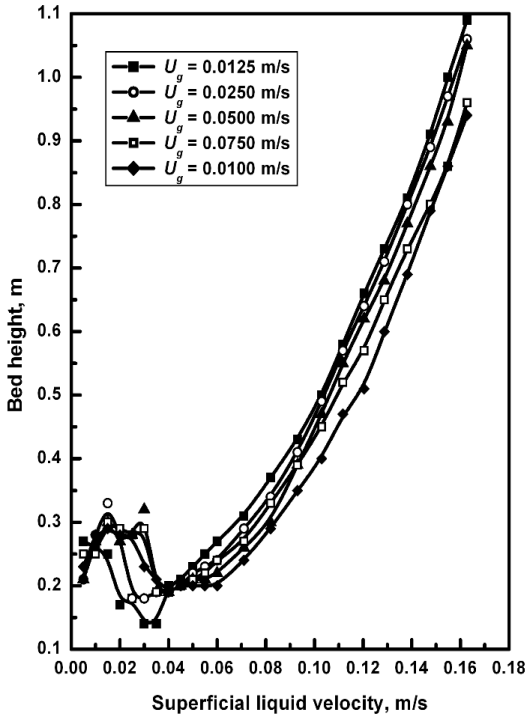

Fig. 5.11. CFD simulation result of bed expansion behaviour of 2.18 mm glass beads at H_s=0.171 m.

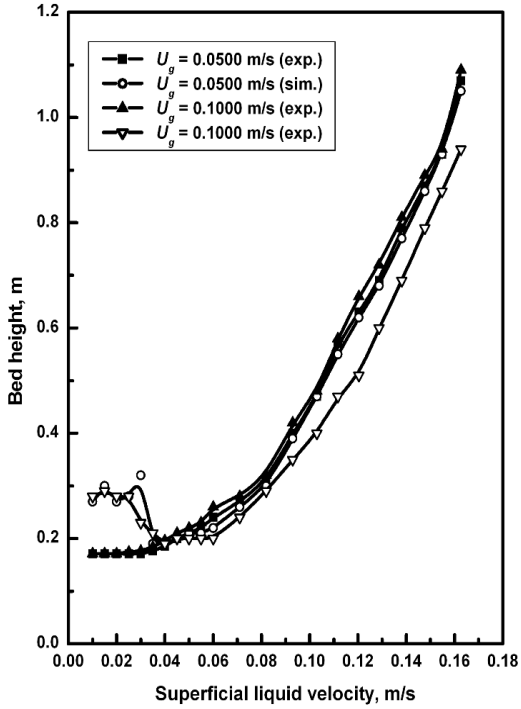

Fig. 5.12. Comparison of bed height obtained from experiment and CFD simulation.

Fig. 5.12 shows a comparison of the simulated and the experimental values of expanded bed height. A very good agreement is seen between the values for the gas velocity of 0.05 m/s, while for gas velocity of 0.10 m/s, the values have been found to deviate. At this higher gas velocity the simulated bed height has been found to be less than the experimental one. In experiment, a slight increase in bed height has been observed with the increase in the gas velocity. The computational model used is based on the prescription by some investigators. They might have found a decrease in bed height with the increase in gas velocity. The bed contraction truly occurs for particles of sizes close to 1 mm or less than that. Above all in the bed expansion regime (condition above minimum fluidization), the expanded bed height value from experiment and from simulation agrees within 10 %. In Figs. 5.11 and 5.12 at low liquid velocity, the bed height has been found to be higher, then it decreases and further increases with increase in liquid velocity. This indicates the presence of an agitation in the bed by the larger size gas bubbles where few particles are lifted giving the pseudo feeling of fluidization. Larger size bubbles appear at low liquid velocities and as liquid velocity increases the bubble size decreases. In experiment the agitated bed height has been neglected while measuring the bed height. CFD simulation result shows the agitated bed. In CFD result the agitated bed vanished near the minimum fluidization state.

5.4.2. Bed pressure drop

The axial pressure drop in a fluidized bed varies from higher value at the bottom of the bed to zero value at top of the column in the gauge pressure scale. Similar variation has been observed in the CFD simulation result as shown in Fig. 5.13, the contour plot of the static gauge pressure. The figure represents the contours of static gauge pressure (mixture phase) in the column obtained at water velocity of 0.12 m/s and air velocity of 0.0125 m/s. The bed pressure drop can be determined from the difference of pressure at the inlet (bottom) and the outlet (top).

As it was shown in Fig. 3.4 in chapter-3, a similar pressure profile for increased gas velocity is also resulted from CFD simulation. Fig 5.14 shows the plot of bed pressure drop vs. liquid velocity obtained at different inlet values of air velocity. It is evident that pressure drop increases when water velocity is increased. Also when the air velocity is small (U_g = 0.0125 m/s) there is no substantial increase in pressure drop with liquid velocity. This can be attributed to the fact that at low air velocity, volume fraction of the gas is low and does not change a lot with the variation in liquid velocity. But at higher gas velocity, the gas holdup is more and increase in liquid velocity cause a decrease in the gas holdup (increase in liquid holdup), thus leading to increase in pressure drop. Fig 5.15 presents the variation of bed pressure drop with superficial gas velocity. In the plot the effect of liquid velocity on pressure drop is also seen. Fig. 5.16 shows a comparison of bed pressure drop values obtained from the experiment and the CFD simulation. A fairly good agreement is seen between the two values.

5.4.3. Gas holdup

Gas holdup is obtained as mean area-weighted average of volume fraction of the gas phase at sufficient number of axial positions in the fluidized portion of the bed. As it can be seen from the XY plot (Fig. 5.17) of gas (air) volume fraction along the axis of the column that the volume fraction of air is not the same at all positions in the fluidized portion of the column, it varies with axial position and radial position. Hence area weighted average of volume fraction of air is determined at heights 0.05 m apart along the length of the column. These values are averaged to give the average gas holdup in the bed.

The variation of gas holdup with superficial liquid velocity obtained from CFD simulation is shown in Fig. 5.18. The figure shows a decrease in gas holdup with liquid velocity. The same has been obtained from experiments as discussed in chapter-3 and chapter-4. A steady decrease in gas holdup has been obtained from CFD simulation;

where as experimental finding shows a fast decrease in gas holdup at low values of liquid velocity but the rate decreases at higher liquid velocity ranges.

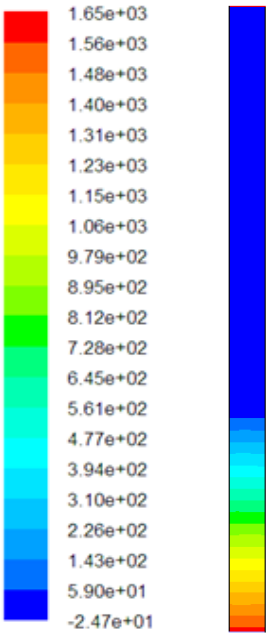

Fig. 5.13. Contours of static gauge pressure.

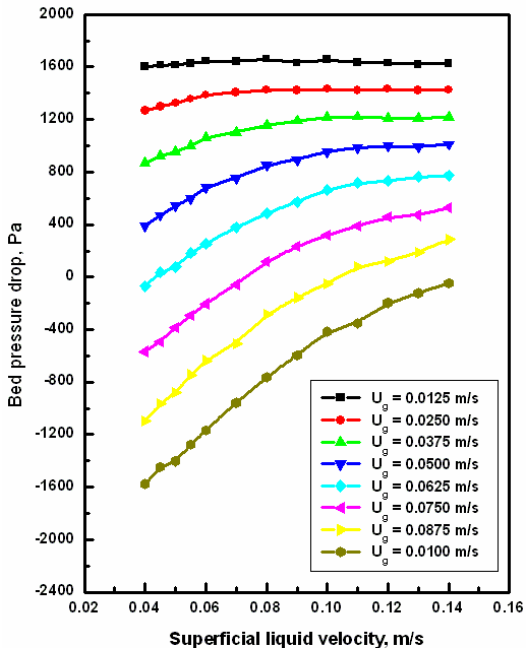

Fig. 5.14. Variation of pressure drop with liquid velocity at different values of gas velocity for 2.18 mm glass beads at H_s = 0.171 m.

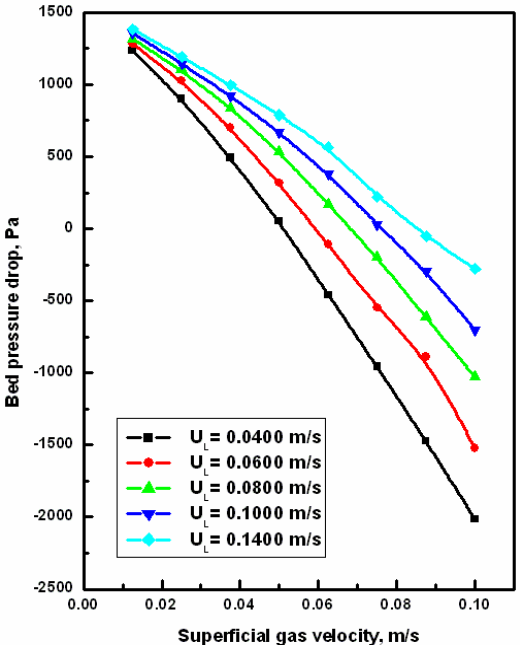

Fig. 5.15. Variation of pressure drop with gas velocity at different liquid values of velocity for 2.18 mm glass beads at H_s = 0.171 m.

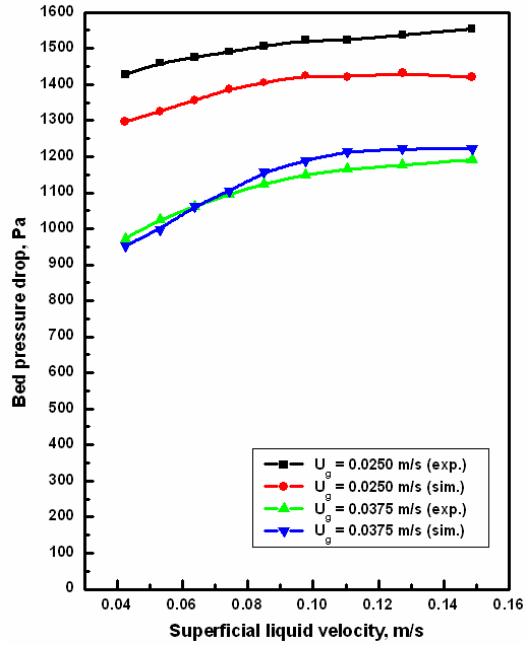

Fig. 5.16. Comparison of bed pressure drop.

Similarly from Fig. 5.19, it is seen that the gas holdup monotonically increases with increase in gas velocity. Fig. 5.20 shows a comparison of the gas holdup values obtained

from CFD simulation and the experimental. Good agreement between the two has been observed. As already discussed, decrease in gas holdup nearly at a constant rate has been observed with increase in the liquid velocity.

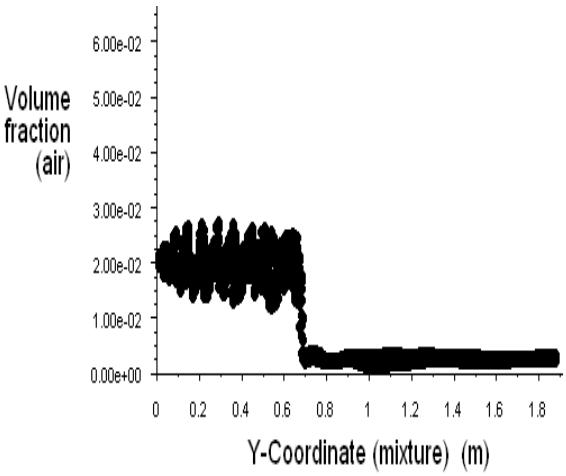

Fig. 5.17. XY plot of air volume fraction at water velocity of 0.12 m/s and air velocity of 0.0125 m/s for 2.18 mm glass beads with static bed height 0.213 m.

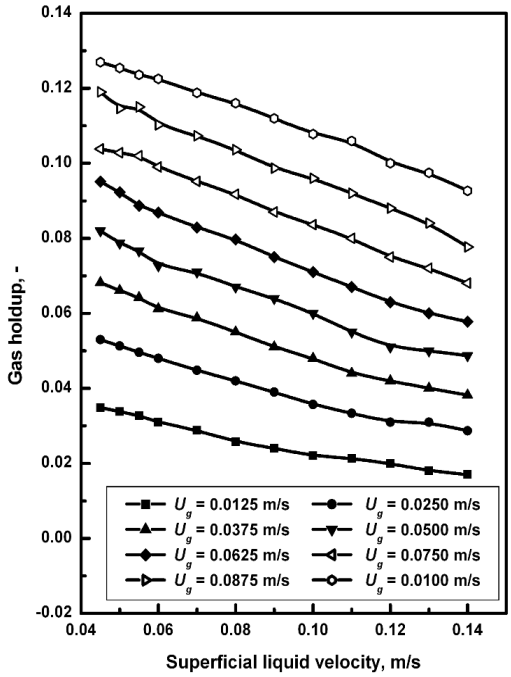

Fig. 5.18. Variation of gas holdup with liquid velocity at different values of gas velocity for 2.18 mm glass beads at H_s = 0.213 m.

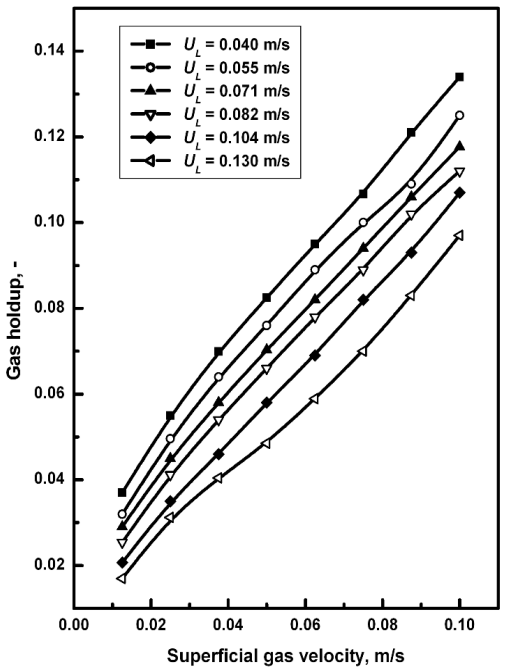

Fig. 5.19. Variation of gas holdup with gas velocity at different values of liquid velocity for 2.18 mm glass beads at H_s = 0.171 m.

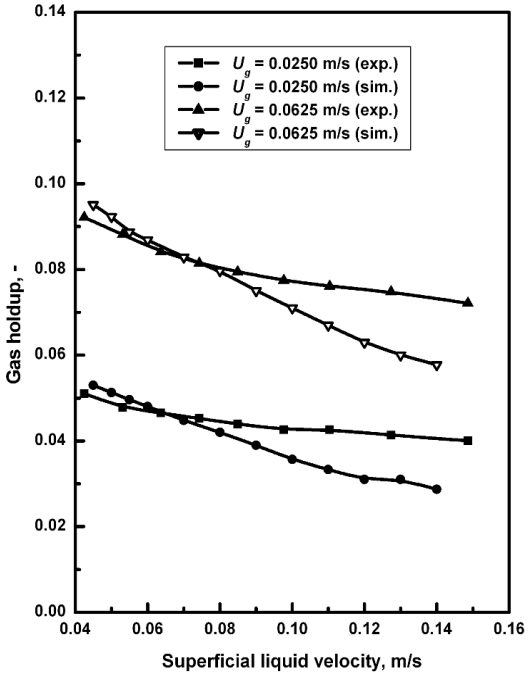

Fig. 5.20. Comparison of gas holdup.

5.5. Conclusion

CFD simulation of hydrodynamics of gas–liquid–solid fluidized bed has been carried out for different operating conditions by employing the Eulerian-Eulerian granular multi-phase approach. The CFD simulation results have shown good agreement with experimental data for solid phase hydrodynamics in term of expanded bed height of the present experimental findings and for gas and liquid phase hydrodynamics in terms of phase velocities and hold up. The bed pressure drop obtained from CFD simulation agree well with the experimental values. Both the bed expansion and pressure drop values indicate that the drag model used in CFD simulation has satisfactorily describe the three-phase (gas-liquid-solid) phenomena. The bed expansion behaviour with variation in gas velocity obtained from CFD simulation to some extent has corroborated the experimental findings. Experimental result has shown an increase in bed expansion with gas velocity, on the other hand CFD simulation has shown slight decrease in bed expansion.

The CFD simulation exhibited a solid circulation pattern for all the operating conditions, which is consistent with the observations reported by various earlier investigators. For liquid velocity of 0.04 m/s and a gas velocity of 0.10 m/s, the gas holdup in the bed has been found to be 0.1294. The gas hold up values have tallied very well at lower liquid velocity range, while at higher values of liquid velocity the values differed within 20 %. The good agreement between the values obtained from CFD simulation and experimental ones for the range of the present operating variables justify that the Eulerian-Eulerian multi-phase granular flow approach is capable to predict the overall performance of gas–liquid–solid fluidized bed.

Chapter 6

Hydrodynamics of Regular Particles in Semi-fluidized Bed

Chapter-6

Hydrodynamics of Regular Particles in Semi-fluidized Bed

6.1. Introduction

A semi-fluidized bed has the advantages of both the packed and the fluidized beds. The disadvantages of fluidized beds, namely back-mixing of solids, attrition of particles and erosion of surfaces, and those of packed beds, such as non-uniform bed temperatures, segregation of solids and channeling, are taken care of, at least partially in a semi-fluidized bed. The development and advantages of the semi-fluidized bed relating to studies on hydrodynamics, mass transfer, reaction kinetics and filtration have been highlighted by Fan and Wen (1961), Babu Rao et al. (1965, 1970), Murthy and Roy (1986) and Ho et al. (1987). Semi-fluidized beds have been applied successfully to many industrial processes (physical, chemical and biochemical) such as in the filtration, adsorption, catalytic reactions, heavy metal removal and recovery, coal pyrolysis, bio-oxidation, ethanol fermentation, granule tablet manufacturing etc. as discussed in chapter-1. A fairly good number of patents claimed since year 1958, relating to the best possible applications of the semi-fluidized bed in many industrial processes as reported by Liu et al. (2006).

Gas-liquid-solid semi-fluidized bed is possible in both co-current and counter current operation of the fluid phases. The use of two common types of gas-liquid solid semi-fluidized bed as reported in literature are the one with the co-current up flow of the liquid and the gas and the second an inversed fluidized bed, where counter flow of gas and liquid flow with liquid flow from top to bottom and the gas in up flow mode. Among these the most striking one is the co-current three-phase semi-fluidization with the liquid as the continuous phase (Chern et al., 1984). In a three-phase semi-fluidized bed a higher pressure drop than the fluidized bed is experienced due to formation of a packed bed at the top. This results a higher value of gas holdup, finer bubbles and ultimately higher interfacial area in the system.

The co-current gas-liquid-solid semi-fluidization is defined as an operation in which a bed of solid particles is partly fixed to a top grid or restraining plate whereas the rest of the particles are in a suspended state with upward flowing gas and/or liquid media. Such an operation generates considerable intimate contact among the gas, liquid and solid particles in the system and provides substantial advantages for applications in physical,

chemical or biochemical processing involving gas, liquid and solid phases (Fan, 1983; Chern et al., 1984).

For successful design and operation of a gas-liquid-solid semi-fluidized bed system, knowledge of fundamental characteristics of the system, viz. the hydrodynamics, heat and mass transfer characteristics are highly essential. The most important among the hydrodynamic characteristics are the semi-fluidized bed pressure drop, minimum and maximum semi-fluidization velocity, top packed bed height, porosity of the fixed and the fluidized sections in the semi-fluidized bed, distribution of solids between the packed and the fluidized sections, and phase holdups. Chern et al., (1984) have studied a few of these characteristics.

As evidenced from a comprehensive literature survey of the hydrodynamics of both liquid-solid and gas-liquid-solid semi-fluidized beds there is hardly any literature available on the hydrodynamic study of a gas-liquid-solid semi-fluidized bed. Chern et al. (1984) have reported the hydrodynamic parameters like pressure drop, minimum semi-fluidization velocity, height of packed section and fluidized section, and gas holdup based on separate experiments conducted in fluidized and packed beds. Singh et al. (2005) have investigated the pressure drop of semi-fluidized bed with irregular solid particles in a single experiment and developed a correlation from dimensional analysis. Literature survey reveals that almost no study is available where the semi-fluidized bed experiment has been conducted in the same vessel for a gas-liquid-solid up flow semi-fluidized bed with liquid as the continuous phase and using spherical particles. As far as the two-phase liquid-solid semi-fluidization is concerned, although a good number of research articles are available, the study is limited to a narrow range of operating variables. The particle sizes studied are either too small (< 1 mm) or large (> 4 mm). Mostly in the hydrodynamic studies irregular particles have been used and the literature on the use of spherical particles is scanty in liquid-solid bed, where as in gas-liquid-solid fluidized bed the use regular spherical particles is plenty. Viscosity effect has not been addressed in the earlier studies.

In this chapter the hydrodynamic characteristics of both the liquid-solid and the gas-liquid-solid semi-fluidized beds have been studied. The liquid-solid semi-fluidized bed behaviour has been extensively studied basically for two reasons i.e. firstly to develop more generalized correlations for the hydrodynamic parameters and secondly for the comparison of the hydrodynamics of the gas-liquid-solid system with that of the liquid-solid one in the same experimental set-up. Fan and Hsu (1980) and Fan (1983) have

discussed the suitability of the semi-fluidized bed as a bioreactor for aerobic and anaerobic applications. Later Dias (1991) has mentioned the significant performance of the semi-fluidized bed system in the extractive fermentation of ethanol. In the immobilized cell bioreactors the preferred size of the solid matrix is nearly 2-4 mm. In the present work spherical glass beads of size 2-4 mm have been used.

Further, the experimental system used ultimately aims at use of a semi-fluidized bed as an aerobic as well as an anaerobic bioreactor. The objective of the work outlined in this chapter is to develop a better understanding of the hydrodynamics of the liquid-solid and gas-liquid-solid semi-fluidization. The parameters studied in this chapter include the minimum and the maximum semi-fluidization velocities, the top packed bed height, the pressure drop across the semi-fluidized bed and the gas holdup. Experimental setup used for the study of gas-liquid-solid fluidization with modification has been used in this study.

6.2. Experimental set-up and techniques

A schematic representation of the experimental setup is shown in Fig. 6.1. This experimental setup is a modified version of the set-up as shown in Fig. 2.1 and discussed in chapter-2. The experimental semi-fluidized bed set-up consists of a fluidized bed assembly, a top restraining plate with handle to control and pressure taps. The fluidized bed assembly consists of a fluidizer, liquid distributor, liquid disengagement and recirculation facility, liquid pump, liquid storage tank, a set of calibrated liquid rotameters. The scope of the experiment is presented in Table 6.1. Accurately weighed amount of material is fed the column, fluidized and de-fluidized slowly with the liquid and adjusted for a specified reproducible initial static bed height. Liquid was pumped to the fluidizer at a desired flow rate using calibrated rotameter. The air was then injected into the column through the air sparger at a desired flow rate. Approximately five minutes were allowed to make sure that the steady state has been reached. The readings for pressure drop using mercury manometers, expanded bed heights or the top packed bed height (as the case may be) of the bed were then noted. All experiments have been conducted at temperature of (30 ± 5) ^{O}C. The procedure has been repeated varying the particle size, viscosity and density of the liquid, bed expansion ratio (R) and initial static bed height. For gas holdup measurement the phase isolation method has been used as discussed in chapter-3.

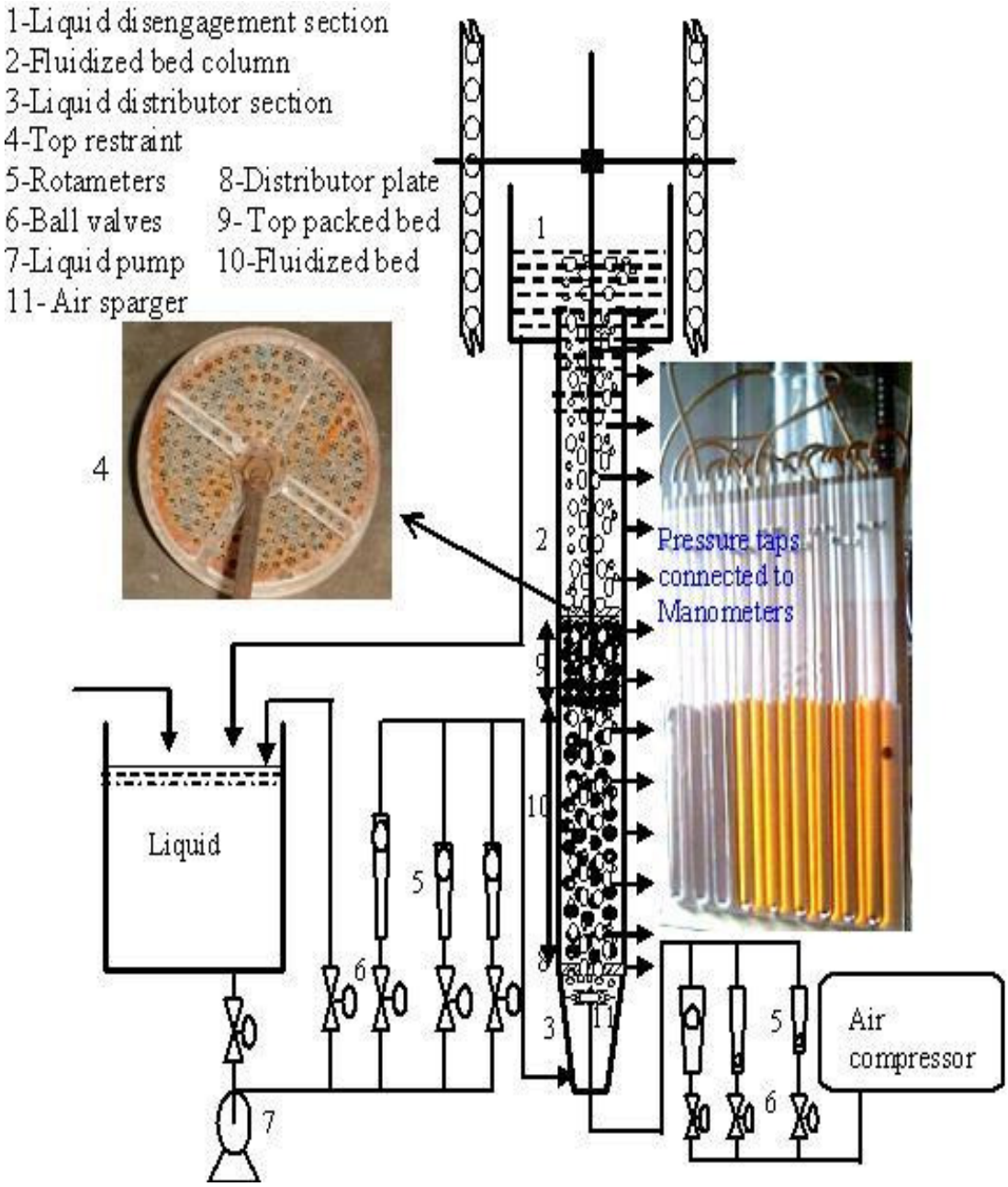

Fig. 6.1. Experimental setup of the semi-fluidized bed.

Table 6.1: Scope of the experiment

Solid-liquid system	d_p, mm	ρ_p, kg/m^3	ε_s, -	ρ_L, kg/m^3	μ_Lx10^3, Pa.s	H_s, m	R, -
Air-water-glass beads	2.18	2470	0.425	995.7	0.789	0.171	2.5
do	2.18	2470	0.425	995.7	0.789	0.213	2.5
do	2.18	2470	0.425	995.7	0.789	0.256	2.5
do	2.18	2470	0.425	995.7	0.789	0.301	2.5
do	2.58	2470	0.423	995.7	0.789	0.171	2.5
do	3.07	2470	0.420	995.7	0.789	0.171	2.5
do	4.05	2470	0.415	995.7	0.789	0.171	2.5
do	2.18	2470	0.425	995.7	0.789	0.171	2.0
do	2.18	2470	0.425	995.7	0.789	0.171	3.0
do	2.18	2470	0.425	995.7	0.789	0.171	3.5
do	3.07	2470	0.420	995.7	0.789	0.171	2.0
Air-aqueous solution of glycerol-glass beads % by mass of glycerol							
6.0	3.07	2470	0.420	1009.7	0.948	0.171	2.0
12.0	3.07	2470	0.420	1024.0	1.082	0.171	2.0
18.0	3.07	2470	0.420	1039.0	1.268	0.171	2.0
24.0	3.07	2470	0.420	1054.0	1.567	0.171	2.0
Superficial gas velocity:	$0.0 < U_g < 0.1274$ m/s						
Superficial liquid velocity:	$0.0 < U_L < 0.3057$ m/s						
Temperature:	$(30\pm5)^0$C						
Gas phase:	Air, density = 1.166 kg/m^3, viscosity = 1.794x10^{-5} Pa.s						

6.3. Minimum semi-fluidization velocity

In liquid-solid system minimum semi-fluidization velocity also called the onset velocity of semi-fluidization (U_{osf}) is the superficial liquid velocity at which a bed particle of the expanded fluidized bed first touches the top restraint of the semi-fluidizer. For gas-liquid-solid system with liquid as the continuous phase, the minimum semi-fluidization velocity is also referred to as the minimum liquid semi-fluidization velocity (onset liquid velocity of semi-fluidization) (U_{Losf}). Experimentally the minimum semi-fluidization velocity can be determined by the following methods. (i) From the plot of the ratio of the height of the top restraint to the height of the expanded fluidized bed (H_f/H_t) versus the superficial liquid velocity (U_L) as illustrated in Fig. 6.2. (ii) From the plot of pressure drop across the bed versus the superficial liquid velocity as illustrated in Fig. 6.3. (iii) For comparatively large particles from the visual observation. As the top portion of the fluidized bed is dilute in particles, it is practically difficult to ascertain the exact height of the expanded bed. In such a case, if the height of the expanded bed is taken as the height of the moderately dense bed then it predicts a higher value of U_{osf}. On the other hand if the top surface of the dilute bed is considered for the purpose, it predicts a lower value of U_{osf}. The pressure drop method seems to be the most reliable one. Fan and Wen (1961), Roy and Sarma (1972), Roy and Sharat Chandra (1976) and Ho et al. (1987) have recommended the pressure drop method for the prediction of U_{osf}. Chern et al. (1984)

have measured U_{osf} (or U_{Losf}) by extrapolation of the bed expansion relationship of the fluidized bed.

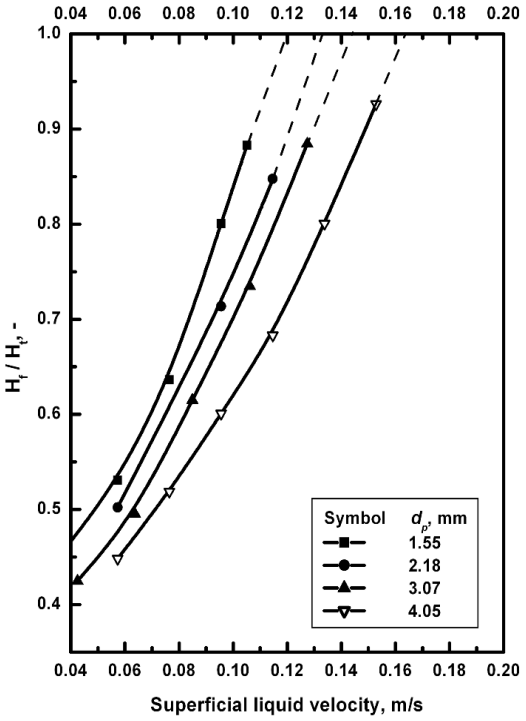

Fig. 6.2. Variation of H_f/H_f with superficial liquid velocity for glass beads and water with H_s=0.171 m and R=2.5.

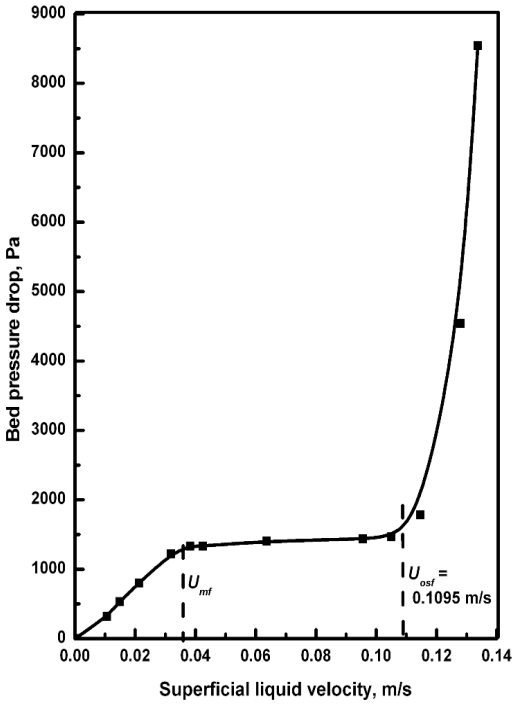

Fig. 6.3. Variation of bed pressure drop with U_L for 2.18 mm particles in water with h_s=0.171 m and R=2.5.

In the present study the values of the minimum semi-fluidization velocity have been experimentally obtained by both the methods (i) and (ii) and reported in Table 6.2, but the values from method-(ii) have been used for the development of the model equations. In the present investigation the values of the minimum semi-fluidization velocity obtained from method-(i) have been found to be higher than those obtained from method-(ii). Fig. 6.4 shows the almost negligible effect of initial static bed height on the minimum semi-fluidization velocity. The independency of U_{osf} on static bed height for the liquid-solid system has been reported by Roy and Sarma (1972) and Roy and Sharat Chandra (1976). But Ho et al. (1987) have reported that the marginal effect of initial static bed height on the minimum semi-fluidization velocity in a gas-solid semi-fluidized bed. They have reported a decrease in the minimum semi-fluidization velocity with the increase in initial static bed height. According to them is that an increase in static bed height corresponds to an increase in bubble size, which in turn promotes the bed expansion and accelerates the semi-fluidization process. But the phenomenon is not observed in case of a liquid-solid system, thus the minimum semi-fluidization velocity being practically un-affected by the initial static bed height.

The effect of particle size on U_{osf} is presented in Fig. 6.5. This shows that larger the particle size higher is the minimum semi-fluidization velocity. This is true as higher drag force and ultimately the higher fluid velocity is required to lift the bigger size particle which bears a higher mass. The bed expansion ratio has a strong effect on the minimum semi-fluidization velocity as indicated in Fig. 6.6. The reason is the requirement of higher fluid velocity to lift the particle to a relatively higher position of the top restraint in the bed. U_{osf} increases with the increase in bed expansion ratio. The same behaviour has been observed by other investigators also.

To study the effect of liquid viscosity, aqueous solutions of glycerol (0 – 24 % by mass) have been used as the liquid phase. The properties of the solutions are given in Table 6.1. For the glycerol solutions there is an increase both in the density and viscosity with increase in the percentage of glycerol in the solution. The increase in viscosity is predominant over density as increase in viscosity is 96.7% for 24% glycerol solution over the water; where as the increase in density is only 5.85% for the same solution. Thus the study on viscosity effect using these solutions is not far away from the assumption of the constant density. The effect of liquid viscosity on the minimum semi-fluidization velocity is shown in Fig. 6.7. The figure indicates the decrease in the minimum semi-fluidization velocity with increase in the liquid viscosity. This is due to the fact that the particle experiences a higher drag at lower velocity of the liquid possessing higher viscosity.

Kurian and Raja Rao (1970) have suggested two theoretical methods for the estimation of U_{osf}. The first method is based on the correlation for the expanded bed voidage. Use of this method is not convenient as one has to use the proposed expanded bed voidage correlation along with the correlation graph given in their published article (Kurian and Raja Rao, 1970). The second method is based on the correlation for the height of the top packed section (H_{pa}), which is discussed in detail in the following section *3.4* on height of packed bed. At the onset of semi-fluidization, H_{pa}=0, the correlation is given by,

$$\frac{U_{osf} - U_{mf}}{U_t - U_{mf}} = 0.61\left(\frac{R}{R-1}\right)^{-1.2} \tag{6.1}$$

In the present work, the observed minimum semi-fluidization velocity has been correlated with the static bed height, bed expansion ratio, particle size and liquid viscosity. The following equation with a correlation coefficient of 0.977 has been obtained.

$$U_{osf} = 0.14R^{0.887}d_p^{0.468}\mu_L^{-0.254} \tag{6.2}$$

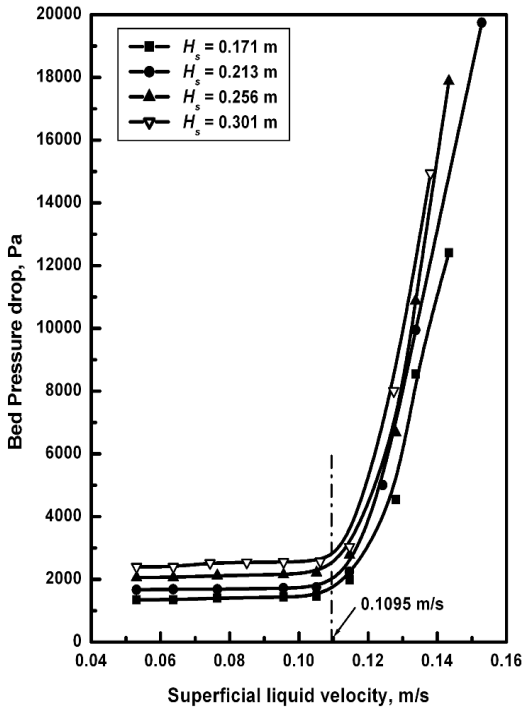

Fig. 6.4. Variation of bed pressure drop with U_L for 2.18 mm particles in water at different H_s with R=2.5.

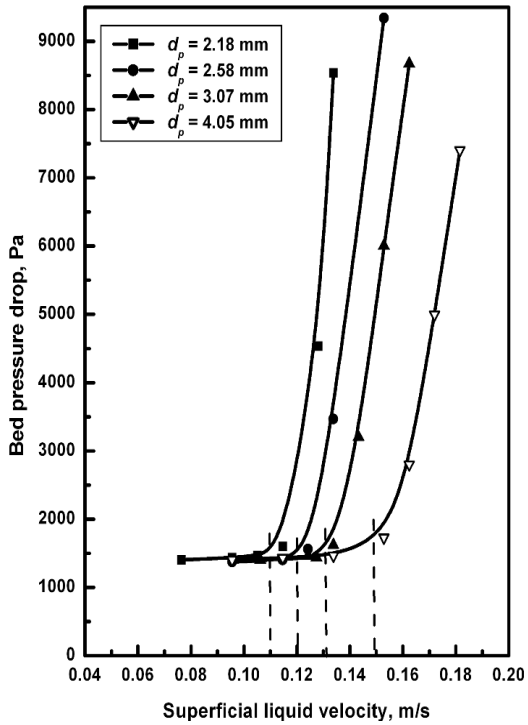

Fig. 6.5. Variation of bed pressure drop with U_L for different particle sizes in water with H_s =0.171 m and R=2.5.

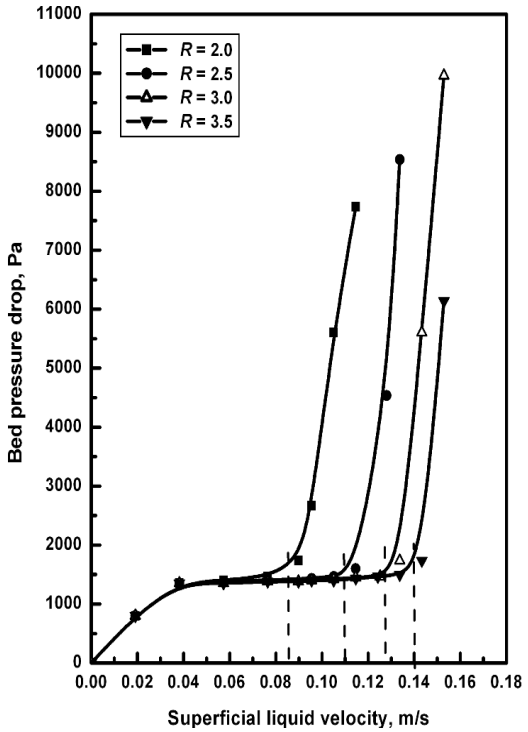

Fig. 6.6. Variation of bed pressure drop with $U_{:L}$ for 2.18 mm particles in water at different values of R with H_s=0.171 m.

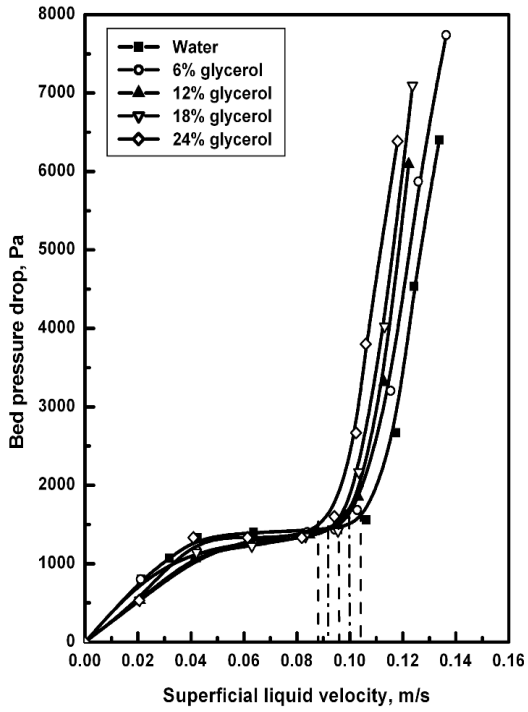

Fig. 6.7. Variation of bed pressure drop with U_L for 3.07 mm particles in aqueous solution of glycerol of different composition at H_s=0.171 m and R=2.0.

It is interesting to note that the minimum semi-fluidization velocity is independent of static bed height. To test the validity of the above correlation, a few more experimental runs have been carried out with glass bead of size 1.55 mm, bed expansion ratios of 1.5, 1.75, 2.25, 2.75, 3.25, 3.75 and 4.0 and liquid viscosity of 0.001752 Pa.s (30% by mass of glycerol solution) which are near the range of variables studied. Values of U_{osf} predicted from Eqs. (6.1) and (6.2) and the experimental ones have been reported in Table 6.2 and compared in Fig. 6.8. The Eq. (6.2) adequately describes the observed data with a standard deviation value of 0.0235 as indicated in Fig. 6.8. Values of U_{osf} predicted from Eq. (6.1) also shows a good agreement except for four points deviating more than 10%. In the figure the legend indicating the other data points means those which have not been used for the development of the empirical model.

Table 6.2: Minimum and maximum semi-fluidization velocities (liq.-sol. system)

H_s (m)	d_p (mm)	R	μ_Lx10^3 (Pa.s)	U_{mf}^{*} (m/s)	U_{osf}^{**1} (m/s)	U_{osf}^{**2} (m/s)	U_{osf}^{***} (m/s)	U_{msf}^{**} (m/s)	$U_t^{\$}$ (m/s)	$U_{msf}^{\#}$ (m/s)
0.171	2.18	2.5	0.798	0.0256	0.1214	0.1095	0.1195	0.3310	0.3098	0.2163
0.213	2.18	2.5	0.798	0.0256	0.1214	0.1095	0.1195	0.3516	0.3098	0.2163
0.256	2.18	2.5	0.798	0.0256	0.1214	0.1095	0.1195	0.3677	0.3098	0.2163
0.301	2.18	2.5	0.798	0.0256	0.1214	0.1095	0.1195	0.3956	0.3098	0.2163
0.171	2.58	2.5	0.798	0.0302	0.1326	0.1204	0.1315	0.3683	0.3370	0.2413
0.171	3.07	2.5	0.798	0.0348	0.1444	0.1311	0.1449	0.4045	0.3679	0.2705
0.171	4.05	2.5	0.798	0.0428	0.1639	0.1492	0.1682	0.4642	0.4222	0.3235
0.171	2.18	2.0	0.798	0.0256	0.0989	0.0855	0.1011	0.2733	0.3098	0.2163
0.171	2.18	3.0	0.798	0.0256	0.1385	0.1280	0.1322	0.3602	0.3098	0.2163
0.171	2.18	3.5	0.798	0.0256	0.1520	0.1397	0.1414	0.3801	0.3098	0.2163
0.171	3.07	2.0	0.798	0.0348	0.1180	0.1043	0.1232	0.3278	0.3679	0.2705
0.171	3.07	2.0	0.948	0.0331	0.1113	0.0998	0.1068	0.3074	0.3104	0.2628
0.171	3.07	2.0	1.082	0.0316	0.1065	0.0958	0.0943	0.2846	0.2680	0.2559
0.171	3.07	2.0	1.268	0.0297	0.1035	0.0918	0.0822	0.2687	0.2273	0.2486
0.171	3.07	2.0	1.567	0.0275	0.0983	0.0881	0.0784	0.2492	0.2193	0.2410

[*] Calculated from the correlation of Wen and Yu (1966).
[**] Experimental values. [1] method-1, [2] method-2.
[***] Calculated from the correlation of Kurian and Raja Rao (1970).
[$] Calculated from Intermediate law or Newton's law (Gupta and Sathiyamoorthy, 1999).
[#] Calculated from the correlation of Roy (1975).

Similarly, the minimum liquid semi-fluidization velocity (U_{Losf}) for gas-liquid-solid system has been determined. For a constant gas velocity, the liquid velocity has been varied and the semi-fluidization behaviour has been observed. Figs. 6.9 and 6.10 show the variation of bed pressure drop with liquid velocity at different values of gas velocity and bed expansion ratio. The U_{Losf} has been found to decrease with increase in gas velocity and increase with increase in bed expansion ratio. The values of bed pressure drop have been plotted against the superficial liquid velocity for different particle sizes and aqueous solutions of glycerol with other parameters maintained at constant level and presented in Figs 6.11 and 6.12. The minimum liquid semi-fluidization velocity is a strong function of the particle size. As particle size increases minimum liquid semi-

fluidization velocity increases and with increase in liquid viscosity the U_{Losf} decreases. U_{Losf} has been found to decrease with increase in liquid viscosity at a fixed gas velocity. It has been found that the influence of initial static bed height on minimum liquid semi-fluidization velocity is not significant. There is very little increase in minimum liquid semi-fluidization velocity with increase in initial static bed height,

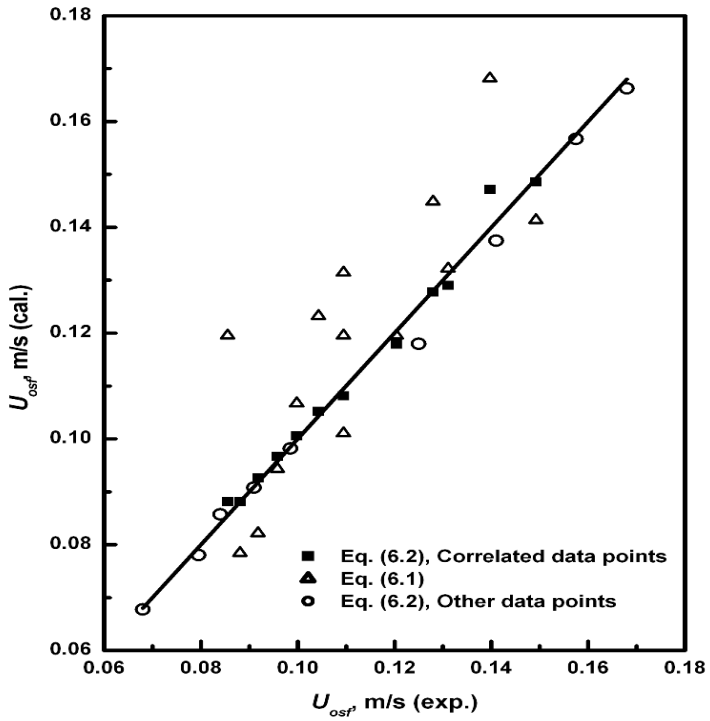

Fig. 6.8. Comparison of the values of minimum semi-fluidization velocity in liquid-solid system.

For the prediction of minimum liquid semi-fluidization velocity in gas-liquid-solid system, a correlation from the non-linear regression analysis has been developed as given below (Eq. (6.3))

$$U_{Losf} = 0.037 U_g^{-0.267} R^{0.497} d_p^{0.228} \mu_L^{-0.157} \tag{6.3}$$

The correlation (Eq. (6.3)) has been found to agree well with experimentally determined minimum liquid semi-fluidization velocities with an AARE of 1.23 %. The values of U_{Losf} calculated from the model of Chern et al. (1984) have also been compared with the experimental values in Fig. 6.13. Most of the calculated values have been found to deviate even more than 30 % from those obtained in the present work. Further the calculated values of U_{Losf} have been found be higher than the U_{osf} for the liquid-solid system. The values of U_{osf} for the liquid-solid system were found to agree with the model of Kurian and Raja Rao (1970). The higher values of U_{Losf} calculated from model of

Chern et al. (1984) may be due to the difference in the values of the expanded bed voidage calculated by them from the k-x generalized wake model.

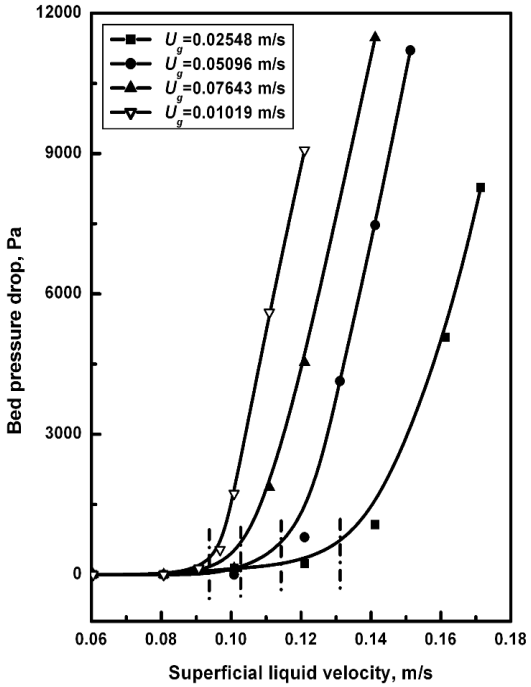

Fig. 6.9. Variation of bed pressure drop with superficial liquid velocity at different fixed values of gas velocity for 4.05 mm glass beads at R=2.5 and H_s=0.171 m.

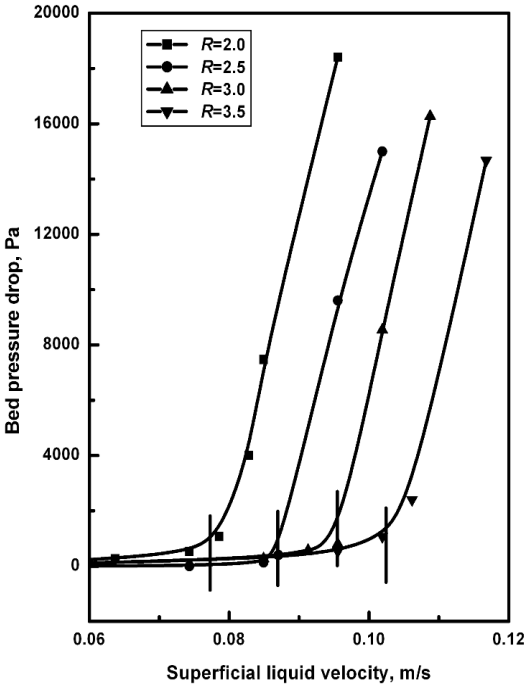

Fig. 6.10. Variation of bed pressure drop with superficial liquid velocity at different values of bed expansion ratio for 2.18 mm glass beads at H_s=0.171 m and U_g=0.07643 m/s.

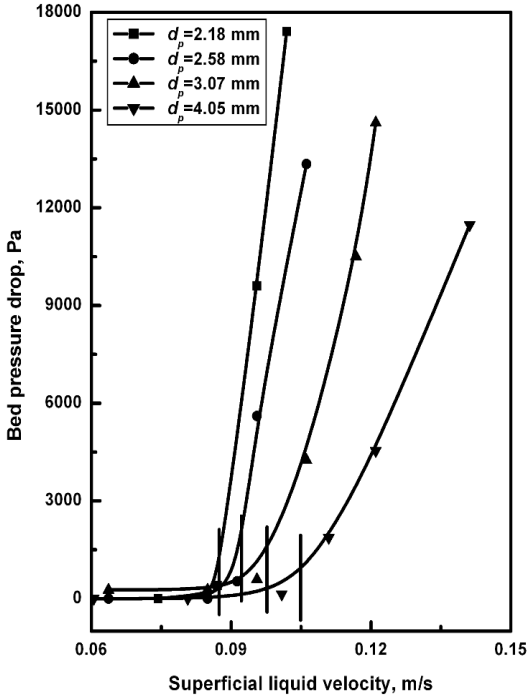

Fig. 6.11. Variation of bed pressure drop with superficial liquid velocity for different particle sizes of glass beads at R=2.5, H_s=0.171 m and U_g=0.07643 m/s.

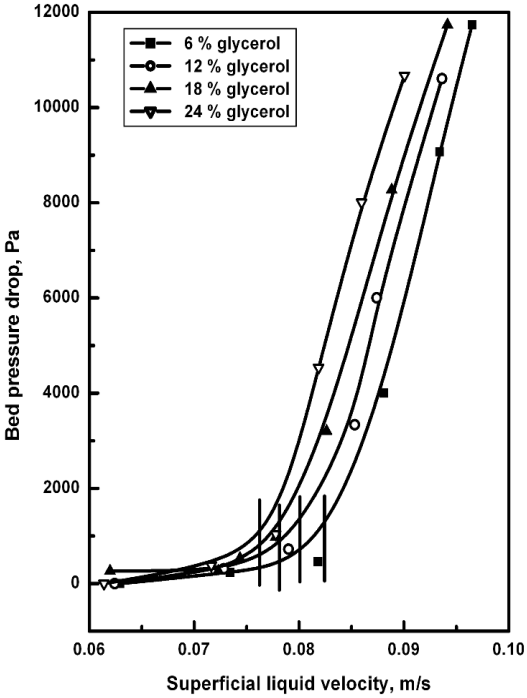

Fig. 6.12. Variation of bed pressure drop with superficial liquid velocity for aqueous solutions of glycerol and for 3.07 mm glass beads at R=2.0, H_s=0.171 m and U_g=0.07643 m/s.

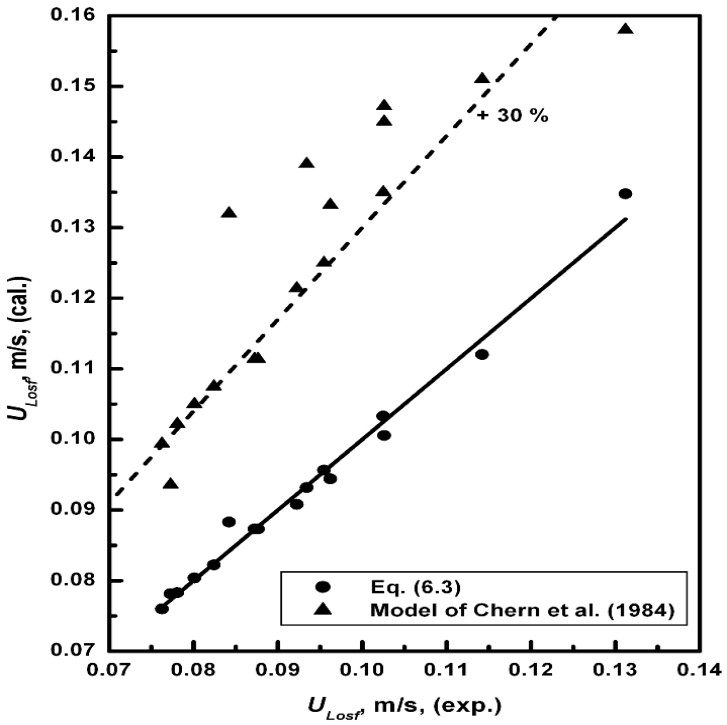

Fig. 6.13. Comparison of experimental Values of U_{oLsf} with the calculated ones from Eq. (6.33) and model of Chern et al. (1984).

6.4. Maximum semi-fluidization velocity

The maximum semi-fluidization velocity (U_{msf}) is the fluid velocity at which the entire bed of solid particles is transferred to the top packed bed. Theoretically this velocity corresponds to the terminal (free fall) velocity (U_t) of the particles. The intermediate law for gravity settling (intermediate flow) or the Newton's law (turbulent flow) as given by Gupta and Sathiyamoorthy (1999) is valid for most of the experimental conditions and has been used for the calculation of terminal velocity.

For intermediate flow:

$$\mathrm{Re}_t = 0.1527 Ar^{0.7143} \tag{6.4}$$

For turbulent flow:

$$\mathrm{Re}_t = 1.74 Ar^{0.5} \tag{6.5}$$

Fan and Wen (1961) and Kurian and Raja Rao (1970) have shown some sort of suitability of these laws for their experimental conditions. But many other investigators have suggested the use of experimental determination of the maximum semi-fluidization velocity. The reason may be the following. The terminal velocity predicted from the intermediate law or Newton's law is actually valid for a single particle. These laws may not predict the accurate values of the maximum semi-fluidization velocity due to definite influence of the presence of the other particles, as well as the effect of column wall and

supports. There is a definite effect of the position of the top restraining plate relative to the static bed height on U_{msf}, but the terminal velocity for a specific particle system is independent of the grid position. The terminal velocity may be used to represent U_{msf} when the position of the top grid is at a much higher level (say at infinite position). Thus it is meaningful to find the maximum semi-fluidization velocity from the experiment if possible.

In actual experiment, very often it is not possible to transfer the entire particles to the top packed bed. There are two methods used for the prediction of the maximum semi-fluidization velocity from extrapolation of the experimental data. (i) By extrapolation of the porosity of the fluidized section (ε_f) vs. superficial liquid velocity curve to $\varepsilon_f = 1$ or (ii) by extrapolation H_{pa}/H_s vs. superficial liquid velocity curve to $H_{pa}/H_s = 1$. The extrapolation of ε_f produce quite higher values of maximum semi-fluidization velocity for the liquid-solid system. Fan and Wen (1961), Kurian and Raja Rao (1970) and Roy (1975) have suggested the use of the second method i.e. the extrapolation H_{pa}/H_s vs. superficial liquid velocity curve to $H_{pa}/H_s = 1$ over the former. In the present study, the second method has been used to determine the values of the maximum semi-fluidization velocity.

For the liquid-solid system, the maximum semi-fluidization velocity has been found to increase with the initial static bed height, the particle size and the bed expansion ratio, but to decrease with the increase in the liquid viscosity as indicated in Figs. (6.14) through (6.17). Roy (1975) has shown the independency of U_{msf} on initial static bed height and bed expansion ratio, but in the present work a significant effect of these variables has been observed. The discrepancy may be due to the difference in geometry and design of the components of the semi-fluidized bed, particle size and shape of the particles.

The experimental values of U_{msf} have been reported in Table 6.2. This table also gives the values of U_{msf} calculated from the equation proposed by Roy (1975) and the terminal velocity calculated from Eq. (6.4) or (6.5) for the given experimental conditions. The experimental values and the values of U_{msf} calculated from correlations have been compared in Fig. 6.18. As observed from the figure, the experimental values U_{msf} are in some close agreement with those predicted from Eq. (6.4) or (6.5), but deviate a lot from the prediction using the correlation of Roy (1975). Like Eq. (6.2), a correlation for U_{msf} has been developed as given by Eq. (6.6) below with a correlation coefficient of 0.972.

$$U_{msf} = 0.5051 H_s^{0.3474} R^{0.6659} d_p^{0.6152} \mu_L^{-0.4651} \qquad (6.6)$$

The equation adequately describes the observed data with a standard deviation of 0.0274 as indicated in Fig. 6.18.

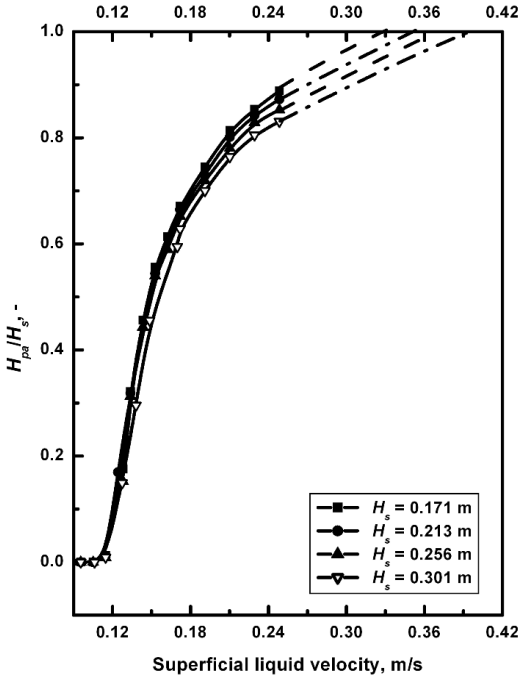

Fig. 6.14. Variation of H_{pa}/H_s with U_L for 2.18 mm particles in water at different values of initial static bed height with R=2.5.

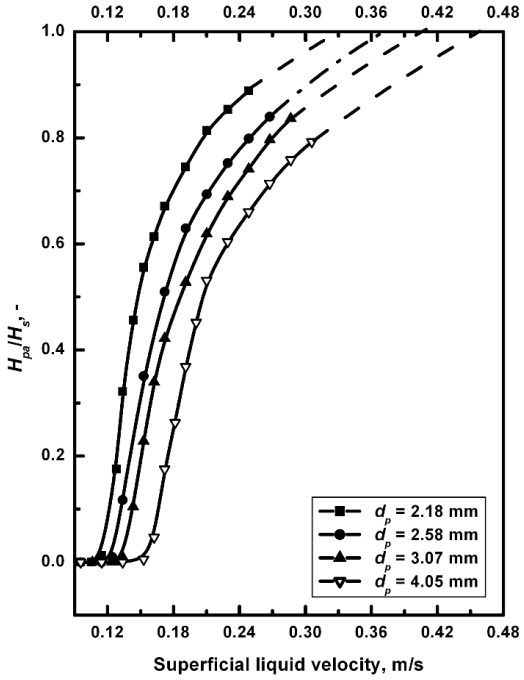

Fig. 6.15. Variation of H_{pa}/H_s with U_L for different particle sizes in water with H_s=0.171 m and R=2.5.

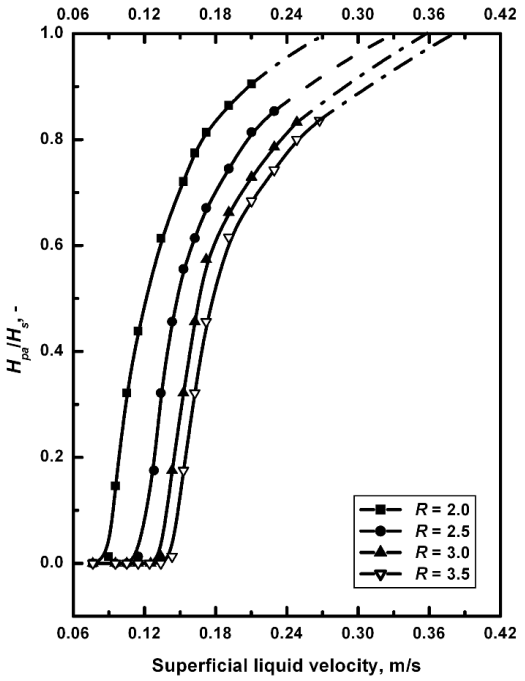

Fig. 6.16. Variation of H_{pa}/H_s with U_L for 2.18 mm particles of glass bead in water for different values of bed expansion ratio at H_s=0.171 m.

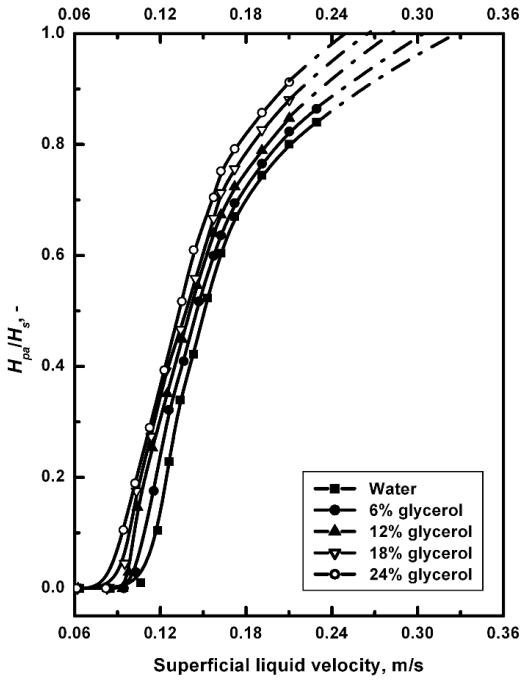

Fig. 6.17. Variation of H_{pa}/H_s with U_L for 3.07 mm glass beads in aqueous solutions of glycerol at H_s=0.171 m and R=2.0.

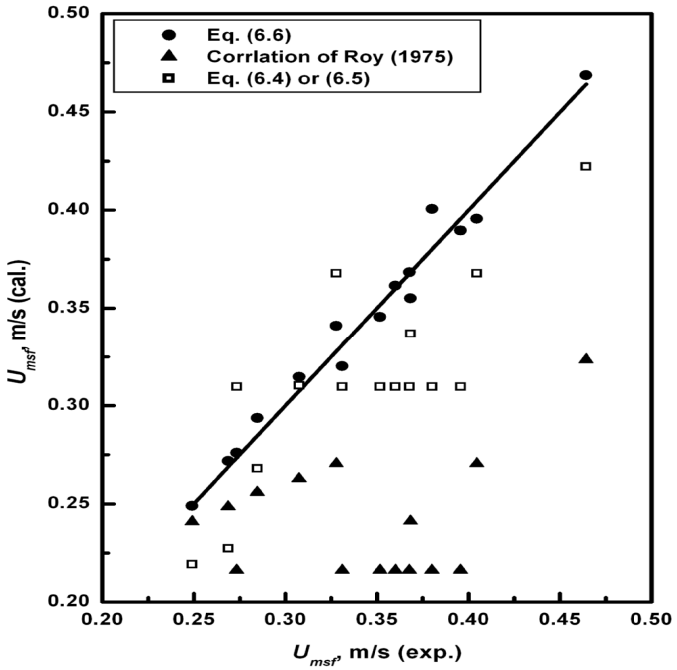

Fig. 6.18. Comparison of the values of maximum semi-fluidization velocity in liquid-solid system.

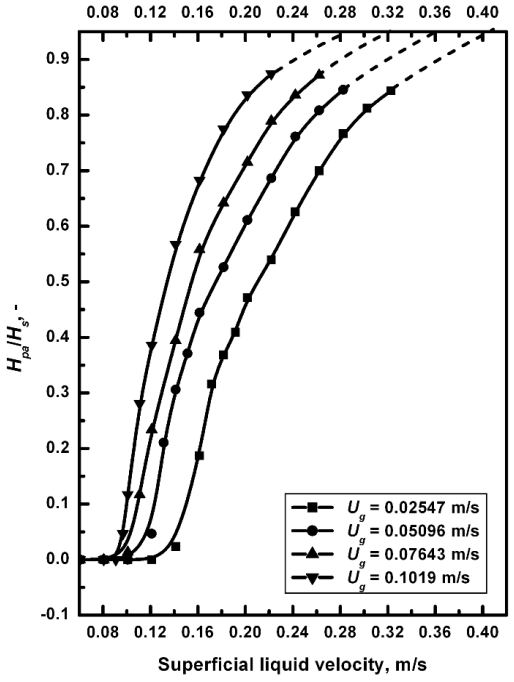

Fig. 6.19. Variation of H_{pa}/H_s with U_L at different fixed values of gas velocity for 4.05 mm glass beads at R=2.5 and H_s=0.171 m.

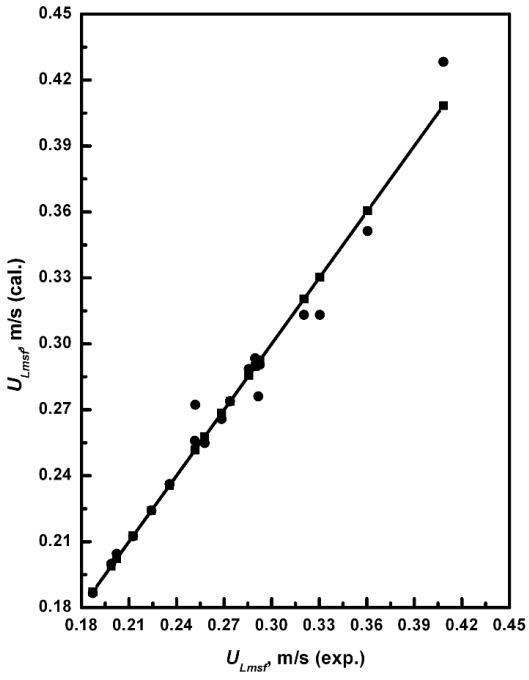

Fig. 6.20. Comparison of experimental values of maximum liquid Semi-fluidization velocity with those calculated from Eq. (6.7).

For gas-liquid-solid system in a similar manner the maximum liquid semi-fluidization velocity (U_{Lmsf}) has been determined keeping the gas velocity at a fixed value. It has been observed that U_{Lmsf} decreases with gas velocity as indicated in Fig. 6.19, which represents the contribution of the gas to fluidization and so also to semi-fluidization.

Similarly it has been observed that U_{Lmsf} increases with bed expansion ratio, particle size, static bed height and density difference between solid and liquid phase, and decreases with liquid viscosity.

A correlation for the prediction of minimum liquid semi-fluidization velocity in gas-liquid-solid system has been developed from non-linear regression analysis of the data and has been presented as Eq. (6.7).

$$U_{Lmsf} = 0.144 U_g^{-0.285} R^{0.646} d_p^{0.455} H_s^{0.367} \mu_L^{-0.366} \tag{6.7}$$

The values of U_{Lmsf} calculated from the developed correlation (Eq. (6.7)) has been found to agree well with experimental values of U_{Lmsf} with an AARE of 1.81 %.

6.5. Dimensionless minimum and maximum semi-fluidization velocity

The onset of fluidization and semi-fluidization are two consecutive events in the sequence of the operation of the semi-fluidization phenomenon. Thus many investigators have found it convenient to represent the correlation for minimum semi-fluidization velocity in the dimensionless form as ratio of the minimum semi-fluidization velocity to the minimum fluidization velocity i.e. U_{osf}/U_{mf}. A few of them have represented the dimensionless minimum semi-fluidization velocity as the function of the system and operating variables directly viz. Ho et al. (1987), but some other researchers (Roy and Sarma, 1972, Roy and Sharat Chandra, 1976) have used the system and operating variables in dimensionless form. In the present work empirical equations for U_{osf}/U_{mf} have been represented in both the forms for the convenient use of the designers. There are many correlations available for the prediction of the minimum fluidization velocity from the knowledge of the fluid and solid properties. In the present communication, the minimum fluidization velocity has been predicted from the correlation of Wen and Yu (1966), used widely.

$$\mathrm{Re}_{mf} = \sqrt{33.7^2 + 0.0408 Ar} - 33.7 \tag{6.8}$$

The experimental values of the dimensionless minimum semi-fluidization velocity in liquid-solid semi-fluidized bed have been reported in Table 6.3. The dimensionless minimum semi-fluidization velocity is independent of the static bed height. For all other variables at constant value, the smaller the particle size the higher is the dimensionless minimum semi-fluidization velocity. The dimensionless minimum semi-fluidization velocity increases with the increase in bed expansion ratio. There is a slight increase in the dimensionless minimum semi-fluidization velocity (U_{osf}/U_{mf}) with the increase in liquid viscosity. In terms of system and operating variables and the variables in their

dimensionless term, the dimensionless minimum semi-fluidization velocity (U_{osf}/U_{mf}) can be represented as;

$$\frac{U_{osf}}{U_{mf}} = f(H_s, D_c, d_p, \rho_s, \rho_L, \mu_L, R) \tag{6.9}$$

$$\frac{U_{osf}}{U_{mf}} = f\left[\frac{H_s}{D_c}, \frac{d_p}{D_c}, \frac{\rho_s}{\rho_L}, \frac{\mu_L}{\mu_w}, R\right] \tag{6.10}$$

Since the column diameter and the density of solid are constant, the variation in the liquid density is negligible and the effect of static bed height is not relevant, with the help of the remaining experimental parameters, the equations developed are;

$$\frac{U_{osf}}{U_{mf}} = 0.388 d_p^{-0.369} \mu_L^{0.099} R^{0.916} \tag{6.11}$$

$$\frac{U_{osf}}{U_{mf}} = 0.449 \left(\frac{d_p}{D_c}\right)^{-0.369} \left(\frac{\mu_L}{\mu_w}\right)^{1.14} (R)^{0.916} \tag{6.12}$$

Both the equations possess a correlation coefficient of 0.9804 and predict the same value of the dimensionless minimum semi-fluidization velocity, but appear in different forms. The values of the dimensionless minimum semi-fluidization velocity predicted from Eqs. (6.11) and (6.12) are in very close agreement with the experimental values with a standard deviation of 2.59%.

Table 6.3: Values of dimensionless minimum and maximum semi-fluidization velocity in liquid-solid semi-fluidized bed

$\frac{h_s}{D_c}$	$\frac{d_p}{D_c}$	R	$\frac{\mu_l}{\mu_w}$	$\frac{U_{osf}}{U_{mf}}$ *	$\frac{U_{osf}}{U_{mf}}$ **	$\frac{U_{osf}}{U_{msf}}$ *	$\frac{U_{osf}}{U_{msf}}$ &	$\frac{U_{msf}}{U_{mf}}$ *	$\frac{U_{msf}}{U_{mf}}$ #
1.71	0.0218	2.5	1.000	4.272	7.208	0.3308	0.3638	12.91	15.49
2.13	0.0218	2.5	1.000	4.272	7.208	0.3114	0.3638	13.72	15.49
2.56	0.0218	2.5	1.000	4.272	7.208	0.2978	0.3638	14.35	15.49
3.01	0.0218	2.5	1.000	4.272	7.208	0.2768	0.3638	15.44	15.49
1.71	0.0258	2.5	1.000	4.013	6.892	0.3269	0.3763	12.28	14.43
1.71	0.0307	2.5	1.000	3.767	6.578	0.3241	0.3897	11.62	13.41
1.71	0.0405	2.5	1.000	3.486	6.113	0.3214	0.4118	10.85	11.94
1.71	0.0218	2.0	1.000	3.336	6.326	0.3128	0.3342	10.66	15.49
1.71	0.0218	3.0	1.000	4.994	8.019	0.3556	0.3899	11.62	13.41
1.71	0.0218	3.5	1.000	5.451	8.776	0.3676	0.4134	10.85	11.94
1.71	0.0307	2.0	1.000	2.997	5.773	0.3182	0.3580	9.419	13.41
1.71	0.0307	2.0	1.188	3.011	5.791	0.3247	0.3572	9.276	13.53
1.71	0.0307	2.0	1.378	3.036	5.809	0.3366	0.3563	9.091	13.66
1.71	0.0307	2.0	1.629	3.092	5.829	0.3416	0.3554	9.050	13.79
1.71	0.0307	2.0	1.967	3.204	5.848	0.3538	0.3546	9.024	13.93

* Experimental values.
** Calculated from the correlation of Roy and Sarma (1972).
& Calculated from the correlation of Roy and Sharat Chandra (1976).
# Calculated from the correlation of Roy and Sarma (1974).

The values of the dimensionless minimum semi-fluidization velocity also calculated from the correlations available in the literature pertaining to the liquid-solid system (Roy and Sarma, 1972) have been indicated in Table 6.4. The values predicted are much higher than the present findings. This may be due to delayed semi-fluidization in their system with difference in particle size, geometry of the bed and the design of the top grid which one is a fructo-conical perforated one attached to a wire mesh. But a similar dependency on the system variables has been observed in both the cases. The main contribution might be that of the particle size and the pressure gradient at the top grid. As the particle size becomes smaller the dimensionless minimum semi-fluidization velocity increases. The correlation by Roy and Sarma (1972) has been developed for very small particles, thus predicting higher values of the dimensionless minimum semi-fluidization velocity.

Roy (1975) and Roy and Sharat Chandra (1976) have proposed different correlations for predicting the minimum semi-fluidization velocity in the dimensionless form. The different dimensionless minimum semi-fluidization velocity (U_{osf}/U_{msf}) is the ratio of the minimum semi-fluidization velocity to the maximum semi-fluidization velocity. For the prediction of the maximum semi-fluidization velocity they have proposed an empirical equation from there experimental findings. The values of the dimensionless minimum semi-fluidization velocity (U_{osf}/U_{msf}) calculated from the experimental findings of minimum and maximum semi-fluidization velocities and predicted from the proposed correlation by Roy (1975) has been reported in Table 6.4. The equation proposed by Roy (1975) predicts a higher value of U_{osf}/U_{msf}. This is due to the higher predicted values of the minimum semi-fluidization velocity as pointed earlier and lower value of maximum semi-fluidization velocity. A new correlation (Eq. (6.13)) has been proposed here for the prediction of U_{osf}/U_{msf}.

$$\frac{U_{osf}}{U_{msf}} = 0.254\left(\frac{H_s}{D_c}\right)^{-0.302}\left(\frac{d_p}{D_c}\right)^{-0.045}\left(\frac{\mu_L}{\mu_w}\right)^{0.155}(R)^{0.295} \qquad (6.13)$$

Like the dimensionless minimum semi-fluidization velocity, the maximum semi-fluidization velocity can also be represented in a dimensionless form as dimensionless maximum semi-fluidization velocity (U_{msf}/U_{mf} or U_{msf}/U_{osf}). U_{msf}/U_{osf} is the inverse of U_{osf}/U_{msf} and can be predicted from Eq. (6.13) just by inversion. Earlier Roy and Sarma (1974) have proposed a correlation for U_{msf}/U_{mf} for the liquid-solid system with irregular particles, where only the effect of two variables i.e. the particle size and the particle density is shown. In the present work, a new correlation (Eq. (6.14)) has been developed

from experimental values of U_{msf}/U_{mf} with a correlation factor of 0.973. The values of U_{msf}/U_{mf} predicted from the correlation of Roy and Sarma (1974) have been indicated in Table 6.4 along with the experimental values. Most of the values are within 20 % except those corresponding to the bed expansion ratio, R = 2 and for values with viscosity variation. The difference may be due to the absence of variable like: liquid viscosity, expansion ratio and static bed height in the correlation of Roy and Sarma (1974).

$$\frac{U_{msf}}{U_{mf}} = 1.565\left(\frac{H_s}{D_c}\right)^{0.359}\left(\frac{d_p}{D_c}\right)^{-0.330}\left(\frac{\mu_L}{\mu_w}\right)^{-0.077}(R)^{0.687} \tag{6.14}$$

The relation between minimum liquid fluidization velocity, minimum liquid semi-fluidization velocity and maximum liquid semi-fluidization velocity for gas-liquid-solid system has been expressed in the form of dimensionless minimum and maximum semi-fluidization velocities as it has been done for liquid-solid system above. The dimensionless minimum and maximum semi-fluidization velocities have been represented in the form of empirical equations developed from non-linear regression analysis of the experimental data and given below as (Eqs. (6.15), (6.16) and (6.17)).

$$\frac{U_{Losf}}{U_{Lmf}} = 4.153U_g^{0.001}R^{0.491}d_p^{-0.322}\mu_L^{0.299} \tag{6.15}$$

(with a correlation coefficient of 0.979)

$$\frac{U_{Losf}}{U_{Lmsf}} = 0.257U_g^{0.018}R^{-0.149}d_p^{-0.227}H_s^{-0.369}\mu_L^{0.209} \tag{6.16}$$

(with a correlation coefficient of 0.966)

$$\frac{U_{Lmsf}}{U_{Lmf}} = 15.94U_g^{-0.017}R^{0.639}d_p^{-0.096}H_s^{0.365}\mu_L^{0.089} \tag{6.17}$$

(with a correlation coefficient of 0.947)

The prediction of dimensionless minimum and maximum semi-fluidization velocities from Eqs. (6.15), (6.16) and (6.17) agree with experimental ones with an AARE of 1.09, 1.18 and 1.89 % respectively.

6.6. Height of the top packed bed

Between the two limiting conditions of semi-fluidization i.e. the minimum and the maximum, a part of the total solid form a packed bed beneath the top restraint, while the balance of the solid remain in the fluidized state. By adjusting the position of the top grid and / or by varying the velocity of the fluid, the extent of packed bed formation can be controlled to suit to a particular requirement. The extent of packed bed formation is also

closely related to the pressure drop across the semi-fluidized bed. The prediction of packed bed formation is therefore important in the study of semi-fluidization.

In the present study the packed bed formation has been represented as dimensionless quantity such as H_{pa}/H_s and $(H_{sf}\text{-}H_{pa})/(H_{sf}\text{-}H_s)$. The voidage of the top packed bed has been assumed to be equal to the voidage of the reproducible initial static bed. The dependency of H_{pa}/H_s on superficial liquid velocity, bed expansion ratio, static bed height, particle size and liquid viscosity for liquid-solid system has been presented in Fig. (6.14) through (6.17) and the effect of gas velocity for the gas-liquid-solid system has been presented in Fig. 6.19. The results indicate that the packed bed section starts to form at a velocity right above the minimum semi-fluidization velocity, and the section increases in height as the velocity is increased. The packed bed height increases with the liquid velocity, but decreases with bed expansion ratio, particle size and to a lesser extent on the initial static bed height. For gas-liquid-solid system the packed bed height has been observed to increase with the increase in gas velocity. As mentioned by Ho et al. (1987), in the present study the formation of packed bed for the liquid-solid system has not been uniform. The mean packed bed height from the repeat of the experiments has been taken as the packed bed height under each operating condition.

Fan and Wen (1961), using dimensional analysis and the momentum and continuity equations, obtained the following relationship.

$$[(H_{sf}\text{-}H_{pa})/(H_{sf}\text{-}H_s), (U_s\text{-}U_{mf})/(U_t\text{-}U_{mf})] = 0. \tag{6.18}$$

Using this relation Kurian and Rao (1970), proposed the following correlation from their experimental finding.

$$\frac{U_s - U_{mf}}{U_t - U_{mf}} = 0.61\left(\frac{H_{sf} - H_{pa}}{H_{sf} - H_s}\right)^{-1.2} \tag{6.19}$$

Singh et al. (1980), have proposed a different correlation in the logarithmic form from their experimental finding as indicated below.

$$\frac{H_{sf} - H_s}{H_{sf} - H_{pa}} = 0.974 + 0.324\ln\left(\frac{U_s - U_{mf}}{U_t - U_{mf}}\right) \tag{6.20}$$

Mydlarz (1987), from his experimental finding has shown the validity of Eq. (6.19) for the range of the dimensionless packed bed height as; $1.3 < (H_{sf}\text{-}H_{pa})/(H_{sf}\text{-}H_s) < R$. He has proposed a different relation for the range $1.0 < (H_{sf}\text{-}H_{pa})/(H_{sf}\text{-}H_s) < 1.3$ as;

$$\frac{U_s - U_{mf}}{U_t - U_{mf}} = \left(\frac{H_{sf} - H_{pa}}{H_{sf} - H_s}\right)^{-3.15} \tag{6.21}$$

In the present study an attempt has been made to correlate the experimental data for the larger regular particles in the form of the Eqs. (6.19) – (6.21). The following relationships have been obtained which are valid for the entire range of experimentation.

$$\frac{H_{sf}-H_s}{H_{sf}-H_{pa}}=1.1037\left(\frac{U_s-U_{mf}}{U_{msf}-U_{mf}}\right)^{0.484} \tag{6.22}$$

and

$$\frac{H_{sf}-H_s}{H_{sf}-H_{pa}}=1.04+0.3514\ln\left(\frac{U_s-U_{mf}}{U_{msf}-U_{mf}}\right) \tag{6.23}$$

The values of $(H_{sf}\text{-}H_{pa})/(H_{sf}\text{-}H_s)$ predicted from the Eqs. (6.22) and (6.23) have been compared with the experimental values and a fairly good agreement has been found with standard deviation values of 7.62 % and 7.46 % respectively. Fig. 6.21 shows the comparison of the values of $(H_{sf}\text{-}H_s)/(H_{sf}\text{-}H_{pa})$ predicted from Eqs. (6.19) – (6.22) with the experimental ones for the liquid-solid system. Almost all values are within 15 % of the experimental ones in case of these equations. The recommendation for the use of two different power law correlation for the two different range of the values of $(H_{sf}\text{-}H_{pa})/(H_{sf}\text{-}H_s)$ by Mydlarz (1987) is found to be true as it is seen from Fig. 6.21.

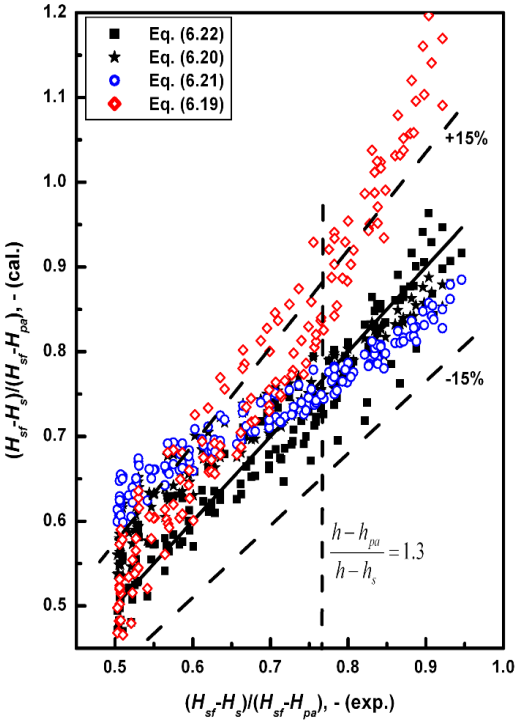

Fig. 6.21. Comparison of dimensionless packed bed height ($(H_{sf}\text{-}H_s)$ /$(H_{sf}\text{-}H_{pa})$).

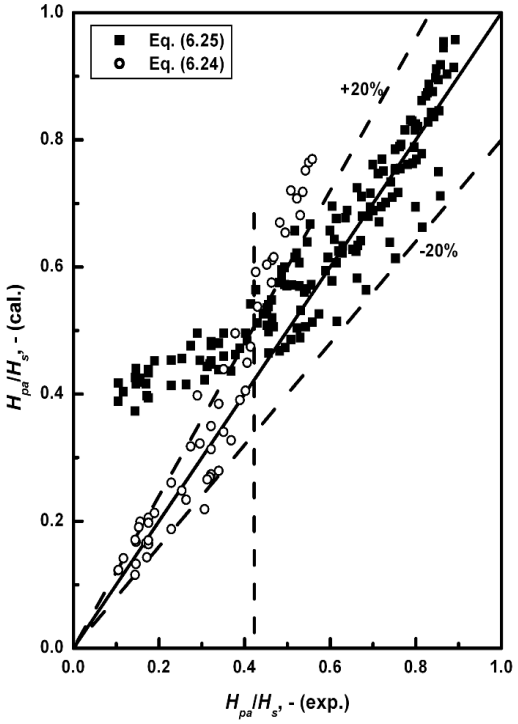

Fig. 6.22. Comparison of dimensionless packed bed height (H_{pa}/H_s).

An attempt has been made to develop dimensionless correlation for H_{pa}/H_s in terms of dimensionless parameters U_s/U_{osf}, H_s/D_c, d_p/D_c, R and μ_L/μ_w to realize the direct effect of these variables on the top packed bed height. It has been observed that up to 42% of the particles in the top packed bed i.e. $H_{pa}/H_s = 0.42$, the dependency of H_{pa}/H_s on U_s/U_{osf} is different from that of $H_{pa}/H_s > 0.42$. Thus two different correlations have been proposed to predict the packed bed formation for the two different ranges of the values of H_{pa}/H_s as Eqs. (6.24) and (6.25). Over the specified range the predicted values of H_{pa}/H_s from Eq. (6.24) agrees with the experimental ones with a standard deviation value of 16.7%, where as the values predicted from Eq. (6.25) agrees with a standard deviation value of 9.45% as indicated in Fig. 6.22. This indicates the instability in the packed bed formation up to nearly 42% of the particles forming the top packed bed.

$$\frac{H_{pa}}{H_s} = 0.0497\left(\frac{U_s}{U_{osf}}\right)^{6.562}\left(\frac{H_s}{D_c}\right)^{-0.075}\left(\frac{d_p}{D_c}\right)^{-0.214}\left(\frac{\mu_L}{\mu_w}\right)^{0.086}(R)^{-0.419} \qquad (6.24)$$

for $H_{pa}/H_s < 0.42$.

$$\frac{H_{pa}}{H_s} = 0.3248\left(\frac{U_s}{U_{osf}}\right)^{0.965}\left(\frac{H_s}{D_c}\right)^{-0.053}\left(\frac{d_p}{D_c}\right)^{-0.133}\left(\frac{\mu_L}{\mu_w}\right)^{0.053}(R)^{-0.258} \qquad (6.25)$$

for $H_{pa}/H_s > 0.42$.

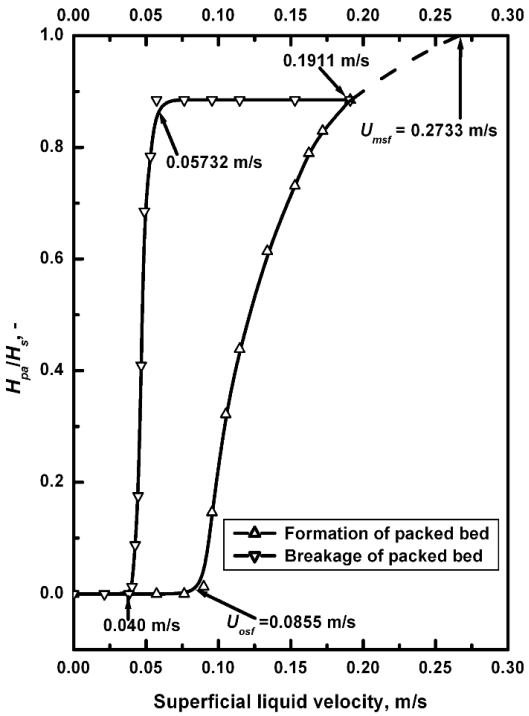

Fig. 6.23. Formation and breakage of packed bed with variation of liquid velocity for 2.18 mm particles at H_s=0.171 m and R=2.0.

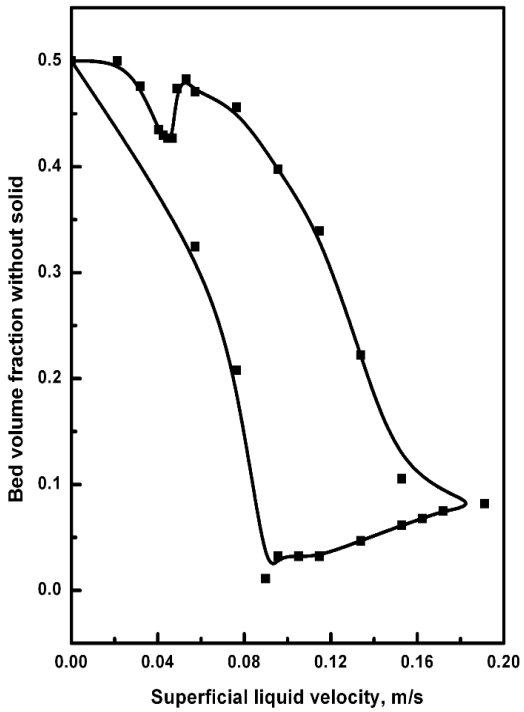

Fig. 6.24. Variation of Bed volume fraction without solids with liquid velocity for 2.18 mm particles at H_s=0.171 m and R=2.0.

Fig. 6.23 shows the formation of and breakage behaviour of the top packed bed with increase and decrease in the liquid velocity respectively of 2.18 mm particles with R=2.0. A hysteresis loop results with significant gap between the formation and breakage of the packed bed. As seen from the plot the liquid velocity increased from 0 to 0.1911 m/s and then decreased to 0 m/s. At 0.1911 m/s liquid velocity H_{pa}/H_s = 0.885. With decrease in liquid velocity from this value, the amount of particles in the top packed bed remain intact, the expanded fluidized bed height decreases and the clear zone (portion of the bed without solid, i.e. between fluidized bed and top packed bed or top grid) in the bed increases as seen in Fig. 6.24. At the liquid velocity of 0.0573 m/s, particle from the top packed bed begins to fall, the clear zone in the bed decreases and in a very narrow range of liquid velocity (0.0573-0.04 m/s) all the particles from the top packed bed falls to the fluidized bed at the bottom. With further decrease in the liquid velocity, the clear zone increases up to the liquid velocity reaching the minimum fluidization velocity, where the expanded bed height becomes equal to the reproducible static bed height. Thus a valley for clear zone is created between the liquid velocities corresponding to the starting of packed bed breakage and the minimum fluidization velocity as seen in Fig. 6.24.

From the packed bed formation behaviour in gas-liquid-solid system, it has been observed that the height of the top packed bed increases with increase in liquid velocity, gas velocity and liquid viscosity but decreases with increase in the value of bed expansion ratio and particle size. The influence of initial static bed height on the height of top packed bed has been found to be negligible up to nearly 60 % solids in the top packed bed, but with further increase in top packed bed height the value of the same has been found to be less for higher initial static bed height.

For the prediction of the height of the packed bed in the gas-liquid-solid semi-fluidized bed, Chern et al. (1984) have suggested a model based on the material balance of the solid particles as given by Eq. (1.4) in chapter-1. The details of the calculation procedure and equations used have been discussed in chapter-1. For the calculation of solid holdup in the fluidized bed (ε_s), the k-x generalized wake model (Eq. (1.2)) as used by Chern et al. (1984) has been used first. Using Eq. (1.2) for fluidized bed solid holdup calculation, Eq. (1.4) has predicted the top packed bed heights which deviating widely from that of the experimental values and some the values predicted are unrealistic. This large deviation may be due to the lower values of bed voidage predicted by the k-x wake model than the experimentally observed ones under the same flow conditions. The large error has also been confirmed in case of the minimum liquid semi-fluidization velocity

calculation. Thus in using the model equation (Eq. (1.4)) for packed bed height prediction, the solid holdup in the fluidized bed (ε_s) has been calculated from Eq. (3.12) as $\varepsilon_s = 1-\varepsilon$, and for the solid holdup in the packed bed ($\varepsilon_{s,p}$), the solid holdup of the initial static bed has been used.

The values calculated from Eq. (1.4) have been compared with experimental determined values of top packed bed height and has been represented in Fig. 6.25. A good agreement has been observed between the experimental and values predicted from the model. Most of the values agree within ± 12 %. In the lower range of the values of the top packed bed height, the deviation has been found to be little more than 12 %. This may be due to the delayed semi-fluidized bed formation at the top restraint than that is expected.

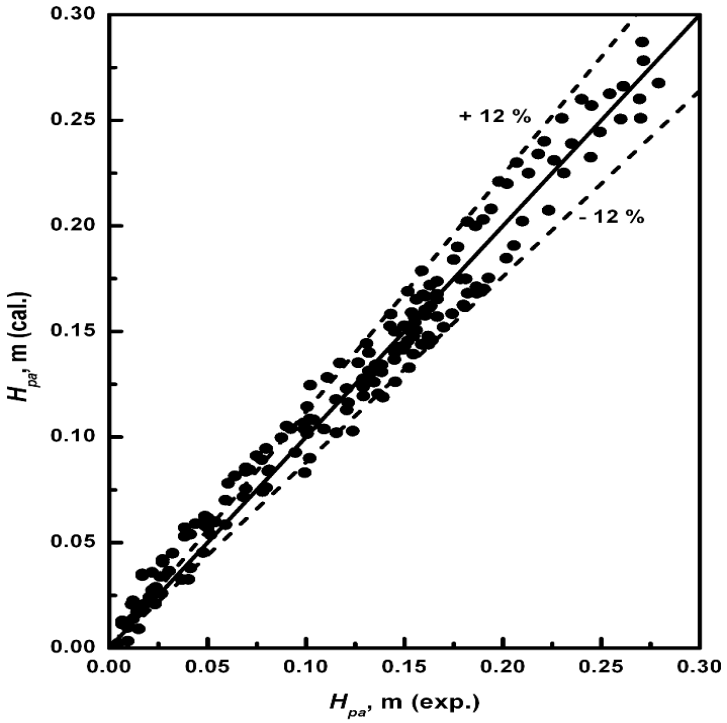

Fig. 6.25. Comparison of experimental and calculated values of the top packed bed height in semi-fluidized bed for regular particles.

6.7. Pressure drop across the bed

The pressure drop across a semi-fluidized bed can be viewed as the combination of the pressure drop across the fluidized section, the packed section and the constraint (top restraining) plate.

$$\Delta P_{sf} = \Delta P_f + \Delta P_{pa} + \Delta P_r \tag{6.26}$$

Fan and Wen (1961), Kurian and Raja Rao (1970) and Ho et al. (1987) have proposed models for the prediction of bed pressure based on the above assumption. Fan and Wen

(1961) have neglected the pressure drop across the top restraint plate where as, Ho et al. (1987) in their work with gas-solid system and Kurian and Raja Rao (1970) for liquid-solid system have shown significant contribution of the pressure drop across the top restraint towards the total pressure drop in the semi-fluidized bed. In these models for the fluidized bed pressure drop, they have considered the amount of solids in the fluidized section of the semi-fluidized bed, but actually when the operation starts from the initial static bed, first all the solids come to the fluidization mode and thereafter a portion of the solids form the packed bed beneath the top grid with increase in the liquid velocity. Thus the pressure drop for the total solids of the bed for fluidization should be taken into account. This pressure drop actually gets added to the packed bed pressure drop and the pressure drop for the top restraining plate.

In the present study we have taken the pressure equivalent to the buoyant weight of whole of the solids as the fluidized bed pressure drop. The mass of the solids used in each experiment have accurately been measured and have been used for the calculation of buoyant mass.

$$\Delta P_f = (1-\varepsilon_f)(\rho_s - \rho_L)H_f = M_b g / A_c \tag{6.27}$$

For the prediction of the packed bed pressure drop Ergun's equation has been used.

$$\Delta P_{pa} = 150\frac{(1-\varepsilon_{pa})^2}{(\varepsilon_{pa})^3}\frac{\mu_L U_L H_{pa}}{(\varphi_s d_p)^2} + 1.75\frac{1-\varepsilon_{pa}}{(\varepsilon_{pa})^3}\frac{\rho_L U_L^2 H_{pa}}{\varphi_s d_p} \tag{6.28}$$

The pressure drop across the top grid depends on its design. With the column being empty the pressure drop across the top grid has been measured by increasing the liquid velocity. For the maximum liquid velocity of 0.3057 m/s used in the study the pressure drop across the bed has been found to be 400 Pa where as at the same liquid velocity the pressure drop in case of a semi-fluidized bed has been measured to be 52032 Pa for 4.05 mm particles with bed expansion ratio of 2.5. Thus the pressure drop across the top grid can be neglected in comparison to the semi-fluidized bed pressure drop. The semi-fluidized bed pressure drops have been calculated from the following equation.

$$\Delta P_{sf} = \frac{M_b g}{A_c} + 150\frac{(1-\varepsilon_{pa})^2}{(\varepsilon_{pa})^3}\frac{\mu_L U_L H_{pa}}{(\varphi_s d_p)^2} + 1.75\frac{1-\varepsilon_{pa}}{(\varepsilon_{pa})^3}\frac{\rho_L U_L^2 H_{pa}}{\varphi_s d_p} \tag{6.29}$$

In predicting the semi-fluidized bed pressure drop from Eq. (6.29), the packed bed voidage (ε_{pa}) has been assumed to be equal to the voidage of the reproducible initial static bed ($\varepsilon_{,s}$). Fig. 6.26 shows the comparison of the experimentally measured semi-fluidized bed pressure drop with the values calculated from Eq. (6.29). Fairly good

agreement between the values is obtained as most of the values are within 10%, but almost all the values predicted from Eq. (6.29) have been found to be lower than the experimental ones. The higher experimental pressure drop is expected for the packed bed voidage little lower than the voidage of the static bed which has been used in the model Eq. (6.29). The top packed bed may be more compact than the initial static bed. The same phenomenon is prominent for small and irregular particles as reported by many earlier investigators. The compaction is not prominent in the present investigation as the particles are regular in shape and larger in size and hence the deviations have been within -10%.

The pressure drop in the gas-liquid-solid semi-fluidized bed has been measured using manometers with mercury as the manometric fluid. The semi-fluidized bed pressure drop has been found to increase with the liquid and the gas velocity due to increase in the packed bed height and friction loss at higher velocities. For the gas-liquid-solid semi-fluidized bed, the pressure drop has been calculated from the model of Chern et al. (1984) as given by Eq. (1.5). The calculated values of semi-fluidized bed pressure drop have been compared with the experimental ones as presented in Fig. 6.27. A fairly good agreement between the experimental and the calculated values has been obtained. More than 80 % of the data agree with in ± 10 %. The model of Chern et al. (1984) can be suitably used for the prediction of semi-fluidized bed pressure drop.

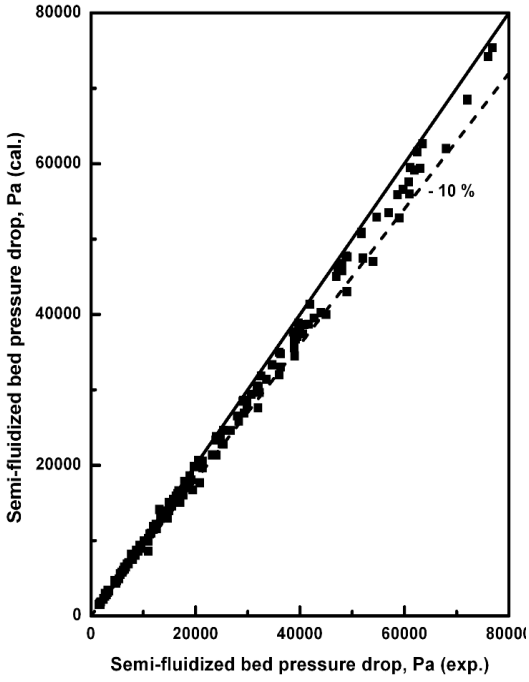

Fig. 6.26. Comparison of semi-fluidized bed pressure drops in liquid-solid semi-fluidization.

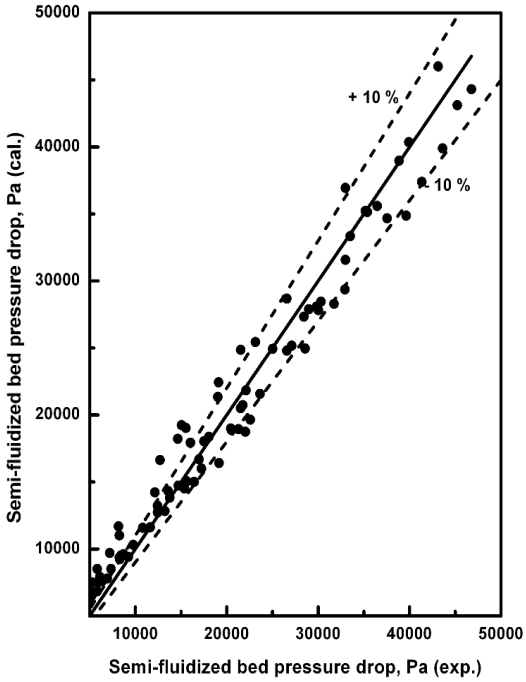

Fig. 6.27. Comparison of semi-fluidized bed pressure drops in gas-liquid-solid semi-fluidization.

6.8. Gas holdup

In the gas-liquid-solid semi-fluidized bed, the gas holdup has been measured by the phase isolation method as the bed pressure drop drastically changes for little increase in the height of the top packed bed. Also the contribution of the voidage of the top packed bed to pressure drop is quite large and little error in the measurement of this affects the bed pressure drop to a considerable extent. Above all the variations in pressure drop in the gas-liquid-solid semi-fluidized bed due to gas holdup w.r.t. liquid-solid bed is negligible than the pressure drop occurred when the height of packed bed is relatively more. It seems the bed pressure drop may likely to give erroneous result for the gas holdup. Thus the phase isolation can be the ideal method to measure the gas holdup in the system.

The phase isolation method of determination of gas holdup for the gas-liquid-solid fluidized bed (chapter-3) has been followed here. In the phase isolation method the quick closing valves (9, Fig. 2.1) in the water and air line were closed simultaneously. Unlike it was done in chapter-3, here the holdup in the two-phase region above the top restraint which is to be subtracted from the total holdup of the column has been found from the pressure drop measurement with the help of manometers using the pressure tappings above the position of the top grid.

Fig. 6.28 presents the variation of gas holdup with superficial liquid velocity at different values of fixed gas velocities. In the figure the abbreviation 'SFB' represents the semi-fluidized bed gas holdup and the abbreviation 'FB' represents fluidized bed gas holdup. The experimental values of semi-fluidized bed gas holdup has been compared with the semi-fluidized bed gas holdup calculated from the model (Eq. (1.18)) of Chern et al. (1984) and the fluidized bed gas holdup of regular particles calculated using Eq. (3.18). The experimental gas holdup in the semi-fluidized bed has been found to be much higher than the gas holdup values predicted from the model of Chern et al. (1984). The model (Eq. (1.18)) has been found to predict the gas holdup value which is lower than the fluidized bed gas holdup calculated from Eq. (3.18) for the same experimental conditions. Thus the model of Chern et al. (1984) may not be suitable for the prediction of gas holdup in a true semi-fluidized bed. In a semi-fluidized bed the higher values of gas holdup may be due to the higher pressure drop with increased value of the height of the top packed bed, which might have led to severe bubble disintegration. Visual observation confirms the presence of large number of smaller size bubbles in the

fluidized section of the semi-fluidized bed than that is seen in a conventional fluidized bed.

From the experimental data a correlation (Eq. (6.30)) has been developed for the calculation of semi-fluidized bed gas holdup in the air-water system. The influence of other variables than the liquid and the gas velocity is being clear; the correlation with a R-square value of 0.989 is given by;

$$\varepsilon_{g,sf} = 1.005 U_L^{-0.176} U_g^{0.836} \tag{6.30}$$

A comparison of the values of semi-fluidized bed gas holdup calculated from Eq. (6.30) with the experimental ones has been presented in Fig 6.29. The calculated values have been found to agree well with experimental ones with an AARE of 4.09%.

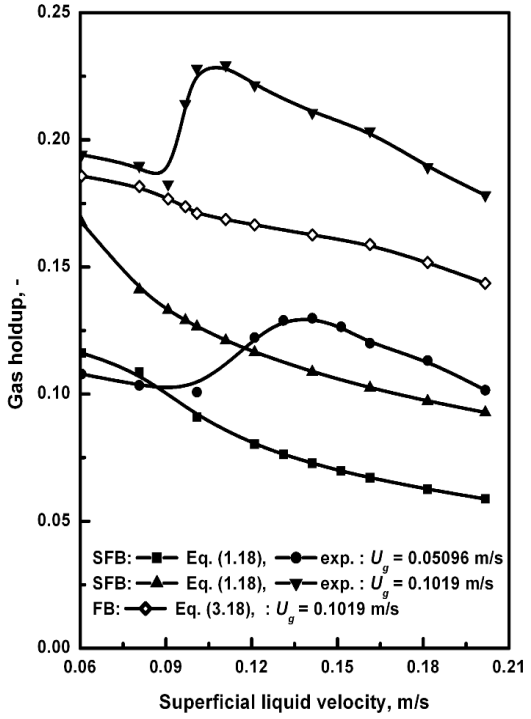

Fig. 6.28. Variation of gas holdup with liquid velocity at different values of fixed gas velocity for 4.05 mm glass beads at H_s = 0.171 m and R = 2.5.

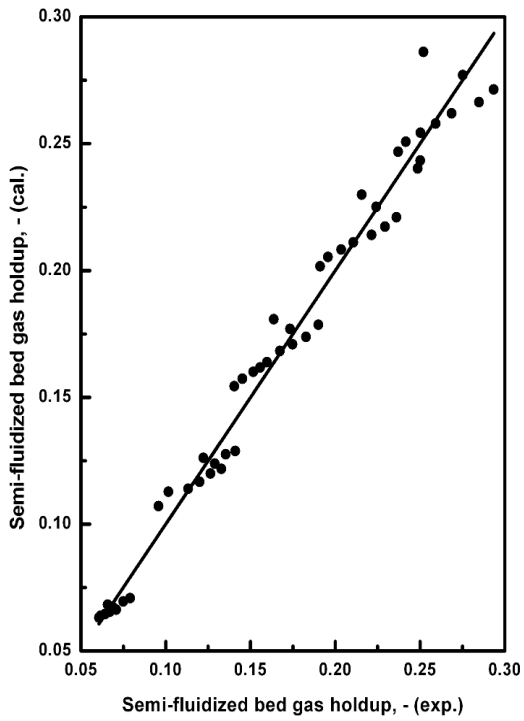

Fig. 6.29. Comparison of experimental values of gas holdup with the calculated ones from Eq. (6.30) in gas-liquid-solid semi-fluidized bed.

6.9. Conclusions

In the present investigation hydrodynamic study of the liquid-solid and gas-liquid-solid semi-fluidized beds has been carried out. The hydrodynamic parameters studied include: minimum and maximum semi-fluidization velocities, height of the top packed bed section in the semi-fluidized bed, pressure drop and gas holdup. The effects of various operating and geometric variables have been studied on hydrodynamic properties within the experimental conditions. The following conclusions have been drawn from the study.

In case of the liquid-solid semi-fluidized bed, both the minimum and the maximum semi-fluidization velocities increase with the increase in particle size and bed expansion ratio, but decrease with the increase in liquid viscosity. The minimum semi-fluidization velocity is independent of the variation of initial static bed height, but the maximum semi-fluidization velocity increases with increase in the static bed height. Proposed Eqs. (6.2) and (6.6) in dimensional form and Eqs. (6.11) to (6.14) in dimensionless form can be suitably used for the prediction of the minimum and the maximum semi-fluidization velocities in liquid-solid system by selecting the appropriate one. Height of the top packed bed increases with superficial liquid velocity and liquid viscosity, but decreases with bed expansion ratio, particle size and initial static bed height. Proposed Eqs. (6.22) through (6.25) can be used for the prediction of packed bed height in the semi-fluidized system with a caution that the Eq. (6.24) introduces a bit of uncertainty. Eq. (6.29) can suitably be used for the prediction of semi-fluidized bed pressure drop for the liquid-solid system.

The hydrodynamic study of the three-phase semi-fluidized bed with spherical particles reveals that the minimum liquid semi-fluidization velocity (U_{Losf}) shows the similar dependency on the variables like the one in case of liquid-solid system. Additionally U_{Losf} decreases with increase in gas velocity. U_{Losf} has been found to be a strong function of gas superficial velocity, particle size, bed expansion ratio. Height of the top packed bed increases with gas superficial velocity. The maximum semi-fluidization velocity (U_{Lmsf}) decreases with gas superficial velocity. Eq. (6.3) and Eq. (6.7) can be used to predict the values of the minimum and the maximum liquid semi-fluidization velocity respectively. The model of Chern et al. (1984) has not been found suitable for the prediction of U_{Losf} as well as the top packed bed height may be due to the lower value of bed expansion with the k-x generalized wake model used by them. Using the bed expansion value found in the present experiment in chapter-3, the model of Chern et al.

(1984) has been found to suitably predict the height of the top packed bed section in the gas-liquid-solid semi-fluidized bed.

The pressure drop has been found to increase with superficial gas velocity due to increase in top packed bed height in the semi-fluidized bed. The model of Chern et al. (1984) has been found to be suitable for the prediction semi-fluidized bed pressure drop in the gas-liquid-solid system. The existing model of Chern et al. (1984) is not suitable for the prediction of semi-fluidized bed gas holdup and a new empirical model has been proposed.

The outcome of the present investigation may be useful for the scale-up and successful design and operation of a liquid-solid and a gas-liquid-solid semi-fluidized bed system for various process applications with moderate size of particles.

Chapter 7

Hydrodynamics of Irregular Particles in Semi-fluidized Bed

Chapter-7

Hydrodynamics of Irregular Particles in Semi-fluidized Bed

7.1. Introduction

Semi-fluidization is a novel fluid solid contacting technique. The increasing popularity of semi-fluidized bed, as it overcomes some inherent disadvantages of both the fluidized and the fixed beds has necessitated for more investigations into its bed dynamics to learn it more. The semi-fluidized beds find wide applications as exothermic reactors and bioreactors, in ion exchange and in filtration operation for the removal of suspended particles from gases or liquids. In semi-fluidized bed the fluidization section acts as a CSTR and the packed bed section acts as a tubular flow reactor which results in better performance specifically for first order exothermic reactions (Fan and Hsu, 1978). The application of semi-fluidized bed to various physical, chemical and biochemical processes has been discussed in chapter-1 and subsequently in chapter-6. A systematic literature survey as presented in chapter-1 reveals that different aspects of liquid-solid semi-fluidized bed with irregular particles have been studied by various investigators in narrow columns and particles of smaller (< 1 mm) or larger (> 4 mm). The hydrodynamics of particles of sizes in between the above have not been studied, which can be used in aerobic and anaerobic reactors as discussed in chapter-6. Liquid viscosity effect on semi-fluidized bed behaviour has not been studied by earlier investigators. Further studies relating to a large number of operating variables in a particular investigation is rare in literature. The present reinvestigation has therefore been taken up to give a relook to liquid-solid semi-fluidization with irregular particles. The outcome can be used for a better comparison with the gas-liquid-solid hydrodynamics to be studied later using the same experimental setup with additional facility.

A review of literature reveals that the hydrodynamics of irregular shape particles in gas-liquid-solid semi-fluidized bed has not been studied so far. The study of gas-liquid-solid semi-fluidization is limited to spherical and cylindrical particles where the liquid viscosity and density and the solid density have not been studied (Chern, 1984). Effect of position of the grid and static bed height has also not been investigated by previous investigators. Therefore, the hydrodynamic study of co-current gas-liquid-solid semi-fluidized bed with liquid as the continuous phase has been taken up to have a better understanding of the bed behaviour.

In this chapter the hydrodynamic characteristics of both the liquid-solid and the co-current up flow gas-liquid-solid semi-fluidized beds with irregular particles have been studied. The parameters studied in this chapter include the minimum and the maximum semi-fluidization velocities, the top packed bed height, the pressure drop across the semi-fluidized bed and the gas holdup. Experimental setup that was used in the hydrodynamic study of regular particles in semi-fluidized bed (chapter-6) has been used in the present investigation. The effect of operating variables investigated include liquid velocity, gas velocity, initial static bed height, bed expansion ratio, viscosity of liquid, particle size and density.

7.2. Experimental set-up and procedure

The experimental setup used in this study is the same as shown has been presented in Fig. 6.1. Accurately weighed amount of materials like coal, dolomite, laterite or iron ore was fed into the column, fluidized and de-fluidized slowly with the liquid and adjusted for a specified reproducible initial static bed height. Liquid was pumped to the fluidizer at a desired flow rate using calibrated rotameters of different range. The air was then injected into the column through the air sparger at a desired flow rate. Approximately five minutes was allowed the steady state to be reached after which the readings were taken. The readings for pressure drop, expanded bed heights or the height of the top packed bed (as the case may be) were then noted. For gas holdup measurement phase isolation method was used as described in chapter-3 and chapter-6. All experiments were conducted at temperature of $(30\pm5)^0$C. The procedure was repeated varying the particle size, particle density, viscosity and density of the liquid, bed expansion ratio and initial static bed height. The scope of the experiment has been presented in Table 7.1. This table includes the physical properties of the system used and the operating variables.

7.3. Minimum semi-fluidization velocity

The values of the minimum semi-fluidization velocities have been experimentally obtained from the plot of pressure drop across the bed versus the superficial liquid velocity and have been used for the development of the model equations. As it was observed for regular particles (chapter-6) almost negligible effect of initial static bed height on the minimum semi-fluidization velocity (U_{osf}) has also been observed for the irregular particles. The effect of particle size on U_{osf} shows an increase in the same with the increase in particle size. The bed expansion ratio has a strong effect on the minimum semi-fluidization velocity. U_{osf} of irregular particles increases with the increase in bed expansion ratio. The effect of liquid viscosity on the minimum semi-fluidization

velocity indicates a decrease in the minimum semi-fluidization velocity with increase in the liquid viscosity. A similar behaviour has been observed as it was observed for spherical particles in chapter-6, but the quantitative dependence of U_{osf} on different variables has been found to be different from the regular particles. Fig. 7.1 shows the effect of particle density on U_{osf}. It is seen from the plot that U_{osf} increases with particle density. This may be due to requirement of higher drag to lift the particles of higher mass to the top grid, which can be achieved at a higher liquid velocity.

Table 7.1: Scope of the experiment

Liquid-solid system	d_px10^3 **m**	ρ_p **kg/m^3**	ε_s, -	Φ_s, -	H_s **m**	ρ_L **kg/m^3**	μ_Lx10^3 **Pa.s**	R, -	ε_{pa}, - **(exp.)**
Water-glass beads	3.07	2652	0.49	0.71	0.176	995.7	0.789	2.0	0.44
do	3.07	2652	0.49	0.71	0.216	995.7	0.789	2.0	0.44
do	3.07	2652	0.49	0.71	0.256	995.7	0.789	2.0	0.435
do	3.07	2652	0.49	0.71	0.296	995.7	0.789	2.0	0.445
do	1.55	2652	0.47	0.72	0.176	995.7	0.789	2.0	0.45
do	2.18	2652	0.48	0.715	0.176	995.7	0.789	2.0	0.48
do	4.05	2652	0.50	0.70	0.176	995.7	0.789	2.0	0.448
do	4.05	2652	0.50	0.70	0.176	995.7	0.789	2.5	0.435
do	4.05	2652	0.50	0.70	0.176	995.7	0.789	3.0	0.44
do	4.05	2652	0.50	0.70	0.176	995.7	0.789	3.5	0.44
Water-Coal	4.05	1492	0.52	0.63	0.176	995.7	0.789	2.0	0.47
Water-Laterite	4.05	3313	0.51	0.68	0.176	995.7	0.789	2.0	0.465
Water-Iron ore	4.05	3994	0.47	0.73	0.176	995.7	0.789	2.0	0.43
Aqueous solution of glycerol-glass beads (% by mass of glycerol)									
6.0	3.07	2652	0.49	0.71	0.216	1009.7	0.948	2.0	0.434
12.0	3.07	2652	0.49	0.71	0.216	1024.0	1.082	2.0	0.44
18.0	3.07	2652	0.49	0.71	0.216	1039.0	1.268	2.0	0.443
24.0	3.07	2652	0.49	0.71	0.216	1054.0	1.567	2.0	0.436
Superficial gas velocity:	$0.00 < U_g < 0.1274$ m/s								
Superficial liquid velocity:	$0.00 < U_L < 0.3057$ m/s								
Temperature:	$(30\pm2)^0$C								
Gas phase:	Air, density = 1.166 kg/m^3, viscosity = 1.794x10^{-5} Pa.s								

The proposed equation (Eq. 6.1) of Kurian and Raja Rao (1970) based on the correlation for the height of the top packed section (H_{pa}), which has been discussed in detail in the section 6.6 was found suitable in predicting the onset velocity of fluidization for the present case. Here the same equation has taken for the comparison of U_{osf} found experimentally. Like Eq. (6.2), the observed minimum semi-fluidization velocity for irregular particles has been correlated with the static bed height, bed expansion ratio, particle size, particle density and liquid viscosity. The following equation with a correlation coefficient of 0.992 has been obtained.

$$U_{osf} = 2.12\times10^{-4} R^{0.373} d_p^{0.523} \mu_L^{-0.369} \rho_s^{0.801} \qquad (7.1)$$

It has been indicated that the minimum semi-fluidization velocity is independent of static bed height. Values of U_{osf} predicted from Eqs. (6.1) and (7.1) and from the correlation of Roy and Sarma (1972) for non-spherical particles have been compared with the experimental ones in Fig. 7.2. The Eq. (7.1) adequately describes the observed data with an Average Absolute Relative Error (AARE) of 0.0235. The values of U_{osf} predicted from Eq. (6.1) are also in good agreement. The values predicted from the correlation of Roy and Sarma (1972) is much higher than the experimental ones except for a few combinations. This may be due to delayed semi-fluidization in their system with difference in particle size, bed geometry of the bed and the design of the top grid which was a fructo-conical perforated one attached to a wire mesh. But a similar dependency on the system variables has been observed in both the cases.

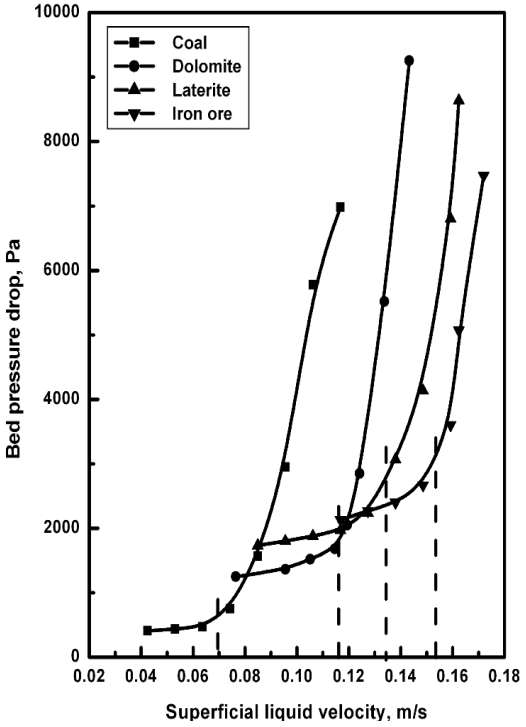

Fig. 7.1. Variation of bed pressure drop with U_L for 4.05 mm particles of different density in water at H_s=0.176 m and R=2.0.

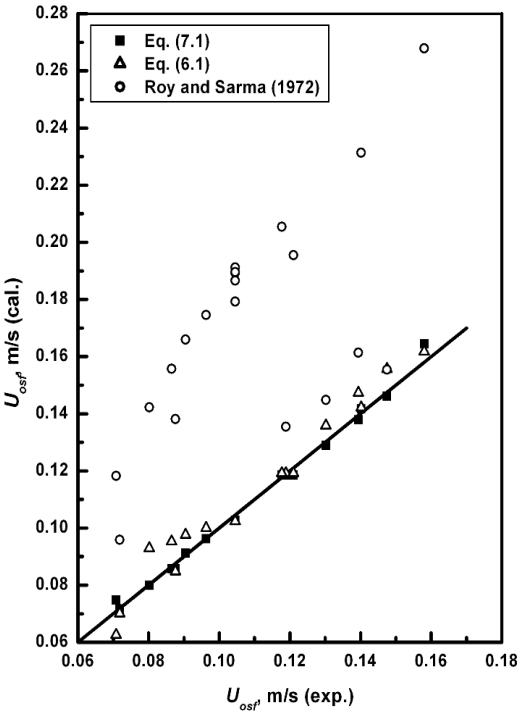

Fig. 7.2. Comparison of the values of minimum semi-fluidization velocity.

The minimum semi-fluidization velocity (minimum liquid semi-fluidization velocity, U_{Losf}) for gas-liquid-solid system has been determined in the similar method. For a constant gas velocity, the liquid velocity is varied and the semi-fluidization behaviour has been observed. The U_{Losf} has been found to decrease with increase in gas velocity and increase with increase in the bed expansion ratio. It has been observed that with increase in gas velocity the bed pressure drop decreases. This is due to higher top packed

bed height for smaller particles. The minimum liquid semi-fluidization velocity increases with particle size since higher drag as well as higher liquid velocity is required for a larger particle to reach the top grid.

As it was observed for the liquid-solid system, in the gas-liquid solid system U_{Losf} also decreases with the increase in liquid viscosity. The variation of bed pressure drop with liquid velocity for different particle density (particles of different material) is shown in Fig 7.3. The figure indicates increase in U_{Losf} with the solid phase density. The values of U_{Losf} at different superficial gas velocities are listed in Table 7.2. A comparison of the experimentally found U_{Losf} with the ones calculated from the bed expansion ratio equation (Eq. (4.7)) of chapter-4 has been made in Fig. 7.4. In calculating U_{Losf} from Eq. (4.7), the bed expansion ratio (H/H_s) of the fluidized bed has been equated to the bed expansion ratio of the semi-fluidized bed ($R=H_l/H_s$) and the corresponding liquid velocity has been considered as U_{Losf}. For most of the cases the experimental values of fU_{Losf} have been found to agree within 10 % with those calculated from the bed expansion ratio equation (Eq. (4.7)). The positive deviation of experimental values of U_{Losf} may be due to formation of permanent fixed bed at a little higher liquid velocity. From visual observation it is confirmed that the particles actually touch the top grid at a velocity close to the velocity calculated from Eq. (4.7), and thereafter return back without remaining fixed to the top grid. The particles get fixed to the top grid a velocity relatively higher than U_{Losf} calculated from Eq. (4.7). This phenomenon is prominent for low density particle i.e. coal.

A correlation from non-linear regression analysis of the data has been developed for the minimum liquid semi-fluidization velocity in gas-liquid solid system as given by Eq. (7.2) with a correlation factor of 0.998.

$$U_{Losf} = 9.8\times10^{-6} U_g^{-0.267} R^{0.918} d_p^{0.672} \mu_L^{-0.516} (\rho_s - \rho_L)^{0.681} \phi_s^{-1.126} \qquad (7.2)$$

The minimum liquid semi-fluidization velocity has been found to be independent of the initial static bed height. The values of U_{Losf} predicted from Eq. (7.2) have been compared with the values obtained from experiment in Fig. 7.5. Fairly good agreement has been observed between the experimental and the predicted values with an AARE of 1.1 %. This signifies the robustness of the correlation. In Fig. 7.5 the values of U_{Losf} predicted from the model of Chern et al. (1984) have also been indicated. For all the cases, the model of Chern et al. (1984) has been found to predict higher values of the minimum liquid semi-fluidization velocity. The packed bed height and semi-fluidized bed pressure drop depend on the onset of semi-fluidization condition. Comparison of these parameters

predicted from the model of Chern et al. (1984) with experimental ones is not done due to the large difference in U_{Losf}.

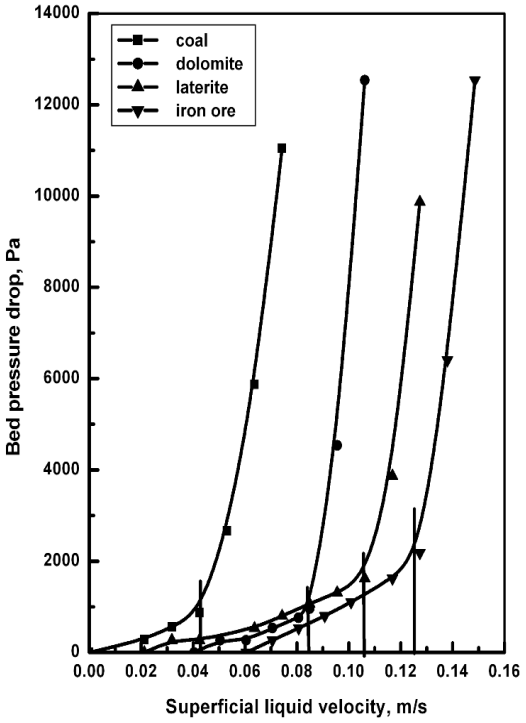

Fig. 7.3. Variation of bed pressure drop with U_L for 4.05 mm particles of different density in water at [H_s=0.176 m, R=2.0, U_g= 0.07643 m/s].

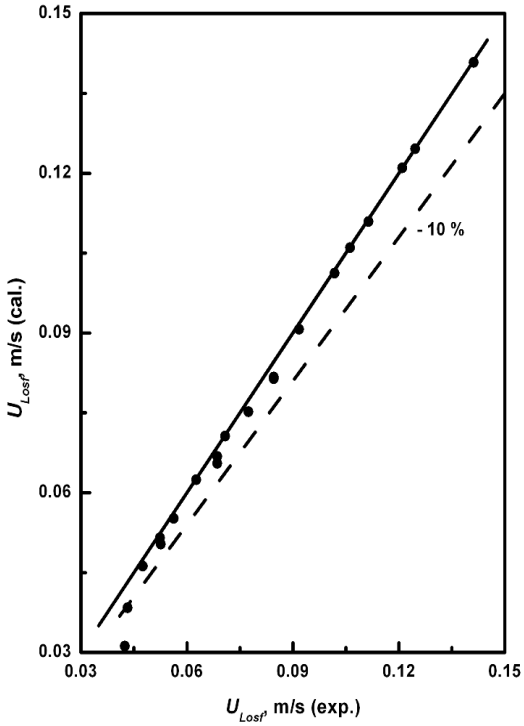

Fig. 7.4. Comparison of the values of minimum liquid semi-fluidization velocity obtained from experiment and those calculated from Eq. (4.7).

Table 7.2: Values of minimum semi-fluidization velocity (gas-liquid-solid system)

For d_p**=4.05 mm** R**=2** H_s**=0.176m** μ_L**=0.000798 Pa.s** ρ_s**=2652 Kg/m3**		**For** d_p**=4.05 mm** U_g**=0.0764 m/s** H_s**=0.176m** μ_L**=0.000798 Pa.s** ρ_s**=2652 Kg/m3**		**For** R**=2** U_g**=0.0764 m/s** H_s**=0.176m** μ_L**=0.000798 Pa.s** ρ_s**=2652 Kg/m3**		**For** d_p**=3.07 mm** R**=2** H_s**=0.216m** U_g**=0.0764 m/s** ρ_s**=2652 Kg/m3**		**For** d_p**=4.05 mm** R**=2** H_s**=0.176m** U_g**=0.0764 m/s** μ_L**=0.000798 Pa.s**	
U_g **(m/s)**	U_{Losf} **(m/s)**	R **(-)**	U_{Losf} **(m/s)**	d_p **(mm)**	U_{Losf} **(m/s)**	μ_L **(Pa.s)**	U_{Losf} **(m/s)**	ρ_s **(Kg/m3)**	U_{Losf} **(m/s)**
0.02547	0.1114	2	0.0846	1.55	0.0432	0.000798	0.0686	1492	0.0425
0.05096	0.0918	2.5	0.1018	2.18	0.0526	0.000948	0.0626	2652	0.0846
0.07643	0.0846	3	0.1210	3.07	0.0686	0.001082	0.0563	3313	0.1062
0.1019	0.0774	3.5	0.1412	4.05	0.0846	0.001268	0.0524	3994	0.1246
0.1274	0.0708					0.001567	0.0475		

7.4. Maximum semi-fluidization velocity

Maximum semi-fluidization velocity is the one at which all the particles are lifted to the top packed bed. A semi-fluidized bed should practically be operated below this velocity. Theoretically this velocity corresponds to the terminal (free fall) velocity (U_t) of the particles. The terminal velocity of non-spherical particles can be calculated from the knowledge of fluid-solid properties using the equations of Haider and Levenspiel (1989)

or Geldart (1990) or from the equation and graph of drag coefficient as given by Chattopadhayay (1993).

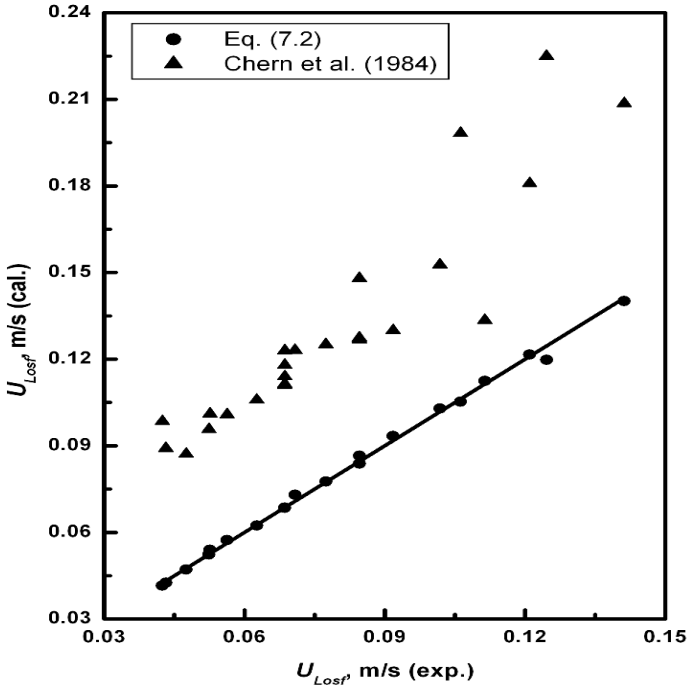

Fig. 7.5. Comparison of U_{Losf} obtained from experiment with those calculated from Eq. (7.2) and the model of Chern et al. (1984).

The merit of finding the maximum semi-fluidization velocity from experiment has been discussed in chapter-6. In the present investigation the maximum semi-fluidization velocity for both the liquid-solid and the gas-liquid-solid systems has been obtained by extrapolation of the plot of H_{pd}/H_s vs. superficial liquid velocity curve to H_{pd}/H_s=1. The suitability of this method has been described in chapter-6. The maximum semi-fluidization velocity has been found to increase slightly with the initial static bed height. This agrees with the findings for the regular particles. U_{msf} increase significantly with the particle size and the bed expansion ratio, but decrease with the increase in the liquid viscosity. These findings are also in agreement with those observed for regular particles in chapter-6. The maximum semi-fluidization velocity has been found to increase with the particle density as indicated in Fig. 7.6. A correlation for U_{msf} has been developed as given by Eq. (7.3) below with a correlation coefficient of 0.9846.

$$U_{msf} = 1.267\times10^{-4} H_s^{0.212} R^{0.305} d_p^{0.354} \mu_l^{-0.435} \rho_s^{0.848} \qquad (7.3)$$

The equation adequately describes the observed data with an Average Absolute Relative Error (AARE) of 2.33 %. In Fig 7.7 the experimental values of U_{msf} have been compared with those calculated from Eq. (7.3), the equation proposed by Roy (1975), the terminal

velocity calculated from the equations suggested by Haider and Levenspiel as given in Kunii and Levenspiel (1991), the equations given by Geldart (1990) and from the equation and graph of drag coefficient as given in Chattopadhayay (1993) for the given experimental conditions. As seen from Fig. 7.7, the experimental values of U_{msf} agree with the values calculated from the proposed correlation of Roy (1975) except for a few points. The experimental values of U_{msf} are higher than those calculated from the equation suggested by Haider and Levenspiel as given in Kunii and Levenspiel (1991) but lower than those calculated from the equations given by Geldart (1990) and from the equation and graph of drag coefficient as given in Chattopadhayay (1993).

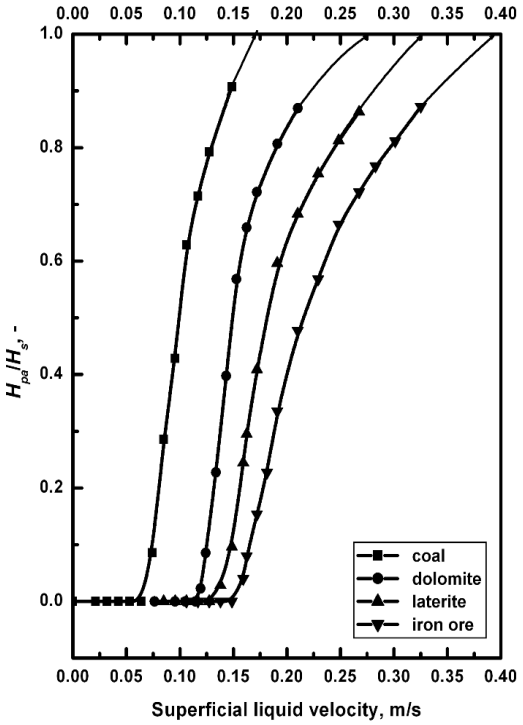

Fig. 7.6. Variation of H_{pa}/H_s with U_L for 4.05 mm particles of different density in water at [H_s=0.176 m, R=2.0].

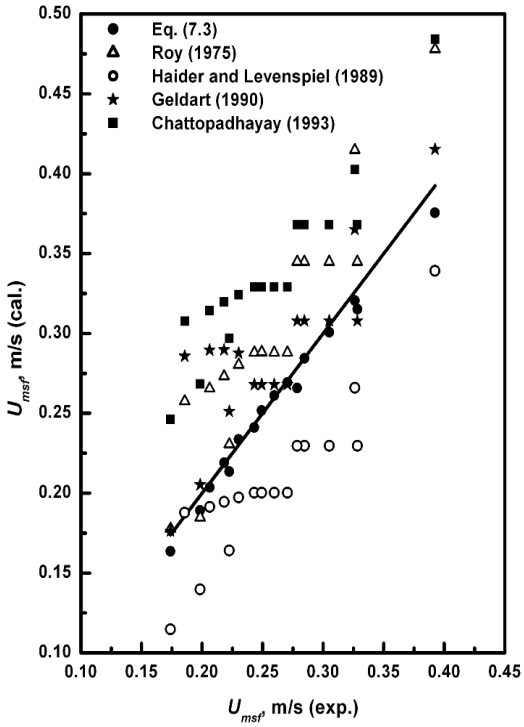

Fig. 7.7. Comparison of the values of maximum liquid semi-fluidization velocity and terminal velocity.

For gas-liquid-solid system in a similar manner the values for the maximum semi-fluidization velocity or the maximum liquid semi-fluidization velocity (U_{Lmsf}) have been determined. It is seen from Fig. 7.8 that U_{Lmsf} decreases with the increase of gas velocity, which represents the contribution of the gas to fluidization and so also to semi-fluidization. Similarly it has been observed that U_{Lmsf} increases with bed expansion ratio, particle size, initial static bed height and particle density of the solid, but decreases with liquid viscosity as shown in Figs. 7.9, 7.10, 7.11, 7.12, and 7.13 respectively. Except the particle density similar influence of other variables on the maximum liquid semi-

fluidization velocity has been observed for regular particles but with different quantitative dependence.

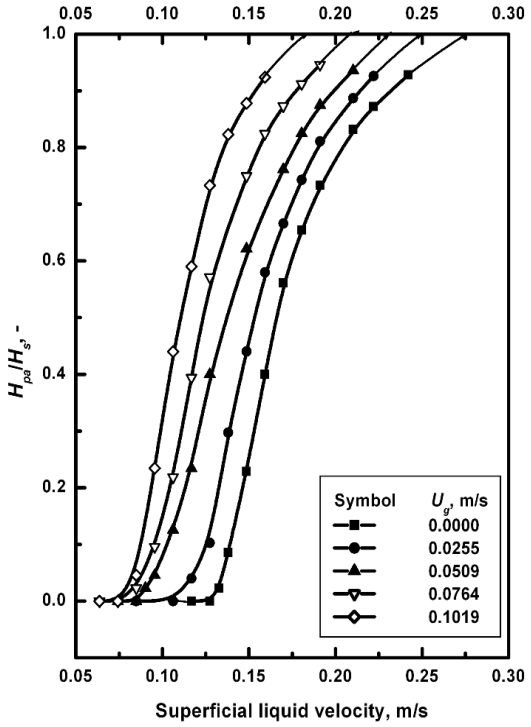

Fig. 7.8. Variation of H_{pa}/H_s with U_L of 4.05 mm particles in water for different values of gas velocity at [H_s=0.176 m, R=2.0].

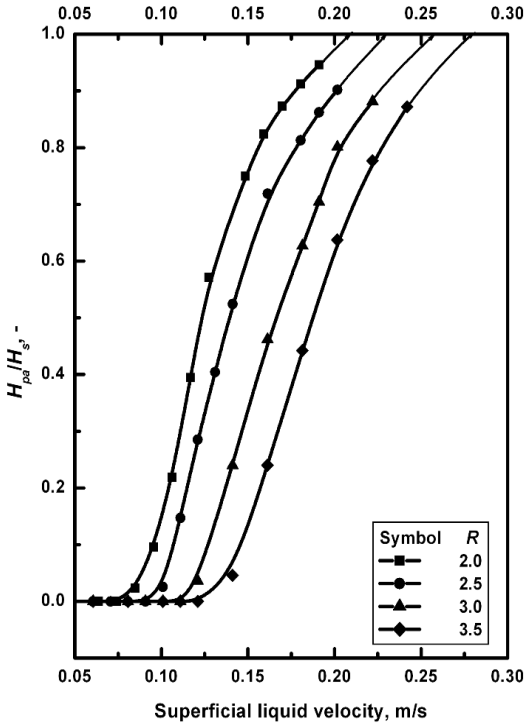

Fig. 7.9. Variation of H_{pa}/H_s with U_L of 4.05 mm particles in water for different values of bed expansion ratio at [H_s=0.176 m, U_g=0.0764 m/s].

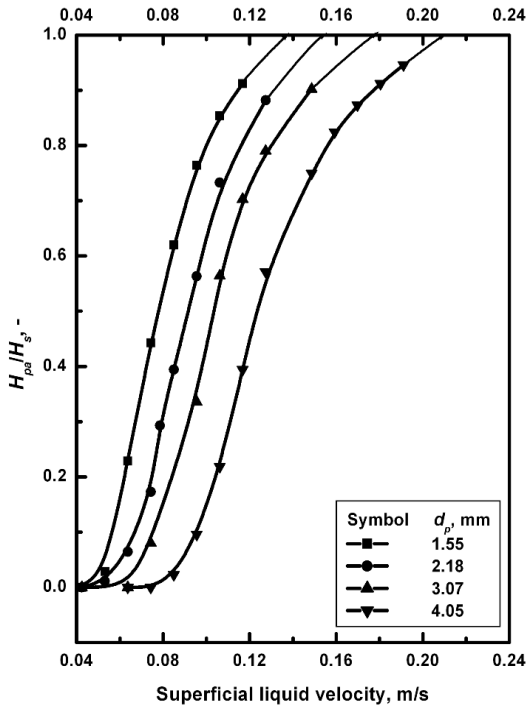

Fig. 7.10. Variation of H_{pa}/H_s with U_L for dolomite particles of different size in water at [H_s=0.176 m, R=2.0, U_g=0.0764 m/s].

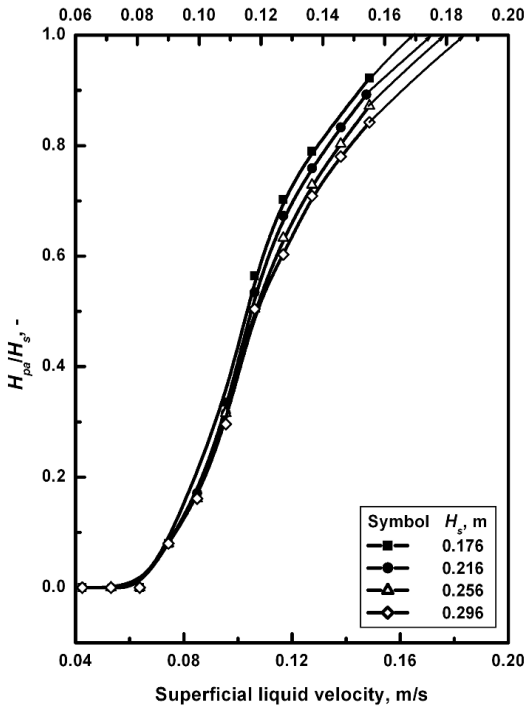

Fig. 7.11. Variation of H_{pa}/H_s with U_L for 3.07 mm dolomite particles in water for different values of initial static bed height at [R=2.0, U_g=0.0764 m/s].

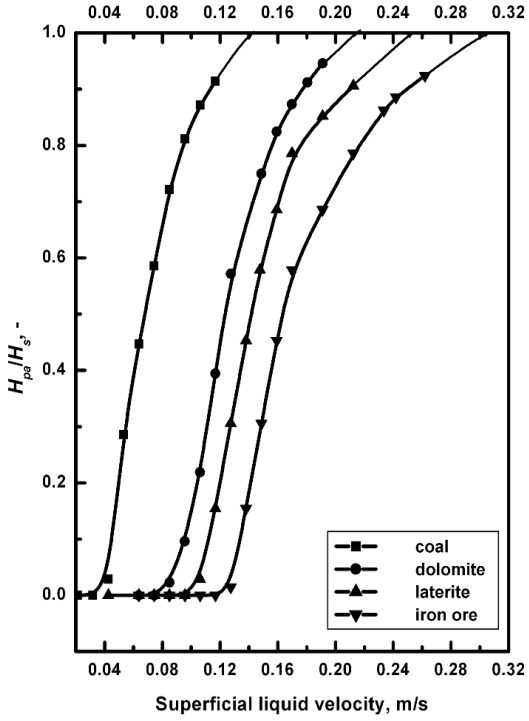

Fig. 7.12. Variation of H_{pa}/H_s with U_L for 4.05 mm particles of different density in water at [H_s=0.176 m, R=2.0, U_g=0.0764 m/s].

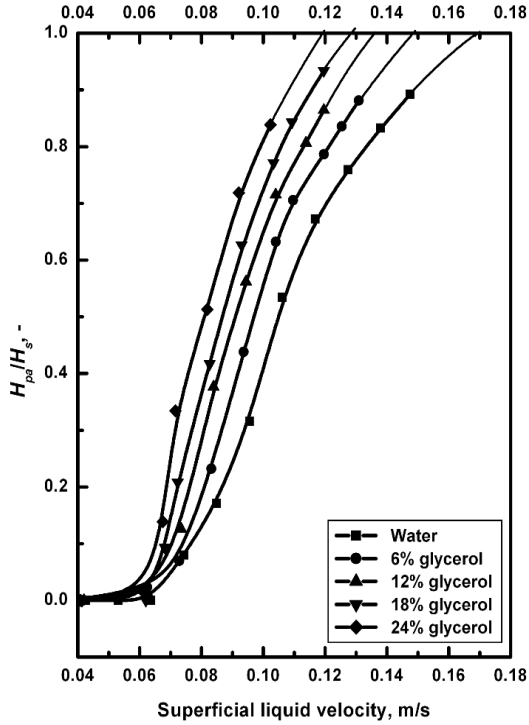

Fig. 7.13. Variation of H_{pa}/H_s with U_L for 3.07 mm dolomite particles in aqueous solutions of glycerol of varying concentration at [H_s=0.216 m, U_g=0.0764 m/s].

Using the values of experimental maximum liquid semi-fluidization velocity, a correlation from regression analysis has been developed as given by Eq. (7.4) with a correlation factor of 0.953. The values of U_{Lmsf} predicted from Eq. (7.4) have been compared with the experimental values in Fig. 7.14. Good agreement has been observed between the experimental and the predicted values with an AARE of 3.83 %. This signifies the robustness of the correlation. The correlation therefore can be used suitably for the prediction maximum liquid semi-fluidization velocity over the range of the operating variables investigated.

$$U_{Lmsf} = 9.92\times10^{-6} U_g^{-0.246} R^{0.581} d_p^{0.326} H_s^{0.007} \mu_L^{-0.605} (\rho_s - \rho_L)^{0.683} \phi_s^{-3.704} \qquad (7.4)$$

7.5. Dimensionless minimum and maximum semi-fluidization velocity

Correlations in dimensionless form for the prediction of minimum and maximum semi-fluidization velocities have been developed and represented as Eqs. (7.5) to (7.8) for the liquid-solid system in a similar manner as was developed for regular particles in the previous chapter. Unlike the values of the minimum fluidization velocity that were calculated from equation of Wen and Yu (1966), the experimental values of minimum fluidization velocity have been used in the present case as was obtained in chapter-4. This is done because of the wide deviations in experimental and predicted values of the

minimum fluidization velocity from various prescribed equations as has been discussed earlier (chapter-4, section 4.4).

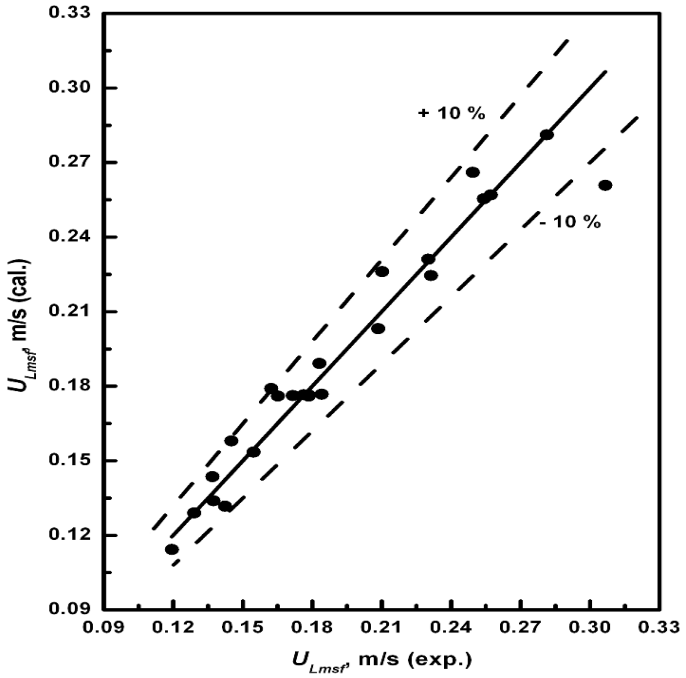

Fig. 7.14. Comparison of the values of maximum semi-fluidization velocity for irregular particles in gas-liquid-solid system.

The correlations for the dimensionless minimum semi-fluidization velocity (U_{osf}/U_{mf}) has been presented in two different forms are given by Eqs. (7.5) and (7.6).

$$\frac{U_{osf}}{U_{mf}} = 0.913 d_p^{-0.209} \mu_L^{0.057} \rho_s^{-0.114} R^{0.4} \tag{7.5}$$

$$\frac{U_{osf}}{U_{mf}} = 1.01 \left(\frac{d_p}{D_c}\right)^{-0.209} \left(\frac{\mu_L}{\mu_w}\right)^{-0.057} \left(\frac{\rho_s}{\rho_L}\right)^{-0.114} (R)^{0.4} \tag{7.6}$$

The correlation coefficients for Eqs. (7.5) and (7.6) are 0.963 and 0.967 respectively. Both the equations predict nearly the same value of the dimensionless minimum semi-fluidization velocity, but appear in different forms. The values of the dimensionless minimum semi-fluidization velocity predicted from Eqs. (7.5) and (7.6) are in very close agreement with the experimental values with an ARRE of 0.879 % and 0.921 % respectively.

The experimental values of the dimensionless minimum semi-fluidization velocity for liquid-solid systems have been compared with those predicted from Eq. (7.6) and the correlations of Ho et al. (1987) and Roy and Sarma (1972) in Fig. 7.15. The values predicted from the correlation of Roy and Sarma (1972) are much higher than the present

findings. This may be due to the same reason as discussed in section 7.3. Here the main contribution might be that of the particle size and the pressure gradient at the top grid. As the particle size becomes smaller, the values of the dimensionless minimum semi-fluidization velocity increase. The correlation by Roy and Sarma (1972) has been developed for very small particles, thus predicting higher values of the dimensionless minimum semi-fluidization velocity. The calculated values from correlations of Ho et al. (1987) are lower than the experimental ones.

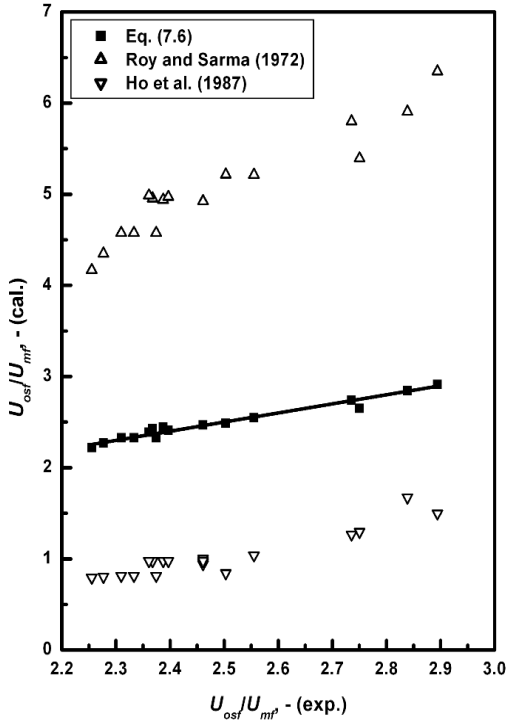

Fig. 7.15. Comparison of dimensionless minimum semi-fluidization velocity (U_{osf}/U_{mf}).

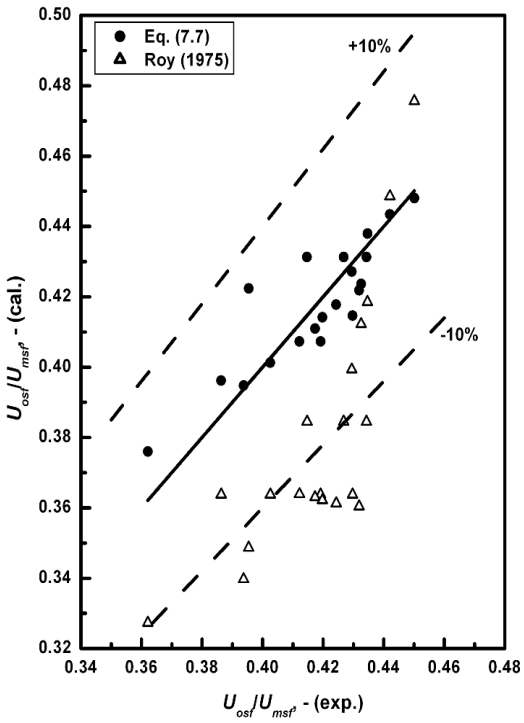

Fig. 7.16. Comparison of dimensionless minimum semi-fluidization velocity (U_{osf}/U_{msf}).

The dimensionless minimum semi-fluidization velocity (U_{osf}/U_{msf}) as the ratio of the minimum semi-fluidization velocity to the maximum semi-fluidization velocity has been correlated as Eq. (7.7). The experimental values of U_{osf}/U_{msf} have been compared with those predicted from Eq. (7.7) and the proposed correlation of Roy (1975) in Fig. 7.16. The equation proposed by Roy (1975) predicts lower values of U_{osf}/U_{msf} but agrees within 20 % deviation. A fairly good agreement between experimental values and those predicted from Eq. (7.7) has been observed.

$$\frac{U_{osf}}{U_{msf}} = 0.714\left(\frac{H_s}{D_c}\right)^{-0.088}\left(\frac{d_p}{D_c}\right)^{0.143}\left(\frac{\mu_L}{\mu_w}\right)^{0.048}\left(\frac{\rho_s}{\rho_L}\right)^{-0.044}(R)^{0.068} \qquad (7.7)$$

A new correlation (Eq. (7.8)) has been developed from the experimental values of U_{msf}/U_{mf}. The experimental values of U_{msf}/U_{mf} have been compared with those predicted

from the Eq. (7.8) and the correlation of Roy and Sarma (1974) in Fig. 7.17. Most of the values are within 20 % except those corresponding to the bed expansion ratio, R = 2 and for the values with viscosity variation. The difference may be due to the absence of variable like: liquid viscosity, expansion ratio and initial static bed height in the correlation of Roy and Sarma (1974).

$$\frac{U_{msf}}{U_{mf}} = 1.786\left(\frac{H_s}{D_c}\right)^{0.164}\left(\frac{d_p}{D_c}\right)^{-0.367}\left(\frac{\mu_L}{\mu_w}\right)^{-0.080}\left(\frac{\rho_s}{\rho_L}\right)^{-0.326}(R)^{0.229} \tag{7.8}$$

Similarly for gas-liquid-solid system the dimensionless minimum and maximum semi-fluidization velocities have been represented in the form of empirical equations as given below (Eqs. (7.9), (7.10) and (7.11)). These empirical equations have been developed from the non-linear regression analysis of the experimental data.

$$\frac{U_{Losf}}{U_{Lmf}} = 0.032U_g^{0.103}R^{0.920}d_p^{-0.143}\mu_L^{-0.245}(\rho_s - \rho_L)^{0.142}\phi_s^{-2.101} \tag{7.9}$$

(with a correlation coefficient of 0.988)

$$\frac{U_{Losf}}{U_{Lmsf}} = 9.77U_g^{-0.021}R^{0.338}d_p^{0.346}H_s^{-0.004}\mu_L^{0.088}(\rho_s - \rho_L)^{-0.001}\phi_s^{2.560} \tag{7.10}$$

(with a correlation coefficient of 0.958)

$$\frac{U_{Lmsf}}{U_{Lmf}} = 0.003U_g^{0.125}R^{0.581}d_p^{-0.488}H_s^{0.007}\mu_L^{-0.336}(\rho_s - \rho_L)^{0.141}\phi_s^{-4.632} \tag{7.11}$$

(with a correlation coefficient of 0.936)

The prediction of dimensionless minimum and maximum semi-fluidization velocities from Eqs. (7.9), (7.10) and (7.11) agree with the experimental ones with an AARE of 1.28 %, 3.35 % and 3.84 % respectively.

7.6. Height of the top packed bed

Similar treatment for expressing the height of the top packed bed of both in liquid-solid and in gas-liquid-solid semi-fluidized bed has been presented here as it was done in chapter-6. The equations of Kurian and Rao (1970), Singh et al. (1980), and Mydlarz (1987) as were presented in chapter-6 as Eqs. (6.19) to (6.21) have been taken up in the present case for the prediction of dimensionless top packed bed height in liquid-solid semi-fluidized bed. Empirical equations in the similar form have been developed as presented by Eqs. (7.12) and (7.13) which represent a different quantitative influence of the operating variables on the height of the top packed bed.

$$\frac{H_{sf}-H_s}{H_{sf}-H_{pa}}=1.061\left(\frac{U_s-U_{mf}}{U_{msf}-U_{mf}}\right)^{0.634} \tag{7.12}$$

$$\frac{H_{sf}-H_s}{H_{sf}-H_{pa}}=0.993+0.4287\ln\left(\frac{U_s-U_{mf}}{U_{msf}-U_{mf}}\right) \tag{7.13}$$

These equations are valid for the entire range of experimentation. The values of (H_{sf}-H_s)/(H_{sf}-H_{pa}) predicted from the Eqs. (7.12) and (7.13) have been compared with the experimental values and a fairly good agreement has been found with AARE values of 3.54 % and 3.66 % respectively. The recommendation for the use of two different power law correlation for the two different range of the values of (H_{sf}-H_{pa})/(H_{sf}-H_s) by Mydlarz (1987) is found to be true also for irregular particles in the liquid-solid semi-fluidized bed.

An attempt has been made to develop dimensionless correlation for H_{pa}/H_s in terms of dimensionless parameters viz. U_s/U_{osf}, H_s/D_c, d_p/D_c, ρ_s/ρ_L, μ_L/μ_w and R to realize the direct effect of these variables on the top packed bed height. The detailed procedure and steps have been used in this case is discussed in Chapter-6. It has been observed that up to 42% of the particles in the top packed bed i.e. $H_{pa}/H_s = 0.42$, the dependency of H_{pa}/H_s on U_s/U_{osf} is different from that of $H_{pa}/H_s > 0.42$. The same behaviour was also observed for spherical particles. Thus two different correlations have been proposed to predict the packed bed formation for the two different ranges of the values of H_{pa}/H_s as Eqs. (7.14) and (7.15). It has been found that over the specified range the predicted values of H_{pa}/H_s from Eq. (7.14) agrees with the experimental ones with an AARE of 13.7%, where as the values predicted from Eq. (7.15) agrees with an AARE of 6.77 %.

$$\frac{H_{pa}}{H_s}=1.316\left(\frac{U_s}{U_{osf}}\right)^{5.560}\left(\frac{H_s}{D_c}\right)^{-0.442}\left(\frac{d_p}{D_c}\right)^{0.411}\left(\frac{\mu_L}{\mu_w}\right)^{-0.225}\left(\frac{\rho_s}{\rho_L}\right)^{0.039}(R)^{-0.270} \tag{7.14}$$

for $H_{pa}/H_s < 0.42$.

$$\frac{H_{pa}}{H_s}=0.617\left(\frac{U_s}{U_{osf}}\right)^{1.351}\left(\frac{H_s}{D_c}\right)^{-0.092}\left(\frac{d_p}{D_c}\right)^{0.144}\left(\frac{\mu_L}{\mu_w}\right)^{-0.114}\left(\frac{\rho_s}{\rho_L}\right)^{0.087}(R)^{-0.058} \tag{7.15}$$

for $H_{pa}/H_s > 0.42$.

The packed bed formation behaviour in gas-liquid-solid system has been presented in Figs. 7.8 through 7.13. As indicated in these figures the height of the top packed bed increases with increase in liquid velocity, gas velocity and liquid viscosity but decreases with increase in the value of bed expansion ratio, particle size and particle density. The influence of initial static bed height on the height of top packed bed has been found to be

negligible, but at much higher values of H_{pa}/H_s, the dimensionless packed bed height decrease with the increase in initial static bed height.

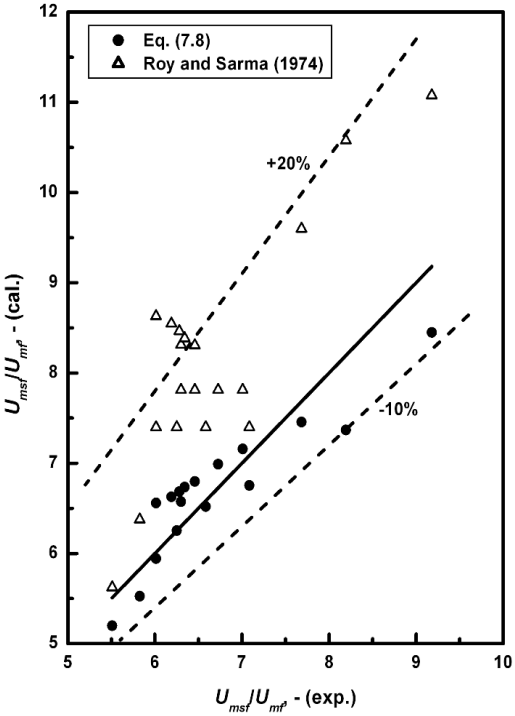

Fig. 7.17. Comparison of dimensionless minimum semi-fluidization velocity (U_{msf}/U_{mf}).

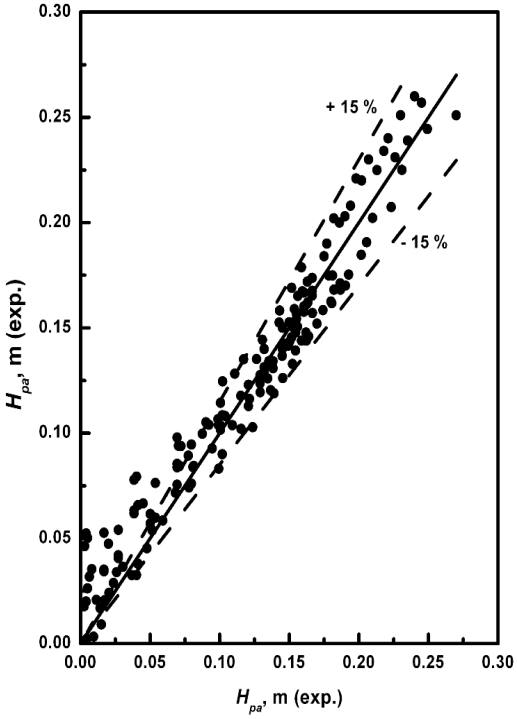

Fig. 7.18. Comparison of top packed bed height in gas-liquid-solid semi-fluidized.

The model suggested by Chern et al. (1984) has been used for the prediction of packed bed height in the gas-liquid-solid semi-fluidized bed. In using the model equation (Eq. (1.4), the solid holdup in the fluidized bed ($\varepsilon_S = 1-\varepsilon$) has been calculated from Eq. (4.8), the packed bed voidage (ε_{pa}) that was obtained experimentally (as reported in Table 7.1) for the liquid-solid bed has been used for the calculation of solid holdup in the packed bed ($\varepsilon_{s,p} = 1-\varepsilon_{pa}$). The values calculated from Eq. (1.4) have been compared with experimental values of top packed bed height and has been represented in Fig. 7.18. It is seen from the plot that the packed bed height predicted by the model is more than the experimental ones for lower values of H_{pa} i.e. at the early stage of the semi-fluidization phenomenon. This may be due to the delayed semi-fluidized bed formation as discussed in the minimum semi-fluidization velocity section 7.3. For relatively higher values of H_{pa} the predicted and experimental values agrees well within 15 %.

7.7. Pressure drop across the bed

For the prediction of pressure drop across the liquid-solid semi-fluidized bed Eq. (6.29), rewritten here as Eq. (7.16) has been used.

$$\Delta P_{sf} = \frac{M_b g}{A_c} + 150\frac{(1-\varepsilon_{pa})^2}{(\varepsilon_{pa})^3}\frac{\mu_L U_L H_{pa}}{(\varphi_s d_p)^2} + 1.75\frac{1-\varepsilon_{pa}}{(\varepsilon_{pa})^3}\frac{\rho_L U_L^2 H_{pa}}{\varphi_s d_p} \tag{7.16}$$

In Eq. (6.29), the top packed bed voidage (ε_{pa}) has been considered equal to the voidage of the reproducible initial static bed ($\varepsilon_{,s}$) was used for regular particles in the previous chapter and satisfactory result was obtained. In present case of irregular particles, it has been found that the top packed bed is more compact than the initial static bed due to reorientation of the irregular particles. The pressure drop calculated taking packed bed voidage (ε_{pa}) equal to the voidage of the reproducible initial static bed ($\varepsilon_{,s}$) has been found to be much less than the experimental values. In predicting the semi-fluidized bed pressure drop Fan and Wen (1961) and Kurian and Raja Rao (1970) have used the packed bed voidage as the voidage of the initial static bed but Ho et al. (1987) have used the experimentally determined voidage of the top packed bed. However Fan and Wen (1961) and Kurian and Raja Rao (1970) have recommended additional term for the pressure drop correction.

In this work the packed bed voidage has been obtained from the experimental pressure drop measured across the packed bed by using Ergun's equation (6.28). For comparison purpose, the semi-fluidized bed pressure drop has been calculated from Eq. (7.16) using both the packed bed voidage (ε_{pa}) (equal to the voidage of the reproducible initial static bed ($\varepsilon_{,s}$)) and the experimentally determined one from the measurement of packed bed pressure drop and the use of Eq. (6.28). The reproducible initial static bed voidage ($\varepsilon_{,s}$) and the experimentally determined packed bed voidage (ε_{pa}) have been reported in Table 7.1. Fig. 7.19 shows the comparison of the experimentally measured semi-fluidized bed pressure drop with the values calculated from Eq. (7.16) using the voidage of reproducible initial static bed and the packed bed voidage obtained from experiment. The calculated semi-fluidized bed pressure drop values using the static bed voidage have been found to deviate largely from the experimental ones. This is due to the packed bed formed at the top is much compact and possesses a low bed voidage than the initial static bed. This is the reason for the large deviation in the predicted pressure drop from the

experimental values. Fairly good agreement between the experimental pressure drop and those calculated from Eq. (7.16) using packed bed voidage found experimentally is seen.

In case of the gas-liquid-solid semi-fluidized bed for the calculation of pressure drop, the model of Chern et al. (1984) has been used. The calculated values of semi-fluidized bed pressure drop have been compared with the experimental ones as presented in Fig. 7.20. From comparison, it has been observed that about 60 % of the data agree within ± 20 %, but the rest deviate a lot. In case of higher deviation, the experimentally measured values of pressure drop have been found to be more than those predicted from the model of Chern et al. (1984). This may possibly be due to the compactness of the top packed bed where the channel diameter for the liquid flow might be less than the effective diameter of the channel calculated from the model of Chern et al. (1984). Chern et al. (1984) have shown a good agreement between their experimental and predicted values from the model. The reason may be that they have conducted separate experiment for the packed bed and the fluidized bed and combined the behaviour of the two to explain the hydrodynamic behaviour of a semi-fluidized bed, which may not exactly coincide with the situation that is realized in a true semi-fluidized bed. But in a true semi-fluidized bed experiment where a static bed is converted to a fluidized bed and then a semi-fluidized bed is formed with increase in fluid velocity, there may be a different orientation of the particles forming a more compact top bed than that of the initial static bed.

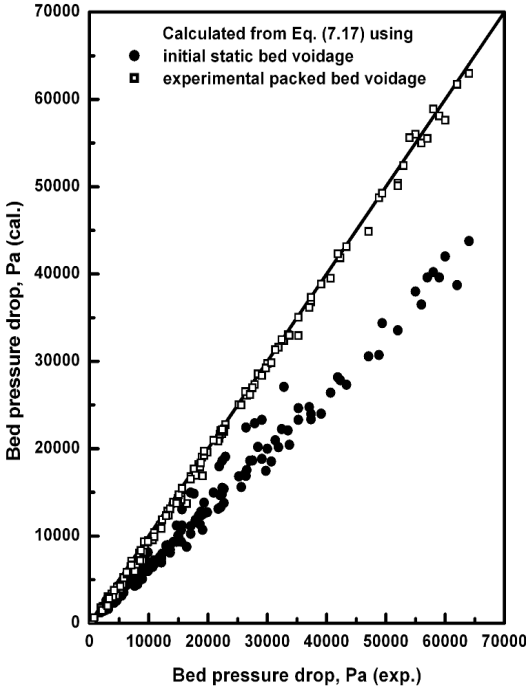

Fig. 7.19. Comparison of the values of the experimental and the calculated semi-fluidized bed pressure drop in liquid-solid system.

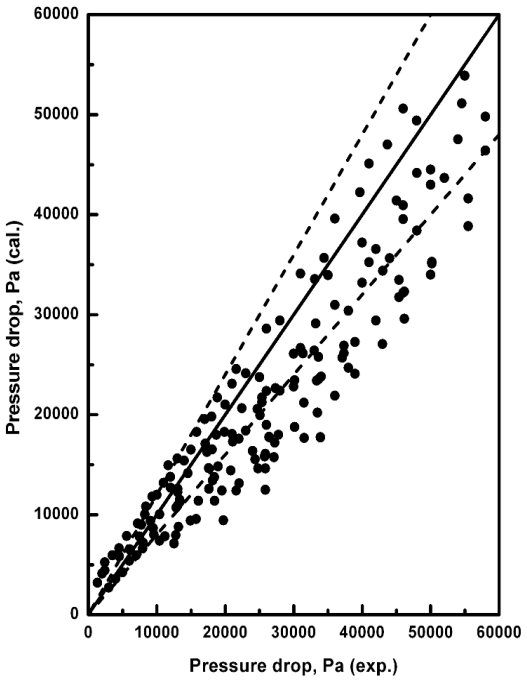

Fig. 7.20. Comparison of the values of the experimental and the calculated semi-fluidized bed pressure drop in gas-liquid-solid system.

7.8. Gas holdup

For the gas-liquid-solid system with irregular particles, the gas holdup has been measured by the phase isolation method. The reason for measuring gas holdup by the phase isolation method has been discussed in chapter-6. The gas holdup in the semi-fluidized bed has found to be more than that obtained in a fluidized bed. The reason as explained in chapter-6 may be due to the increase in pressure drop in the system where severe bubble disintegration takes place and the gas holdup in the fluidized bed portion is higher than that observed in a fluidized bed without a top restraint. The visual observation of the semi-fluidized has confirmed the existence larger number of small bubbles in the fluidized portion of the bed.

Fig. 7.21 presents the variation of gas holdup with superficial liquid velocity at different values of fixed gas velocity. In the figure the abbreviation SFB represents the semi-fluidized bed gas holdup. The semi-fluidized bed gas holdup has been compared with the fluidized bed gas holdup of irregular particles calculated using Eq. (4.11), the empirical model developed in chapter-4. The experimental values of gas holdup have found to be close to the calculated values of fluidized bed gas holdup in the fluidized bed before the particles touched the top restraint in the semi-fluidized bed experiment. The marginally higher values of the experimental gas holdup before the formation of the top packed bed than those calculated ones from Eq. (4.11) may be due to the presence of a top restraint in the semi-fluidized bed. The top restraint might have restricted the bubble motion and the bubble coalescence.

For the liquid velocity higher than the minimum liquid semi-fluidization velocity, the gas holdup has been found to be much more than the fluidized bed. After the starting of the formation of top packed bed, the gas holdup has been found to increase with the increase in liquid velocity, but subsequently decreases as it happens in a fluidized bed. This increase in gas holdup in the semi-fluidized bed with liquid velocity may be due to the higher pressure drop with increased value of the height of the top packed bed, which might have led to severe bubble disintegration. After the initial increase, the decrease in gas holdup with liquid velocity may be due to attainment of saturation condition of bubble disintegration, decrease in the residence time of bubbles at higher liquid velocity and increased top packed height and a reduced value of fluidized bed height. In a semi-fluidized bed the contribution of the bottom fluidized bed to the average gas holdup is more than the top packed bed. The decrease in the bottom fluidized bed portion and increased liquid velocity might have reduced the gas holdup in the bed. The rate of

decrease in gas holdup in a semi-fluidized bed than a normal fluidized bed can thus be the effect of several contributing factors.

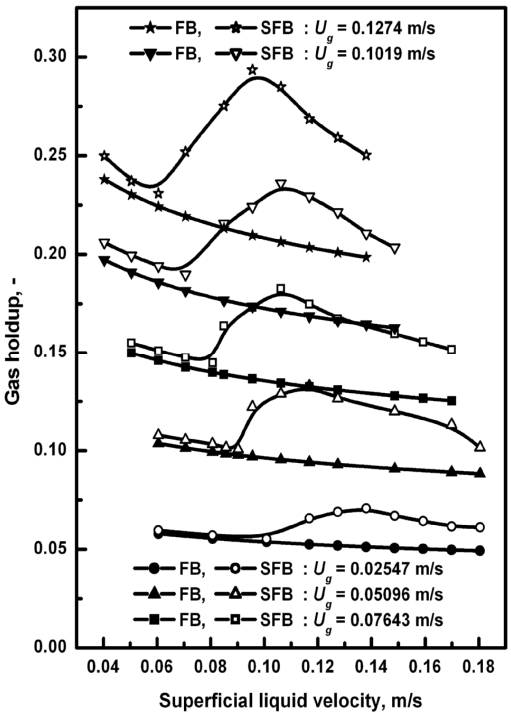

Fig. 7.21. Variation of gas holdup in semi-fluidized bed and in normal fluidized bed with liquid velocity at different values of fixed gas velocity.

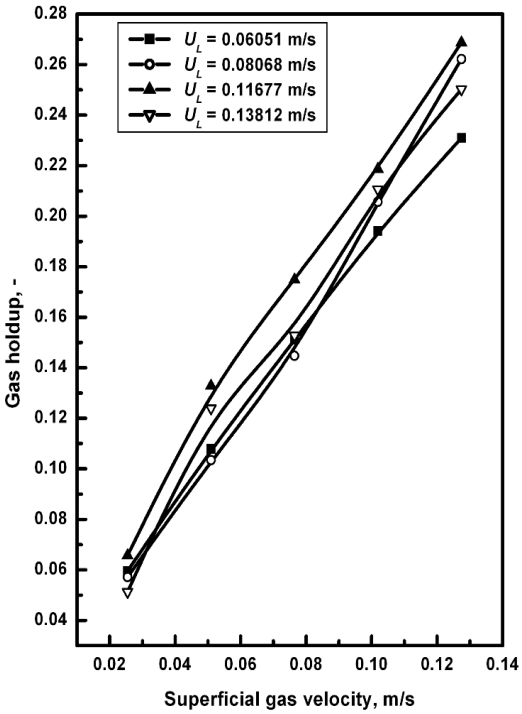

Fig. 7.22. Variation of gas holdup in semi-fluidized bed with gas velocity at different values of fixed liquid velocity.

Fig 7.22 shows the variation of semi-fluidized bed gas holdup with the gas velocity. A sharp increase in gas holdup has been observed with gas velocity, but the effect of liquid velocity is not clear in the semi-fluidized bed due to the interference of the top packed and its amount in the semi-fluidized bed.

7.9. Conclusions

In this chapter the hydrodynamic study of the liquid-solid and gas-liquid-solid semi-fluidized bed with irregular particles has been presented. The results show a similar influence of particle size, initial static bed height, bed expansion ratio, liquid and gas velocities and liquid viscosity on various hydrodynamic parameters as it was observed in the earlier chapter. Quantitatively the influence of the variables has been found to be different. The quantitative influence has been presented in the form of empirical equations. Both the minimum semi-fluidization velocity and the maximum semi-fluidization velocity have been found to increase with the particle density in case of both the liquid-solid and gas-liquid-solid semi-fluidized beds.

Equations proposed for the prediction of packed bed height in the liquid-solid semi-fluidized bed has been found to be suitable in describing the packed bed behaviour and agree with a few literature models. In case of the gas-liquid-solid bed, the model of Chern et al. (1984) developed from material balance to predict the packed bed height has found to be suitable using the fluidized bed voidage model (Eq. (4.8) developed in the present study. However the use of generalized k-x wake model as used by Chern et al (1984) has been found to deviate significantly from the experimental values.

The prediction of semi-fluidized bed pressure drop for liquid-solid system using Eq. (7.16) results in large error for the irregular particles if the bed packed bed voidage is taken as that of the initial static bed voidage. But, it is interesting to note that by using the experimentally measured voidage of the top packed bed, the model has resulted in accurate prediction of the semi-fluidized bed pressure drop in liquid-solid system, which has been a maiden attempt. For a gas-liquid-solid semi-fluidized bed, the pressure drop prediction agrees within 20 % for nearly sixty percent of the data, but deviate more than 20 % from that of the others. This may be because of the formation of a more compact bed with irregular particles than regular ones where the deviation has been observed to be less.

The hydrodynamics of a co-current gas-liquid-solid (three-phase) semi-fluidized bed with liquid as the continuous phase has shown an increased gas holdup value than for a fluidized bed. For some liquid and gas velocity combinations, the gas holdup has been found to be 41 % higher than that occurs in a fluidized bed under similar conditions. An initial increase in gas holdup with liquid velocity at a fixed gas velocity has been observed, which may possibly be due to increase in packed bed height and pressure drop with enhanced bubble disintegration and longer residence time of the bubbles in the bed. But with further increase in liquid velocity, the gas holdup has been found to decrease which may be due to the saturation in bubble disintegration phenomenon, reduced fluidized bed portion and lower residence time of the gas bubbles at higher liquid velocity.

The outcomes of the present findings will be useful for better understanding of the semi-fluidized bed hydrodynamics for both liquid-solid and gas-liquid-solid system with irregular particles. The quantitative expressions in the form of derived and empirical models presented in this chapter will help in the successful design, scale-up and operation of a semi-fluidized bed.

Chapter 8

Conclusions and future scope of the work

Chapter-8

Conclusions and future scope of the work

8.1. Introduction

Critical appraisal of the literature reveals that both the fluidized bed and the semi-fluidized beds are useful for efficient gas-liquid-solid contacting process and can be used in chemical reactors for catalytic as well as non-catalytic ones, biochemical process and wastewater treatment. During the last four decades, considerable research efforts have been made to understand the hydrodynamic aspects of fluidization as well as micro scale structure, identification and characterization of various regimes, gas-solids mixing, etc. Over the years newer applications of fluidized bed systems are being explored which necessitate further understanding of the two and the three phase fluidization and semi-fluidization systems. The problems related to the effect of distributor, irregular and regular shape particles, liquid viscosity and surface tension, scaling up, particle size and density, which affect the hydrodynamics, and its structure still create practical dilemma. Even though a large number of experimental studies have been directed towards the quantification of various hydrodynamic parameters of gas-liquid-solid fluidized beds, the complicated phenomena have not yet been fully understood. Thus, there exist many grey areas requiring further extensive fundamental studies in fluidized and semi-fluidized bed systems.

The work reported in this is an attempt to understand and quantify the hydrodynamic parameters in a larger domain of the operating variables and validate the experimental results by CFD analysis. Thus a gas-liquid-solid fluidized bed (0.1 m x 1.88 m) and a semi-fluidized bed (0.1 m x 1.24 m) have been designed, fabricated and fitted with all accessories. Detailed experimental studies to determine the hydrodynamic behaviour of both the gas-liquid-solid fluidized and the semi-fluidized beds have been carried out using regular shape spherical particles (1.55 mm to 6.29 mm of density nearly 2470 kg/m^3), hollow cylindrical particles (6.684 mm, 1670 kg/m^3) and irregular particles (1.55 mm to 4.05 mm, density from 1492 to 3994 kg/m^3). The hydrodynamic characteristics for gas-liquid-solid fluidization studied include pressure drop, minimum fluidization velocity, bed expansion and phase holdup. For semi-fluidization hydrodynamics the characteristics like minimum and maximum semi-fluidization velocity, height of the top packed bed, pressure drop and gas holdup have been studied.

8.2. Conclusions

The antenna type air sparger used in the present study has resulted in lower pressure drop in the distributor section and generation of fine bubbles those are well distributed across the column cross-section. A comparatively higher gas holdup of about 82.6% and 25.4% respectively than the gas holdup reported by Ramesh and Murugesan (2002) and by Safoniuk et al. (2002) for air-glycerol solution (44% by mass) at a gas Froude number of 0.01148 has been obtained in the present study (Fig. 3.33). In the CFD simulation, "uniform gas and liquid velocity with a gas bubble size of 2 mm" has been used as the inlet boundary condition for the gas and the liquid phases. The result obtained from CFD simulation has been found to agree well with the experimental results in terms of hydrodynamic parameters like: expanded bed height (Fig. 5.12) and bed pressure drop (Fig. 5.16). This indicates that without affecting the other hydrodynamic parameters the antenna type air sparger has resulted in improved gas holdup for the system in the present study.

The measured pressure drop in a gas-liquid-solid fluidized bed does not represent the true drag exerted by the fluid phase on the particles. Rather the measured pressure drop is used to determine the minimum liquid fluidization velocity (U_{Lmf}) and the phase holdup in the system. Visual observation confirms the increase in bed height with increase in liquid velocity in case of fluidization and height of the top packed bed in case of semi-fluidization. The detailed out come of various hydrodynamic studies and theoretical analysis has been presented in the respective chapters. Following are the brief summary of the conclusions made in the respective chapters.

8.2.1. Hydrodynamics of regular particles in fluidized bed

8.2.1.1. The bed pressure drop has been found to decrease with gas velocity and increase with the static initial bed height.

8.2.1.2. Minimum liquid fluidization velocity decreases with increase in gas velocity and liquid viscosity but increases with increase in particle size, while it is independent of the initial static bed height.

8.2.1.3. The bed expansion ratio has been found to increase with increase in liquid and gas velocity and viscosity of liquid, decrease with particle size but is unaffected by the initial static bed height.

8.2.1.4. The overall gas holdup has been found to be a strong function of Eötvös number and gas Froude number and increases with the increase in both.

8.2.1.5. For the prediction of minimum fluidization velocity, bed expansion and gas holdup, empirical equations have been developed.

8.2.1.6. The optimum operating conditions for gas holdup have been found to be [Mo, Eo, Fr_L, Fr_g, β_d, d_r, h_r] = [$3.21\text{x}10^{-10}$, 1487.6, $1.1\text{x}10^{-3}$, $1.55\text{x}10^{-2}$, 2.28, 0.059, 2.75] with a maximum value of 0.282 determined by Genetic algorithm.

8.2.1.7. Similar qualitative influence of different operating variables has been observed in case of hollow cylindrical particles as observed with the spherical ones, but quantitatively the influences are found to be different.

8.2.2. Hydrodynamics of irregular particles in fluidized bed

8.2.2.1. Similar kind of trend has been observed for almost all the hydrodynamic parameters as it was observed for regular shape particles, but their extent of dependency on various operating variables is different.

8.2.2.2. Additionally, minimum liquid fluidization velocity increases with particle density and expanded bed height decreases with particle density.

8.2.2.3. A different set of empirical equations for the prediction of minimum fluidization velocity, bed expansion and gas holdup has been developed for the irregular particles.

8.2.3. CFD simulation of hydrodynamic characteristics of three-phase fluidized bed

8.2.3.1. Bed pressure drop obtained from CFD simulation has been found to decrease with gas velocity and increase with static bed height and particle density.

8.2.3.2. The expanded bed height has been found to increase with liquid velocity and decrease with particle size and particle density.

8.2.3.3. Gas holdup has been found to increase with gas velocity but decrease with liquid velocity.

8.2.3.4. The dynamic characteristics of gas–liquid–solid flows obtained from the CFD simulation have been validated with the experimental results and a good agreement has been observed.

8.2.3.5. The Eulerian-Eulerian multi-phase granular flow approach is capable of predicting the overall performance of a gas–liquid–solid fluidized bed.

8.2.4. Hydrodynamics of regular particles in semi-fluidized bed

8.2.4.1. The minimum semi-fluidization velocity (U_{osf} or U_{Losf}) has been found to increase with particle size and bed expansion ratio, but decrease with, liquid viscosity and is independent of initial static bed height for both the liquid solid and the gas-liquid-solid systems. However U_{Losf} decreases with gas velocity for the three-phase system.

8.2.4.2. Similar variations in maximum semi-fluidization velocity have been observed with operating variables as it is in case of the minimum semi-fluidization velocity except that there is increase in maximum semi-fluidization velocity with the initial static bed height for both the liquid-solid and the gas-liquid-solid semi-fluidized beds.

8.2.4.3. The top packed bed height increases with the values of liquid and gas velocity, liquid viscosity, but decreases with particle size, initial static bed height and expansion ratio.

8.2.4.4. For the prediction of the values of minimum and maximum semi-fluidization velocity and the height of the top packed bed, empirical and semi-empirical equations have been developed. Predictions from these equations have been found to agree well with the experimental results and a few literature correlations or models.

8.2.4.5. For prediction of semi-fluidized pressure drop the developed model equation using the value of the static bed voidage (ε_s) as the packed bed voidage has been found to agree well with the experimental one in case of liquid-solid fluidized bed. The model of Chern et al. (1984) based on the separated flow for the prediction of gas-liquid-solid semi-fluidized bed pressure drop has been found suitable in case of regular shape particles.

8.2.4.6. The gas holdup in the semi-fluidized bed has been found to be much higher than that observed in a fluidized bed. For some gas and liquid velocity combinations the gas holdup has been found to be nearly 40 % higher than that occurs in a fluidized bed under similar conditions. Empirical model equation has been proposed fro the prediction of gas holdup.

8.2.5. Hydrodynamics of irregular particles in semi-fluidized bed

8.2.5.1. Similar behaviour for minimum semi-fluidization velocity as it was reported for regular particles has been observed. Additionally both U_{osf} and U_{Losf} have been found to increase with particle density.

8.2.5.2. Similar variations for maximum semi-fluidization velocity (U_{msf} or U_{Lmsf}) have been observed with the operating variables.

8.2.5.3. The top packed bed height in dimensionless form as H_{pa}/H_s has been found to behave differently as packed bed formation begins and attains a higher value i.e. two different packed regimes have been observed.

8.2.5.4. The dependency of hydrodynamic parameters on operating variables has been found to be different for the regular and the irregular particles. Thus a different set of empirical and semi-empirical equations has been developed for the prediction of the

values of minimum and maximum semi-fluidization velocity and the height of the top packed bed.

8.2.5.5. Prediction of pressure drop using the model equation with the initial static bed voidage has resulted in large deviation from the experimental values for irregular particles. But using the measured packed bed voidage a good agreement has been observed in case of the liquid-solid semi-fluidized bed. As far as the gas-liquid-solid semi-fluidized bed pressure drop is concerned, the prediction with the existing model does not agree with the experimental findings.

8.3. Future scope of the work

From the hydrodynamic study of gas-liquid-solid fluidized and semi-fluidized beds with a wide range of operating variables in the same experimental set-up, a clear understanding of the behaviour of semi-fluidized bed w.r.t. the fluidized has been obtained. Hydrodynamics of both regular and irregular particles have been studied separately. The followings are the recommendations for the future work.

8.3.1. Mathematical analysis for the unification of hydrodynamic parameters of regular and irregular particles and development of more generalized correlations.

8.3.2. Further validation of the dimensionless approach is required. This would include significant variation in the Eotvos number, M-group, and the density ratio.

8.3.3. A method for proper design an effective and simple distributor system for the three-phase fluidized bed is required. For this a combination of a different distributor system can be studied.

8.3.4. Computational fluid dynamics study on flow regime identification and bubble behaviour and using different types of particles, liquids and bed geometries can be carried out.

8.3.5. Theoretical analysis of semi-fluidized bed hydrodynamics using CFD are to be carried out for better understanding of the phenomena involved.

8.3.6. Experimental investigation relating to semi-fluidized bed as a bioreactor will be quite relevant in the context of efficient waste treatment keeping in view the inherent advantages of such a bed.

8.3.7. Scale-up studies relating various hydrodynamic parameters in three-phase fluidized and semi-fluidized beds are necessary for their potential industrial application.

References

References

Agaletskii, F.N., Ruban, N. M., 1959. Reduction of iron ores in semi-fluidized bed. Institute of Metal 5, 25-35.

Anata, I., Subroto, M.A., Doran, P.M., 1995. Oxygen transfer and culture characteristics of self-immobilized Solanum aviculare aggregates. Biotechnology and Bioengineering 47, 541-549.

Babu Rao, K., Mukherjee, S. P., Doraiswamy, L. K., 1965. New adiabatic MT reactor system. AIChE Journal 11, 741-746.

Babu Rao, K, Doraiswamy, L.K., 1970. Combined Reactors: Formulation of Criteria and Operation of a Mixed Tubular Semi-fluidized Reactor. AIChE Journal 16, 273-280.

Babu, S.P., Shah, B., Talwalkar, A., 1978. Fluidization correlations for coal gasification materials - minimum fluidization velocity and fluidized bed expansion ratio. AIChE Symposium Series 74, 176-186.

Bahary, M., 1994. Experimental and computational studies of hydrodynamics in three-phase and two-phase fluidised beds. Ph.D. Thesis, Illinois Institute of Technology, Chicago.

Bakopoulos, A., 2006. Multiphase fluidization in large-scale slurry jet loop bubble columns for methanol and or dimethyl ether production. Chemical Engineering Science 61, 538 – 557.

Barkat, O., and Diboun, M., 1995. Hydrodynamics of Two- and Three-Phase Bubble Flow in Counter and Co-curent Systems", Fluidization and Fluid-Particle Svstems: AIChE 1995 Annual Meeting Preprints, Arastoopour, H. ed., 200-204.

Barthe, L., Desportes, S., Steinmetz, D., Hemati, M., 2009. Metallic salt deposition on porous particles by dry impregnation in fluidized bed: Effect of drying conditions on metallic nanoparticles distribution. Chemical Engineering Research and Design 87, 915-922.

Beaton, W.L, McDaniel, N.K., McWhirter, W.E., Petersen, R.D., van Dnesen, R.P., 1986. Resid hydrocracker expands cnide processing flexibility. Oil Gas Journal 84 (27), 47-53.

Beaver, L.E., Fan, L.S., 1984. Experimental observations in a cocurrent gas-liquid-solid semifluidized bed with gas as the continuous phase. Journal of the Chinese Institute of Chemical Engineers 15, 159-68.

Begovich, J.M., Watson, J.S., 1978. Hydrodynamic characteristics of three-phase fluidized beds. In “Fluidization”. J.F. Davison and D.L. Keairns (Eds.), Cambridge University Press, Cambridge, 190-195.

Beyenal, H., Tanyolac, A., 1998. The effects of biofilm characteristics on the external mass transfer coefficient in a differential fluidized bed biofilm reactor. Biochemical Engineering Journal 1, 53-61.

Bhatia, V.K., Epstein, N. 1974. Three Phase Fluidization: A Generalized Wake Model. In: Fluidization and its Applications. H. Angelino et al., Eds., Cepadues Editions, Toulouse, 380-392.

Bloxom, V.R., Costa, J.M., Herranz, S., MacWilliam, G.L., and Roth, S.R., 1975. Determination and Correlation of Hydrodynamic Variables in a Three-Phase Fluidized Bed (part IV)", Oak Ridge National Laboratory -MIT, Report no. 219.

Blum, D.B., Toman, J.J., 1977. Three-phase fluidization in a liquid phase methanator, AIChE Symposium series 73 (161), 115-120.

Briens, L.A., Briens, C.L., Margaritis, A., Hay, J., 1997a. Minimum Liquid Fluidization Velocity in Gas-Liquid-Solid Fluidized Beds. AIChE Jounal 43, 1181-1189.

Briens, L.A., Briens, C.L., Margaritis, A., Hay, J., 1997b. Minimum Liquid Fluidization Velocity in Gas-Liquid-Solid Fluidized Beds of Low Density Particles. Chemical Engineering Science 52, 4231-4238.

Briens, L.A., Ellis, N., 2005. Hydrodynamics of three-phase fluidised bed systems examined by statistical, fractal, chaos and wavelet analysis methods. Chemical Engineering Science 60, 6094–6106.

Brownell, L.E., 1951. In: Encyclopaedia of Chemical Technology. R.E. Kirk and D.F. Othmer, Ed., Interscience Encyclopaedia, New York 6, 516-517.

Buffiėre, P., Fonado, C., Moletta, R., 1998. Liquid mixing and phase hold-ups in gas producing fluidized bed bioreactors. Chemical Engineering Science 53, 617-627.

Bunner, B., Tryggvason, G., 1999. Direct numerical simulations of dispersed flows. In: Proceedings of the Ninth Workshop on Two-Phase Flow Predictions, Germany, 13–19.

Cao, C., Liu, M., Guo, Q., 2007. Experimental investigation into the radial distribution of local phase holdups in a gas-liquid-solid fluidized bed. Industrial & Engineering Chemistry Research 46, 3841-3848.

Cao, C., Liu, M., Wen, J., Guo, Q., 2009. Experimental measurement and numerical simulation for liquid flow velocity and local phase hold-ups in the riser of a GLSCFB. Chemical Engineering and Processing: Process Intensification 48, 288-295.

Catros, A., Bernard, J.R., Briens, C. Bergougnou, M.A., 1985. Gas Holdup above the Bed Surface and Grid Gas Jet Hydrodynamics for Three-Phase Fluidized Beds. Canadian Journal of Chemical Engineering 63, 754-759.

Chatib, B., Grasmick, A., Elmalch, S., Aim, R. B., 1981. Biological wastewater treatment in a three-phase fluidised-bed reactor. In: P. F. Cooper and B. Atkinson (eds.), Biological Fluidized Bed Treatment of Water and Wastewater. Ellipse Horwood Limited, Chichester, UK, 192-204.

Chattopadhaya, P., 1993. Unit operations of Chemical Engineering. Khanna Publishers, Delhi, 1, 251.

Chen, R.C., Reese, J., Fan, L.S., 1994. Flow structure in a three-dimensional bubble column and three-phase fluidized bed. AIChE Journal 40, 1093-1104.

Chen, Z., Zheng, C., Feng, Y., 1995. Distributions of flow regimes and phase holdups in three-phase fluidised beds. Chemical Engineering Science 50, 2153–2159.

Chen, C., Fan, L.S., 2004. Discrete Simulation of Gas-Liquid Bubble Columns and Gas-Liquid-Solid Fluidized Beds. AIChE Journal 50, 288-301.

Chern, S.H., Muroyama, K., Fan, L.S., 1983. Hydrodynamics of Constrained Inverse Fluidization and Semi-fluidization in a Gas-Liquid-Solid System. Chemical Engineering Science 38, 1167 – 1174.

Chern, S-H., Fan, L-S., Muroyama, K., 1984. Hydrodynamics of Cocurrent Gas-Liquid-Solid Semifluidization with Liquid as the Continuous Phase. AIChE Journal 30, 288-294.

Cheung, S.C.P., Yeoh, G.H., Tu, J.Y., 2007. On the numerical study of isothermal vertical bubbly flow using two population balance approaches. Chemical Engineering Science 62, 4659–4674.

Chitester, D.C., Kornosky, R.M., Fan, L.-S., Danko, J.P., 1984. Characteristics of fluidization at high pressure. Chemical Engineering Science 39, 253-261.

Choi, J-W., Min, J., Lee, W-H., Lee, S.B., 1999. Mathematical Model for a Three-Phase Fluidized Bed Biofilm Reactor in Wastewater Treatment. Biotechnology and Bioprocess Engineering 4, 51-58.

Costa, E., De Lucas, A., Garcia, P., 1986. Fluid Dynamics of Gas-Liquid-Solid Fluidized Beds. Industrial & Engineering Chemistry Process Design and Development 25, 849-854.

Cover, A.E., Schreiner, W.C., Skaperdas, G.T., 1973. Kellogg's Coal Gasification Process. Chemical Engineering Progress 69 (3), 31-37.

Dakshinamurty, P., Subrahmanyam, V., Rao, J. N., 1971. Bed porosities in gas-liquid fluidization. Industrial and Engineering Chemistry Process Design and Development 10, 322-328.

Dakshinamurty, P., Subrahmanyam, V., Rao, J. N., 1972. Bed porosities in gas-liquid fluidization. Industrial and Engineering Chemistry Process Design and Development 11, 318-319.

Dargar, P., Macchi, A., 2006. Effect of Surface-Active Agents on the Phase Holdups of Three-Phase Fluidized Beds. Chemical Engineering and Processing 45, 764–772.

Darton, R.C., Harrison, D., 1975. Gas and Liquid Holdup in Three-Phase Fluidization. Chemical Engineering Science 50, 581-586.

Darton, R.C., 1985. "The Physical Behaviour of Three-Phase Fluidized Beds", in Fluidization, 2nd edition, Davidson, J.F., Clifi, R., and Harrison, D., ed., Academic Press, London. 495-528.

Davies, O.L., 1978. The design and analysis of industrial experiments, 2nd edn, Longman Publishers, London.

Deckwer, W.D., Becker, F.U., Ledakowicz, S., Dobler, I.W., 2004. Microbial removal of ionic mercury in a three-phase fluidized bed reactor. Environmental Science and Technology 38, 1858-1865.

Delebarre, A., Morales, J. M., Ramos, L., 2004. Influence of bed mass on its fluidization characteristics. Chemical Engineering Journal 98, 81-88.

Dhanuka, V.R., Stepanek, J.B., 1978. Gas and Liquid Hold-up and Pressure Drop Measurements in a Three-Phase Fluidized Bed. in “Fluidization”, J.F. Davison and D.L. Keairns, Eds., Cambridge University Press, UK, 179-183.

Dehkissia, S., Baçaoui, A., Iliuta, I., Larachi, F., 2008. Dynamics of Fines Deposition in an Alternating Semifluidized Bed. A.I.Ch.E. Journal 54, 2120-2131.

Dias, S.M.M., 1991. Extractive fermentation of ethanol by immobilized yeast cells. NTIS. Report, Dep. Eng., Tech. Univ. Lisbon, Lisbon, 218.

Donaldson, T.L., Strandberg, G.W., Hewitt, J.D., Shields, G.S., 1984. Bio oxidation of coal gasification wastewaters. Environmental Progress 3, 248–253.

Donath, E.E., 1963. In: Chemistry of coal utilization. Supplementary volume. H.H. Lowry ed., John Wiley, 1041-1043.

Dudukovic, M.P., Larachi, F., Mills, P.L., 1999. Multiphase reactors-revisited. Chemical Engineering Science 54, 1975–1995.

El-Temtamy, S.A., Epstein, N., 1978. Bubble wake solids content in three-phase fluidized beds. International Journal of Multiphase Flow 4, 19-31.

El-Temtamy, S.A., Epstein, N., 1979. Contraction or expansion of three-phase fluidized beds containing fine/light particles. Canadian Journal of Chemical Engineering 57, 520-522.

Ermakova, A., Ziganshin, G.K., Slin’ko, M.G., 1970. Hydrodynamics of a gas–liquid reactor with a fluidized bed of solid matter, Theoretical Foundations of Chemical Engineering 4, 84–89.

Epstein, N., and Nicks, D., 1976. Contraction or Expansion of Three-Phase Fluidized Beds. In: Fluidization Technology, Keairns, D.L., ed., Washington, Hemisphere Publishing, 389-397.

Epstein, N., 1981. Review: Three-Phase Fluidization-Some Knowledge Gaps. Canadian Journal of Chemical Engineering 59, 649-757.

Euzen, J.P., Trambouze, P., Wauquier, L.P., 1993. Scale-up Methodology for Chemical Processes, Editions Technip, Paris.

Fan, L.T., Yang, Y.C., Wen, C.Y., 1959. Semifluidization: Mass transfer in semifluidized beds. AIChE Journal 5, 407-409.

Fan, L.T., Yang, Y.C., Wen, C.Y., 1960. Mass transfer in semifluidized beds for solid-liquid system. AIChE Journal 6, 482-487.

Fan, L.T., Wen, C.Y., 1961. Mechanics of semi-fluidization of single size particles in solid-liquid systems, AIChE Journal 7, 606-610.

Fan, L.T., Hsu, E.H., 1980. Semifluidized Bed Bioreactor. In: Advances in Biotechnology (Proceedings of the VIth International Fermentation Symposium, London, Ontario, Canada, M. Moo-Young, ed., Pergamon Press, New York, N.Y. 1981.1, 663-669.

Fan, L.S., 1983. Mechanism of Semifluidized Bed Bioreactorfor Biological Phenol Degradation. Final Project Report No. A-060. The Ohio State University Columbus, Ohio.

Fan, L.S., Matsuura, A., Chern, S.H., 1985. Hydrodynamic characteristics of a gas-liquid-solid fluidized bed containing a binary mixture of particles. A.I.Ch.E. Journal 31, 1801-1810.

Fan, L.S., Satija, S., Wisecarver, K., 1986. Pressure fluctuation measurements and flow regime transitions in gas-liquid-solid fluidized beds. A.I.Ch.E. Journal 32, 338-340.

Fan, L.S., Bavarian, F.R., Gorowara, I., and Kreischer, B.E., 1987. Hydrodynamics of Gas-Liquid-Solid Fluidization under High Gas Hold-Up Conditions. Powder Technology 53, 285-293.

Fan, L.S., Attia, Y.A., 1988. A Novel Three Phase Fluidized Bed Process for Simultaneous Selective Flocculation and Microbial Desulfurization of High Sulfur Coal. Project No.RN-1-87-090. The Ohio State University, Columbus, Ohio.

Fan, L.S., 1989. Gas-Liquid-Solid Fluidization Engineering. Butterworth Series in Chemical Engineering, Butterworth Publishers, Boston, MA.

Farhadian, M., Duchez, D., Vachelard, C., Larroche, C., 2008. Monoaromatics removal from polluted water through bioreactors—A review. Water Research 42, 1325-1341.

Feng, W., Wen, J., Fan, J., Yuan, Q., Jia, X., Sun, Y., 2005. Local hydrodynamics of gas–liquid–nano particles three-phase fluidization. Chemical Engineering Science 60, 6887–6898.

Fluent 6.2.16. Fluent 6.2.16 User's Guide, Fluent Inc. 2004.

Fonts, I., Azuara, M., Gea, G., Murillo, M.B., 2009. Study of the pyrolysis liquids obtained from different sewage sludge. Journal of Analytical and Applied Pyrolysis 85, 184-191.

Foot, D.G., MacKay, J.D., Huiatt, J.L., 1986. Column Flotation of Chromite and Fluorite Ores. Canadian Metallurgical Quarterly 25, 15–21.

Forster, C.F., Boyes, A.P., Hay, B.A., Butt, J.A., 1986. An aerobic fluidised bed reactor for wastewater treatment. Chemical Engineering Research and Design 64, 425-430.

Fortin, Y. 1984. Réacteurs à lit fluidisé triphasique: Caractéristiques hydrodynamiques et mélange des particules solides. Ph.D. Thesis, Institut National Polytechnique de Lorraine, Nancy, France.

Fraguío, M.S., Cassanello, M.C., Larachi, F., Chaouki, J., 2006. Flow regime transition pointers in three-phase fluidised beds inferred from a solid tracer trajectory. Chemical Engineering and Processing 45, 350–358.

Fuerstenau, D.W., 1980. Fine Particle Flotation. in "Fine Particle Processing", P. Somasundaran, Ed., The Society of American Institute of Mining, Metallurgical and Petroleum Engineers, New York, NY, USA, 669-705.

Gartsman, A.N, Ermakova, A., Bakhbolva, V.P., Rassadnikova, N.I., 1977. Mass transfer with chemical reaction in the three-phase system gas-liquid-solid catalyst. International Chemical Engineering 17, 697-702.

Geldart, D., 1990. Estimation of basic properties for use in fluid-particle process calculations. Powder Technology 60, 1-13.

Gidaspow, D., 1994. Multiphase Flow and Fluidization: Continuum and Kinetic Theory Descriptions. Academic Press, New York.

González, G., Herrera, G., García, Ma.T., Peña, M., 2001. Biodegradation of phenolic industrial wastewater in a fluidized bed bioreactor with immobilized cells of Pseudomonas putida. Bioresource Technology 80, 137-142**.**

Gorowara, R.L., Fan, L.S., 1990. Effect of surfactants on three-phase fluidized bed hydrodynamics. Industrial and Engineering Chemistry Research 29, 882-891.

Grasmick, A., Chatib, B., Elmaleh, S., Ben Aim, R., 1981. Hydrocarbon removal in a three-phase fluidized experimental bed and modelling of the process. Water research 15, 719-727.

Grevskott, S., Sannaes, B.H., Dudukovic, M.P., Hjarbo, K.W., Svendsen, H.F., 1996. Liquid circulation, bubble size distributions, and solids movement in two-and three-phase bubble columns. Chemical Engineering Science 51, 1703–1713.

Gupta, C.K., Sathiyamoorthy, D., 1999. Fluid bed technology in material processing CRC Press, Florida, 38.

Haider, A., Levenspiel, O., 1989. Drag coefficient and terminal velocity of spherical and nonspherical particles. Powder Technology 58, 63-70.

Han, J.H., Wild, G., Kim, S.D., 1990. Phase Hold-Up Characteristics in Three-Phase Fluidized Beds. Chemical Engineering Journal 43, 67–73.

Heard, W.B., Richter, G.R., 1996. Numerical Mutiphase, Multicomponent Flow Modeling. Computational Fluid Dynamics in Chemical Reaction Engineering, United Engineers Foundation, San Diego, Ca.

Herzberg, M., Dosoretz, C.G., Green, M., 2005. Increased biofilm activity in BGAC reactors. AIChE Journal 51, 1042-1047.

Hikita, H., Kikukawa, H., 1974. Liquid-Phase Mixing in Bubble Columns: Effect of Liquid Properties. Chemical Engineering Journal 8, 191–197.

Hikita, H., Asai, K., Segawa, K., Kuan, M. 1980, Gas Holdup in Bubble Columns. Chemical Engineering Journal 20, 59–67.

Hirata, A., Takemoto, T., Ogawa, K., Auresenia, J., Tsuneda, S., 2000a. Evaluation of kinetic parameters of biochemical reaction in Three-phase fluidized bed biofilm reactor for wastewater treatment. Biochemical Engineering Journal 5, 165-171.

Hirata, A., Meutia, A.A., Osawa, M., Arai, M., Tsuneda, S., 2000b. Effects of oxygen supply condition and specific biofilm interfacial area on phenol removal rate in a three-phase fluidized bed bioreactor, The Canadian Journal of Chemical engineering 78, 95-101.

Ho, T.C., Yau, S.J., Hopper, J.R., 1987. Hydrodynamics of Semi-fluidization in gas-solid systems, Powder Technology 50, 25-34.

Ho, T.C., Kobayashi, N., Lee, Y.K., Lin, C.J., Hopper, J.R., 2002. Modeling of mercury sorption by activated carbon in a confined, a semi-fluidized, and a fluidized bed. Waste Management 22, 391–398.

Ho, T.C., Lee, Y.K., Hopper, J.R., Lin, C.J., Kobayashi, N., 2005. Mercury emission control from combustion flue gas employing semi-fluidized bed activated carbon adsorption, Journal of the Chinese Institute of Chemical Engineers 36, 77-84.

Hogrefe, W., Grossenbacher, H., Cook, A.M., Hütter, R., 1986. Biotreatment of *s*-triazine-containing wastewater in a fluidized bed reactor. Biotechnology and Bioengineering 28, 1577-1581.

Holladay, D.W., Hancher, C.W., Scott, C.D., Chilcote, D.D., 1978. Biodegradation of phenolic waste liquors in stirred tank, packed-bed, and fluidized bed bioreactors, Journal of Water Pollution Control Federation 50, 2573–2589.

Holland J.H., 1975. Adaptation in natural and artificial systems. MIT Press, Cambridge, MA.

Horn, H., Hille, A., Nue, T.R., Ochmann, C., 2008. Biofilm technologies - A review [Neue biofilmverfahren zur industrieabwasserreinigung]. GWF, Wasser - Abwasser 149, S67-S72.

Hu, T.T., Yu, B.T., Wang, Y.P., 1986. Holdups and Models of Three Phase Fluidized Bed. In: Fluidization, V, Ostergaard, K., and Sorenson, A., ed., Engineering Foundation, New York, 353-360.

Hughmark, G. A., 1967. Holdup and Mass Transfer in Bubble Columns. Industrial & Engineering Chemistry Process Design and Development 6, 218–220.

Hwang, S. J., Chiou, S. N., 1990. Packed bed height and liquid dispersion in gas-liquid-solid semifluidized beds. Journal of the Chinese Institute of Chemical Engineers 21, 53-60.

Hwang, S.-J., Lu, W.-J., 1995. Ion exchange in a semifluidized bed. Industrial and Engineering Chemistry Research 34, 1434-1439.

Is'emin, R.L., Zaitseva, N.A., Osipov, A.D., Akol'zin, A.P., 1995. Formation of nitrogen oxides and deposits on the heating surfaces of boilers with semi-fluidized bed furnaces fired with low grade coal. Promyshlennaya Energetika 2, 37-38.

Is'emin, R.L., Konyakhin, V.V., Kuz'min, S.N., Budkova, E.V., 2001. Boiler for central heating operating on low-grade solid fuel. Promyshlennaya Energetika 9, 22-25.

Jean, R.H., Fan, L.S., 1986. A Simple Correlation for Solids Holdup in a Gas-Liquid-Solid Fluidized Bed. Chemical Engineering Science 41, 2823-2828.

Jean, R.H., Fan, L.S., 1987. On the particle terminal velocity in a gas-liquid medium with liquid as the continuous phase. Canadian Journal of Chemical Engineering 65, 881-886.

Jena, H.M., Roy, G.K., Meikap, B.C., 2005. Development and Comparative Study of a Semi-Fluidized Bed Bioreactor for Treatment of Wastewater from Process Industries. Process & Plant Engineering – Environment Management 23, 70-75.

Jena, H.M., Roy, G.K., Meikap, B.C., 2008a. Prediction of gas holdup in three-phase fluidized bed from bed pressure drop measurement. Chemical Engineering Research and Design 86, 1301-1308.

Jena, H.M., Sahoo, B.K., Roy, G.K., Meikap, B.C., 2008b. Characterization of hydrodynamic properties of a gas–liquid–solid three-phase fluidized bed with regular shape spherical glass bead particles. Chemical Engineering Journal 145, 50-56.

Jena, H.M., Roy, G.K., Meikap, B.C., 2009a. Hydrodynamics of a gas-liquid-solid fluidized bed with hollow cylindrical particles. Chemical Engineering and Processing: Process Intensification 48, 279-287.

Jena, H.M., Sahoo, B.K., Roy, G.K., Meikap, B.C., 2009b. Statistical Analysis of the Phase Holdup Characteristics of a Gas–Liquid–Solid Fluidized Bed. The Canadian Journal of Chemical Engineering 87, 1-10.

Jiang, P., Arters, D., Fan, L.S., 1992. Pressure Effects on the Hydrodynamic Behaviour of Gas-Liquid-Solid Fluidized Beds. Industrial and Engineering Chemistry Research 3, 2322-2327.

Jianping, W., Shonglin, X., 1998. Local hydrodynamics in a gas–liquid–solid three-phase bubble column reactor. Chemical Engineering Journal 70, 81–84.

Jianping, W., Lei, P., Liping, D., Guozhu, M., 2003. The denitrification treatment of low C/N ratio nitrate-nitrogen wastewater in a gas-liquid-solid fluidized bed bioreactor. Chemical Engineering Journal 94, 155-159.

Jiradilok, V., Gidaspow, D., Breault, R.W., 2007. Computation of gas and solid dispersion coefficients in turbulent risers and bubbling beds. Chemical Engineering Science 62, 3397–3409.

Johnson, T.E., Murphy, J.R., Tasker, K.G., 1985. Combined cracking processes boost fuel yields from low-quality crudes and residua Oil and Gas Journal 83 (26), 50-55.

Joshi, J.B., Abichandani, J.S., Shah, Y.T., Ruether, J.A., Ritz, H.J., 1981. Kinetics of Oxydesulfurization of Minshall-Indiana Coal. AIChE Journal 27, 937-945.

Kato, Y., Uchida, K., Kago, T., Morooka, S., 1981. Liquid Hold-Up and Heat Transfer Coefficient between Bed and Wall in Liquid-Solid and Gas-Liquid-Solid Fluidized Beds. Powder Technology 28, 173–179.

Kato, Y., Morooka, S., Kago, T., Saruwatari, T., Yang, S.Z., 1985. Axial Hold-up Distributions of Gas and SoIid Particles in Three-Phase Fluidized Beds for Gas-Liquid (Slurry)-Solids Systems. Journal of Chemical Engineering Japan 18, 308-318.

Kelkar, B.G., Godbole, S.P., Honath, M.F., Shah, Y.H., 1983. Effect of Addition of Alcohols on Gas Holdup and Backmixing in Bubble Columns. A.I.Ch.E. Journal 29, 361-369.

Kiared, K., Larachi, F., Chaouki, J., Guy, C., 1999. Mean and turbulent particle velocity in the fully developed region of a three-phase fluidised bed. Chemical Engineering & Technology 22, 683–689.

Kim, S.P., Baker, C.G.J., Bergougnou, M.A., 1972. Hold-Up and Axial Mixing Characteristics of Two and Three-Phase Fluidized Beds. Canadian Journal of Chemical Engineering 50, 695–701.

Kim, S.P., Baker, C.G.J., Bergougnou, M.A., 1975. Phase Holdup Characteristics of Three Phase Fluidized Beds. Canadian Journal of Chemical Engineering 53, 134-139.

Kim, S.D., Baker, C.G.J., Bergougnou, M.A., 1977. Bubble Characteristics in Three-Phase Fluidized Beds. Chemical Engineering Science 32, 1299-1 306.

Kim, S.D., Tsutsurni, A., Yoshida, K., 1987. Effect of Particle Size on Gas Holdup in Three-Phase Reaction. Sadhana, 10, 261-268.

Kim, S.D., Kim, H.S., Han, J.H., 1992. Axial Dispersion characteristics in Three-Phase Fluidized Beds. Chemical Engineering Science 52, 3419-3426.

Kim, S.D., Kang, Y., 1997. Heat and Mass Transfer in Three-Phase Fluidized-Bed Reactors-An Overview. Chemical Engineering Science 52, 3639-3660.

Kim, S.J., Jeung, S.Y., Moon, H., 1998. Removal and recovery of heavy metal ions in fixed and semi-fluidized beds. Korean Journal of Chemical Engineering 15, 637-643.

Kim, S.J., Hwang, K.R., Cho, S.Y., Moon, H., 1999. Simultaneous Removal of Cyanide and copper Ions in a Semi-Fluidized Ion Exchanger Bed. Korean Journal of Chemical Engineering 16, 664-669.

Kim, S.J., Hwang, K.R., Cho, S.Y., 2001. Study on Ion-Exchange Behavior of Cu-CN Complexes. Journal of Chemical Engineering of Japan 34, 193-198.

Kim, S-J., Lim, K-H., Joo, K-H., Lee, M-J., Kil, S-G., Cho, S.Y., 2002. Removal of Heavy Metal-Cyanide Complexes by Ion Exchange. Korean Journal of Chemical Engineering 19, 1078-1084.

Knesebeck, A., Guardani, R., 2004a. Estimation of particle concentration profiles in a three-phase fluidized bed from experimental data and using the wake model. Brazilian Journal of Chemical Engineering 21, 47-57.

Knesebeck, A., Guardani, R., 2004b. Particle distribution in a three-phase fluidized bed under low-to-intermediate Reynolds conditions. Powder Technology 140, 30-39.

Kohl, A.L., Harty, R.B., Johnson, J.G., 1978. The molten salt coal gasification process. Chemical Engineering Progress 74, 73–79.

Koppatz, S., Pfeifer, C., Rauch, R., Hofbauer, H., Marquard-Moellenstedt, T., Specht, M., 2009. H_2 rich product gas by steam gasification of biomass with in situ CO_2 absorption in a dual fluidized bed system of 8 MW fuel input. Fuel Processing Technology 90, 914-921.

Kulkarni, A.A., Ekambara, K., Joshi, J.B., 2007. On the development of flow pattern in a bubble column reactor: experiments and CFD. Chemical Engineering Science 62 (4), 1049–1072.

Kunii, D., Levenspiel, O., 1991. Fluidization Engineering. 2nd ed. Butterworth-Heinemann, MA, USA.

Kurian, J., Raja Rao, M., 1970. Hydrodynamics of semi-fluidized bed, Indian Journal of Technology 8, 275-284.

Kusakabe, K., Morooka, S., Kato, Y., 1981. Characteristics of three-phase fluidized-bed electrodes for an alkaline fuel cell cathode. Journal of Chemical Engineering Japan 14(3), 208-214.

Larachi, F., Cassanello, M., Chaouki, J., Guy, C., 1996. Flow structure of the solids in a 3-D gas–liquid–solid fluidised bed. AIChE Journal 42, 2439–2452.

Larachi, F., Illiuta, I., Rival, O., Grandjean, B. P. A., 2000. Prediction of Minimum Fluidization Velocity in Three-Phase Fluidized-Bed Reactors. Industrial Engineering Chemistry and Research 39, 563-572.

Larachi, F., Belfares, L., Iliuta, I., Grandjean, B.P.A., 2001. Three-phase Fluidization Macroscopic Hydrodynamics Revisited. Industrial Engineering Chemistry and Research 40, 993-1008.

Lee, J.C., Al-Dabbagh, N., 1978. Three-Phase Fluidized Beds: Onset of Fluidization at High Gas Rates. in "Fluidization", J.F. Davison and D.L. Keairns, Eds., Cambridge University Press, UK. 184-189.

Lee, D.D., Scott, C.D., Hancher, C.W., 1979. Fluidized-bed bioreactor for coal-conversion effluents. Journal of Water Pollution Control Federation 51, 974-984.

Lee, S.L.P., de Lasa, H.I., 1987. Phase holdups in three-phase fluidised beds. AIChE Journal 33, 1359–1370.

Lee, S.L.P., Soria, A., and de Lasa, H.I., 1990. Evolution of Bubble Length Distributions in Three-Phase Fluidized Beds. AIChE Journal 36, 1763-1767.

Lee, D.H., Macchi, A., Grace, J.R., Epstein, N., 2001a. Fluid Maldistribution Effects on Phase Holdups in Three-Phase Fluidized Beds. Chemical Engineering Science 56, 6031–6038.

Lee, D.H., Epstein, N., Grace, J.R., 2001b. Models for minimum liquid fluidization velocity of gas-liquid-solid fluidized beds. Journal of Chemical Engineering of Japan 34 (2), 95–101.

Lee, D.H., Macchi, A., Epstein, N., Grace, J.R., 2001c. Transition velocities and phase holdups at minimum fluidization in gas-liquid-solid systems. The Canadian Journal of Chemical Engineering 79, 579–583.

Le Page, J.-F., Chatila, S.G., and Davidson, M., 1992. Resid and Heavy Oil Processing. IFP, Editions Technip, Paris.

L'Homme, G.A., 1979. Chemical engineering of gas-liquid solid catalyst reactions. CEBEDOC, Liege.

Li, A., Liu, D., 1981. In proceeding of second world congress of chemical engineering, Montreal, 170-176.

Li, Y., Zhang, J., Fan, L.-S., 1999. Numerical simulation of gas–liquid–solid fluidization systems using a combined CFD–VOF–DPM method: bubble wake behavior. Chemical Engineering Science 54, 5101–5107.

Liang, W., Yu, Z., Jin, Y., Wang, Z., Wu, Q., 1995. The phase holdups in a gas-liquid-solid circulating fluidized bed. The Chemical Engineering Journal and The Biochemical Engineering Journal 58, 259-264.

Lin, T.J., Tzu, C.H., 2003. Effects of macroscopic hydrodynamics on heat transfer in a three-phase fluidized bed. Catalysis Today 79–80, 159–167.

Lin, C-N., Wu, S-Y., Chang, J-S., Chang, J-S., 2009. Biohydrogen production in a three-phase fluidized bed bioreactor using sewage sludge immobilized by ethylene–vinyl acetate copolymer. Bioresource Technology 100, 3298-3301.

Liu, , Li, Z., Zheng, W., Wen, X., Liu, H., 2006. Method for manufacturing charging coal from blend coal for coking Anshan Coking and Refractory Engineering Consulting Corporation, China Metallurgical Construction Group, Peop. Rep. China, Chinese Patent: CNXXEV CN 1834204 A 20060920.

Liu, X., Xu, G., Gao, S., 2008. Fluidization of extremely large and widely sized coal particles as well as its application in an advanced chain grate boiler. Powder Technology 188, 23–29.

Lun, C.K.K., Savage, S.B., Jeffrey, D.J., Chepurniy, N., 1984. Kinetic Theories for Granular Flow: Inelastic Particles in Couette Flow and Slightly Inelastic Particles in a General Flow Field. Journal of Fluid Mechanics 140, 223-256.

Luo, X., Jiang, P., Fan, L.S., 1997. High pressure three-phase fluidization: hydrodynamics and heat transfer, AIChE Journal 43, 2432-2445.

Mathews, A.P., Fan, L.T., 1983. Comparison of performance of packed and semifluidized beds for adsorption of trace organics. AIChE Symposium Series 79 (No. 230), 79-85.

Matonis, D., Gidaspow, D., Bahary, M., 2002. CFD simulation of flow and turbulence in a slurry bubble column. AIChE Journal 48, 1413–1429.

Matsuura, A., Fan, L.S., 1984. Distribution of Bubble Properties in a Gas-Liquid-Solid Fluidized Bed. AIChE Journal 30, 894-903.

Meikap, B.C., Roy, G.K., 1995. Recent advances in biochemical reactors for treatment of wastewater, Indian Journal of Environmental Protection 15, 44-49.

Meikap, B.C., 2000. Abatement of particulate Laden SO2 in a Modified Multi-Stage Bubble Column. Ph.D. Thesis, Indian Institute of Technology, Kharagpur, India.

Meikap, B.C., Kundu, G., Biswas M.N., 2002. Prediction of dispersed phase holdup in a modified multi-stage bubble column scrubber. Canadian Journal of Chemical Engineering 80, 306-312.

Minina, S.A., Pryakhina, N.I., Chemesova, I.I., Chizhikov, D.V., A Pediatric Medicinal Preparation Containing an Extract of the Milk-White Iris (*IRIS LACTEA*). Pharmaceutical Chemistry Journal 42, 37-39.

Mirata, M.A., Heerd, D., Schrader, J., 2009. Integrated bioprocess for the oxidation of limonene to perillic acid with *Pseudomonas putida* DSM 12264. Process Biochemistry 44, 764-771.

Mitra-Majumdar, D., Farouk, B., Shah, Y.T., 1997. Hydrodynamic modeling of three- phase flows through a vertical column. Chemical Engineering Science 52, 4485 –4497.

Miura, H., Takahashi, T., Kawase, Y., 2001. Effect of pseudoplastic behaviour of liquid in co-current three-phase fluidized beds on bed expansion. Chemical Engineering Science 56, 6047-6053.

Muroyama, A., Fan, L.S., 1985. Fundamentals of gas–liquid–solid fluidization. A.I.Ch.E. Journal 30, 1–34.

Murthy, J.S.N., Roy, G.K., 1986. Semifluidization: A Review. Indian Chemical Engineer 29 (2), 1-14.

Murthy, J. S. N., Roy, G. K., Subramanyam, N., Zutshi, D.K., Naik, S.C., 1990. Residence Time distribution in Semi-fluidized beds. Journal of Institution of Engineers (India) 71, 42-43.

Mydlarz, J., 1987. Prediction of the packed bed height in liquid-solid semi-fluidization of homogeneous mixtures, Chemical Engineering Journal 34, 155-158.

Nacef, S., 1991. Hydrodynamique des Lits Fluidisés Gaz-Liquide-Solide. Effets du Distributeur et de la Nature du Liquide, Ph.D. thesis, Institut National Polytechnique de Lorraine, Nancy, France.

Nacef, S., Wild, G., Laurent, A., Kim, S.D., 1992. Scale effects in gas-liquid-solid fluidization. International chemical engineering 32, 51-72.

Nacef, S., Poncinb, S., Bouguettouchaa, A., Wild, G., 2007. Drift flux concept in two- and three-phase reactors. Chemical Engineering Science 62, 7530 –7538.

Nicolella, C., Van Loosdrecht, M.C.M., Heijnen, J.J., 2000. Wastewater treatment with particulate biofilm reactors. Journal of Biotechnology 80, 1-33.

Nikov, I., Grandjean, B.P.A., Carreau, P.J., Paris, J., 1990. Viscosity Effects in Co current Three-Phase Fluidization. A.I.Ch.E. Journal 36, 1613–1616.

Nurmi, P., Özkaya, B., Kaksonen, A.H., Tuovinen, O.H., Puhakka, J.A., 2009. Inhibition kinetics of iron oxidation by *Leptospirillum ferriphilum* in the presence of ferric, nickel and zinc ions. Hydrometallurgy 97, 137-145.

Oloman, C., Watkinson, A.P., 1975. On the role of the surfactant aliquat® 336 on the kinetics of oxygen reduction reaction and on the rate of hydrogen peroxide electro synthesis, Canadian Journal of Chemical Engineering 53, 268–273.

Onysko, K.A., Robinson, C.W., Budman, H. M., 2002. Improved modeling of the unsteady-state behaviour of an immobilized-cell, fluidized-bed bioreactor for phenol biodegradation. The Canadian Journal of Chemical engineering 80, 239-252.

O'Rourke, P.J., Zhao, P.(P.), Snider, D., 2009. A model for collisional exchange in gas/liquid/solid fluidized beds. Chemical Engineering Science 64, 1784-1797.

Ostergaard, K., 1977. Chemical Engineering with Per Soltoft. in K. Ostergaard and A. Fredenslund Eds., Teknisk Forlag, Copenhague, 165.

Padial, N.T., Van der Heyden, W.B., Rauenzahn, R.M., Yarbro, S.L., 2000. Three-dimensional simulation of a three-phase draft-tube bubble column. Chemical Engineering Science 55, 3261–3273.

Pan, Y., Dudukovic, M.P., Chang, M., 1999. Dynamic simulation of bubbly flow in bubble columns. Chemical Engineering Science 54, 2481–2489.

Pan, Y., Dudukovic, M.P., Chang, M., 2000. Numerical investigation of gas-driven flow in 2-D bubble columns. A.I.Ch.E. Journal 46, 434–449.

Panneerselvam, R., Savithri, S., Surender, G.D., 2007. CFD based investigations on hydrodynamics and energy dissipation due to solid motion in liquid fluidised bed. Chemical Engineering Journal 132, 159–171.

Panneerselvam, R., Savithri, S., Surender, G.D., 2009. CFD simulation of hydrodynamics of gas–liquid–solid fluidised bed reactor. Chemical Engineering Science 64, 1119-1135.

Patankar, S.V., 1980. Numerical HeatTransfer and Fluid Flow. McGraw-Hill, NewYork.

Patil, D.J., van Sint Annaland, M., Kuipers, J.A.M., 2005. Critical comparison of hydrodynamic models for gas–solid fluidised beds-Part I: bubbling gas–solid fluidised beds operated with a jet. Chemical Engineering Journal 60, 57–72.

Poddar, S.K., Dutt, D.K. 1969. Semifluidization characteristics for solid-liquid systems: Prediction of minimum and maximum semifluidization velocity. Indian Chemical Engineer 11(3), 80-88.

Potumarthi, R., Mugeraya, G., Jetty, A., 2008. Biological treatment of toxic petroleum spent caustic in fluidized bed bioreactor using immobilized cells of Thiobacillus RAI01. Applied biochemistry and biotechnology 151, 532-546.

Prenosil, J.E., Pedersen, H., 1983. Immobilized plant cell reactors. Enzyme and Microbial Technology 5, 323–331.

Qian W. X., 1980. Research report no.5, Wuhan institute of municipal engineering, China.

Rafique, M., Chen, P., Dudukovic, M., 2004. Computational modeling of gas–liquid flow in bubble columns. Reviews in Chemical Engineering 20, 225–375.

Rajasimman, M., Karthikeyan, C., 2007. Aerobic digestion of starch wastewater in a fluidized bed bioreactor with low density biomass support. Journal of Hazardous Materials 143, 82-86.

Ramachandran, P.A., Chaudhari, R.V., 1983. Three-phase catalytic reactors. New York: Gordon and Breach.

Ramesh, K., Murugesan, T., 2002. Minimum fluidization velocity and gas holdup in gas-liquid-solid fluidized bed reactors. Journal of Chemical Technology and Biotechnology 77, 129-136.

Ramesh, K.V., Raju, G.M.J., Sarma, G.V.S., Sarma, C.B., 2009. Effect of internal on phase holdups of a three-phase fluidized bed. Chemical Engineering Journal 145, 393-398.

Razzak, S.A., Barghi, S., Zhu, J.-X., 2007. Electrical resistance tomography for flow characterization of a gas–liquid–solid three-phase circulating fluidized bed. Chemical Engineering Science 62, 7253 – 7263.

Razzak, S.A., Barghi, S., Zhu, J.-X., Mi, Y., 2009a. Phase holdup measurement in a gas–liquid–solid circulating fluidized bed (GLSCFB) riser using electrical resistance tomography and optical fibre probe. Chemical Engineering Journal 147, 210–218.

Razzak, S.A., Zhu, J.-X., Barghi, S., 2009b. Radial Distributions of Phase Holdups and Phase Propagation Velocities in a Three-Phase Gas-Liquid-Solid Fluidized Bed (GLSCFB) Riser. Industrial Engineering Chemistry and Research 48, 281–289.

Richardson, J.F., Zaki,W.N., 1954. Sedimentation and fluidisation: Part-1. Transaction of Institution of Chemical Engineers 32, 35-53.

Rigby, G.R., Van Brokland, G.P., Park, W.H., Capes, C.E., 1970. Properties of bubbles in three-phase fluidised bed as measured by an electroresistivity probe. Chemical Engineering Science 25, 1729–1741.

Roshchin, N.I., 1992. Granulated Tablet Mixtures in Semifluidized Bed Apparatuses, No. 8, Medprom, Central Office for Scientific and Technical Information, Moscow.

Roy, G.K., Sarma, K.J.R., 1972. Dynamics of liquid-solid semi-fluidization III: Relation between onset of semi-fluidization and minimum fluidization velocity, Chemical Engineering Journal 4, 294-296.

Roy, G.K., Sarma, K.J.R., 1973. Dynamics of Liquid-Solid Semi-fluidization: Prediction of Semi-fluidization Velocity & Packed Bed Formation. Indian Journal of Technology 11, 237-241.

Roy, G.K., Sarma, K.J.R., 1974. Relation between Maximum Semi-Fluidization and Minimum Fluidization Velocity in Liquid-Solid Systems. Journal of the Institution of Engineers (*CH*) 54, 34-35.

Roy, G.K., 1975. Studies on certain aspects of semi-fluidization, PhD Thesis, Sambalpur University, India.

Roy, G.K., Sharat Chandra, H.N., 1976. Liquid-solid semi-fluidization of heterogeneous mixtures II: Prediction of minimum semi-fluidization velocity, Chemical Engineering Journal 12, 77-80.

Roy, G.K., Sarma, K.J.R., 1978. Prediction of Pressure Drop across a Liquid-Solid Semi-fluidized Bed. Indian Journal of Technology 16, 89-93.

Roy, S., Dudukovic, M.P., 2001. Flow mapping and modeling of liquid–solid risers. Industrial Engineering Chemistry and Research 40, 5440–5454.

Ruiz, R.S., Alonso, F., Ancheyta, J., 2004. Minimum Fluidization Velocity and Bed Expansion Characteristics of Hydrotreating Catalysts in Ebullated-Bed Systems. Energy & Fuels 18, 1149-1155.

Saberian-Broudjenni, M., Wild, G., Charpentier, J.-C., Fortin, Y., Euzen, J.-P., Patoux, R., 1987. Contribution to the hydrodynamic study of gas-liquid-solid fluidized-bed reactors. International Chemical Engineering 27, 423-440.

Safoniuk, M., Grace, J.R., Hackman, L., Mcknight, C.A., 1999. Use of dimensional similitude for scale-up of hydrodynamics in three-phase fluidized beds. Chemical Engineering Science 54, 4961-4966.

Safoniuk, M., Grace, J.R., Hackman, L., Mcknight, C.A., 2002. Gas Hold-Up in a Three-Phase Fluidized Bed. AIChE Journal 48, 1581-1587.

Sajc, L., Grubisic, D., Vunjak-Novakovic, G., 2000. Bioreactors for plant engineering: an outlook for further research. Biochemical Engineering Journal 4, 89–99.

Samejima, H., Nagashima, M., Azuma, M., Noguchi, S., Inuzuka, K., 1984. Annals New York Academy of Sciences 434, 394-395.

Sastri, N.V.S., Epstien, N., Hirata, A., Koshijama, I., Izumi, M., 1983. Zinc hydrosulphite by three-phase fluidization: Experiments and model. Canadian Journal of Chemical Engineering 61,635-646.

Schallenberg, J., Enß, J.H., Hempel, D.C., 2005. The important role of local dispersed phase hold-ups for the calculation of three-phase bubble columns. Chemical Engineering Science 60, 6027–6033.

Schiller, L. and Naumann. Z., 1935. A drag coefficient correlation. Z. Ver. Deutsch. Ing. 77, 318.

Schügerl, K., 1997. Three-phase-biofluidization application of three-phase fluidization in the biotechnology - A review. Chemical Engineering Science 52, 3661-3668.

Schweitzer, J.M., Bayle, J., Gauthier, T., 2001. Local Gas Hold-Up Measurements in Fluidized Bed and Slurry Bubble Column. Chemical Engineering Science 56, 1103–1110.

Scott,C.D., Hancher, C.W., 1976. Use of a tapered fluidized bed as a Continuous bioreactor. Biotechnology and Bioengineering 18, 1393-1403.

Shah, Y.T., 1979. Gas-liquid-solid reactor design. McGraw-Hill, New York.

Shcherbakov, A.A., Smidovich, E.V., 1963. Comparative analysis of technical design variations of the reactor system in equipment for continuous coking in a semi-fluidized bed. Transaction Mosk. Institute Neftekhim. i Gaz. Prom. 44, 197-202.

Shen,Y.M., Wang, B.L., 1980. Research report No.2. Chen-du Institute of Municipal Engineering, china.

Sherwin, M.B., Frank, M.E., 1976. Make methanol by three phase reaction. Hydrocarbon Processing 55, 122-124.

Singh, A.N., Takhalate, H.R., Storck, A., Sen Gupta, P., 1980. A correlation for the prediction of packed bed height in liquid-solid semi-fluidization. Chemical Engineering Journal 20, 69-73.

Singh R.K., Maharathy, A.K., Mahapatra, A.K., 2005. Prediction of Pressure Drop in Three-phase Semi-fluidized Bed for Non-spherical Particles. Chemical Engineering World 40 (9), 86-88.

Sinha, V.T., Butensky, M., Hyman, D., 1986. Comparison of cylinders and spheres in three-phase fluidization. Industrial & Engineering Chemistry Process Design and Development 25, 321-324.

Smith, J.M., 1981. Chemical Engneerine Kinetics, 3rd edition, McGraw-Hill, New York.

Sokol, W., Halfani, M.R., 1999. Hydrodynamics of a gas-liquid-solid fluidized bed bioreactor with a low-density biomass support. Biochemical Engineering Journal 3, 185-192.

Sokol, W., 2001. Operating parameters for a gas-liquid-solid fluidized bed bioreactor with a low density biomass support. Biochemical Engineering Journal 8, 203-212.

Sokol, W., 2003. Treatment of refinery wastewater in a three-phase fluidized bed bioreactor with a low-density biomass support. Biochemical Engineering Journal 15, 1-10.

Sokol, W., Korpal, W., 2004. Determination of the optimal operational parameters for a three-phase fluidized bed bioreactor with a light biomass support when used in treatment of phenolic wastewaters. Biochemical Engineering Journal 20, 49-56.

Sokolichin, A., Eigenberger, G., Lapin, A., 2004. Simulation of buoyancy driven bubbly flow: established simplifications and open questions. AIChE Journal 50, 24–45.

Soleimani, M., Bassi, A., Margaritis, A., 2007. Biodesulfurization of refractory organic sulfur compounds in fossil fuels. Biotechnology Advances 25, 570-596.

Son, S-M., Kang, S-H., Kang, T-G., Song, P-S., Kim, U-Y., Kang, Y., Kang, H-K., 2007. Gas Holdup and Gas-Liquid Mass Transfer in Three-Phase Circulating Fluidized-Bed Bioreactors. Journal of Industrial Engineering Chemistry13, 14-20.

Song, G.H., Bavarian, F., Fan, L.S., 1989. Hydrodynamics of three-phase fluidized bed containing cylindrical hydrotreating catalysts. Canadian Journal of Chemical Engineering 67, 265-275.

.

Soung, W.Y., 1978. Bed Expansion in Three-Phase Fluidization. Industrial & Engineering Chemistry Process Design and Development 17, 33-36.

Squires, A.M., Kwauk, M., Avidan, A.A., 1985. Fluid Beds: At Last, Challenging Two Entrenched Practices. Science, 230, 1329-1 337.

Sun, Y., Furusaki, S., 1990. Continuous production of acetic acid using immobilized *Acetobacter aceti* in a three phase fluidized bed bioreactor. Journal of Fermentation and Bioengineering 69, 102-110.

Takase, H., Ishibashi, D., Sugimoto, M., 1983. In: Symposium on biological wastewater treatment, Society of Chemical Engineers, Japan, Sendai, Japan, 17-22.

Tang, W.-T., Fan, L.-S., 1989. Hydrodynamics of Three-Phase Fluidized Bed Containing Low Density Particles. AIChE Journal 35, 355-363.

Tarmy, B.L., Chang, M., Coulaloglou, C.A., Ponzi, P.R., 1984. The three phase hydrodynamics of the EDS coal liquefaction reactors: their development and use in reactor scale up. 8th International Symposium on Chemical Reaction Engineering 87, 303–317.

Tarmy, B.L., Coulaloglou, C.A., 1992. Alpha-Omega and Beyond: Industrial View of Gas/Liquid/Solid Reactor Development. Chemical Engineering Science 47, 3231-3246.

Thompson, A.R., 1955. In: Encyclopaedia of Chemical Technology. R.E. Kirk and D.F. Othmer, Ed., Interscience Encyclopaedia, New York 4, 619-620.

Thompson, V.S., Worden, R.M., 1997. Phase holdup, liquid dispersion, and gas-to-liquid mass transfer measurements in a three-phase magnetofluidized bed. 52, 279-295.

Thorat, B.N., Shevade, A.V., Bhilegaonkar, K.N., Aglawe, R.H., Parasu Veera, U., Thakre, S.S., Pandit, A.B., Sawant, S.B., Joshi, J.B., 1998. Effect of sparger design and height to diameter ratio on fractional gas hold-up in bubble columns. Transaction of Institution of Chemical Engineers Part A 76, 823-834.

Vinod, A.V., Reddy, G.V., 2003. Dynamic behaviour of a fluidised bed bioreactor treating wastewater. Indian Chemical Engineer 45, 20-27.

Vinod, A.V., Ajeesh, K.N., Reddy, G.V., 2004. Studies on gas hold-up in a Draft tube fluidised bed column. Indian Chemical Engineer 46, 229-233.

Volpicelli, G., Massimilla, L., 1970. Three-phase fluidized bed reactors an application to the production of calcium bisulphite acid solutions. Chemical Engineering Science 25, 1361-1373.

Wang, T., Wang, J., Yang, W., Jin, Y., 2003. Experimental study on bubble behavior in gas–liquid–solid three-phase circulating fluidized beds. Powder Technology 137, 83–90.

Wang, F., Mao, Z.S., Wang, Y., Yang, C., 2006. Measurement of phase holdups in liquid–liquid–solid three-phase stirred tanks and CFD simulation. Chemical Engineering Science 61, 7535–7550.

Wang, X., Li, Z., Wang, Z., Li, J., Li, J., Chen, R., 2009. Effectiveness of fluidized pellet bed for removing soluble contaminants. Journal of Environmental Sciences 21, 13-17.

Warsito, W., Fan, L.S., 2001. Measurement of real-time flow structures in gas–liquid and gas–liquid–solid flow systems using electrical capacitance tomography (ECT). Chemical Engineering Science 56, 6455–6462.

Warsito, W., Fan, L.S., 2003. ECT imaging of three-phase fluidised bed based on three-phase capacitance model. Chemical Engineering Science 58, 823–832.

Wen C. Y., Yu, Y. H., 1966. Mechanics of Fluidization, Chemical Engineering Symposium Series, 62, 100-111.

Wen, C. Y., Fan, L. T., 1979. Method of filtration using convertible (semifluidized) beds. US Patent 4,157,959.

Wen, J., Lei, P., Huang, L., 2005. Modeling and simulation of gas-liquid-solid three-phase fluidization. Chemical Engineering Communications 192, 941-955.

Weiss, D.E., Swinton, E.A., 1958. Continuous extraction from solution with granular adsorbents. Patent: AU 212370 19580129, Commonwealth Scientific and Industrial Research Organization.

Wild, G., Poncin, S., 1996. Chapter 1: Hydrodynamics. In: Three-Phase Sparged Reactors, Nigam, K.D.P., and Schumpe, A., ed., Gordon and Breach Publishers, Amsterdam, The Netherlands.

Wild, G., Saberian, M., Schwartz, J.-L., Charpentier, J.-C., 1984. Gas-Liquid-Solid Fludidized-Bed Reactors. State of the Art and Industrial Possibilities", International Chemical Engineering, 24, 639-678.

Xianling, L., Jianping, W., Qing, Y., Xueming, Z., 2005. The pilot study for oil refinery wastewater treatment using a gas–liquid–solid three-phase flow airlift loop bioreactor. Biochemical Engineering Journal 27, 40–44.

Yang, G.Q., Du, B., Fan, L.S., 2007. Bubble formation and dynamics in gas–liquid–solid fluidization—A review. Chemical Engineering Science 62, 2-27.

Yu, Y.H., Kim, S.D., 1988. Bubble characteristics in the radial direction of three-phase fluidised beds. AIChE Journal 34, 2069–2072.

Yu, H., Rittman, B.E., 1997. Predicting Bed Expansion and Phase Hold-Up for Three-Phase fluidized Bed Reactors with and without Biofilm. Water Research 31, 2604-2616.

Zhang, J.-P., Epstein, N., Grace, J.R., Zhu, J., 1995. Minimum Liquid Fluidization Velocity of Gas-Liquid Fluidized Beds. Transaction of Institution of Chemical Engineers 73, Part A, 347 – 353.

Zhang, J., 1996. Bubble Columns and Three-Phase Fluidized Beds: Flow Regimes and Bubble Characteristics, PhD thesis, UBC, Vancouver.

Zhang, J., Grace, J.R., Epstein, N., 1997. Flow Regime Identification in Gas-Liquid Flow and Three-Phase Fluidized Beds. Chemical Engineering Science 52, 3979-3992.

Zhang, J.-P., Epstein, N., Grace, J. R., 1998. Minimum Fluidization Velocities for Gas-Liquid-Solid Three-Phase Systems. Powder Technology 100, 113-118.

Zhang, J.-Y., Lin, C., Lin, C.-S., 2002. Axial distribution of solids holdup for both hydrophilic and hydrophobic particles in three-phase fluidized beds. Canadian Journal of Chemical Engineering 80, 37-43.

Zhang, X., Ahmadi, G., 2005. Eulerian–Lagrangian simulations of liquid–gas–solid flows in three-phase slurry reactors. Chemical Engineering Science 60, 5089–5104.

Zhang, N., Lu, B., Wang, W., Li, J., 2008. Virtual experimentation through 3D full-loop simulation of a circulating fluidized bed. Particuology 6, 529-539.

Zheng, C., Yao, B., and Feng, Y., 1988. Flow Regime Identification and Gas Hold-up of Three-phase Fluidized Systems. Chemical Engineering Science 43, 2195-2200.

Zhou, D., Dong, S., Wang, H., Bi, H.T., 2009. Minimum fluidization velocity of a three-phase conical fluidized bed in comparison to a cylindrical fluidized bed. Industrial and Engineering Chemistry Research 48, 27-36.

Curriculum Vitae

HARA MOHAN JENA

E-mail: hara.jena@gmail.com, hmjena@nitrkl.ac.in

Permanent Address: AT: Bambilo, PO: Hariank, VIA: Danpur
Dist: Kendrapara, Orissa, India
Pin Code - 754210

Education:

2009	Ph. D. Dissertation Submitted
2002	M.Tech, R.E.C, Rourkela
1997	AMIE, IE, Kolkata
1995	MSc, Berhampur University

Personal Information:

Date of Birth:	12-04-1971
Nationality	Indian

Employment:

1998 - 2000	***Shift Engineer***, Akay Organics Ltd. MIDC Tarapur (MS)
2002 - 2003	***Adhoc Lecturer***, Dept. of Chem. Engg., NIT, Rourkela, Orissa
2007 - Till Date	***Lecturer***, Dept. of Chem. Engg., NIT, Rourkela, Orissa

Publications:

1. **Jena, H.M.**, Roy, G.K., Meikap, B.C., 2005. Development and Comparative Study of a Semi-Fluidized Bed Bioreactor for Treatment of Wastewater from Process Industries. *Process & Plant Engineering – Environment Management* 23 (1), 70-75.
2. **Jena, H.M**., Roy, G.K., Meikap, B.C., 2007. Gas holdup in a three-phase fluidized bed with cylindrical particles. *International Journal of Chemical Sciences* 5(4), 1712-1722.
3. **Jena, H.M.**, Roy, G.K., Meikap, B.C., 2008. Prediction of gas holdup in three-phase fluidized bed from bed pressure drop measurement. *Chemical Engineering Research and Design* 86, 1301-1308.
4. **Jena, H.M.**, Roy, G.K., Biswal, K.C., 2008. Studies on Pressure Drop and Minimum Fluidization Velocity of Gas-Solid Fluidization of Homogeneous Well Mixed Ternary Mixtures in Un-Promoted and Promoted Square Bed. *Chemical Engineering Journal* 145, 16-24.
5. **Jena, H.M.**, Sahoo, B.K., Roy, G.K., Meikap, B.C., 2008. Characterization of hydrodynamic properties of a gas–liquid–solid three-phase fluidized bed with regular shape spherical glass bead particles. *Chemical Engineering Journal* 145, 50-56.
6. **Jena, H.M.**, Roy, G.K., Meikap, B.C., 2009. Hydrodynamics of a gas-liquid-solid fluidized bed with hollow cylindrical particles. *Chemical Engineering and Processing: Process Intensification* 48, 279-287.
7. **Jena, H.M.**, Sahoo, B.K., Roy, G.K., Meikap, B.C., 2009. Statistical Analysis of the Phase Holdup Characteristics of a Gas–Liquid–Solid Fluidized Bed. *The Canadian Journal of Chemical Engineering* 87, 1-10.
8. **Jena, H.M.**, Roy, G.K., Mahapatra, S.S., 2009. Determination of optimum gas holdup conditions in a three-phase fluidized bed by Genetic Algorithm. *Computers & Chemical Engineering* doi:10.1016/j.compchemeng.2009.07.003.
9. **Jena, H.M.**, Roy, G.K., Meikap, B.C., 2009. Hydrodynamics of regular particles in a liquid- solid semi-fluidized bed. *Powder Technology* doi:10.1016/j.powtec.2009.07.022.